

UNIVERSITÀ DEGLI STUDI DI NAPOLI Federico II

DOTTORATO DI RICERCA IN FISICA

CICLO XXXII

COORDINATORE: PROF. SALVATORE CAPOZZIELLO

THE FATE OF LATE-TYPE GALAXIES IN THE FORNAX CLUSTER, MAPPED WITH DEEP IMAGING DATA

Dottorando
Maria Angela RAJ

Tutori
Dr. Enrichetta IODICE
Prof. Nicola R. NAPOLITANO

Settore Scientifico Disciplinare FIS/05

Anni 2017/2020

Dedicated to my beautiful mother and memory of my father

Abstract

"The fate of late-type galaxies in the Fornax cluster, mapped with deep imaging data"

by Maria Angela RAJ

The main objective of the work presented in this thesis is to study the bright ($m_B < 16$ mag) late-type galaxies (LTGs) in the Fornax cluster core and compare their structure and relevant properties (e.g. stellar mass, $g - i$ colours) to those in the Fornax A subgroup. In this thesis, I present the surface photometry of 22 LTGs in the Fornax cluster i.e. 13 in the core and nine in the subgroup, observed with the Fornax Deep Survey (FDS). With the multi-band (u, g, r, i) and deep images of FDS, I investigate the faint outskirts of the LTGs and estimate the amount of intra-group light (IGL). Since the Fornax cluster is observed in multiple wavelengths, I use some ancillary data to discuss the individual LTGs and trace their evolutionary path in the cluster. The main results of this work suggest that the dense environment of the cluster core inhibits the formation of spiral galaxies and therefore, the very late-type galaxies with morphological type $5 < T \leq 9$ are located beyond the high-density (> 0.8 deg) regions of the Fornax cluster. From the analysis of the break-radius and break type, six out of nine LTGs in the Fornax A group are of Type-III, which is either suggestive of strangulation halting the star-formation in their outer discs or a consequence of HI-richness, while the cluster core LTGs have Type-II and Type-III profiles. In the Fornax A group, the absence of morphology and colour segregation of LTGs with group-centric distance, and the low IGL fraction (16%) suggest that the evolutionary phase of the group is different from that of the cluster core. This is further supported by the effect of the environment on the structure of LTGs, where we find that the break-radius of most ($\sim 80\%$) of the cluster core LTGs are located within $1R_e$, contrary to those in the group ($> 1R_e$). By comparing the aforementioned properties and analysing them in projected phase-space, I discuss 'pre-processing' of galaxies before cluster infall thereby providing clues to the hierarchical merging of groups into the main cluster. During the merging of groups, the IGL mixes with the intra-cluster light thus forming the bulk of the intra-cluster baryons inside the core of the Fornax cluster. All of the mentioned work not only helps us to understand the evolution of LTGs in the Fornax cluster but also provides clues to their structure-transformation in other dense clusters. Finally, by comparing observational results to those from simulations, I predict the fate of LTGs in the Fornax cluster.

Contents

Abstract **v**

1 Introduction **1**
1.1 Galaxies: a 'library of the Universe' . . . 2
1.2 Late-type galaxies: the cradle of structure - formation . . . 6
1.2.1 Spiral galaxies . . . 6
1.2.2 Barred spiral galaxies . . . 7
1.2.3 Galaxies with pseudo-rings/outer rings . . . 7
1.3 The densest parts of the large scale structures in the Universe . . 7
1.3.1 Groups . . . 8
1.3.2 Clusters . . . 8
1.4 Evolution and structure transformation of LTGs in dense environments . . . 9
1.4.1 Ram-pressure stripping . . . 9
1.4.2 Galaxy-galaxy harassment . . . 10
1.4.3 Strangulation . . . 10
1.4.4 Merging . . . 10
1.5 The Fornax-Eridanus complex . . . 11
1.5.1 The Fornax cluster core . . . 13
1.5.2 The Fornax A subgroup . . . 13
1.5.3 Surveys . . . 15
1.6 The era of deep imaging data . . . 17
1.6.1 Exploring faint outskirts of galaxies . . . 18
Truncations and disc-breaks . . . 18
1.6.2 Studying the intra-cluster light and intra-group light . . 19
1.6.3 Deep data: a probe for investigating the effect of the environment on galaxy evolution . . . 20
1.7 The Fornax Deep Survey . . . 21
1.8 Scientific motivation of this thesis . . . 22
1.9 Thesis Outline . . . 23

2 Evolution and structure of late-type galaxies inside the virial radius of the Fornax cluster **25**
2.1 Introduction . . . 27
2.2 The Fornax Deep Survey: data . . . 29
2.3 Analysis: surface photometry . . . 32
2.3.1 Method: isophote fitting . . . 34
2.3.2 Products: total magnitude, effective radius, colour, and stellar mass-to-light ratio . . . 34
2.4 Analysis: the break radius . . . 37

2.4.1 Surface brightness profile deconvolution 37
2.4.2 Algorithm: break radius 38
2.5 Morphological segregation of LTGs inside the virial radius of the Fornax cluster 43
2.6 Analysis of disc-breaks 47
2.7 Summary of results and discussion 50
2.7.1 Evolution of LTGs inside the virial radius of the Fornax cluster 51
Late-type spiral (Scd-Sdm) galaxies 52
Galaxies transitioning into S0 53
2.7.2 Break radius as a proxy for the structural evolution of LTGs 53
Type III disc-break 54
Type II disc-break 54
What can the average $(g - i)$ colour of the inner and outer discs of LTGs indicate? 55
2.8 Concluding remarks and future perspectives 55

Appendices **57**
2.A The sample: LTGs inside the virial radius 57
2.A.1 FCC113 57
2.A.2 FCC115 57
2.A.3 FCC121 57
2.A.4 FCC176 58
2.A.5 FCC179 58
2.A.6 FCC263 58
2.A.7 FCC267 58
2.A.8 FCC285 59
2.A.9 FCC290 59
2.A.10 FCC302 59
2.A.11 FCC306 60
2.A.12 FCC308 60
2.A.13 FCC312 60
2.B The sample: images and profiles 61
2.C Methodologies 74
2.C.1 Reliability test 74
2.C.2 Algorithm 76

3 On the assembly history of the bright galaxies in the Fornax A sub-group **83**
3.1 Introduction 85
3.2 The Fornax Deep Survey: data 87
3.3 Analysis 88
3.3.1 Isophote fitting 90
3.3.2 Products: total magnitude, effective radius, colours, stellar mass 91
3.3.3 Products: break radius, scale-lengths, disc colours 91
3.4 Results 97

3.4.1 Morphology and colour analysis of galaxies in the Fornax A subgroup . . . 97
3.4.2 Analysis of the discs . . . 99
3.5 Assembly history of the bright LTGs in Fornax A . . . 101
3.6 The tale of the Fornax environment . . . 104
3.6.1 Galaxy populations . . . 104
3.6.2 Morphological segregation . . . 104
3.6.3 Colour segregation . . . 105
3.6.4 Structure of LTGs . . . 105
3.6.5 X-ray emission . . . 105
3.6.6 Disc-breaks of LTGs . . . 107
3.7 Summary and conclusions . . . 107

Appendices **111**
3.A Bright LTGs in the Fornax A subgroup . . . 111
3.A.1 FCC013 . . . 111
3.A.2 FCC022 . . . 111
3.A.3 FCC028 . . . 111
3.A.4 FCC029 . . . 112
3.A.5 FCC033 . . . 112
3.A.6 FCC035 . . . 112
3.A.7 FCC037 . . . 112
3.A.8 FCC039 . . . 113
3.A.9 FCC062 . . . 113
3.B The sample: images and profiles . . . 114
3.C Methodologies: Multi-component fits of the light distribution . . . 123

4 The intra-cluster baryons in Fornax **127**
4.1 Introduction . . . 129
4.1.1 An overview of the outskirts of NGC 1316 . . . 130
Faint features . . . 130
Formation history . . . 130
4.2 The ICL in the Fornax cluster . . . 130
4.2.1 The stellar bridge connecting NGC 1399 and NGC 1387 . . . 132
4.2.2 The diffuse light in the central regions of Fornax cluster core . . . 132
4.2.3 The intracluster GCs and PNe . . . 132
4.2.4 The ICL of Fornax cluster compared to other local clusters 134
4.3 Estimation of the IGL . . . 134
4.4 On the build-up of the IGL in the Fornax A subgroup . . . 136
4.4.1 The HI content versus diffuse light . . . 139
4.4.2 IGL as the progenitor of the ICL . . . 140
4.5 Summary and conclusions . . . 140

5 Discussion and future perspectives **141**
5.1 Discussion . . . 142
5.1.1 On the account of pre-processing of galaxies in the Fornax cluster core . . . 143

Clues from phase-space diagrams 145
Evidence from break-radius 146
5.1.2 The fate of LTGs in the Fornax cluster 146
5.2 Conclusions and future perspectives 147

Acknowledgements **149**

Bibliography **151**

List of Figures

1.1 Simulated image of millions of galaxies in clusters, super clusters, forming the galactic filament. 2
1.2 Hubble sequence by Delgado-Serranp et al. (2010) 4
1.3 Revised morphological classification scheme 5
1.4 Elmegreen classification of spiral arms in galaxies. 6
1.5 The Fornax-Eridanus complex 12
1.6 VST colour composite image of the Fornax cluster core 14
1.7 VST colour composite image of the Fornax A subgrpup 16
1.8 Comparison of images at different surface brightness limiting depth 19
1.9 Smoothed VST images of NGC 1427A 20
1.10 Area spanning 26 deg^2 around NGC 1399 and NGC 1316 observed with the Fornax Deep Survey. 22

2.1 VST mosaic in g-band of Fornax cluster's virial radius, at about 9 deg^2 32
2.2 Impact of PSF on galaxies with different angular extent 39
2.3 Type II disc breaks 41
2.4 Surface brightness profiles of galaxies with Type III disc-break, similar to Fig. 2.3. 42
2.5 Hubble type T as function of projected cluster-centric distance . 45
2.6 Stellar mass as function of cluster-centric distance (top panel) and colour-magnitude relation (lower panel) for LTGs and ETGs in the Fornax cluster core 46
2.7 $g - i$ (top panel) and $g - r$ (lower panel) colours as function of projected distance from Fornax cluster's centre in degrees and Mpc. 47
2.8 Histogram of surface brightness at break radius (μ_{B_r}) for Type II and Type III galaxies. 48
2.9 Analysis of galaxies with disc-breaks 49
2.10 Molecular gas mass (top panel) and molecular gas-fractions (lower panel) as function of break radius 50
2.B.1 Surface photometry of FCC113 61
2.B.2 Surface photometry of FCC115 62
2.B.3 Surface photometry of FCC121 63
2.B.4 Surface photometry of FCC176 64
2.B.5 Surface photometry of FCC179 65
2.B.6 Surface photometry of FCC263 66
2.B.7 Surface photometry of FCC267 67
2.B.8 Surface photometry of FCC285 68

2.B.9 Surface photometry of FCC290 . . . 69
2.B.10 Surface photometry of FCC302 . . . 70
2.B.11 Surface photometry of FCC308 . . . 71
2.B.12 FCC306 in zoom . . . 72
2.B.13 Surface photometry of FCC306 . . . 72
2.B.14 Surface photometry of FCC312 . . . 73
2.C.1 Reliability test for deconvolution . . . 75
2.C.2 An example of the 'best fits' produced by the algorithm . . . 77
2.C.3 Appendix 2.C.2 continued . . . 78
2.C.4 Appendix 2.C.2 continued . . . 79
2.C.5 Type-II original versus deconvolved profiles . . . 80
2.C.6 Type-III original versus deconvolved profiles . . . 81

3.2.1 VST mosaic in g-band of the Fornax A subgroup covering 3×2 deg^2 . . . 88
3.3.1 Surface brightness profiles of galaxies with Type III disc break 96
3.4.1 Hubble Type T as a function of group/cluster-centric distance for bright galaxies in the Fornax A subgroup (left panel) and Fornax cluster core (right panel). . . . 98
3.4.2 Stellar mass as function of projected distance from NGC 1316 (top panel) and colour-magnitude relation (lower panel) for bright spiral galaxies inside the virial radius of the Fornax A subgroup. . . . 99
3.4.3 Size-mass relation (top panel) and effective radius as a function of projected distance from NGC 1316 (lower panel) for all the bright spiral galaxies in the Fornax A subgroup . . . 100
3.4.4 $g - i$ (top panel) and $g - r$ (lower panel) colours as a function of projected distance from NGC 1316 in degrees and Mpc . . . 101
3.4.5 Analysis of galaxies with a break in their surface brightness profiles . . . 102
3.5.1 Projected phase-space diagram of galaxies in the Fornax A subgroup within a group-centric distance of 1.1 deg $\sim$ 0.38 Mpc . 103
3.6.1 Histogram of the colour $(g - i)$ distribution (left) and of the stellar mass (right) for the bright galaxies in the Fornax core and Fornax A subgroup. . . . 106
3.B.1 Surface Photometry of FCC013 . . . 114
3.B.2 Surface Photometry of FCC022. Top left panel: g-band image in SB level. Top right panel: SB profiles in g, r, i bands. Bottom panels: $g - i$ colour map (left) and $g - i$ colour profile (right). 115
3.B.3 Surface Photometry of FCC028 . . . 116
3.B.4 Surface Photometry of FCC029 . . . 117
3.B.5 Surface Photometry of FCC033 . . . 118
3.B.6 Surface Photometry of FCC035 . . . 119
3.B.7 Surface Photometry of FCC037 . . . 120
3.B.8 Surface Photometry of FCC039 . . . 121
3.B.9 Surface Photometry of FCC062 . . . 122
3.C.1 Multi-component fits of the surface brightness profiles (r-band) of galaxies with Type III disc break . . . 124

4.1.1 Image of NGC 1316 in SB level with all the detected loops . . . 131
4.2.1 Diffuse patches of ICL detected in the Fornax cluster core . . . 133
4.2.2 Radial density of the galaxy population as a function of the cluster-centric distance . . . 134
4.3.1 Residual image in g-band used for the estimation of the IGL. . 136
4.4.1 Radial density of the galaxy population as a function of the group-centric distance . . . 137
4.4.2 Fraction of IGL by mergers and fraction of IGL accreted 138
4.4.3 Fraction of IGL as a function of the total HI mass for four loose groups and Hickson Compact Groups . . . 139

5.1.1 Bright galaxies in the Fornax cluster in projected phase-space . 144

List of Tables

1.1 Main properties of the Fornax cluster 13
1.2 Main properties of the Fornax A subgroup 13

2.1 Image quality of FDS fields 31
2.2 LTGs brighter than $m_B \leq 16.6$ mag inside Fornax cluster's virial radius 33
2.3 Limiting radius of intensity profiles 35
2.4 Derived Parameters of LTGs inside Fornax cluster's virial radius 36
2.5 Stellar mass estimates of LTGs in i -band 37
2.6 Parameters of LTGs with disc-breaks 44
2.C.1 Parameters of the best fit of LTGs with disc-breaks, inside the virial radius 76

3.2.1 Image quality of FDS fields used in this work 87
3.3.1 LTGs brighter than $m_B < 16$ mag in the Fornax A subgroup . . 89
3.3.2 Limiting radius of intensity profiles 90
3.3.3 Derived Parameters of LTGs in Fornax A subgroup 92
3.3.4 Stellar mass estimates of LTGs in the i -band 94
3.3.5 Parameters of LTGs with a disc break 95
3.C.1 Best-fitting parameters for five galaxies with detected disc-breaks in the Fornax A subgroup 125

Chapter 1

Introduction

Abstract

In this chapter, I define and give an overview of the morphological classification of galaxies. I then briefly describe the structure of late-type galaxies (LTGs) e.g. spiral galaxies, which are prone to changes in dense environments. Hence, I give a short summary of the current knowledge we have of galaxy clusters and groups, which form the densest parts of the large-scale-structures in the Universe. In order to understand *how* dense environments can transform the structures of LTGs, I explain the significant processes (e.g. ram pressure stripping) which take place in clusters/groups. I then introduce the Fornax cluster and provide the motivation of choice for studying its constituent LTGs and the impact of the environment on their evolution. The motivation also includes the large coverage of the Fornax cluster in multiple wavelengths and therefore, I give a brief overview of the surveys involved in observing and studying this cluster; one of the surveys is the Fornax Deep Survey (FDS), which is a deep, multi-band imaging survey. Since the work presented in this thesis is based on data from FDS, I describe how the era of deep imaging data has helped us to explore a great amount of the light distribution of galaxies in the cluster down to faint surface brightness levels. On this note, I also briefly describe the observations, goals, and the main results of FDS. Finally, I provide the scientific motivation of the work undertaken in this thesis, how it contributes to the overall goals of FDS and in the study of the Fornax cluster itself, and then give the thesis outline.

1.1 Galaxies: a 'library of the Universe'

It was not until the twentieth century that astronomers discovered that our Galaxy, the Milky Way was not the entire Universe. Since then, there have been dedicated studies to look beyond our Milky Way. Especially in the last few decades, astronomy has reached new milestones by imaging the farthest known galaxy yet at redshift $z > 10$ (Oesch et al. 2016) and this field of research continues to reach further.

The most commonly asked question is *why do we study galaxies?* Since the dawn of the early-Universe, the attractive force of gravitation has played a prominent role in creating the large structures of the Universe we know of today— spanning from stars to superclusters of galaxies to galaxy filaments and voids. Fig. 1.1 shows a simulated image of the large structures of the Universe.

In simplest terms, a *galaxy* is defined as a massive gravitationally bound object consisting of stars, dust, gas, and dark matter. Galaxies vary in shape, size, mass, structure, composition and most importantly, are at different distances to us. The finite velocity of light helps us determine these distances and hence, we are able to look at galaxies in different epochs. Moreover, they can be found in isolation (the field) or clumped together in different environments— groups, clusters. Studying them in different environmental conditions at various look-back times[1], particularly analysing their formation, evolution, and morphology has proven to be vital in understanding our Universe.

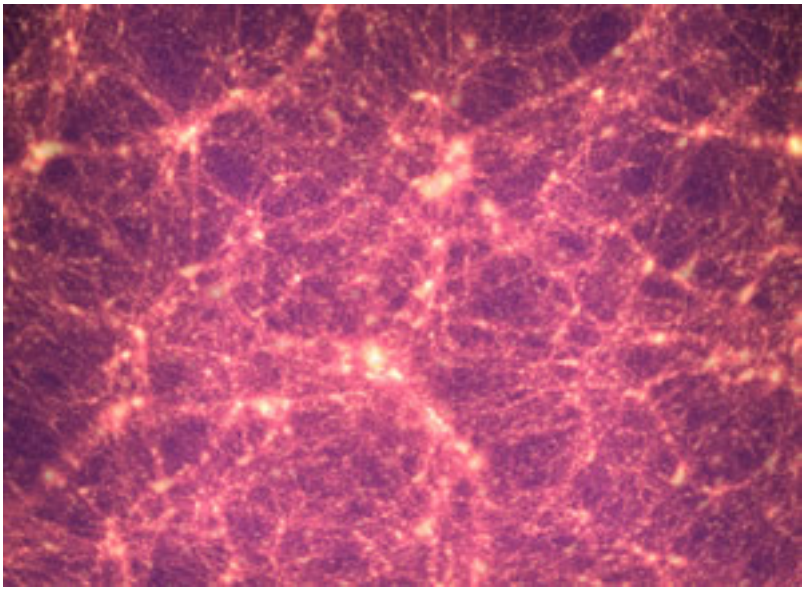


FIGURE 1.1: Simulated image of millions of galaxies in clusters, superclusters, forming the galactic filament. Credit: Paul Bourke and Alexander Knebe, Swinburne University of Technology.

[1]The look-back time (t_L) to an object is the difference between the age (t_0) of the Universe at the time of observation and the age (t_e) of the Universe at the time the light was originally emitted by the object (see Hogg 1999).

The original model for galaxy formation was the *monolithic collapse* (Eggen, Lynden-Bell, and Sandage 1962). According to this model, a galaxy was formed by the gravitational collapse of a primordial cloud of gas in the early-Universe. Contrary to this approach, White and Rees (1978) proposed that small fluctuations in the density field of the hot, young Universe created the first seeds of galaxies; this has since been supported by the cold dark matter (CDM) model. Peculiarities in the density field caused dark matter (DM) to collapse onto dark haloes, which was then followed by cosmic inflation and subsequent cooling of the baryonic matter. Stars were then formed by the concentration of cold gas in the aforementioned dark haloes; these stars became the luminous part of galaxies. The galaxies we observe in the Local Universe are the final result of the evolution (external and internal) of the *early galaxies*. Based on the ΛCDM cosmological model, structures thereafter grow through hierarchical clustering of dark matter and gas (White and Frenk 1991); this has also been shown in cosmological simulations (e.g. Schaye et al. 2015; Pillepich et al. 2018).

'Galaxy morphology' is the product of the formation and evolution of a galaxy and therefore, characterises it based on its interactions with the environment, structure, and star-formation history (Buta 2011). In 1926, Edwin Hubble studied the diverse nature of galaxies and proposed a morphological classification scheme. This well-known 'tuning-fork diagram' (Hubble 1926) which groups galaxies based on their bulge/disc ratio, gas fractions, and rotational support, set the premises of determining the nature of galaxies. The main classes of this morphological classification are elliptical (E), lenticular (S0), spiral (S), and irregular galaxies (Ir). Sub-classes were then introduced based on their ellipticity for elliptical galaxies (E0–E9), tightness of the spiral arms (Sa–Sc) and presence of bars (SB) for spiral galaxies.

According to the Hubble-Sandage (1961) classification scheme, galaxies on the left part of the Hubble sequence were referred to as 'early-type' galaxies (ETG) and those on the right part were referred to as 'late-type' galaxies (LTG). Under the same scheme, Sa-SBa galaxies were called 'early-type spirals' and Sc-SBc galaxies were called 'late-type spirals'. A qualitative method of classifying galaxies based on their morphology is using the *Hubble stage T* parameter (de Vaucouleurs 1959, 1963, 1974). In this method, galaxy morphology is represented as a three-dimensional volume with a long axis and short axis. The long axis is the *type* as given in the Hubble sequence, and the short axis is the family i.e. if a galaxy is barred, or has an inner-ring. In addition to Hubble's classification, other classes were included; they are late ellipticals (E^+), very-late spirals (Sd), magellanic spirals (Sm) and magellanic irregulars (Im). The stages are denoted as numbers ranging from -6 (compact E; cE) to +10 (Im) or +11 (compact Im). Since then, the Hubble classification scheme was improved to include various other classes like peculiar (Arp 1966), dwarfs, and central dominant (cD) galaxies (Sandage 2005). Fig.1.2 shows the Hubble sequence of galaxies in the local and distant Universe ($0.4 < z < 0.8$).

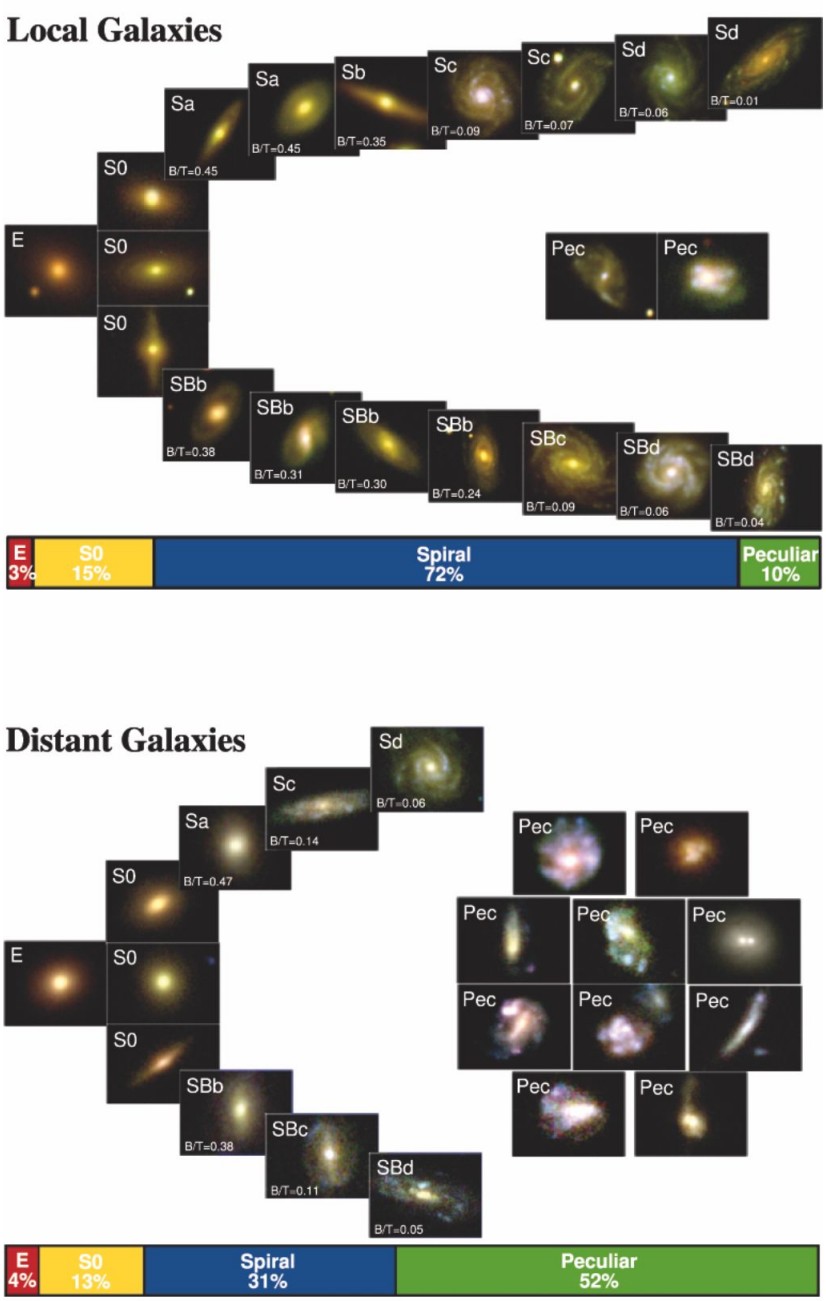


FIGURE 1.2: Hubble sequence by Delgado-Serrano et al. (2010).

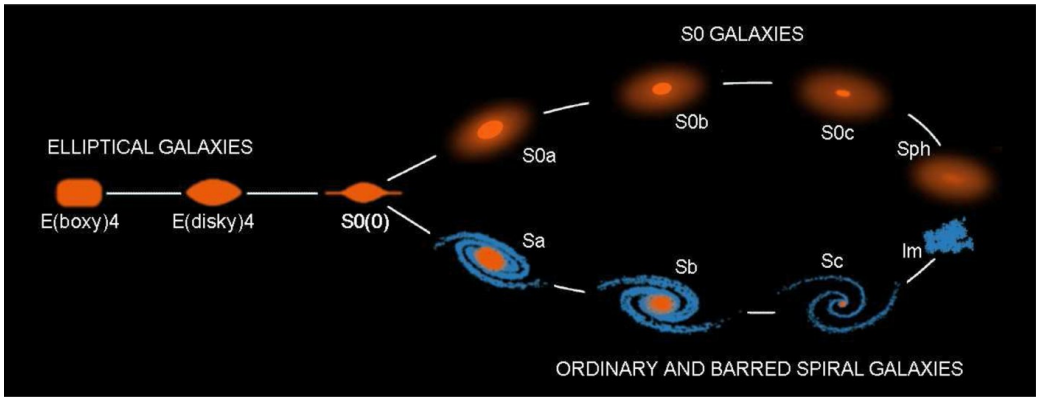


FIGURE 1.3: Revised parallel-sequence morphological classification scheme of galaxies by Kormendy and Bender (2012).

Alternative to Hubble's approach, van den Bergh (1976) provided a classification scheme that put S0s (S0a-S0b-S0c) parallel to spiral galaxies (Sa-Sb-Sc). This was done from observational results which showed that S0s with small bulge-to-total light (B/T) ratio did not fit into the transition sequence from Sa to E, rather they are structurally similar to Sa–Sc galaxies. The classification scheme was then modified by Kormendy and Bender (2012) to include spheroidal (Sph) galaxies parallel to irregular galaxies (see Fig. 1.3).

In this thesis, I focus on LTGs which include spiral and irregular galaxies. Spiral galaxies make up about two-third of the massive galaxy population (Lintott et al. 2011; Dobbs and Baba 2014). As mentioned above, the general morphological classification scheme for spiral galaxies is based on the presence of bars and spiral arms[2] (de Vaucouleurs 1974). Another classification scheme by Elmegreen and Elmegreen (1987) includes sub-types of the spiral galaxies that is based on the number and length of the spiral arms. In simple terms, the classification scheme of spiral arms by (Elmegreen 1990) has three main types: (i) grand-design galaxies (two main spiral arms); (ii) flocculent spiral galaxies (many short spiral arms); (iii) multi-armed spiral galaxies. An example for each of the types of galaxies, based on the classification of their spiral arms is shown in Fig. 1.4. Overall, galaxies are classified with the above notations. Recently, the classification scheme by Buta et al. (2015) incorporates more finer morphological measurements such as nuclear rings, box/peanut structures, thick discs.

In this thesis, we select LTGs based on their original classification, but in their individual analysis, we include recent morphological classifications to provide a better framework of their substructures and evolution. These substructures e.g. spiral arms are the regions where star-formation occurs. Hence, understanding the formation of these substructures in spiral galaxies provides clues on star-formation and the evolution of the Universe. In the next section, I give a brief overview on the formation of substructures (e.g. spiral arms, bars) in LTGs.

[2]The De Vaucouleurs classification scheme also included the presence of arms that spiral into a ring (denoted as r) or pseudo-rings/outer-rings (denoted by R, preceding the Hubble type).

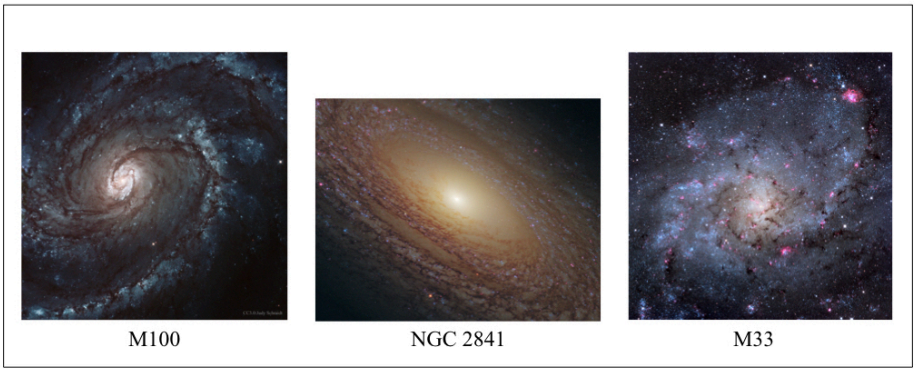


FIGURE 1.4: Examples for the Elmegreen (1990) classification of spiral arms in galaxies: M100 (grand design spiral galaxy; image credits: Hubble Legacy Archive, NASA, ESA; Processing & Licence: Judy Schmidt; https://apod.nasa.gov/apod/ap150211.html), NGC 2841 (multi-armed spiral galaxy; image credits: NASA, ESA and the Hubble Heritage; https://www.spacetelescope.org/images/heic1104a/), M33 (flocculent spiral galaxy; image credits: Adam Block/Mount Lemmon SkyCenter/University of Arizona; https://www.messier-objects.com/wp-content/uploads/2015/04/Messier-33.jpg).

1.2 Late-type galaxies: the cradle of structure - formation

Initially, all galaxies form as a disc in a CDM context for galaxy formation (e.g. Abadi et al. 2003). Signatures of this disc are erased through mergers (Barnes 1992). Unlike a purely stellar disc, the disc of a spiral galaxy contains both gas and stars which not only interact through their mutual gravity but also because gas fuels star-formation. In this section, I give a brief overview on the formation of spiral arms, bars, and rings in LTGs.

1.2.1 Spiral galaxies

A galaxy can form spiral arms only if its disc is sufficiently and gravitationally stabilised. This approximation is based on the Toomre parameter Q. From literature (see e.g. Dobbs and Baba 2014), the three main mechanisms proposed to form flocculent or grand design spiral arms are: (i) quasi-stationary density wave theory; (ii) local instabilities or perturbations which induce spiral arms; (iii) tidal interactions. Flocculent spiral arms may have been formed from local instabilities and are shortly lived (few 100 Myr) whereas tidal interactions can produce grand design structures which last longer ($\sim$ 1 Gyr). Over the past century, there have been many theories on the formation of spiral structure (Lindblad 1927; Safronov 1960; Lindblad 1963; Lin and Shu 1964b; 1966; Lynden-Bell and Kalnajs 1972, to name a few), and now it is evident that these spiral arms are dominated by gas and young stars (e.g. Elmegreen et al. 2011).

1.2.2 Barred spiral galaxies

In the Local Universe, more than 60% of disc galaxies are barred (e.g. Knapen, Shlosman, and Peletier 2000; Barazza, Jogee, and Marinova 2008). These bars are non-axisymmetric structures in spiral galaxies. Through N-body simulations of galaxies with two components (self-consistent disc and spheroidal halo), Combes and Sanders (1981) showed that bars develop over a large range of halo mass-to-disc mass ratios, and that these barred systems evolve at a rate which depends on this ratio. Our current knowledge of the formation of bars comes from simulations that show various scenarios (e.g. Elmegreen et al. 1991; Barnes and Hernquist 1991; Miwa and Noguchi 1998). Also, Saha and Elmegreen (2018) showed the impact of classical bulges on the growth of bars such that compact bulges prevent the formation of bars. Rotating bars, under the influence of gravity torque can drive spiral patterns into a closed, ring-like feature (Schwarz 1981, 1984).

1.2.3 Galaxies with pseudo-rings/outer rings

Ring-structures are found in about one-fifth of the spiral galaxy population, and partial-ring structures are observed in one-third of them (Buta and Combes 1996). These rings are associated to the kinematic locations known as resonances. Hence, the types of resonances are important in understanding the formation of rings (Sellwood and Wilkinson 1993). The exact location of the associated resonance cannot be determined without knowing the bar pattern speed and the rotation curve of the galaxy. Among them, the outer-Lindblad resonance (OLR) is related to the occurrence of outer rings found at a radius twice the size of the bar. Rings are regions where star-formation is high and young blue stars are present (e.g. Buta and Crocker 1993; Knapen et al. 1995). Elmegreen et al. (1992) found a dependence of outer rings on the density of the environment such that companion galaxies can convert outer rings into pseudo rings through tidal forces and sometimes can destroy the outer ring. They also found that outer rings are present mostly in early-type barred galaxies, and are less frequent in dense environments. As such, these substructures can be transformed in dense environments e.g. core of clusters and groups.

In the next section, I give a short summary of the current knowledge we have about galaxy clusters and groups, which together form the large scale structures (LSS) in the Universe we know of today.

1.3 The densest parts of the large scale structures in the Universe

Galaxies are not uniformly distributed in the Universe. In the scenario of hierarchical structure formation, they can belong to (i) small scale structures ($\sim$ 1–3 h^{-1}Mpc): binaries, groups, clusters; (ii) large scale structures ($>$ 10h^{-1}Mpc): superclusters, voids, sheets, walls, and filaments (see Coil

2013). This distribution forms a pattern that resembles a spider web and is therefore called the 'cosmic web' (see Fig. 1.1). On scales larger $>$ 100 Mpc, the distribution of galaxies is homogeneous (see Coil 2013). In order to understand these LSS, it is important to analyse their densest parts: clusters and groups. In this thesis, I focus on LTGs in different environments. In particular, on small scales; they are groups and clusters. Below, I give a short description of these structures.

1.3.1 Groups

It is well-known that 85% of the galaxies reside outside of rich clusters. About half of them belong to groups and the remaining are along the 'filament' otherwise known as the 'field' (Karachentsev 2005). According to the ΛCDM model of structure formation, galaxies from the field fall into small groups due to gravity. These groups then merge to form clusters (e.g. Rudick et al. 2009). Galaxies spend a significant amount of time in their evolution in such low-density environments (Miles et al. 2004). The typical range of mass in groups is $10^{12.5}$–$10^{14} h^{-1}$ $M_\odot$ (Bahcall 1996; Bower and Balogh 2004). Groups have low velocity dispersion (100–500 km/s) in comparison to rich clusters (400–1500 km/s; Bahcall 1996), which favour processes like merging and strangulation (see Sect. 1.4). In addition to this, the X-ray temperature is about $<$ 2KeV, unlike rich clusters (2–14 KeV; Bahcall 1996). Depending on the local density of groups, they are classfied into loose groups (LG) and compact groups (CG). The local density in CGs is similar to that of cores in rich clusters, yet they have different velocity dispersions (e.g. Coenda, Muriel, and Martínez 2012; Coenda, Muriel, and Martínez 2015, and references therein).

1.3.2 Clusters

Clusters of galaxies are at the top of the hierarchy of largest objects that have formed by the collapse of their gravity. This means that the structures assembled late in the history of the Universe (Voit 2005). While numerical simulations are required to fully understand the hierarchical merging process of matter in clusters, the basic features in the formation of clusters can be understood in the context of a spherically symmetric collapse model (e.g. Gunn and Gott 1972). These massive structures are bound by gravitational action of dark matter with the luminous (baryonic) matter. However, the baryonic component contributes little to the overall gravitational potential well of the cluster, and is in the form of hot and warm gas in the intra-cluster medium (ICM). Since clusters are dynamically relaxed, their masses are generally estimated using the virial theorem. There are many drawbacks to using this method since it is affected by projection (Danese et al. 1981; Fernley and Bhavsar 1984) and interlopers[3] (Perea, del Olmo, and Moles 1990).

[3]Due to projection effects, samples of galaxy clusters include galaxies which are unbound to the cluster. These galaxies are not good tracers of the gravitational potential of the cluster and hence, they are referred to as interlopers.

Other methods of cluster mass estimation are (i) X-ray emission profile of the hot gas temperature and distribution (Sarazin 1986), assuming hydrostatic equilibrium; (ii) gravitational lensing since the gravitational field distorts the images of the background galaxies (Tyson, Valdes, and Wenk 1990). In cases where clusters have not yet reached equilibrium, the mass is estimated based on the determination of zero-velocity surface[4] (see Nasonova, Freitas Pacheco, and Karachentsev 2011). Typical range of mass (within $r < 1.5h^{-1}$Mpc) for poor clusters can be $10^{12.5}$–$10^{14}h^{-1}M_{\odot}$ and rich clusters, 10^{14}–$2 \times 10^{15}h^{-1}M_{\odot}$ (Bahcall 1995, 1996).

1.4 Evolution and structure transformation of LTGs in dense environments

Over the past decades, there has been a long-standing debate concerning the transformation of spiral galaxies into lenticular systems, either through hierarchical merging or suppression of their star-formation as a consequence of the dense environment in clusters. This is evident through the observation of higher fraction of S0s in local clusters than high-redshift clusters (Oemler 1974). Several mechanisms have been proposed to explain the transformation (which occurs as a result of removing gas that fuels star-formation) of galaxy morphology in dense environments. In this section, I explain some of the important, well-known physical processes that can significantly change the structure of spiral galaxies in clusters and groups.

1.4.1 Ram-pressure stripping

The flat radial HI distribution of LTGs is weakly bound to its host galaxy's gravitational potential well and therefore, it can be easily removed (e.g. Haynes, Giovanelli, and Chincarini 1984; Kenney and Koopmann 1999; Fujita and Nagashima 1999). Due to the hot (usually $T_{IGM} \sim 10^7 K$) and dense ($\rho_{ICM} \sim 10^{-3} atom\ cm^{-3}$) ICM (generally higher than that of the constituent galaxies), the aforementioned gas bound to the galaxy experiences a pressure that results in its removal when it interacts with the hot ICM. Gunn and Gott (1972) first proposed that the pressure experienced by this cold gas is given by $P_{ram} = \rho_{ICM}\Delta v_{cl}^2$, where ρ_{ICM} is the density of the ICM, v_{cl} is the velocity of the galaxy with respect to the hot gas. Ram-pressure stripping has been the likely explanation for the higher fraction of HI-deficient spiral galaxies in clusters (Giovanelli and Haynes 1983). While there is still a debate on the transformation of spiral galaxies into S0 via gas removal and thereafter ceasing star-formation, there have been many observational evidences proving otherwise (e.g. Poggianti et al. 2017).

[4]The motion of galaxies residing at the outskirts of clusters is supposed to be radial and the mass within this surface is estimated using the distance R_0, at which the radial velocity with respect to the centre of mass is zero (see Karachentsev 2005).

1.4.2 Galaxy-galaxy harassment

Galaxy harassment, proposed by Moore et al. (1996) and Moore, Lake, and Katz (1998) is the combined effect of high speed galaxy-galaxy multiple encounters and the interaction with the cluster potential. This process can significantly change the morphology of spiral galaxies in clusters, but depends on the strength of the collision, the tidal field of the cluster, collisional frequency, and the potential distribution of the cluster galaxies. According to simulations by Moore et al. (1996), the multiple galaxy-galaxy encounters heat the stellar component thereby decreasing the angular momentum and increasing the velocity dispersion. This in turn, pushes the gas towards the centre of the galaxy. Due to the difference in potential distribution and masses, galaxies react differently to galaxy harassment. Massive galaxies are not severely affected by the cluster potential well of the cluster or galaxy-encounters; only a slight increase in disc star-formation activity (Mihos 2004) and velocity dispersion in the bulge (Moore et al. 1996). On the other hand, the smallest spheroid galaxies can get completely destroyed in the core of the cluster.

1.4.3 Strangulation

Larson, Tinsley, and Caldwell (1980a) proposed that spiral galaxies in clusters transform to lenticular galaxies through 'strangulation', a process where the warm and hot gas in the halo is stripped, preventing inflow of cold gas, and eventually halting star-formation. Numerical simulations by Bekki, Couch, and Shioya (2002) showed that strangulation is effective even at larger cluster-centric radii, such that spiral galaxies at a pericentre distance ~ 3 core radii would still lose $\sim 80\%$ of its halo within a few Gyr through interactions with the ICM and the tidal field of the cluster. Through these interactions, gas is prevented from accreting onto the galaxy's disc thereby suppressing star-formation and eventually erasing the spiral pattern of these galaxies. While 'galaxy harassment' and 'ram-pressure stripping' are not common in groups, 'strangulation' is the likely mechanism responsible for preventing gas-inflows onto a spiral galaxy's disc and transforming it into an S0 galaxy (Rasmussen, Ponman, and Mulchaey 2006). However, this depends on the dynamical stage of the group (e.g. Kawata and Mulchaey 2007); strangulation is common in groups which are dynamically evolved with an enhanced intra-group medium (IGM).

1.4.4 Merging

Toomre (1977) proposed the formation of elliptical galaxies through repeated galaxy mergers, which was supported by the hierarchical structure formation scenario (White and Rees 1978). However, Ostriker (1980) disagreed with this scenario stating that it was more complex. Subsequent studies showed that the merging event depends on the gas fractions, stellar mass, and morphology of the progenitors (Barnes 1992; Barnes and Hernquist 1996). These assumptions arise from N-body simulations and through the years, many

more studies have shown how galaxy mergers of different mass ratios produce remnants with different properties (e.g. Bournaud, Jog, and Combes 2005, and references therein) and morphology. Galaxy mergers of comparable masses, otherwise known as major merger and with a mass ratio in the range 1:1–3:1 or 1:1–4:1 can result in remnants, elliptical in morphology which can be disky or boxy (Bendo and Barnes 2000). On the other hand, minor mergers are those between a massive galaxy and a satellite galaxy. The mass ratio in the minor merger case is typically around 10:1 (Quinn, Hernquist, and Fullagar 1993) and the outcome is a hot, thickened disc galaxy which would still have an exponential mass distribution similar to that of a spiral galaxy (Freeman 1970). In the past decade, many studies have compared properties (e.g. morphology, atomic and molecular gas fractions, star-formation rate) of merging galaxies to those of non-interacting galaxies (see Hani et al. 2020, and references therein).

The fraction of spiral galaxies has been found to decrease from 80% in the field to 60% in the outskirts of clusters and groups, to ~ 0 in the cores of rich clusters (Dressler 1980; Whitmore 1993). Morphological segregation (Dressler 1980) is the signature of the environmental effects on structure-transformation and evolution of spiral galaxies. Understanding the various processes involved in dense environments is crucial to comprehending *galaxy evolution*. Hence, it is important to study spiral galaxies in clusters and groups. Since different clusters and groups are at different stages of evolution and at different distances to us, studying them individually and thereafter comparing them brings us closer to figuring out the processes and mechanisms responsible for the larger fraction of elliptical and lenticular galaxies in dense environments.

In this thesis, I study spiral galaxies in the Fornax environment, which comprises the Fornax cluster core and the Fornax A subgroup. In the next section, I provide the motivation for the choice of this environment as well as summarise the results and observations of the Fornax cluster and Fornax A subgroup, to date.

1.5 The Fornax-Eridanus complex

The Fornax-Eridanus complex (see Fig.1.5) is made up of the Fornax cluster (NGC 1399), Fornax A subgroup (NGC 1316), Eridanus sub-cluster (NGC 1407), Dorado group, and other neighbouring groups (Nasonova, Freitas Pacheco, and Karachentsev 2011). Among them, the Fornax cluster has the highest mass concentration (Drinkwater, Gregg, and Colless 2001a). The Fornax A subgroup is currently falling into the cluster (Drinkwater, Gregg, and Colless 2001a), and the other groups are about 15 deg away from the Fornax cluster.

The Fornax cluster was first studied by Welch, Chincarini, and Rood (1975), although Reaves (1964) in their study, was the first to suggest that the evolutionary age of the Fornax cluster might be greater than that of the Virgo cluster. Dwarf galaxies in the Fornax cluster were also studied by Hodge, Pyper, and Webb (1965). de Vaucouleurs and de Vaucouleurs (1967)

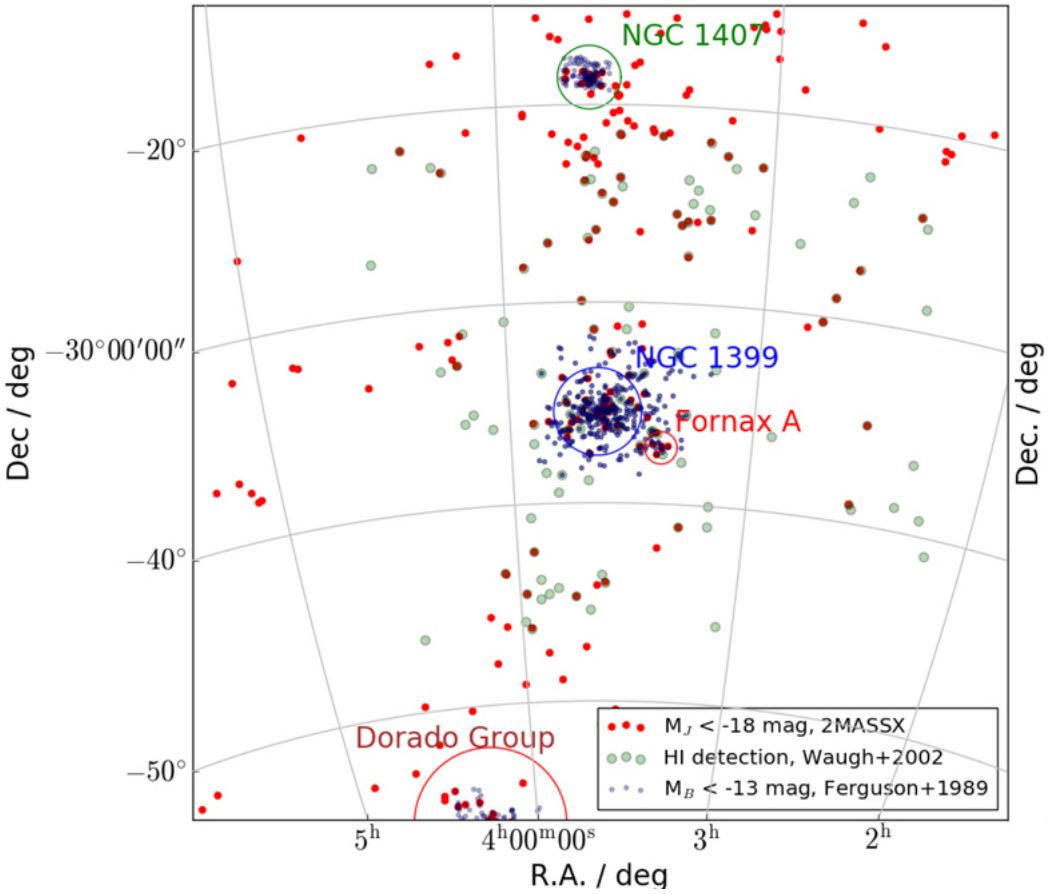


FIGURE 1.5: The Fornax cluster part of the LSS Fornax-Eridanus, as shown by Venhola et al. (2018). As given in Venhola et al., the recession velocities of the galaxies are plotted as a function of declination. The red dots indicate the galaxies with recession velocities $V_r < 4000$ Km/s from the 2 Micron All Sky Survey catalogue (2MASSX; Huchra et al. 2012. Green dots represent galaxies with velocities $V_r < 4000$ Km/s from Waugh et al. (2002). Fornax cluster members are represented with blue dots. The virial radii of the groups are also marked. The adapted image is Fig. 1 in Venhola et al. (2018).

provided a redshift catalogue of bright galaxies that included some Fornax cluster members as well. Based on their velocities, the Fornax cluster is composed of the main cluster centred around NGC 1399 and a subgroup in the south-west (SW) region of the main cluster, centred around NGC 1316, also known as Fornax A. In the 20th century, followed by Welch, Chincarini, and Rood (1975), several others have studied the Fornax environment (e.g. Hodge 1978; Jones and Jones 1980; Caldwell 1987; Davies et al. 1988; Ferguson and Sandage 1988, and references therein). Ferguson (1989) provided the first catalogue of all galaxies in the Fornax cluster (including the SW subgroup). As such, the Fornax cluster is the second nearest cluster ($\sim$ 20 Mpc), after Virgo. Moreover, this environment hosts several spiral and dwarf galaxies located around two massive cD elliptical galaxies. Hence, by studying Fornax, we are able to study two types of environments, the main cluster as well as the subgroup.

In this section, I give a brief review on the properties of the Fornax cluster and Fornax A subgroup.

1.5.1 The Fornax cluster core

The Fornax cluster core is defined as the virialised region within a cluster-centric distance $\sim$ 0.7 Mpc (Drinkwater, Gregg, and Colless 2001a), around NGC 1399. In Table.1.1, I list the important properties of the Fornax cluster, as given in literature.

TABLE 1.1: Main properties of the Fornax cluster

RA;DEC	03h38m; -35d30m
Distance	20$\pm$0.3 Mpc (Blakeslee et al. 2009)
dynamical mass M_{dyn}	$7 \times 10^{13} M_{\odot}$ (Drinkwater, Gregg, and Colless 2001a)
X-ray luminosity L_x	5×10^{41} erg/s (Jones et al. 1997)
Velocity dispersion σ	370 km/s (Drinkwater, Gregg, and Colless 2001a)
Virial radius R_{vir}	0.7 Mpc (Drinkwater, Gregg, and Colless 2001a)

The main cluster consists of 22 bright (< -18 mag) galaxies and 300 fainter galaxies (Ferguson 1989). The first dynamical analysis of the Fornax cluster was presented by Drinkwater, Gregg, and Colless (2001a). The VLT (Very Large Telescope) Survey Telescope (VST) colour composite image of the Fornax cluster core is shown in Fig. 1.6 where most of the bright ETGs in the north-west and two bright LTGs (NGC 1386 and the great barred spiral galaxy NGC 1365) are also indicated.

1.5.2 The Fornax A subgroup

As already mentioned, another important group in the Fornax-Eridanus complex is the Fornax A subgroup, centred around NGC 1316. This group has 16 confirmed members (Drinkwater, Gregg, and Colless 2001a). In Table. 1.2, I list the important properties of this group, taken from literature. The VST colour composite image of the Fornax A subgroup is shown in Fig. 1.7 where all the bright ($m_B < 16$ mag) galaxies including the nine LTGs presented in this work are indicated.

TABLE 1.2: Main properties of the Fornax A subgroup

RA;DEC	03h22m41.7s; -37h12m30s
Distance	20.8$\pm$0.5 Mpc (Cantiello et al. 2018)
dynamical mass M_{dyn}	$6 \times 10^{13} M_{\odot}$ (Drinkwater, Gregg, and Colless 2001a)
Velocity dispersion σ	377 km/s (Drinkwater, Gregg, and Colless 2001a)

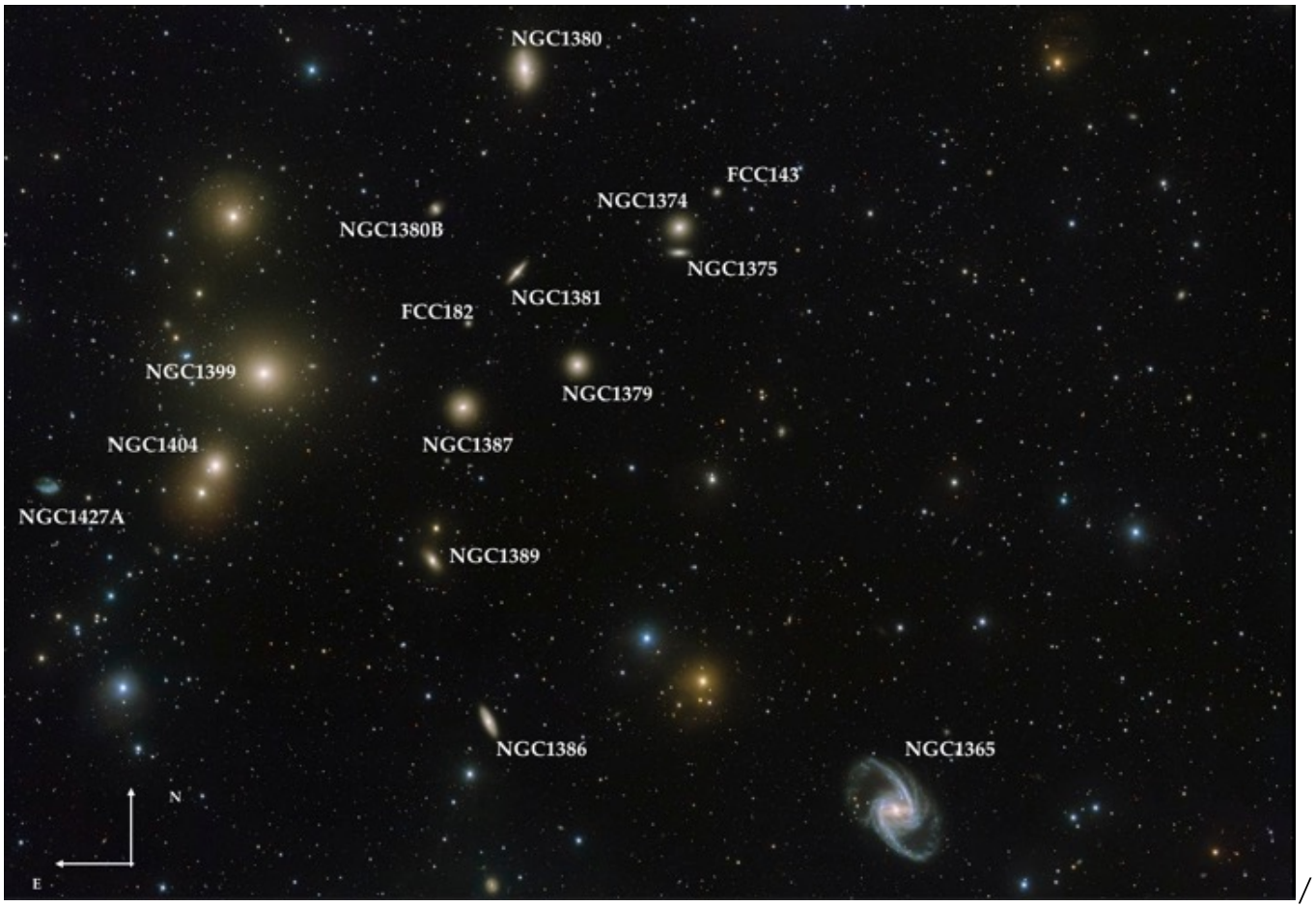


FIGURE 1.6: VST colour composite image of the Fornax cluster core[a]. This image only covers the west side of NGC 1399 with bright ETGs and some LTGs (e.g. the great barred spiral galaxy NGC 1365) indicated. NGC 1427A is also indicated.

[a] https://www.eso.org/public/news/eso1612/

According to Drinkwater, Gregg, and Colless (2001a), Fornax A group is a region with intense star-formation, containing 15% of the total number of galaxies in the Fornax environment, and 31% of the star-forming galaxies. Drinkwater et al. also suggest that it is unlikely that this group has passed through the cluster core as it contains a large amount of neutral hydrogen (Putman et al. 1998).

Since the beginning of the 21st century, there have been several surveys studying the Fornax cluster in multiple wavelengths, which have provided a better understanding of this environment. In Sect. 1.5.3, I summarise past and ongoing studies of the Fornax cluster, thus setting the preliminary stage of my thesis.

1.5.3 Surveys

In this section, I give a list of the past and ongoing surveys observing the Fornax cluster. Some of the ancillary data from the surveys mentioned are used in the work presented in this thesis.

- The Advanced Camera for Hubble Space telescope (ACS; Ford et al. 1998) Fornax Cluster Survey (ACSFCS; Jordán et al. 2007b) is a multi-wavelength imaging survey designed to study globular clusters (GCs) in the Fornax cluster. In addition to this, Blakeslee et al. (2009) provided a distance to the Fornax cluster, which is used throughout this thesis.

- The Herschel Fornax Cluster Survey (HeFoCS; Davis et al. 2013) investigates the far-infrared properties of 11 bright galaxies in the Fornax cluster. Some of the LTGs surveyed by HeFoCS are part of the sample studied in this thesis.

- The Fornax Deep Survey (FDS; Iodice et al. 2016; Venhola et al. 2017) with VST is a deep multi-imaging survey of the Fornax cluster. The work presented in this thesis is based on the data from FDS, which is described in Sect. 1.7.

- The Fornax cluster VLT Spectroscopic Survey (FVSS) studies the GCs (Pota et al. 2018) and planetary nebulae (PNe; Spiniello et al. 2018) in the Fornax cluster.

- MeerKAT Fornax cluster survey (Serra et al. 2016) studies the HI distribution in the Fornax cluster. The aim of the survey is to investigate the HI mass of the Fornax cluster and study the HI tails of the galaxies to quantify the amount of gas stripping events in the context of their evolution.

- Fornax 3D (Sarzi et al. 2018) with MUSE was designed to study a wide range of topics pertaining to the Fornax cluster. One such is the stellar kinematics of the observed 33 Fornax cluster galaxies. Nine LTGs studied in this thesis are also part of the Fornax 3D sample.

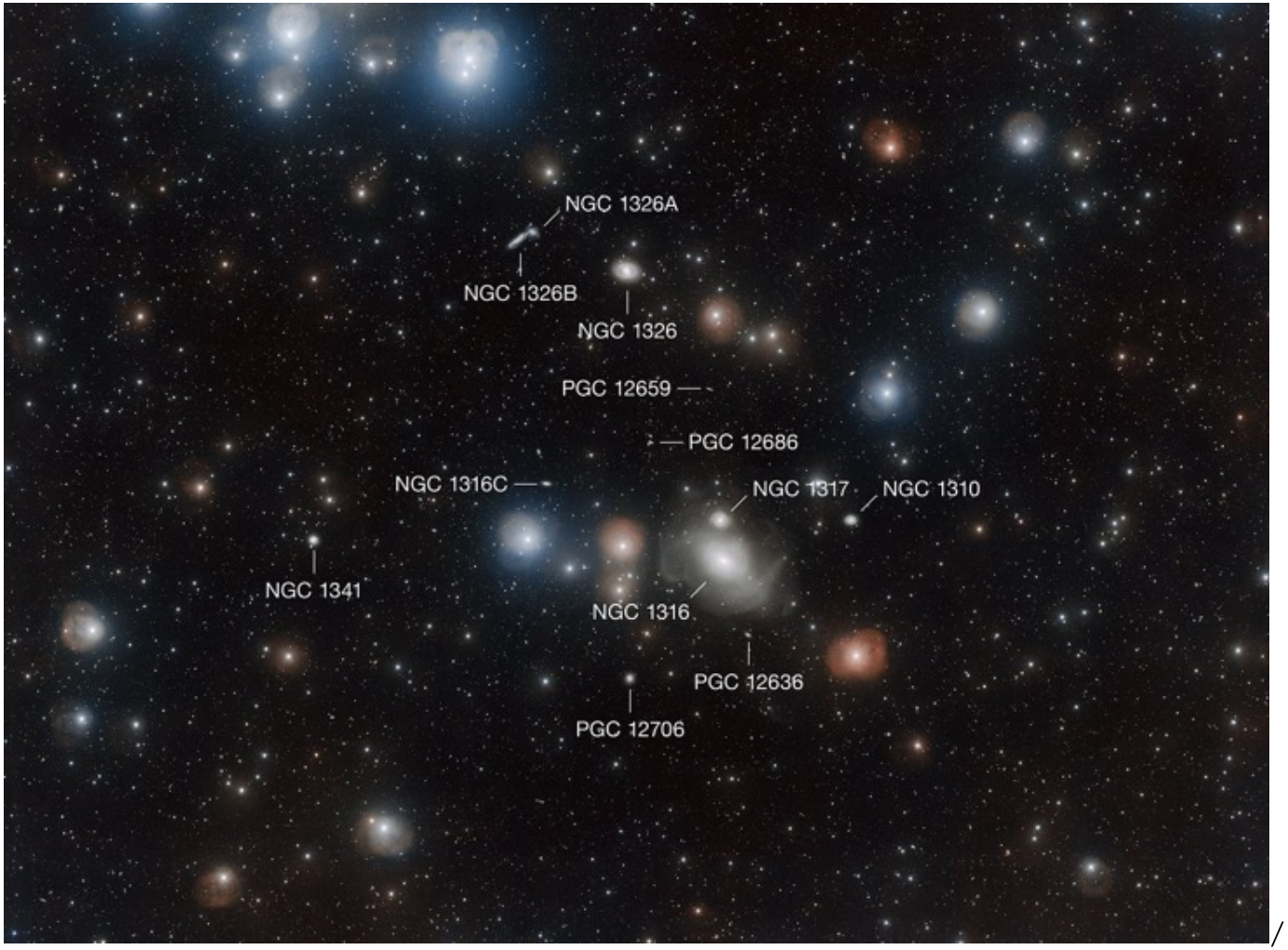


FIGURE 1.7: VST colour composite image of the Fornax A subgrpup[a]. All bright LTGs studied in this work as well as some dwarf ETGs are indicated.

[a] https://www.eso.org/public/news/eso1734/

- The ALMA Fornax Cluster Survey (ALFoCS; Zabel et al. 2019) observes CO and HII regions in 30 Fornax cluster members and investigates the molecular gas content, star-formation activity, and other properties of these galaxies.
- Maddox et al. (2019) presented a spectroscopic census of all the galaxies in the Fornax cluster, covered by FDS which also includes background objects. In this thesis, I use the spectroscopic redshifts of the bright LTGs in the Fornax A subgroup to address their assembly history.
- SAMI Fornax Dwarf Survey (Scott et al., submitted to MNRAS 2020) observes low-mass dwarf-elliptical galaxies (dEs) in the Fornax cluster using the SAMI instrument and addresses the formation mechanism of these dEs.

Apart from the above mentioned surveys, there are also X-ray data of the Fornax cluster (Paolillo et al. 2002; Scharf, Zurek, and Bureau 2005), Hα data of galaxies in the Fornax A group observed with OmegaCAM (P.I. R. Peletier). In the era of deep imaging data (described in the next section), FDS provides a new ground for testing theories from simulations, which are further supported by the large coverage of the Fornax cluster in multiple wavelengths hence giving a comprehensive view of the Fornax cluster and of galaxies therein.

1.6 The era of deep imaging data

The low-velocity dispersion group environment favours interactions and merging which produce tidal tails and plumes in galaxies. The hierarchical merging of such groups onto a cluster results in more expelled material that are fed into the cluster environment. This in turn contributes to the mass accretion of the diffuse stellar component and gradually increases the growth of the intra-cluster baryons. Due to their faint surface brightness levels, the diffuse components were initially difficult to detect and though some works detected them (e.g. de Vaucouleurs and de Vaucouleurs 1970; Bernstein et al. 1995, and references therein), strong constraints on their luminosity were not provided.

In the past couple of decades, studies concerning bright cluster/group galaxies (BCG/BGG) and the intra-cluster/group light (ICL/IGL) in different environments have gained popularity with the advent of deep imaging data (e.g. Arnaboldi et al. 2002; Feldmeier et al. 2004; Zibetti et al. 2005; Arnaboldi et al. 2012; Ferrarese et al. 2012; Duc et al. 2015; Muñoz et al. 2015; Mihos 2015; Mihos et al. 2017; Iodice et al. 2016; Iodice et al. 2017a; Iodice et al. 2017b; Spavone et al. 2018; Cattapan et al. 2019; Iodice et al. 2020, and references therein). In this section, I give a review of the main results obtained with deep imaging data analysis in the past years as per the context of my thesis. The work presented in my thesis focuses on understanding the effect of the environment on the transformation of structure in LTGs and their evolution. As such, I use deep imaging data to study their morphology,

faint outskirts, the intra-cluster/group light (ICL/IGL) and compare them in different environments thus providing the motivation and importance of working with such data in the *era of big data and deep data analysis*.

1.6.1 Exploring faint outskirts of galaxies

The imprints of mass assembly reside in the outskirts of galaxies in dense environments, extending out to about hundreds of kiloparsecs. These regions host the stellar halo which continues to grow over time due to the several processes taking place in dense environments (e.g. Contini et al. 2014). The stellar halo can comprise several stellar components and substructures like tidal tails, streams, and shells. The substructures are a result of the gravitational interactions and merging, which in turn are signatures of the formation history of a galaxy (e.g. Bender et al. 2015). While deep photometry is useful to study stellar haloes, kinematic measurements are also needed to deduce the variation of the orbital distribution of their constituent stars, PNe (e.g. Napolitano et al. 2009; Spiniello et al. 2018, and references therein) and GCs. Exploring the low surface brightness (LSB) structures of galaxies allows us to test and further understand the ΛCDM galaxy formation model (Trujillo and Fliri 2015). In Fig. 1.8, we can see that images with greater depth show more faint features.

It has been known that mergers play a relevant role in the formation of outer regions in spiral galaxies (e.g. Martinez-Delgado et al. 2008). An important formation mechanism of galactic discs in the ΛCDM paradigm is the accretion of satellite galaxies on low-inclination orbits, which is supported by the presence of low-inclination tidal streams in our *Galaxy* (e.g. Grillmair 2006). These tidal streams can last for several Gyr and hence serve as a fossil record of the formation history of spiral galaxies in the Local Universe (Martínez-Delgado et al. 2008). One such example is on the tidal origins of the Fornax cluster member NGC 1427A which were suggested to be the result of a recent merging event that also induced a starburst in this galaxy (see Lee-Waddell et al. 2018) and is evident in its disturbed optical appearance (see Fig. 1.9).

Truncations and disc-breaks

Three out of four spiral galaxies with thin discs exhibit a well-defined feature in their outskirts called a *truncation*. This feature occurs beyond four to five times the exponential scale-lengths of the inner discs in spiral galaxies (van der Kruit and Freeman 2011). Truncations i.e. a decline in the surface brightness profiles of spiral galaxies were first detected by van der Kruit (1979) and since then, their origin has been a debate. Some of the theories postulated to explain the origin of truncations have been linked to (i) a threshold in star-formation (e.g. Roškar et al. 2008); (ii) bar-angular momentum (Debattista et al. 2006); (iii) external mechanisms that strip the stars (Laurikainen and Salo 2001). Truncations are usually detected in edge-on systems and in the case of

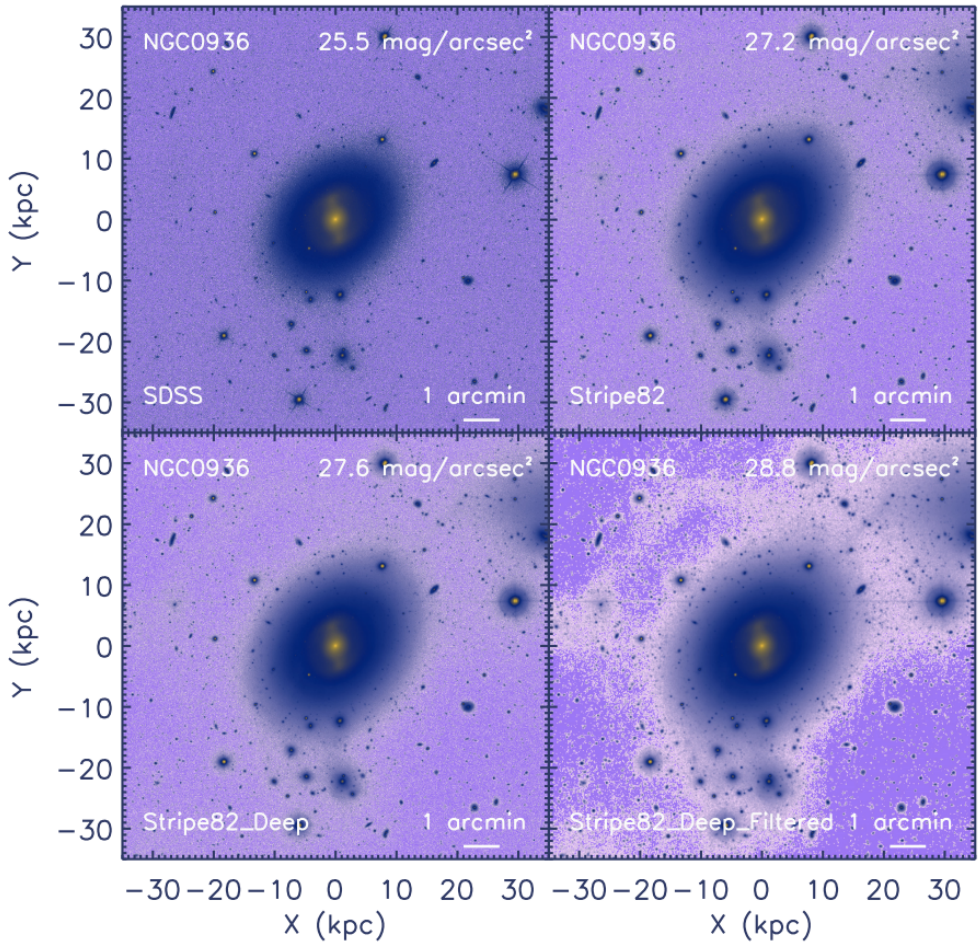


FIGURE 1.8: Comparison of images at different surface brightness limiting depth $\mu_r(3\sigma;9 \text{ arcsec}^2)$ = 25.5, 27.2, 27.6, 28.8 mag/arcsec^2 shown by Trujillo and Fliri (2015). This shows that deep images allow us to study faint outskirts of galaxies. The adapted image is Fig. 1 in Trujillo and Fliri (2015).

face-on systems, they can only be detected with very deep surface photometry (e.g. Martín-Navarro et al. 2012). This is due to the reduced line-of-sight integration through the disc (Martín-Navarro et al. 2012).

Truncations are not the same as disc-breaks; the latter are found at smaller radii (Pohlen and Trujillo 2006). Moreover, their origin can be the result of different phenomena even if they are found to co-exist (Martín-Navarro et al. 2012). As part of the work presented in this thesis, I have developed an algorithm to detect disc-breaks and hence investigate their origin in LTGs in the Fornax cluster.

1.6.2 Studying the intra-cluster light and intra-group light

As mentioned earlier, the LSB Universe has gained popularity in the past decade to further understand the hierarchical formation model. Studying the ICL/IGL is only possible with deep imaging due to their LSB

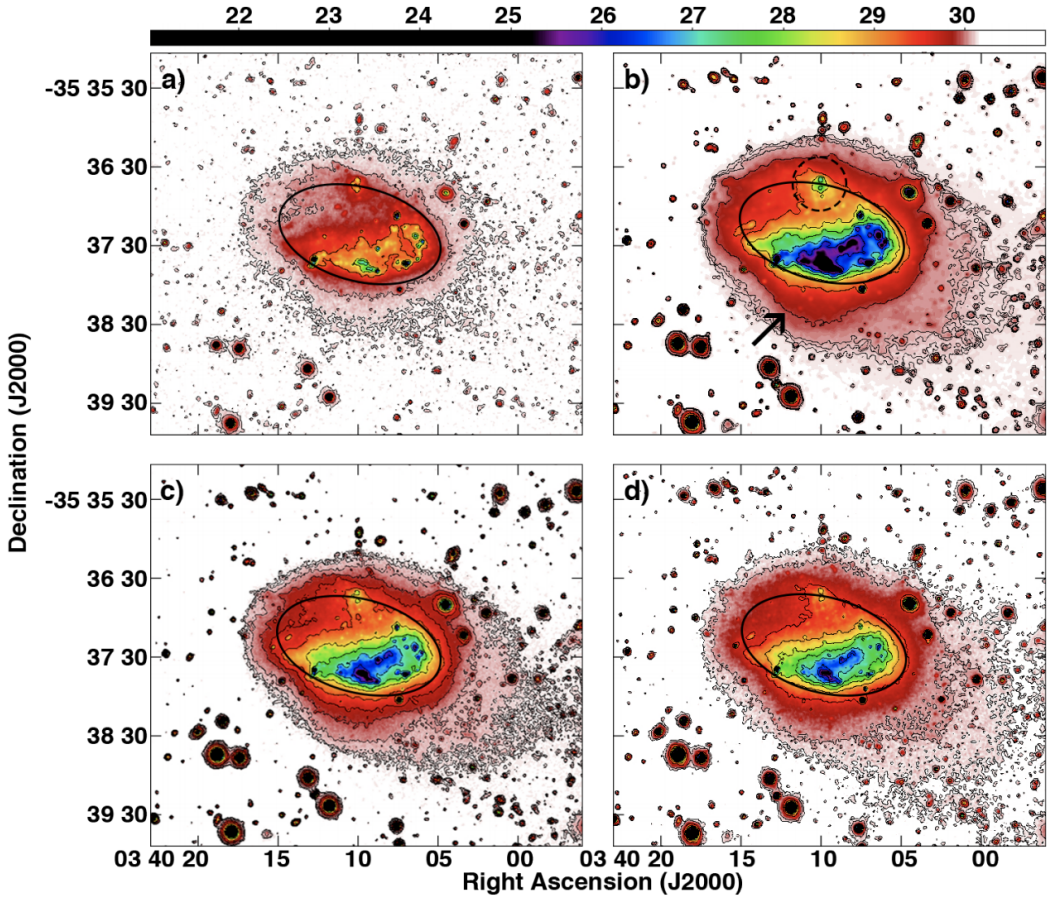


FIGURE 1.9: Smoothed VST images of NGC 1427A in u (panel a), g (panel b), r (panel c), i (panel d) bands. The black ellipse represents the star-forming optical shape of the galaxy as given in Lee-Waddell et al. (2018). In $g-$band (panel b), the dashed circle indicates the northern stellar clump and a faint stellar-overdensity bump is pointed with an arrow. The adapted image is Fig. 2 in Lee-Waddell et al. (2018).

(> 28 mag/arcsec^2). Moreover, in order to map the ICL/IGL, which extend out to > 100 kpc in clusters/groups, wide-field images are required (e.g. Iodice et al. 2016). Multi-wavelength images allow us to investigate the properties (e.g. colour) of the diffuse light and compare them to the population of GCs and PNe therein. In addition to this, observations test theoretical predictions about the formation of the ICL/IGL in different environments (Contini et al. 2014; Contini, Yi, and Kang 2019). The work presented in this thesis includes the estimation and analysis of the IGL in the Fornax A subgroup.

1.6.3 Deep data: a probe for investigating the effect of the environment on galaxy evolution

To summarise, deep data are required to explore the faint outskirts and substructures of galaxies in dense environments as these regions contribute to the growth of the ICL/IGL through various processes. In the last decade, the advancement of technology, instrumentation, and data-analysis have proven

vital in the enhancement of deep imaging surveys exploring faint regions down to a depth of 31.5 mag/arcsec^2 (Trujillo and Fliri 2015). As such, the Fornax cluster is studied in multiple wavelengths making it one of the best environments in the Local Universe to investigate the structure and evolution of galaxies. In particular, the wide-field and deep images of FDS allow us to explore the LSB features, ICL/IGL properties and therefore trace the assembly history of the cluster itself (e.g. Iodice et al. 2019a).

1.7 The Fornax Deep Survey

The work presented in this thesis is based on data from the Fornax Deep Survey. In this section, I describe the survey, their motivation, observations, and data.

FDS observations are part of two Guaranteed Time Observations surveys, Fornax Cluster Ultra-deep Survey (*FOCUS*, P.I. R. Peletier) and VST Early-type GAlaxy Survey (*VEGAS*, P.I. E. Iodice, Capaccioli et al. 2015), with a coverage of 21 deg^2 around NGC 1399 and 6 deg^2 around Fornax A (see Fig. 1.10). The multi-band (u, g, r, i) images were obtained with Omega-CAM (Kuijken 2011) at the VST (Schipani et al. 2012), located at the European Southern Observatory in Cerro Paranal (Chile). The camera with a field of view $\approx$ 1×1 deg^2, consists of 32 CCD chips and has a resolution of 0.21 arcsec/pixel. FDS observations were performed in clear (photometric variation $< 10\%$) or photometric conditions, between November 2013 and November 2017. Observations for u, g, and r bands were carried out in dark time, and for i-band in grey time.

Due to the current generation of telescopes and technology, FDS provides images with greater depth (> 28 mag/arcsec^2) of the Fornax cluster, and was designed to investigate the structure and evolution of galaxies: from the brightest to the faintest (down to the resolution limit of the images). Moreover with such image depth, the faint outskirts and hence, the ICL/IGL can be mapped and studied in detail. The scientific aims of FDS span a wide range of topics that help to comprehend the environment of the Fornax cluster and of galaxies therein.

Within FDS, (i) Iodice et al. (2016) and Iodice et al. (2017b) mapped the surface brightness around BCG NGC 1399, and BGG NGC 1316 out to an unprecedented distance of about $\sim$ 200 kpc (R $\sim 6R_e$) and down to $\mu_g \simeq$ 29–31mag/arcsec^2; (ii) D'Abrusco et al. (2016) and Cantiello et al. (2018) traced the spatial distribution of candidate GCs inside a large fraction of the cluster core; (iii) Iodice et al. (2017a) and Iodice et al. (2019b) studied the galaxy (ETG) outskirts, detected ICL and faint features in the intra-cluster regions of the Fornax core; (iv) Venhola et al. (2019) provided the largest size and magnitude limited catalogue of dwarf galaxies in the Fornax cluster.

As part of FDS, I analyse bright LTGs in the Fornax cluster core and the Fornax A group. In particular, I investigate their structures and faint outskirts, derive their structural parameters, observational properties, and estimate the IGL of the Fornax A group.

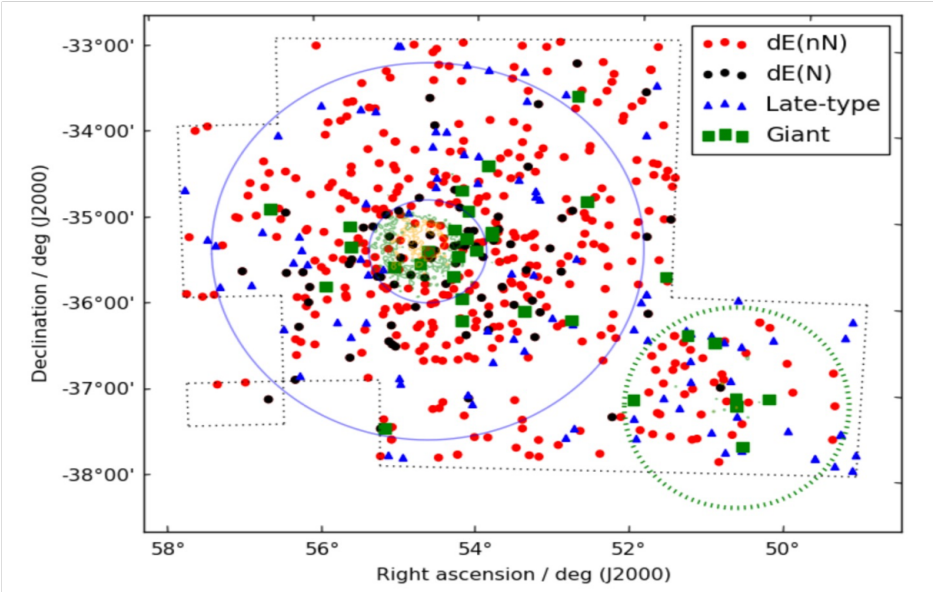


FIGURE 1.10: Area spanning 26 deg^2 around NGC 1399 and NGC 1316 observed with FDS. The red and black dots represent non-nucleated and nucleated dwarf galaxies, and blue triangles represent dwarf LTGs. The giant galaxies are marked with green squares. The virial radius of the Fornax cluster is marked with a blue circle (Ferguson and Sandage 1988), and the green circle encloses a radius of 1 deg around Fornax A (Drinkwater, Gregg, and Colless 2001a). The adapted image is Fig. 1 in Venhola et al. (2019).

1.8 Scientific motivation of this thesis

The morphology-density relation by Dressler (1980) explains the effect of the environment on the structure of galaxies, such that high-density environments inhibit the formation of spirals. With this in mind, the aim of the research work undertaken in my thesis is to study the different environmental mechanisms (e.g. ram-pressure stripping, galaxy-harassment) that contribute to the transformation of LTGs in clusters and groups, in particular the Fornax cluster and Fornax A group. By mapping the light distribution down to faint surface brightness levels, I analyse the morphology, average colours, structural parameters, and outskirts of the LTGs as these regions are the signatures of the processes in dense environments and therefore give a complete picture of their evolution.

Through the work presented in this thesis, the questions I address are: (i) *How different are the structures of LTGs belonging to the cluster core, as compared to the infalling subgroup?* (ii) *What about their structural parameters and observational properties?* (iii) *Do the break-radius and break-type differ in these environments?* (iv) *What does the IGL/ICL in the Fornax cluster indicate in the context of the assembly history of the cluster?* (v) *In the ΛCDM paradigm, how does the IGL contribute to the ICL?* (vi) *Do the studies of the IGL and ICL help us understand 'pre-processing'? Will this help us to further understand the hierarchical merging of groups into the Fornax cluster?* (vi) *Do the studies of the IGL and ICL help us understand 'pre-processing'? Will this help us to further understand*

the hierarchical merging of groups into the Fornax cluster? (vii) *And finally, can we trace the evolutionary history of the cluster core LTGs and predict their fate?*

By answering these questions, I will try to give a comprehensive view of the LTGs in the Fornax cluster and of their hosting environments.

1.9 Thesis Outline

In this chapter, I have defined and described galaxies, their morphology, the dense environments they can reside in, the types of processes involved in their evolution in clusters and groups. In particular, I have given a detail description of the knowledge we have of the Fornax cluster and a small overview of the surveys that contribute to this understanding. Specifically, FDS and the importance of deep imaging surveys. With this, I provided the scientific motivation of this thesis that will help to solve the unanswered questions of the LTGs in the Fornax cluster.

This thesis consists of two scientific papers of which one (Chapter 2) is published and the other, which is split into two chapters (Chapters 3 & 4) is submitted for publication. I give a brief outline of the chapters in this thesis below:

Chapter 2: I investigate the structure and evolution of LTGs in the Fornax cluster core via surface photometry. In the context of deriving break-radii, I present an algorithm I developed and therefore, estimate the break-radius and the break type. I analyse the morphology, average colours and the colours beyond the break radius, and faint outskirts of the cluster core LTGs. By combining data from AlFoCS (Zabel et al. 2019), I show how the dense environment can transform the structures of LTGs therein.

Chapter 3: I address the assembly history of the LTGs in the Fornax A subgroup by using the same approach from Chapter 2. In addition to this, I use available spectroscopic data (Maddox et al. 2019) to analyse the LTGs in projected phase-space. I then compare the results obtained in this analysis to those from Chapter 2 and therefore show how the local environment affects the evolution of LTGs.

Chapter 4: As part of my analysis of the Fornax A subgroup, I also estimate the amount of its IGL. I investigate the formation history of the IGL and compare it to other loose groups. I also give a brief overview of the Fornax cluster ICL and show how the IGL is the progenitor of the ICL, as predicted in past works.

Chapter 5: I summarise the main results of the work and show how they help us understand 'pre-processing' of galaxies, which is important in tracing their evolutionary history and predicting their fate in dense environments. With this, I draw my conclusions and give my future perspectives of the work presented in this thesis.

Chapter 2

Evolution and structure of late-type galaxies inside the virial radius of the Fornax cluster

This chapter is based on the paper:
Raj, M.A.; Iodice,E.; Napolitano,N.R.; Spavone,M.; Su,H.-S.; Peletier,R.F.; Davis, T. A.; Zabel, N.; Hilker, M.; Mieske, S.; Falcon Barroso, J.; Cantiello, M.; van de Ven, G.; Watkins, A. E.; Salo, H.; Schipani, P.; Capaccioli, M.; Venhola, A; *The Fornax Deep Survey with VST, VII. Evolution and Structure of Late Type Galaxies inside the Virial Radius of the Fornax Cluster*, 2019, Astronomy & Astrophysics, 628, A4.
DOI: 10.1051/0004-6361/201935433

Abstract

We present the study of a magnitude limited sample ($m_B \leq$16.6 mag) of 13 late type galaxies (LTGs), observed inside the virial radius, $R_{vir} \sim 0.7$ Mpc, of the Fornax cluster within the Fornax Deep Survey (FDS).The main objective is to use surface brightness profiles and $g-i$ colour maps to obtain information on the internal structure of these galaxies and find signatures of the mechanisms that drive their evolution in high-density environments inside the virial radius of the cluster. By modelling galaxy isophotes, we extract the azimuthally averaged surface brightness profiles in four optical bands. We also derive $g-i$ colour profiles, and relevant structural parameters like total magnitude and effective radius. For ten of the galaxies in this sample, we observe a clear discontinuity in their typical exponential surface brightness profiles, derive their 'break radius', and classify their disc-breaks into Type II (down-bending) or Type III (up-bending). We find that Type II galaxies have bluer average $(g-i)$ colour in their outer discs while Type III galaxies are redder. The break radius increases with stellar mass and molecular gas mass while it decreases with molecular gas-fractions. The inner and outer scale-lengths increase monotonically with absolute magnitude, as found in other works. For galaxies with CO(1−0) measurements, there is no detected cold gas beyond the break radius (within the uncertainties). In the context of morphological segregation of LTGs in clusters, we also find that, in Fornax, galaxies with morphological type $5< T \leq 9$ ($\sim$ 60% of the sample) are located beyond the high-density, ETG-dominated regions, however there is no correlation between T and the disc-break type. We do not find any correlation between the average $(g-i)$ colours and cluster-centric distance, but the colour-magnitude relation holds true. The main results of this work suggest that the disc-breaks of LTGs inside the virial radius of the Fornax cluster seem to have arisen through a variety of mechanisms (e.g. ram-pressure stripping, tidal disruption), which is evident in their outer-disc colours and the absence of molecular gas beyond their break radius in some cases. This can result in a variety of stellar populations inside and outside the break radii.

2.1 Introduction

Spiral galaxies and irregular galaxies, which fall under the late-type galaxies (hereafter, LTGs) morphology classification, have been primarily studied in the past, mostly concerning the formation of grand design structures such as spiral arms (Lin and Shu 1964a). These galaxies are rich in atomic and molecular gas and because of that, they are actively forming stars. Their stellar and (cold and diffuse) gaseous discs are known to be sensitive to effects of the environment and their evolution (or star formation history) is slower (Boselli and Gavazzi 2006) than that of early type galaxies (or lenticular and elliptical galaxies; hereafter ETGs). This makes them interesting probes of a cluster environment (e.g. Blanton and Moustakas 2009; Hwang et al. 2010).

Studying the effect of the environment (e.g. field vs cluster) where LTGs are located, is vital for unravelling the formation of their unique substructures (e.g. Boselli and Gavazzi 2006). Moreover, LTGs are ideal systems to study stellar population gradients (like bulge and disc, inner and outer regions) that may have come about as a consequence of external processes (e.g. Bell and de Jong 2000; Gadotti and Dos Anjos 2001). The relative abundance of galaxies with respect to their morphological types has been shown to be related to the density of their local environment with a fraction of 80% of LTGs in the field, 60% in clusters, and $\sim$0% in the core of rich clusters (Dressler 1980; Whitmore 1993). Their infall into a cluster environment makes their interstellar medium prone to hydrodynamic interactions with the hot intracluster gas (e.g. Binney and Tremaine 1987), and their peculiar morphologies have been the topic of interest, especially concerning their structure formation and star formation regulation through a series of intracluster processes like ram-pressure stripping (Gunn and Gott 1972), star formation quenching (e.g. Abadi, Moore, and Bower 1999), or galaxy-galaxy harassment (e.g. Moore et al. 1996).

Studies have shown that the first stage of evolution of LTGs, as they enter a dense environment, is characterised by the formation of a strong bar, and an open spiral pattern in the disc (Moore, Lake, and Katz 1998; Mastropietro et al. 2005). Further on, their spiral arms and rings can be wiped out by tidal interactions, as shown by galaxy formation and evolution simulations (Mastropietro et al. 2005). Recently, though, numerical simulations (Hwang et al. 2018) have shown that interactions with other galaxies, especially ETGs, in high-density cluster regions can also cause an LTG to lose its cold gas but still have more star formation activity during the collision phase (cold gas interacting with the hot gas of the cluster). Thus, the location of a galaxy in the cluster is a primary parameter to correlate with formation of structure in galaxies. One of the several methods used is to investigate this evolution through the detailed study of the surface brightness profiles and their morphology classification based on their substructures (e.g. lopsided or warped disc, bars, peanut shaped bulges, spiral arms).

Particular insight can be gained from quantitative studies of the light distribution of stellar discs down to the faintest regions, exploring the formation of their substructures and evolutionary paths (e.g. Courteau 1996; Trujillo et

al. 2002). Light distributions of disc galaxies are characterised by an exponential decline (de Vaucouleurs 1959). However, this so-called decline in edge-on spiral galaxies does not continue to its last measured point, but rather truncates after a certain radial scale-length (van der Kruit 1979). The origin of these truncations can be explained though several models suggesting that accretion of external material in the discs of galaxies can produce extended discs which can be interpreted as truncations (e.g. Larson 1976). In de Jong (1996), it was predicted that substantial age gradients exist across these discs, which are not observed yet.

Alternatively, a truncation originates by quenching of star formation activity due to the fall of gas density below a threshold for local instability, for example, interaction with other galaxies, tidal effect of the environment, or stochastic fluctuations due to internal dynamics (Fall and Efstathiou 1980; Schaye 2004). This star-formation threshold is also associated with disc-breaks in light profiles of galaxies (e.g. Martin and Kennicutt 2001).

Truncations should not be confused with disc-breaks. Originally, the former was found to occur in edge-on galaxies at 4.2±0.5 scale-lengths (van der Kruit and Searle 1981a, 1981b), while the latter occurs around 2.5±0.6 scale-lengths (Pohlen and Trujillo 2006). Kregel and van der Kruit (2004) found that the surface brightness at the estimated truncation radius was 25.3±0.6 mag/arcsec^2 (r-band). On the other hand, disc-breaks were found in the surface brightness range 23–25 mag/arcsec^2 (Pohlen and Trujillo 2006). In some cases, disc-breaks and truncations can co-exist, but the mechanisms causing them are different (Martín-Navarro et al. 2012). Depending on the shape of the surface- brightness profiles, disc-breaks are classified into (i) Type I (no break) (ii) Type II (downbending break) (iii) Type III (upbending break; see Erwin, Beckman, and Pohlen 2005; Pohlen and Trujillo 2006; Erwin, Pohlen, and Beckman 2008).

Different mechanisms have been proposed to explain the origin of disc-breaks. Type II disc-breaks occur as a consequence of star-formation threshold (Fall and Efstathiou 1980; Schaye 2004), while Type III disc-breaks have been associated to minor or major mergers (e.g. Younger et al. 2007; Borlaff et al. 2014). Furthermore, disc-breaks are located at closer radial distances to the centre in face-on galaxies than in edge-on systems. Internal mechanisms owing to the formation of bars and rings in spiral galaxies can also cause disc-breaks (Muñoz-Mateos et al. 2013). As such, there has been research on disc-breaks in galaxies of different morphologies (e.g. Pohlen and Trujillo 2006) as well as a function of the environment, that is, field vs cluster (Pranger et al. 2017).

Clusters are suitable for the study of discs in LTGs as they allow us to map the dynamical processes of galaxies in a dense environment. After Virgo, the Fornax cluster is the nearest and second most massive galaxy concentration within 20 Mpc, with a virial mass of M = $9 \times 10^{13} M_{\odot}$ (Drinkwater, Gregg, and Colless 2001a). Fornax is dynamically more evolved than Virgo, as most of its bright ($m_B < 15$ mag) cluster members (Ferguson 1989) are ETGs which are mainly located in its core (Grillmair et al. 1994; Jordán et al. 2007a). However, the mass assembly of the Fornax cluster is still ongoing (Scharf, Zurek,

and Bureau 2005) and the intra-cluster light (ICL; Napolitano et al. 2003) in its core indicates interactions between cluster members (Iodice et al. 2017a; Pota et al. 2018; Spiniello et al. 2018). Iodice et al. (2017a) found that this ICL is the counterpart in the diffuse light of the overdensity in the blue intra-cluster globular clusters (D'Abrusco et al. 2016; Cantiello et al. 2018) and a fraction of the ICL population are low-mass dwarf galaxies (Venhola et al. 2017). The observed number density drop of low surface-brightness (LSB) galaxies below a cluster-centric distance r = 0.6 deg (180 kpc) by Venhola et al. (2017) is a proof of the effect of the dense environment on the evolution of galaxies. In the same regions, the high-velocity planetary nebulae (PNe, Spiniello et al. 2018) and globular clusters (GCs, Pota et al. 2018) show that this ICL component is unbound to galaxies, possibly after gravitational interactions, and is dynamically old. All of these findings indicate that Fornax is an evolved, yet active environment and a rich reservoir for the study of the evolution and the structure of the galaxies in a cluster environment, specifically, inside the virial radius of the Fornax cluster. The aim of this work is to study the structure of LTGs inside the Fornax cluster and address the diverse evolutionary paths these systems can take after falling into a cluster. In particular, by taking advantage of the Fornax Deep Survey (FDS) data, we can map the light distribution down to unprecedented limits in the Fornax cluster. This allows us to detect any asymmetries in the outskirts of the discs as well as tidal tails or streams that would indicate possible interactions. By analysing their surface brightness distribution, we aim at identifying disc-breaks and finding any correlations with the location of galaxies inside the cluster.

In this study, we present the analysis of LTGs, that is, spiral galaxies selected from Ferguson (1989), which are brighter than $m_B \leq$16.6 mag inside the virial radius of the Fornax cluster. We give a short summary of FDS in Sect. 2.2. We describe the procedure and method to derive the radial profiles, colours, and structural parameters like effective radius and total magnitude in Sect. 2.3. We give a detailed description of the algorithm we have developed to derive break radii in Sect. 2.4. A surface photometry analysis of each galaxy presented in this work is described in Appendix 2.A, with their corresponding images in surface brightness, $g-i$ colour maps and profiles, with surface brightness profiles shown in Appendix 2.B. We summarise our results in Sect. 2.5 and 2.6, and discuss the formation of structures caused by secular evolution and the effect the environment in Sect. 2.7. Conclusions and future perspectives are given in Sect. 2.8. The methodologies of some of this work are presented in Appendix 2.C.

2.2 The Fornax Deep Survey: data

The work presented in this chapter focuses on the central 9 deg^2 ($\alpha = 03h\ 38m\ 29.024s, \delta = -35d\ 27'\ 03.18''$), which cover most of the cluster area inside the virial radius, $R_{vir} \sim 0.7$ Mpc (Drinkwater, Gregg, and Colless 2001a). A thorough description of the observing procedure, data reduction pipelines, calibration, and quality-assessment of the final data products were

presented by Venhola et al. (2017), Venhola et al. (2018), Iodice et al. (2016), and Iodice et al. (2017a). The data presented in this work were obtained during several visitor mode runs in dark time for u, g, r bands and in grey time for i-band (see Iodice et al. 2019a for details on the observed FDS fields). Data were reduced with two pipelines: (i) VST-Tube (Grado et al. 2012; Capaccioli et al. 2015); (ii) Astro-WISE (Valentijn et al. 2007). The VST-Tube was used to reduce data for the central 9 deg^2, while Astro-WISE was used for the data reduction of 26 deg^2. We use both data products in this work.

The FDS fields were acquired using a *step-dither* observing strategy, which consists of a cycle of short exposures of 150s each, centred on the core and its adjacent fields (≤ 1 deg) in the Fornax cluster. Fields with few or no bright objects were used to derive an average sky frame for each night and in all bands, which is scaled and subtracted from each science frame. This method has proven to provide an accurate estimation of the sky background around bright and extended galaxies (see Iodice et al. 2016; Iodice et al. 2017a; Iodice et al. 2019a; Venhola et al. 2017; Venhola et al. 2018). For each field, we obtained 76 exposures of 150s each in u band, 54 in g and r bands, and 35 in i band, thus resulting in a total exposure time of 3.17 hr in u band, 2.25 hr in g and r bands, and 1.46 hr in i band. Images with seeing FWHM ≤ 1.5 arcsec were used in the final production of co-added frames (see Iodice et al. 2019a for exposure times of each filter). The FWHM (arcsec) and depth (mag/arsec^2) of FDS fields in each filter (u, g, r, i) are given in Table. 2.1 (see Venhola et al. 2018).

The g-band mosaic covering nine square degrees around the core of the Fornax cluster, with marked circles indicating the galaxies studied and presented in this paper, is shown in Fig. 2.1. This is a complete sample in $m_B \leq 16.6$ mag consisting of 13 LTGs inside the virial radius of the Fornax cluster (see Table. 2.2). The sample of spiral galaxies has been selected from Ferguson (1989), with morphological type $T \geq 1$. To be consistent with the catalogue we refer to (from Ferguson 1989) and keeping in mind that the morphological classification changes over time, we use a generic term, that is, address the galaxies in our sample as LTGs. This work is complementary to that of Iodice et al. (2019a) on ETGs. A detailed description of each galaxy in this sample is given in Appendix 2.A.

TABLE 2.1: **Image quality of FDS fields.** *Col.1* -FDS fields ;*Col.2*- average seeing, and surface brightness corresponding to 1σ signal-to-noise ratio per sq. arcsec for u-band; *Col.3-Col.5*- same as Col. 2 for g, r, and i bands. The PSF FWHM and depth of each filter in all fields are adopted from Venhola et al. (2018).

Field	u band		g band		r band		i band	
	$FWHM$ [arcsec]	depth $[\frac{mag}{arcsec^2}]$	$FWHM$ [arcsec]	depth $[\frac{mag}{arcsec^2}]$	$FWHM$ [arcsec]	depth $[\frac{mag}{arcsec^2}]$	$FWHM$ [arcsec]	depth $[\frac{mag}{arcsec^2}]$
(1)	(2)		(3)		(4)		(5)	
F2	1.21	26.89	1.11	28.35	0.90	27.78	0.79	26.75
F4	1.18	26.95	1.39	28.45	1.19	27.76	0.70	27.01
F5	1.33	27.33	1.15	28.54	1.39	27.85	1.08	26.97
F6	1.11	27.43	0.84	28.47	1.08	27.73	1.21	26.82
F7	1.04	27.3	0.83	28.56	0.95	27.81	1.42	26.62
F12	1.15	27.44	0.83	28.49	1.04	27.84	1.17	26.79
F15	1.30	27.12	1.13	28.35	0.90	27.89	0.97	26.87
F16	1.31	27.27	1.26	28.43	0.94	27.84	1.08	26.96
F17	1.27	27.1	1.11	28.29	0.87	27.96	1.01	26.92

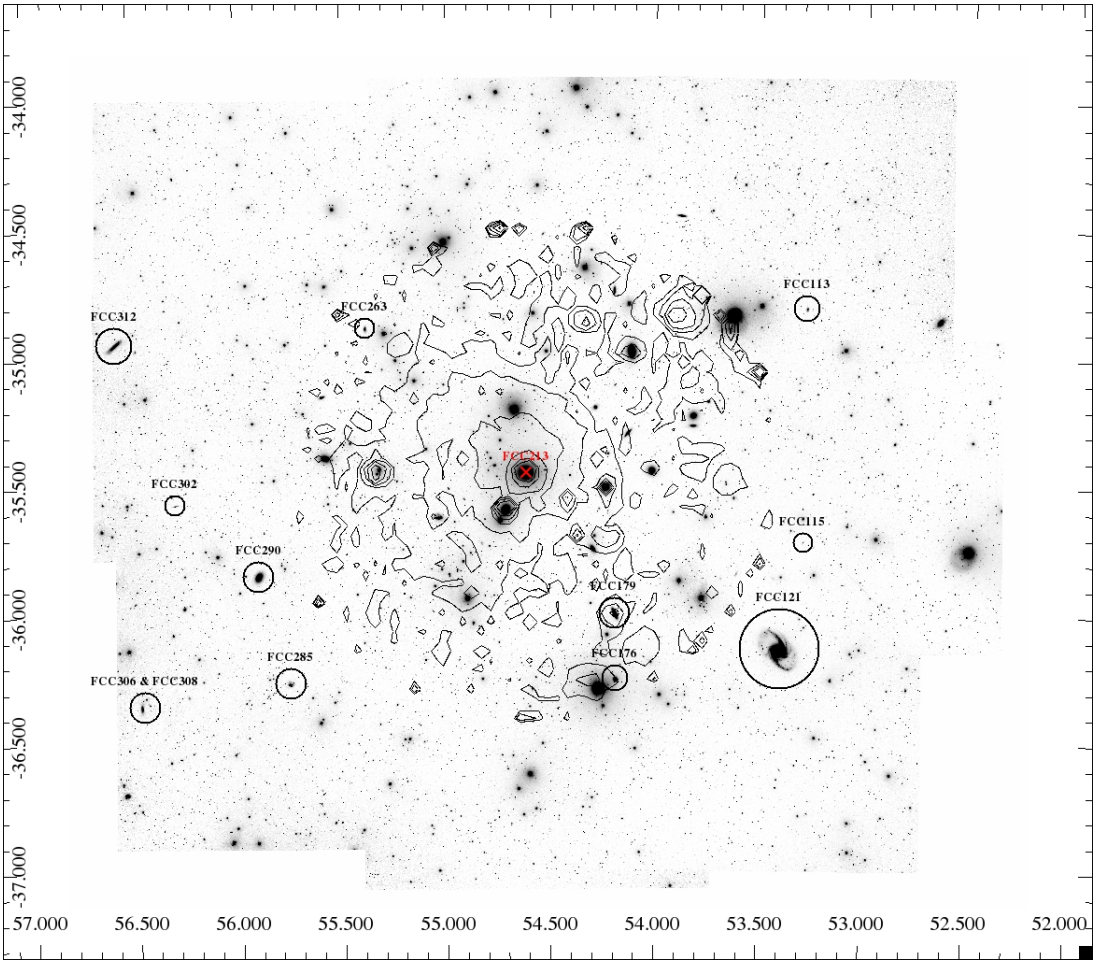


FIGURE 2.1: VST mosaic in g-band of Fornax cluster's virial radius, at about 9 deg^2. The marked circles indicate the 12 LTGs presented in this work, with FCC267 located at the top north of the virial radius, outside this mosaic. Black contours are the X-ray emission from ROSAT (Paolillo et al. 2002). The X-ray contours are spaced by a factor of 1.3, with the lowest level at 3.0×10^{-3} counts/arcmin^2/s.

2.3 Analysis: surface photometry

In this section, we give a brief description of the method we adopt, following Iodice et al. (2017a) and Iodice et al. (2019a), to derive galaxy parameters: total magnitude, effective radius, and stellar mass-to-light (M/L) ratio.

TABLE 2.2: **LTGs brighter than $m_B \leq 16.6$ mag inside Fornax cluster's virial radius.** *Col.1* - Fornax cluster members from Ferguson (1989); *Col.2 & Col.3* - Right Ascension and Declination; *Col.4* - Morphological type; *Col.5* - Heliocentric radial velocity obtained from NED; *Col.6* - total magnitude in *B* band as given in NED; *Col.7* - Location in the FDS Field; *Col.8* - Alternative catalogue names.

object	α	δ	Morph. type	radial velocity	m_B	FDS Field	Alternative Names
	h:m:s	d:m:s		km/s	mag		
(1)	(2)	(3)	(4)	(5)	(6)	(7)	(8)
FCC113	03 33 06.8	-34 48 29	ScdIII pec	1388	14.8	F15-16	ESO358-G15
FCC115	03 33 09.2	-35 43 07	Sdm(on edge)	1700	16.6	F16	ESO358-G16
FCC121	03 33 36.4	-36 08 25	SB(s)b	1635	10.32	F16-F17	NGC 1365, ESO358-G17
FCC176	03 36 45.0	-36 15 22	SBa (SAB(s)a)	1414	13.74	F12-F17	NGC 1369, ESO358-G34
FCC179	03 36 46.3	-35 59 58	Sa	868	12.09	F11-F12	NGC 1386, ESO358-G35
FCC263	03 41 32.6	-34 53 17	SBcdIII	1724	14.04	F6	ESO358-G51
FCC267	03 41 45.4	-33 47 31	SmIV	834	16.1	F4-F5	
FCC285	03 43 02.2	-36 16 24	SdIII	886	14.1	F7	NGC 1437A, ESO358-G54
FCC290	03 43 37.1	-35 51 13	ScII	1387	12.41	F6-F7	NGC 1437, ESO358-G58
FCC302	03 45 12.1	-35 34 15	Sdm (on edge)	803	15.5	F2-F6	ESO358-G060
FCC306	03 45 45.3	-36 20 48	SBmIII	886	15.6	F7	
FCC308	03 45 54.7	-36 21 25	Sd	1487	13.97	F7	NGC 1437B, ESO358-G61
FCC312	03 46 18.9	-34 56 37	Scd	1929	12.83	F2-F6	ESO358-G63

2.3.1 Method: isophote fitting

We extracted azimuthally averaged intensity profiles for each object from the sky-subtracted images in four respective bands, using the ELLIPSE (Jedrzejewski 1987) task in IRAF[5] (for a thorough explanation of this method, see Iodice et al. 2019a).

The main steps are as follows:

1. Create masks for bright objects (galaxy and stars) around our galaxy of interest

2. Fit isophotes in elliptical annuli, starting from the centre of the galaxy, up to its outer edge in the FDS field (out to ~ 0.5 deg). We keep the geometric centre of symmetry fixed while the ellipticity and position angle are free parameters. For lopsided galaxies (FCC113 and FCC285) and barred galaxies (FCC263 and FCC121), we use the galactic centre of one band as the same centre for other bands so that the same regions are mapped in the study and characterisation of their structures.

3. From the intensity profiles, we (i) estimate the limiting radius corresponding to the outer most annulus R_{lim} (see Table. 2.3)[6], where the galaxy's light blends into the average background level [7] and (ii) derive the residual sky background from the outer annuli of all galaxies in each band.

2.3.2 Products: total magnitude, effective radius, colour, and stellar mass-to-light ratio

We adopted the procedure of Iodice et al. (2019a) to derive parameters: total magnitude, effective radius, colour, stellar mass-to-light ratio, for all galaxies in our sample. Firstly, the resulting output of the isophote fit is used to provide their respective intensity profiles, from which we derive the azimuthally averaged surface brightness (SB) profiles. This is followed by a correction for the residual background level estimated at $R \geq R_{lim}$, in each band for all the galaxies in our sample. The error estimates on magnitudes take into account the uncertainties on the photometric calibration and sky subtraction (see Capaccioli et al. 2015; Iodice et al. 2016; Iodice et al. 2019a). Secondly, we derive colour $(g - i)$ profiles from the azimuthally averaged SB profiles for each galaxy (Appendix 2.B). We also show the $g - i$ colour maps for each of these galaxies (Appendix 2.B), obtained from the images. From the isophote fits, we use a growth curve analysis to derive total magnitude and effective radius in each band for all galaxies (see Table. 2.4). We then derive average $(g - i$

[5]IRAF is distributed by the National Optical Astronomy Observatories, which are operated by the Association of Universities for Research in Astronomy, Inc., under cooperative agreement with the National Science Foundation

[6]It should be noted that R_{lim} is different from the depth of the image.

[7]The average background level is the residual after subtracting the sky frame, this results in a value close to zero (see Iodice et al. 2016).

TABLE 2.3: **Limiting radius of intensity profiles**. *Col.1* - Fornax cluster members from Ferguson (1989); *Col.2*- Limiting radius in *r*-band ; *Col.3*- Surface brightness at the limiting radius.

object	R_{lim}	μ
	arcsec	mag/arcsec^2
(1)	(2)	(3)
FCC113	42.23	25.7± 0.2
FCC115	36.04	25.5 ±0.1
FCC121	436.7	26.6 ±0.3
FCC176	86.4	26.5± 0.4
FCC179	139.2	25.8 ±0.3
FCC263	71.41	25.7± 0.1
FCC267	42.23	26.8± 0.4
FCC285	86.4	26.0± 0.1
FCC290	139.2	26.4± 0.03
FCC302	51.1	26.9± 0.2
FCC306	22.75	25.8± 0.1
FCC308	115.0	26.3± 0.1
FCC312	153.1	25.13± 0.1

and $g-r$) colours for each of these galaxies from their radial profiles (see Table. 2.4). Lastly, we estimate the stellar mass M_* from the average $(g-i)$ colour, by using the empirical relation $log_{10}\frac{M_*}{M_\odot} = 1.15 + 0.70(g-i) - 0.4M_i$ from Taylor et al. 2011, where M_i is the absolute magnitude in i-band[8]. According to Taylor et al. (2011), this relation provides an estimate of the stellar mass-to-light ratio M_*/L_i with 1 σ accuracy of ~ 0.1 dex. The M_*/L_i value for each galaxy of the sample is given in Table. 2.5. A full illustration of the SB profiles, $g-i$ colour profiles and maps for individual galaxies are shown in Appendix 2.B.

[8]The empirical relation proposed by Taylor et al. (2011) assumed a Chabrier IMF.

TABLE 2.4: **Derived Parameters of LTGs inside Fornax cluster's virial radius.** *Col.1* - Fornax cluster members from Ferguson (1989); *Col.2 to Col.5* - Total magnitude in the u, g, r and i bands respectively, derived from the isophote fit. Values were corrected for the galactic extinction, using the absorption coefficient by Schlegel, Finkbeiner, and Davis (1998); *Col.6 to Col.9* - Effective radius in the u, g, r and i bands respectively, derived from the isophote fit.

object	m_u	m_g	m_r	m_i	Re_u	Re_g	Re_r	Re_i
	mag	mag	mag	mag	arcsec	arcsec	arcsec	arcsec
(1)	(2)	(3)	(4)	(5)	(6)	(7)	(8)	(9)
FCC113	15.51 ± 0.04	15.01 ± 0.02	14.44 ± 0.01	14.3 ± 0.01	29.74 ± 0.8	19.51 ± 0.2	20.56 ± 0.1	20.64 ± 0.1
FCC115	17.18 ± 0.01	16.35 ± 0.01	15.91 ± 0.4	15.94 ± 0.01	17.9 ± 0.5	19.54 ± 0.1	20.58 ± 0.1	16.58 ± 0.2
FCC121	10.65 ± 0.05	9.33 ± 0.04	8.79 ± 0.03	8.43 ± 0.03	134 ± 4	142.4 ± 3.7	109.8 ± 2.1	132.8 ± 2.9
FCC176	13.95 ± 0.01	12.51 ± 0.01	11.74 ± 0.01	11.45 ± 0.01	56.76 ± 1.6	53.03 ± 0.7	53.73 ± 2.3	47.42 ± 1.2
FCC179	13.17 ± 0.02	11.44 ± 0.01	10.68 ± 0.01	10.34 ± 0.01	22.75 ± 0.4	29.68 ± 0.5	30.03 ± 0.5	28.01 ± 0.7
FCC263	14.72 ± 0.05	12.91 ± 0.05	12.7 ± 0.02	12.58 ± 0.01	21.82 ± 1.6	25.36 ± 1.7	27.15 ± 0.6	21.53 ± 0.1
FCC267	16.6 ± 0.1	15.68 ± 0.03	15.09 ± 0.01	14.8 ± 0.01	14.1 ± 0.5	17.6 ± 0.4	19.4 ± 0.4	20.0 ± 0.3
FCC285	14.57 ± 0.03	13.15 ± 0.02	13.02 ± 0.03	12.77 ± 0.01	40.84 ± 1.6	46.78 ± 1.3	49.9 ± 1.5	51.1 ± 0.6
FCC290	12.6 ± 0.01	11.4 ± 0.01	11.08 ± 0.01	10.74 ± 0.01	49.68 ± 0.5	49.65 ± 0.6	48.52 ± 0.2	48.41 ± 0.1
FCC302	16.29 ± 0.1	15.58 ± 0.01	15.37 ± 0.04	15.06 ± 0.1	28.49 ± 1.7	21.92 ± 0.75	24.15 ± 0.8	28.84 ± 1.6
FCC306	16.54 ± 0.02	15.29 ± 0.03	15.18 ± 0.01	15.0 ± 0.01	9.01 ± 0.2	10.52 ± 0.1	9.7 ± 0.1	9.85 ± 0.1
FCC308	14.36 ± 0.02	12.87 ± 0.01	12.54 ± 0.01	12.17 ± 0.02	53.65 ± 1.4	44.91 ± 0.6	37.11 ± 0.8	46.46 ± 0.4
FCC312	13.38 ± 0.05	11.4 ± 0.02	10.89 ± 0.1	10.45 ± 0.04	49.34 ± 2.1	76.0 ± 3.7	109.5 ± 9.3	117.8 ± 7.3

TABLE 2.5: Stellar mass estimates of LTGs in i -band. *Col.1* - Fornax cluster members from Ferguson (1989); *Col.2*- Projected distance from the galaxy centre in degree, i.e. from NGC 1399 (FCC213); *Col.3*- Absolute magnitude in r-band, derived using the distance modulus from NED and Tully et al. (2009); *Col.4* - Effective radius (kpc) in i-band;*Col.5 & 6*- Average $g-r$ and $g-i$ colours ; *Col.7 & Col. 8*- Stellar mass and mass-to-light (M/L) in i-band.

object	D_{core}	M_i	R_e	$g-r$	$g-i$	M_*	M/L
	deg	mag	kpc	mag	mag	$10^{10}M_\odot$	
(1)	(2)	(3)	(4)	(5)	(6)	(7)	(8)
FCC113	1.21	-16.74	1.98	0.57 ± 0.03	0.71 ± 0.02	0.02	0.56
FCC115	1.05	-15.78	1.59	0.43 ± 0.02	0.41 ± 0.02	0.01	0.35
FCC121	1.06	-22.58	12.74	0.54 ± 0.02	0.90 ± 0.02	6.49	0.77
FCC176	0.82	-19.85	4.55	0.77 ± 0.02	1.06 ± 0.02	0.68	0.99
FCC179	0.55	-20.7	2.68	0.76 ± 0.02	1.10 ± 0.02	1.58	1.06
FCC263	0.79	-18.08	2.06	0.21 ± 0.1	0.32 ± 0.1	0.04	0.3
FCC267	1.73	-15.24	1.92	0.59 ± 0.04	0.88 ± 0.04	0.01	0.74
FCC285	1.17	-17.43	4.90	0.13 ± 0.05	0.38 ± 0.04	0.02	0.33
FCC290	1.05	-20.49	4.64	0.33 ± 0.04	0.66 ± 0.04	0.64	0.52
FCC302	1.30	-15.92	2.76	0.21 ± 0.02	0.52 ± 0.02	0.01	0.41
FCC306	1.69	-15.21	0.94	0.11 ± 0.04	0.29 ± 0.04	0.003	0.29
FCC308	1.69	-17.49	4.46	0.33 ± 0.02	0.69 ± 0.03	0.04	0.55
FCC312	1.59	-20.89	11.30	0.51 ± 0.1	0.95 ± 0.1	1.48	0.83

2.4 Analysis: the break radius

One of the main novelties of this work is the algorithm we have developed to derive break radii of galaxies. It is based on concepts used in literature to derive break radii (e.g. Pohlen and Trujillo 2006), but it is fully automated and reproducible, as it is based on coded rules to define the break radius and bootstraps the results over a variety of initial conditions for the best-fitting procedure. In this section, we illustrate the main steps to derive the break radius from surface brightness profiles, and provide a detailed description of the algorithm we use.

2.4.1 Surface brightness profile deconvolution

We derived the break radius from surface brightness profiles in the r-band as this is one of the highest transmission OmegaCam filters and least-affected by dust absorption, which could be quite high in LTGs.

Since the break radius is derived on the disc regions of LTGs, it is important to account for the effect of the contamination from their bright cores, which scatters their light in the regions around them because of the effect of the point spread function (PSF). The mathematical effect introduced by the PSF over the measured 2D light distribution is equivalent to a convolution of a matrix of the intrinsic intensity values (the surface brightness) and a 2D kernel (the matrix corresponding to the PSF). In order to correct this, we need to invert this operation, that is, perform a deconvolution, assuming the kernel is given.

The first step of deconvolution (assuming the kernel is given) is to accurately measure the PSF out to a radial distance comparable to that of the galaxies' discs. Capaccioli et al. (2015) found that the scattered light can considerably affect the local light profiles in VST images of galaxies of various sizes in different ways. To fully account for the broadening effect of the seeing on their sample of galaxy images, they characterised the PSF from the VST images.

The sample presented in this work consists of galaxies of different angular extent (see Fig. 2.2). FCC306 is the smallest galaxy in our sample ($R_e = 0.94$ kpc in i-band) and FCC121 is the largest galaxy, ($R_e = 12.74$ kpc in i-band). From Fig. 2.2, it is clear that the effect of the PSF (1 arcsec) scatters the light from the central regions to the outer regions. The effect mitigates outside the typical size of the PSF, where, for the conservation of the flux, the light scattered from the core makes the observed profile brighter than the intrinsic (deconvolved) profile. Finally, the effect of the PSF is completely canceled far away from the centre, typically outside ten arcsec. Thus, in order to minimise the effect of the PSF on our structural analysis, we deconvolve galaxies with the PSF, by using the Lucy-Richardson algorithm (Lucy 1974; Richardson 1972), as done by Spavone et al. (2017a, hereafter SP+17). A full description of the deconvolution method used for VST data is presented by Spavone et al. (in prep). The robustness of the deconvolution algorithm is demonstrated in Appendix 2.C.1, where we compare the performance against the method from Borlaff et al. (2017).

The surface brightness profiles and break radii are derived from the deconvolved images in r-band. We also derive the deconvolved profiles in g and i bands. The deconvolved profiles (r-band) are given in Fig. 2.3 and Fig. 2.4, and deconvolved ($g - i$) colour profiles are shown in Appendix 2.B.

2.4.2 Algorithm: break radius

Since discs of LTGs show exponential SB profiles, which become linear in the log-linear plane, the break radius can be defined as the radius where the logarithmic SB, defined as μ =-2.5 log $I(R)$, where $I(R)$ is the SB as a function of the radius R, shows a discontinuity in the slope. The presence of this discontinuity is first guessed by fitting the disc with a single linear model using the following equation,

$$\mu(R) = \beta + \alpha R \tag{2.1}$$

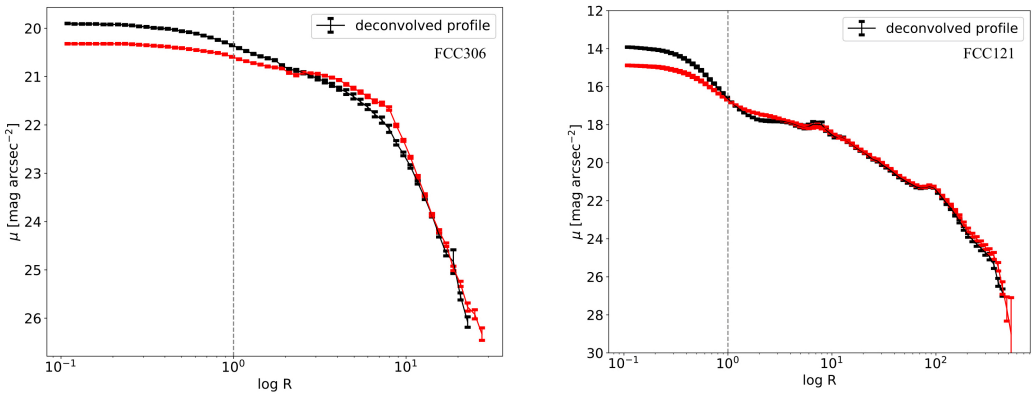


FIGURE 2.2: Impact of PSF on galaxies with different angular extent. Deconvolved SB profiles over-plotted on the original SB profiles (red) for the smallest, FCC306 ($R_e = 0.94$ kpc in i-band) and the largest galaxy, FCC121 ($R_e = 12.74$ kpc in i-band) in the left and right panels. The PSF (1 arcsec) for FDS data is marked in grey dotted lines.

where α is the slope of the linear fit and β is the intercept. The best fit is performed via least square linear fitting of 1D surface brightness profile in r-band (deconvolved). The least square approximation of the linear system is based on the Euclidean norm of the squared residuals.

This is followed by evaluating the residuals of the best fit. If the residuals show monotonic deviations from the best fit (rms residuals > 0.5 mag)[9] that increase with radius, it suggests that the profile has a break and needs a second component. Then, two linear fits are implemented, using Eq. 2.1. In order to take into account different intervals in radius, that is, before and after the discontinuity, we have developed a procedure which automatically defines these intervals (radial ranges) to determine the break radius (B_r). The linear fits are performed outside the bulge component. For most galaxies, the region where the bulge dominates was taken from Salo et al. (2015). Though we initially consider the whole profile (including inner components), we excluded the breaks detected in the inner regions as they are connected to component-transition rather than disc-breaks (e.g. Laine et al. 2014; Laine, Laurikainen, and Salo 2016).

Since the aim of this multi-linear fit approach is to study the disc regions of LTGs and detect any break in this component, it cannot be considered as a tool to decompose the observed profiles into different sub-components. In fact, it makes use of a simple linear regression to define the regions where there is a significant slope change[10] in the light profiles of LTGs to measure the transition point.

In more detail, the first step is to estimate the radial range where the disc component is defined (i.e. an inner disc limit, $range_{in}$, and an outer disc limit, $range_{out}$). This is done by an initial guess of the disc scale-lengths (h_{in}

[9] The residuals in irregular galaxies correspond to the presence of wiggles in their profiles. We checked this before concluding that it is associated with disc-breaks.

[10] This also accounts for a slope error > 0.05.

and h_{out}), from which the range is derived by varying 'n' [11] number of data points ($max_{range_{in}} = range_{in} \pm n$; $max_{range_{out}} = range_{out} \pm n$, we used n=2). The procedure is repeated for the second sub-component and so on (in case there is more than one evident break radius, known from the residuals of the fit).

We stress here that the determination of the fitting range only extends to the limiting radius R_{lim}.
Once the domains of the different disc components are defined, a linear least square fit is done to each of these ranges ($range_{in}$ and $range_{out}$), producing $(n+1)^2$ best fits[12] for the inner and outer ranges. The α and β parameters (in Eq.2.1) of each of these best linear regression fits are stored and used to estimate the point of intersection, otherwise called the break radius (B_r).

The combinations of the fitting for the ranges $range_{in}$ and $range_{out}$ are chosen such that they do not coincide and all points of the disc regions on the surface brightness profile are considered. The selection of these combinations is different from the selection of $max_{range_{in}}$ and $max_{range_{out}}$where these represent the total range considered for $range_{in}$ and $range_{out}$, but not for the fitting itself. This in turn produces $(n+1)^3$ estimates of the break radius. The median of $(n+1)^3$ intersecting points is chosen as the final break radius. The rms residuals (the numerical rank of the scaled Vandermonde matrix) for each linear regression fit are computed and the median of this is shown as the range of variance of the fitted models' scale-lengths h_{in} and h_{out} (see Fig. 2.3 and Fig. 2.4). To show the regions of variance of the intersecting point from the $(n+1)^3$ best fits, the standard deviation of $(n+1)^3$ break radii (σ_{nBr}) is marked as a significant error on the estimation of the break radius. This procedure is repeated by varying the initial guess of the disc scale-lengths until a minimal standard deviation of the $(n+1)^3$ break radii is obtained, resulting in the best selection for h_{in} and h_{out}. The regions (here, $range_{in}$ and $range_{out}$ obtained from the best fit iteration) are given as the disc scale-lengths h_{in} and h_{out} and are used to derive the average $(g-i)$ colour of h_{in} and h_{out}.

The break radius (in arcsec and kpc) of ten galaxies with their σ_{nBr}, surface brightness at the break μ_{B_r}, and average $(g-i)$ colour (derived from deconvolved profiles) for the inner h_{in} and outer h_{out} discs are listed in Table. 2.6, with their deconvolved surface brightness profiles (in r-band), shown in Fig. 2.3 and Fig. 2.4. We also apply the algorithm on irregular galaxies: FCC113, FCC285, and FCC302. In such cases, we do not detect disc-breaks, but rather wiggles and bumps associated to the irregularities (star forming regions) present in these galaxies. This is also checked by subtracting the small-scale wiggles from the profiles of these galaxies, and applying the algorithm on the obtained profile. These three galaxies show a Type I profile.

Most of the galaxies in the sample show clear evidence of a single break radius, however we cannot exclude that further substructures are present beyond their outer disc scale-lengths.

[11] Here n is defined as the number of SB points obtained from ELLIPSE, using a semi-major axis (pixels) step of 0.1 (1.0 + *step*)

[12] This combination is obtained by 'rule of product' i.e. $n+1$ ranges for the upper and lower limits of the radial scale-lengths

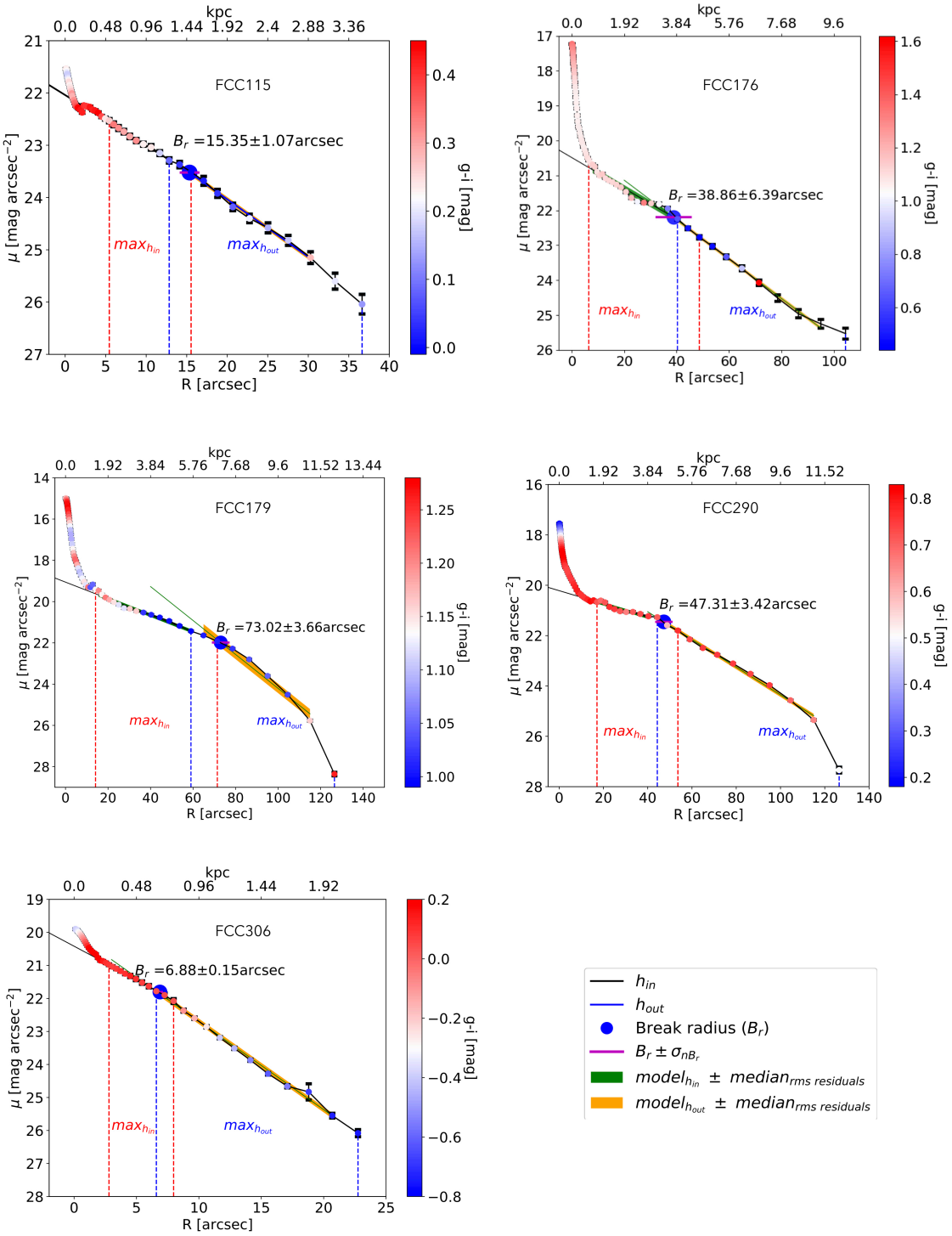


FIGURE 2.3: Surface brightness profiles of galaxies with Type II disc-break, with $(g-i)$ colour as third parameter. In each plot, the break radius (B_r) is marked at the intersecting point of the linear fits performed between h_{in} and h_{out}, with σ_{nB_r} as the median of $(n+1)^3$ combinations of best fits on the inner and outer scale-lengths. The vertical dashed lines ($max_{h_{in}}$ and $max_{h_{out}}$) indicate the regions for $max_{range_{in}} = range_{in} \pm n$ and $max_{range_{out}} = range_{out} \pm n$ where the algorithm produces $(n+1)^2$ linear least square fits. The shaded regions on h_{in} and h_{out} indicate the median of the rms of the residuals for $(n+1)^2$ linear least square fits.

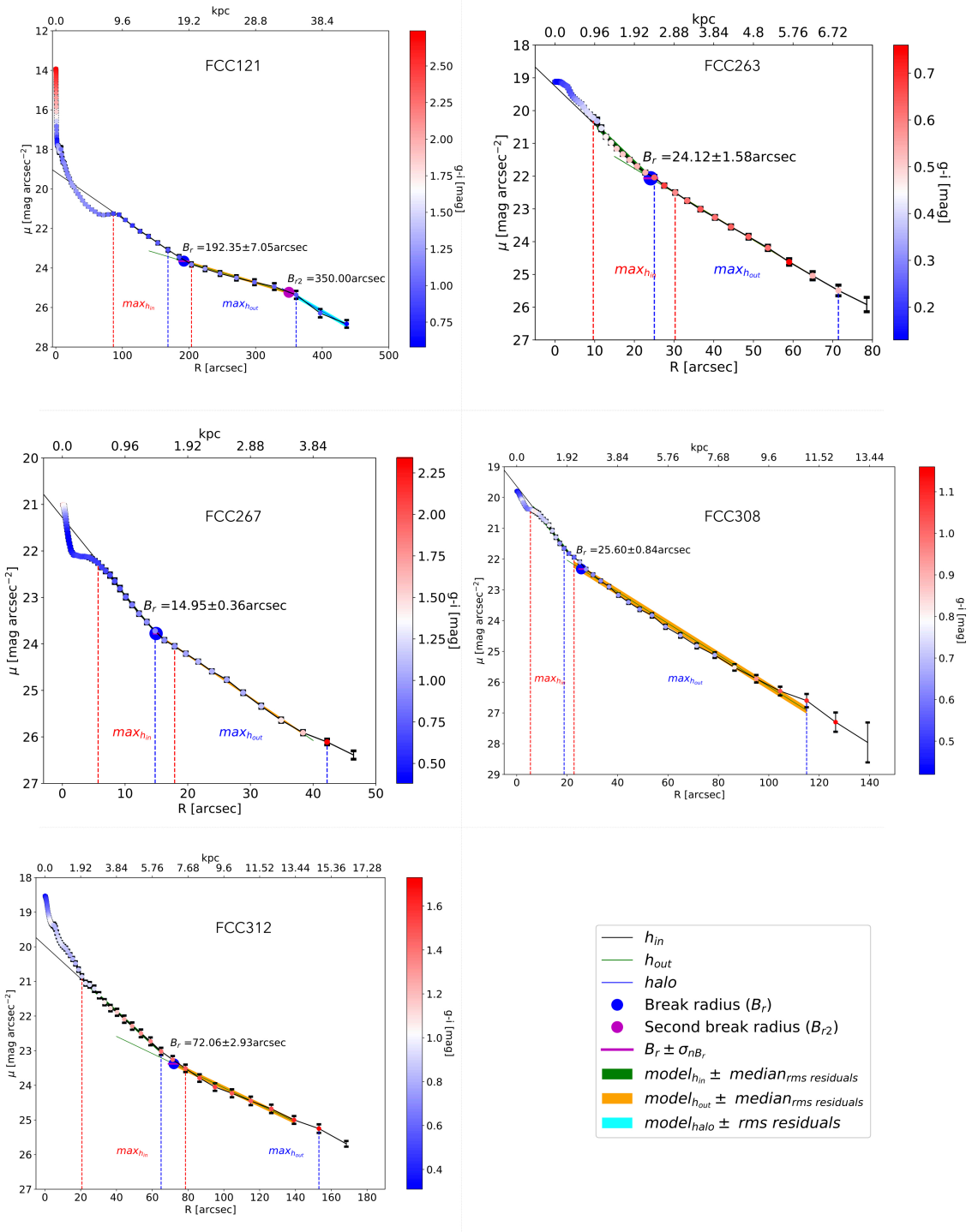


FIGURE 2.4: Surface brightness profiles of galaxies with Type III disc-break, similar to Fig. 2.3.

For example, FCC121 shows a second break (see Fig. 2.4) at $\mu(R) > 25.5$ mag/arcsec^2, which is well detected by the algorithm but it is not discussed in our analysis. This second break could be associated with the truncation radius that occurs in the outermost optical extent of a galaxy (see e.g. Martín-Navarro et al. 2012). Also, we need a minimum of 3 data points to produce $(n+1)^2$ fits (with a lower limit of n=1), that is within the R_{lim}. For this reason, we do not derive a second break for some galaxies of the sample (e.g. FCC267, FCC308) though it seems to be present in their profiles.

An example of the $(n+1)^3$ best fits with minimal standard deviation, produced by the algorithm is shown in Appendices. 2.C.2–2.C.4. Parameters of the best fit for LTGs with disc-breaks are given in Table. 2.C.1. For all galaxies, the break radii (inner and outer disc-breaks as in the case of FCC121) are located within regions where the effects of PSF-convolution are negligible. This is proven by deriving the break radius from deconvolved profiles and the results (original vs deconvolved profiles) are the same, as shown in Appendices. 2.C.5 and 2.C.6.

2.5 Morphological segregation of LTGs inside the virial radius of the Fornax cluster

The sample of LTGs inside the virial radius of the Fornax cluster is heterogeneous in morphology as measured by their T-type Hubble classes. These are shown as a function of the projected distance in Fig. 2.5. The correlation is not as tight as previously reported in other similar environments, for example, Virgo (Binggeli, Tammann, and Sandage 1987) and other clusters (Whitmore 1993). Here, the projected distances have been used as a primary parameter to discern the formation and evolution of the galaxies' substructures as a function of the cluster environment. However, one must also take into account other environment-independent mechanisms like pre-processing (e.g. Fujita 2004), which are independent of the local environment. In this section, we analyse the morphological structures of the galaxies in our sample by grouping them into bins of Hubble stage T as a function of projected cluster-centric distance (D_{core}), shown in Fig. 2.5.

The LTGs in Fornax with morphological type $1 \leq T \leq 4$ are FCC121, FCC176, FCC179, FCC263, and FCC290. These galaxies are located within $D_{core} \leq 1.1$ deg from the cluster centre (see Fig. 2.1 and 2.5), corresponding to 0.54 R_{vir}. Overall, they are among the most luminous ($m_B < 14$ mag, refer Table. 2.2) LTGs in our sample. They show regular spiral or barred-spiral structures with clear grand design features. Three of the above mentioned galaxies (FCC176, FCC179, FCC263) are, in projection, located within the X-ray halo of NGC 1399 (see Fig. 2.1).

TABLE 2.6: **Parameters of LTGs with disc-breaks.***Col.1* - LTGs with a disc-break; *Col.2* - Break radius in units of arcsec and kpc (1 arcsec = 0.096 kpc); *Col.3* - Standard deviation of the break radii from $(n+1)^3$ combinations; *Col.4*- Surface brightness at the break radius; *Col.5* - inner scale-length in units of arcsec, and average $(g-i)$ colour for h_{in}; *Col.6*- outer scale-length in units of arcsec, and average $(g-i)$ colour for h_{out}; *Col.7*- Hubble Type T ;*Col.8*- Profile classification

object	B_r		σ_{nB_r}	μ_{B_r}	h_{in}		h_{out}		Hubble	Break
	[arcsec]	[kpc]	[arcsec]	$[\frac{mag}{arcsec^2}]$	[arcsec]	$g-i$ [mag]	[arcsec]	$g-i$ [mag]	Type (T)	Type
(1)	(2)		(3)	(4)	(5)		(6)		(7)	(8)
FCC113	-	-	-	-	-	-	-	-	6	I
FCC115	15.35	1.47	1.1	23.52	6.84	0.25 ± 0.03	16.15	0.12 ± 0.03	8	II
FCC121	192.35	18.46	7.1	23.65	63.9	0.88 ± 0.02	175.7	1.09 ± 0.04	3	III+II
FCC176	38.86	3.73	6.4	22.20	28.66	1.10 ± 0.02	54.73	0.76 ± 0.2	1	II
FCC179	73.02	7.01	3.7	21.98	43.47	1.10 ± 0.02	50.08	1.05 ± 0.02	1	II
FCC263	24.12	2.32	1.6	22.06	14.42	0.49 ± 0.02	37.39	0.63 ± 0.02	2	III
FCC267	14.95	1.43	0.4	23.83	8.52	0.76 ± 0.03	22.11	1.26 ± 0.13	9	III
FCC285	-	-	-	-	-	-	-	-	7	I
FCC290	47.31	4.54	3.4	21.45	23.22	0.72 ± 0.03	70.66	0.71 ± 0.02	4	II
FCC302	-	-	-	-	-	-	-	-	8	I
FCC306	6.88	0.66	0.2	21.81	2.92	0.09 ± 0.01	14.1	-0.39 ± 0.1	9	II
FCC308	25.60	2.46	0.8	22.32	14.11	0.71 ± 0.02	92.25	0.75 ± 0.04	7	III
FCC312	72.06	6.91	2.9	23.38	42.17	1.16 ± 0.05	67.79	1.54 ± 0.03	7	III

FCC176 and FCC179 are redder than other LTGs inside the virial radius (see Fig. 2.7) with the former devoid of atomic and molecular gas (Fuller et al. 2014; Schröder, Drinkwater, and Richter 2001) and the latter shows dust and molecular gas in its spiral arms. FCC121 and FCC290 are located beyond the X-ray halo with morphological type $T > 3$. FCC290 has spiral arms only inside $1R_e$ (see Appendix 2.B.9). FCC121 has grand design spiral structure with a bar.

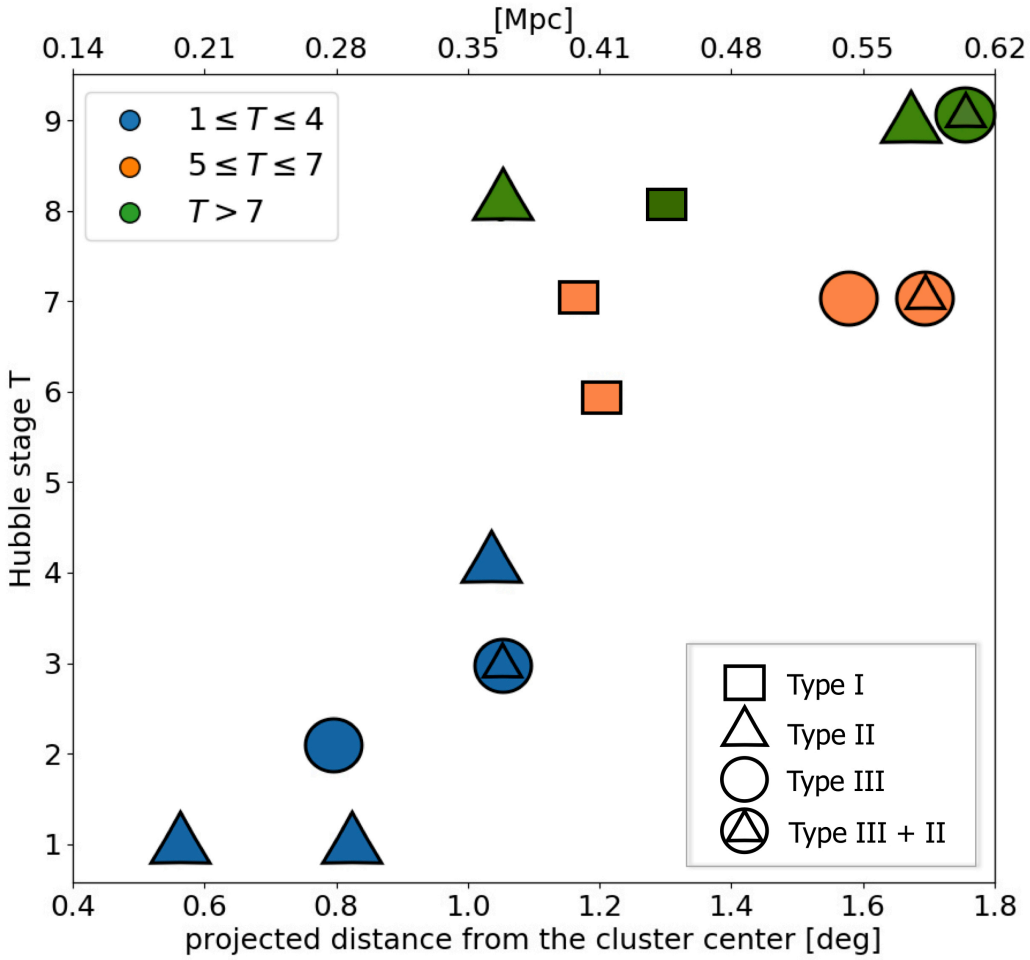


FIGURE 2.5: Hubble type T as function of projected cluster-centric distance. For each galaxy, their disc-break type is represented as squares (Type I) or triangles (Type II), or circles (Type III). For three galaxies with secondary breaks other than their primary break-type, they are represented as circle+triangle(Type III+II).

Galaxies with morphological type $5 \leq T \leq 7$ are FCC113, FCC285, FCC308, and FCC312. These galaxies are located beyond $D_{core} > 1.1$ deg. The former two galaxies (FCC113 and FCC285) are lopsided with luminosities $14 < m_B < 15$ mag and the latter two (FCC308, FCC312) have boxy discs with $m_B < 14$ mag. FCC113 and FCC285 exhibit irregular star-forming regions, which are evident in their SB images (Appendices. 2.B.1 and 2.B.8). They are located on either sides of the cluster centre with their asymmetric discs elongated towards the cluster centre (see Fig. 2.1). FCC308 and FCC312 have irregular star-forming regions in their ill-defined spiral arms. Their

thick discs also have flares which are signs of minor mergers (e.g. Knierman et al. 2012).

The very late morphological type $T > 7$ galaxies are FCC115, FCC302, FCC306, FCC267. FCC115 and FCC302 are edge-on galaxies (making it hard to determine their true morphological T-type), while FCC306 is a bright dwarf galaxy (Drinkwater, Gregg, and Colless 2001a). FCC267 has a double nucleus or a dust-obscured bar (see Appendix 2.B.7). These galaxies have irregular star-forming regions and lumosities in the range $15 < m_B \leq 16.6$ mag (refer Table. 2.2). All the galaxies in this group are located beyond $D_{core} > 1$ deg. None of the aforementioned ($T > 7$) have visible, regular spiral structures with star-forming regions, unlike the galaxies at smaller cluster-centric distances.

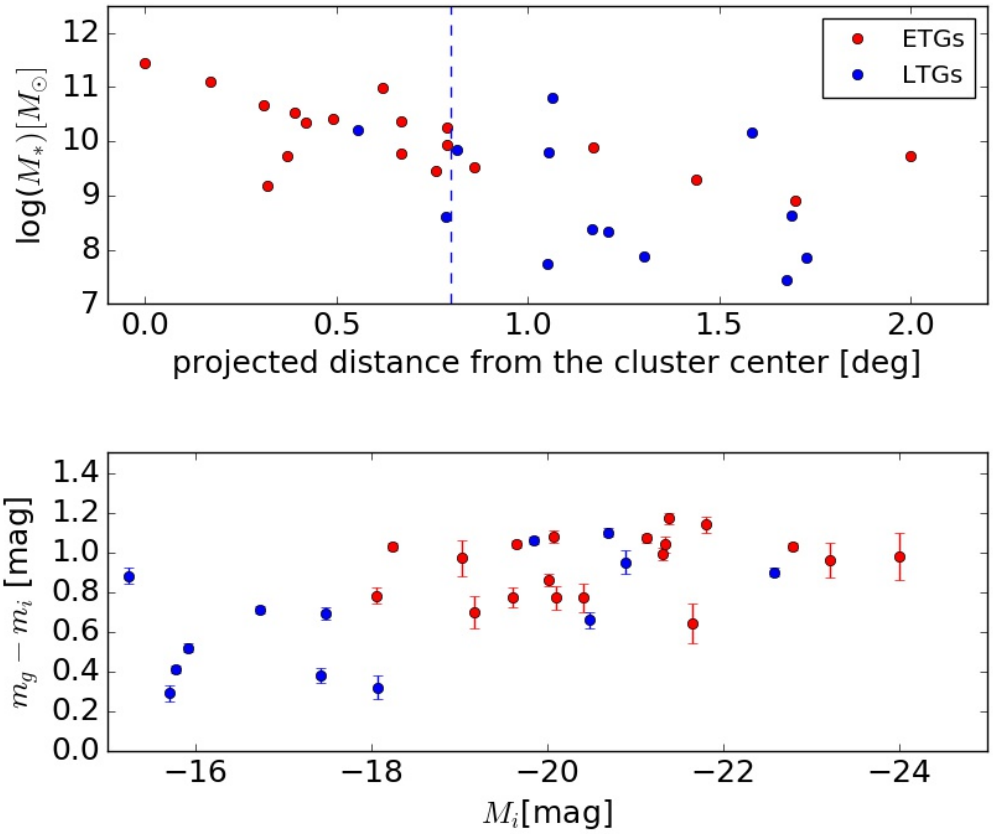


FIGURE 2.6: Stellar mass as function of cluster-centric distance (top panel) and colour-magnitude relation (lower panel) for LTGs and ETGs in the Fornax cluster core (data from Iodice et al. 2019a) inside Fornax cluster's virial radius.

Despite our small heterogeneous sample of LTGs, we can still infer that the overall morphological segregation of galaxies inside the virial radius strongly suggests that the number density of ETGs is higher near the cluster centre ($D_{core} < 0.8$ deg ~ 0.27 Mpc, Iodice et al. 2019a), where only the massive LTGs of earlier types ($1 \leq T \leq 4$) are found (see Fig. 2.6: top panel). Galaxies with morphological type $5 < T \leq 9$ ($\sim 60\%$ of the sample) are

located beyond $D_{core} > 1$ deg ~ 0.36 Mpc, that is beyond the high-density (ETG-dominated) regions defined by Iodice et al. (2019a).

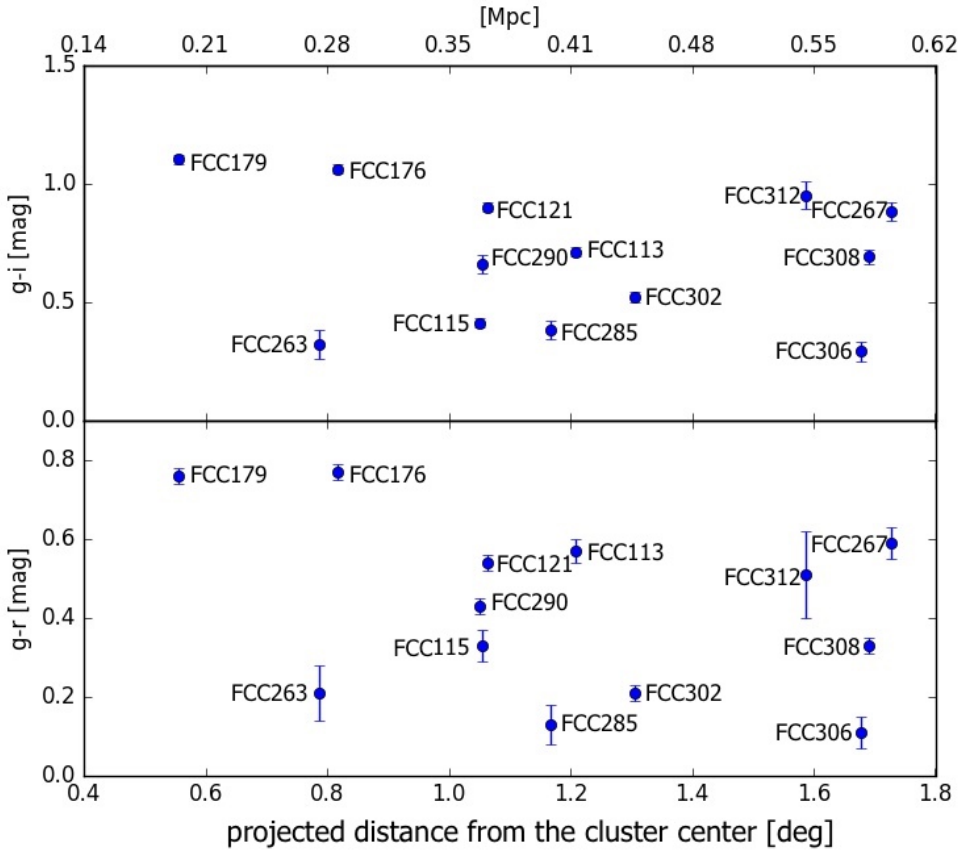


FIGURE 2.7: $g - i$ (top panel) and $g - r$ (lower panel) colours as function of projected distance from Fornax cluster's centre in degrees and Mpc.

We do not find any trends between average ($g - i$ and $g - r$) colours as a function of cluster-centric distance (see Fig. 2.7), as observed by Iodice et al. (2019a) for ETGs. From the colour-magnitude relation diagram (Fig. 2.6), we find a positive correlation as expected and a clear segregation in colours from the bright ETGs in the cluster (see Fig. 2.6: lower panel).

2.6 Analysis of disc-breaks

In this section, we analyse disc-breaks by investigating possible correlations with some global properties such as colours, total magnitudes, stellar mass, molecular gas, and with the galaxy's location in the cluster. Since the sample is limited to 13 galaxies, the results cannot be considered on a statistical basis. However, it represents the complete sample of bright LTGs in the Fornax core and the analysis of their disc properties will provide important information on the assembly history of the cluster. In Fig. 2.5, we show the different disc-break types are distributed as a function of the cluster-centric distance. There is no evident correlation between the morphological type (T) and the

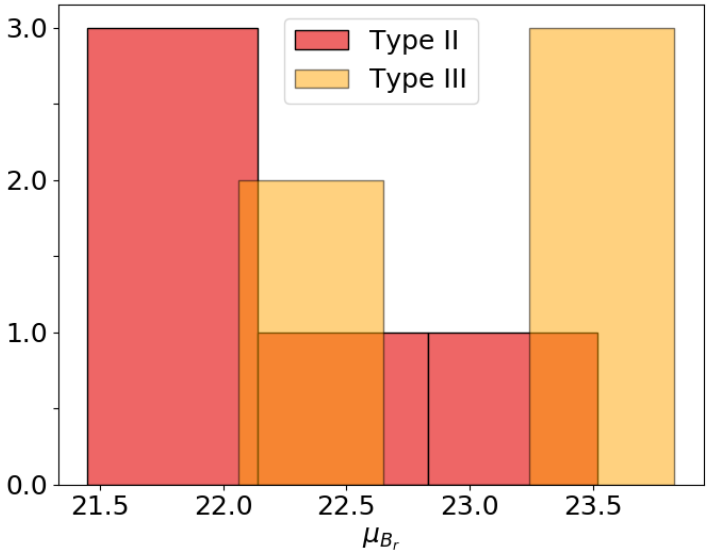


FIGURE 2.8: Histogram of surface brightness at break radius (μ_{B_r}) for Type II and Type III galaxies.

disc-break type. On the whole, we can give the same conclusion about the distribution of different disc-break types inside the virial radius, that is, Type II and Type III breaks are found in galaxies at both small and large cluster-centric distances. It is worth noting that Type I galaxies (only three galaxies) are found around $\sim$ 1.2 deg ($\sim$ 0.4 Mpc).

The surface brightness at the break radius in Type II discs is in the range $22.5 \leq \mu_{B_r} \leq 24$ (see Fig. 2.8).

On average, these galaxies have bluer $(g - i)$ colours in their outer discs (h_{out}) in comparison to their inner discs (h_{in}) (see Fig. 2.9 and refer Table. 2.6). FCC179 and FCC290 have bluer outer discs (than their inner discs), with a difference $\leq$ 0.05 mag, which is above the error (refer Table. 2.6). However, their inner discs have dust and this can cause the observed red colour. FCC115 and FCC306 are very late type galaxies that are bluer on average (see Fig. 2.7) with the former being the faintest in the sample and the latter, a bright dwarf.

Type III disc-breaks have surface brightness levels in the range $21.5 \leq \mu_{B_r} \leq 23$ (see Fig. 2.8), that is, more luminous than the μ_{B_r} of Type II disc-breaks.

These galaxies have redder $(g - i)$ outer discs than their inner discs (see Fig. 2.9 and Table. 2.6). Most of the Type III galaxies show signs of merger events taken place in the past, for example, FCC263 with disturbed molecular gas (Zabel et al. 2019), tidal tails[13] in FCC308 and FCC312 , double nuclei in FCC267, which can produce up-bending profiles. The redder colour may be accounted for the transfer of stellar mass to the outer disc during interactions (Younger et al. 2007). The redder outer discs may also be associated with the

[13]Galaxies with tidal tails were classified as Type IIIa by Watkins et al. (2019).

exhaustion of gas via ram-pressure stripping (see e.g. Steinhauser, Schindler, and Springel 2016; Pranger et al. 2017).

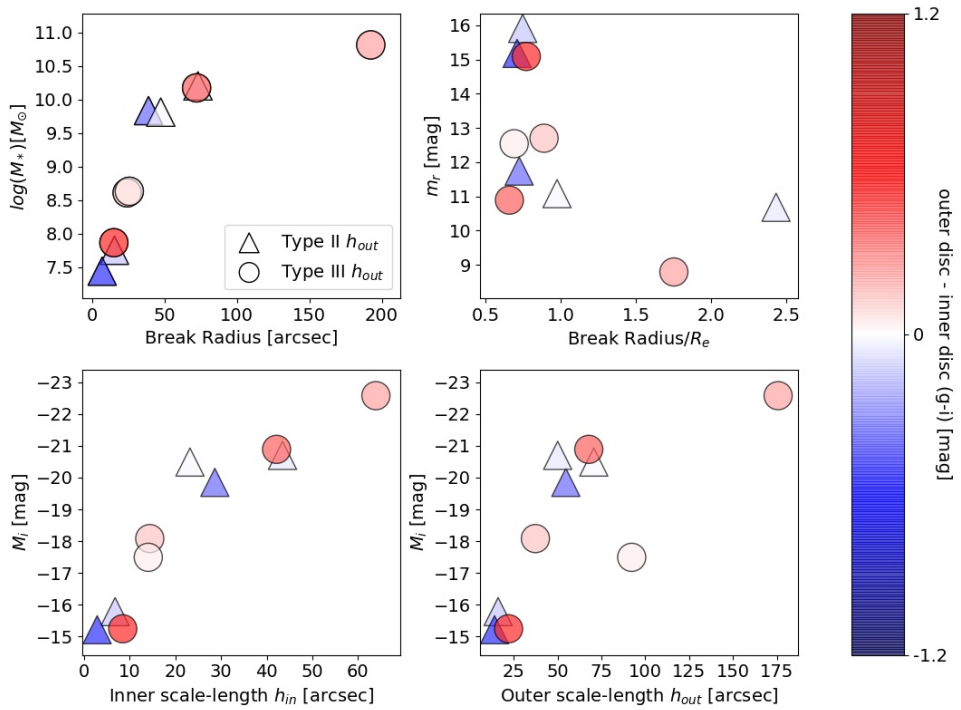


FIGURE 2.9: Analysis of galaxies with disc-breaks. Triangles represent Type II profiles, and circles represent Type III, with average $(g-i)$ colour of h_{out}-h_{in} as colour map. Top panel (left): Stellar mass as a function of break radius; Top panel (right): Total magnitude as a function of break radius normalised to effective radius; Bottom Panel: Absolute magnitude in i-band as a function of inner scale-length h_{in} (left) and outer scale-length h_{out} (right).

We find a positive correlation between stellar mass and the break radius (see Fig. 2.9: top left panel). This trend is expected and has been shown before in literature (e.g. Pohlen and Trujillo 2006). In comparison to the results by Pohlen and Trujillo (2006), we also find that luminous galaxies have larger inner disc scale-lengths as shown in Fig. 2.9 (bottom panel). This trend is still evident in the plot of the total magnitude as a function of the break radius normalised to the effective radius (see Fig. 2.9: top right panel), where most of our sample galaxies have break radius in the range of $0.5\,R_e < B_r < 1.25R_e$, while the two brightest galaxies have $B_r \geq 1.7R_e$.

We used the molecular gas mass M_{H_2} derived from CO (1–0) emission, as part of the ALMA Fornax cluster Survey (Zabel et al. 2019) to obtain molecular gas-fractions (M_{H_2}/M_*) and plot them against the break radius for eight galaxies in our sample, of which six are detected in CO(1–0), and two are non-detected (see Fig. 2.10). The M_{H_2} in the latter cases is the 3σ upper limit. We also plot the CO maps in contours on our g-band images along with the break radius (see Appendix 2.B). From this, we find that the molecular gas

(CO) detection is within the uncertainties of the break radius. Since molecular gas is a prerequisite for star formation, the break radius could also be a sign of a 'break in star formation' (see Roškar et al. 2008; Sánchez-Blázquez et al. 2009; Christlein, Zaritsky, and Bland-Hawthorn 2010). Fig. 2.10 shows that galaxies with larger break radius have higher molecular gas mass, and lower gas-fractions.

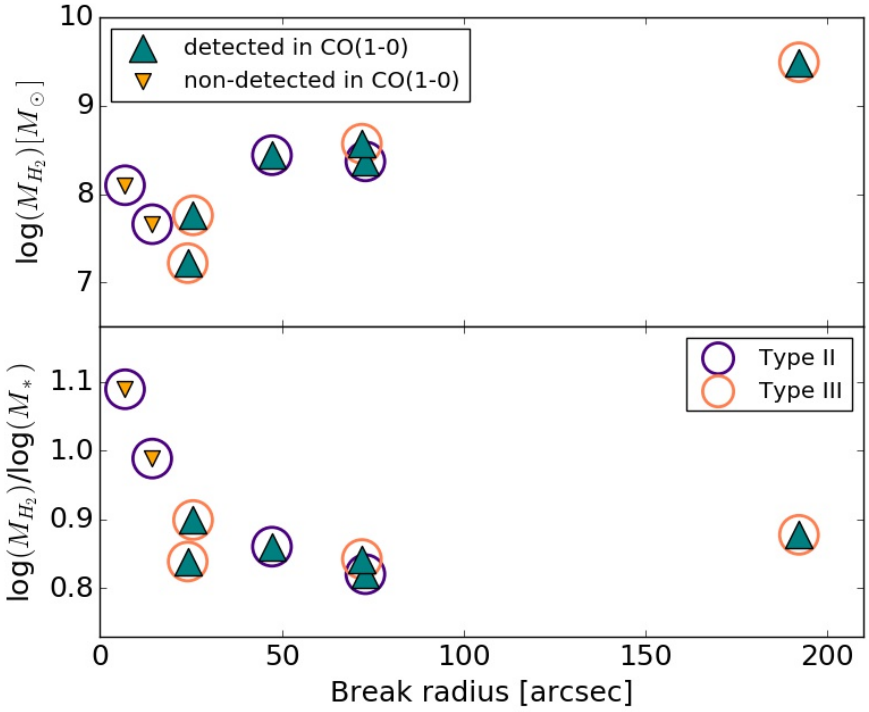


FIGURE 2.10: Molecular gas mass (top panel) and molecular gas-fractions (lower panel) as function of break radius. Green triangles represent galaxies detected in CO(1–0), and orange triangles represent galaxies non-detected in CO(1–0) for eight LTGs in our sample, which were surveyed by Zabel et al. (2019). Orange circles are galaxies with Type II profile, and purple circles are galaxies with Type III profile.

2.7 Summary of results and discussion

Inside the virial radius of the Fornax cluster ($\leq$ 0.7 Mpc), there are 13 LTGs brighter than $m_B \leq 16.6$ mag. In this work, we investigate the structure of this small, yet complete sample of 13 LTGs and in doing so, analyse any possible correlations with their position in the cluster. One aim is to study the disc component and hence, we have developed an algorithm to define and measure break radii in their surface brightness profiles (Sect. 2.6).

The main results of this work are summarised below:

1. From Fig. 2.5, it is evident that our sample of LTGs is heterogeneous in morphology. Still we find that galaxies with morphological type $T \leq 4$ located at smaller cluster-centric distances. Among these, FCC176 and

FCC179 (morphological type T=1) seem to be in a transition phase to S0/SB0. Later morphological types ($5 < T \leq 9$, $\sim$ 60% of the sample) are located at $D_{core} > 1$ deg $\sim$ 0.36 Mpc, that is, beyond the high-density of ETG-dominated regions (D_{core}> 0.8 deg $\sim$ 0.27 Mpc). Most of these show signatures of tidal interactions in the form of lopsidedness (FCC113 and FCC285), thick discs and tidal tails (FCC308 and FCC312) or double nuclei or dust-obscured bar (FCC267).

2. There is an equal fraction (38%) of Type II and Type III discs in the sample, while only three galaxies (23%) show a classical Type I exponential disc. There is no evident correlation between T and the type of disc-break. Type II galaxies have bluer outer discs ($h_{out} - h_{in} = -0.37$ mag), while Type III galaxies have redder outer discs ($h_{out} - h_{in} = 0.25$ mag). Brighter and massive galaxies have larger break radii. For galaxies detected in CO(1–0), the molecular gas is within the break radius.

In the following sections, we discuss the results mentioned above in order to address the evolution of LTGs inside the virial radius of the Fornax cluster.

2.7.1 Evolution of LTGs inside the virial radius of the Fornax cluster

The Fornax cluster has been considered as a classic example of a virialised cluster with regular galaxy distribution (Grillmair et al. 1994; Jordán et al. 2007a). This cluster is dynamically more evolved than the Virgo cluster with a high fraction of ETGs in its core (Grillmair et al. 1994; Jordán et al. 2007a; Iodice et al. 2019a). Inside its virial radius, Iodice et al. (2019a) found that the ETGs are not spherically distributed around NGC 1399, rather, they are located along a stripe, that is, north-south direction in the west side of NGC 1399 (also refer to Fig. 2.1). Along this direction, signatures of an ICL component have been found (Iodice et al. 2017b), mirrored by globular clusters (GC) density substructures (D'Abrusco et al. 2016; Cantiello et al. 2018), and supported by kinematical measurements by PNe (Spiniello et al. 2018) and GCs (Pota et al. 2018). All of this suggests that there are interactions between Fornax cluster members (Iodice et al. 2017b) and among galaxies with the overall cluster potential (Spiniello et al. 2018; Pota et al. 2018). This 'stripe' along the west-north-west direction of NGC 1399, otherwise called as a west-north-west sub-clump, may have resulted from the accretion of a galaxy-group during the build-up of the cluster, hence creating what has been perceived to be an asymmetry (Iodice et al. 2019a). To further substantiate this accretion and the consequences on its surroundings, all the LTGs brighter than $m_B \leq$16.6 mag, presented in this work, are not located spatially anywhere near this sub-clump of ETGs. In fact, these LTGs are located in the opposite direction (east side of NGC 1399, in 2D projection) of this high-density ETG-zone (Fig. 2.1), except for FCC113, a lopsided galaxy. However the lopsided tail of FCC113 appears to be elongated in the direction pointing towards the cluster centre (see Appendix 2.B.1).

Our results concerning the morphological segregation of ETGs crowding the central regions (Iodice et al. 2019a), and LTGs located at larger cluster-centric distance inside the virial radius of the Fornax cluster, is consistent with previous findings of the this relation in Virgo (Binggeli, Tammann, and Sandage 1987) and other clusters (Dressler 1980; Whitmore 1993). Some of the mechanisms that have been proposed to explain the morphological segregation are ram-pressure stripping (Gunn and Gott 1972), galaxy harassment (Moore et al. 1996), truncated star-formation (Larson, Tinsley, and Caldwell 1980a), galaxy-galaxy interaction (Lavery and Henry 1988).

Due to the higher intra-cluster gas density and higher cluster-centric velocities of galaxies, ram-pressure stripping is 16 times more effective in the Virgo cluster (Davies et al. 2013). However, as the Fornax cluster hosts $\sim$ 300 galaxies with $B_T \sim 18$ (Ferguson 1989), which is an order of magnitude lower than the galaxy population in Virgo, it is suggested that galaxy-galaxy interactions play a prominent role in the evolution of Fornax cluster members (e.g. D'Abrusco et al. 2016; Iodice et al. 2017b; Iodice et al. 2017a; Venhola et al. 2017; Venhola et al. 2018; Spiniello et al. 2018). In addition to this, it is also necessary to take into account pre-processing of a galaxy before falling into a cluster, and that the enhanced ram-pressure stripping occurs when the group passes through the cluster pericentre (Vijayaraghavan and Ricker 2013). With these mechanisms stated, we examine the morphological evolution of LTGs inside the virial radius of the Fornax cluster.

Late-type spiral (Scd-Sdm) galaxies

Galaxies with morphological type $5 < T \leq 9$ are located at $D_{core} > 1$ deg ~ 0.36 Mpc. Among these, FCC308 and FCC312 show signs of interactions in the form of tidal tails. The presence of these tails can either be explained by minor-merging events or by the disruption of the outer discs during infall, due to the strong tidal shear in the cluster centre (Whitmore 1993). Galaxies with asymmetric stellar discs (FCC113 and FCC285) could have experienced similar mechanisms during infall, but after the cluster collapse (Whitmore 1993). Since these galaxies have tidal disturbances similar to NGC 1427A, another possible mechanism for this is that it was triggered by a recent fly-by of another galaxy in the cluster (Lee-Waddell et al. 2018). However, more analysis on the HI distribution of these galaxies are required to confirm the possibility of ram-pressure stripping acting on them (e.g. Vollmer 2003).

FCC115, FCC302, FCC267, FCC306 are faint galaxies ($m_B \leq 16.6$) with morphological type $T > 7$ (Sd–Sdm). The former two have ill-defined spiral arms, and the latter two have faint spiral arms. As mentioned in the previous paragraph, these galaxies could have experienced disruptions due to the gravitational potential well of the cluster core, during infall. Since protogalactic clouds which are needed to form Sd galaxies are destroyed during the cluster collapse, these galaxies are dominant at larger cluster-centric distances (Whitmore 1993).

Galaxies transitioning into S0

FCC176 and FCC179, which are located at $D_{core} \leq 0.82$ deg, are classic examples of galaxies transitioning into lenticulars (S0/SB0) in a dense environment. FCC290 (D_{core} = 1.05) also has similar disc structure to FCC179, such that the spiral arms are found only in their central regions (<1R_e) whereas their outer-disc is devoid of any feature (including star-formation blobs and molecular gas). Their discs resemble the smooth structure, that is typically found in the discs of S0 galaxies. FCC176 and FCC179 are close to the cluster core and are the redder and more massive LTGs of our sample, with average $(g-i)$ colour >1 mag and $M_*/10^{10}M_\odot > 0.6$ (see Table. 2.C.1). Larson, Tinsley, and Caldwell (1980a) first explained how blue galaxies evolve to red galaxies over Hubble time, and this was followed by several other supporting evidences of galaxies losing their gas as a consequence of environmental effects (e.g. Boselli and Gavazzi 2006; D'Onofrio, Marziani, and Buson 2015; Gao et al. 2018, and references therein). FCC176 could have formed before the cluster collapse and therefore resides in the X-ray halo of NGC 1399 (e.g. Whitmore 1993). This galaxy's morphological evolution under the influence of the cluster environment has caused it to be HI deficient. However, FCC179 and FCC290 are detected in HI (Schröder, Drinkwater, and Richter 2001) and CO(1–0) (Zabel et al. 2019). The CO disc in spiral galaxies is usually concentrated within 1R_e (see e.g. Davis et al. 2013). The outer gas discs in spirals that extend to their optical radius are typically HI dominated. HI imaging would be required to confirm that these galaxies have been pre-processed (see e.g. Fujita 2004; Vijayaraghavan and Ricker 2013), or that they have experienced ram-pressure or tidal stripping during infall, which has resulted in the loss of their outer disc gas (Larson, Tinsley, and Caldwell 1980a).

2.7.2 Break radius as a proxy for the structural evolution of LTGs

Disc breaks in the light profiles of LTGs have known to occur as a consequence of internal mechanisms (e.g. formation of bars) or external mechanisms (e.g. effect of the environment), or sometimes both (Martín-Navarro et al. 2012). It has proven to be a vital parameter in the study of the stellar and gaseous discs of LTGs (e.g. Martin and Kennicutt 2001; Roediger et al. 2012; Peters et al. 2017, and references therein). As such, we will use the break radius to further discuss the structural and morphological evolution of LTGs inside the virial radius of the Fornax cluster. To this aim, we also take into account the correlation of molecular gas distribution with the break radius, observed for six LTGs in the sample. The CO(1–0) detection (Zabel et al. 2019) is within the uncertainties of the inner break radius (see Appendix 2.B) implying that there could also be a star-formation break, for example, in FCC290, as previously suggested (e.g. Roškar et al. 2008; Sánchez-Blázquez et al. 2009; Christlein, Zaritsky, and Bland-Hawthorn 2010). As the concentration of molecular gas within the break radius could have occurred as a consequence

of a different mechanism from that of the disc-break itself, further analysis on their stellar populations is required to confirm this correlation.

Type III disc-break

Type III breaks in clusters are found in galaxies with past minor or major mergers. Minor mergers can cause gas-inflows towards the centre of the primary gas-rich galaxy which steepens the inner profile, and expands the outer profile as the angular momentum is transferred outwards during the interaction (Younger et al. 2007), while major mergers usually produce Type III S0 galaxies (Borlaff et al. 2014). This process can also explain the presence of molecular gas close the centre, inside their break radius.

FCC308 and FCC312 have boxy discs and morphological type $T = 7$, with flares in their disc, showing signs of minor merger, as already stated. The disc-break of these galaxies could have also occurred as result of external mechanisms in the cluster environment, where the tidal shear of the cluster core causes disruptions in their disc.

FCC121 and FCC263 are barred-spiral galaxies which do not have cold gas beyond their break radius. Within their break radius, these galaxies also show strong star-formation activity (molecular gas and bright blue knots, see Appendix 2.B), whereas the outer disc of FCC263 does not show any signs of current star-formation, and in the case of FCC121, there is a small fraction of bright knots along the spiral arms. External mechanisms as previously stated, result in the removal of gas during infall via tidal stripping by the halo potential (Larson, Tinsley, and Caldwell 1980a).

Type II disc-break

Models for Type II breaks are linked to star-formation threshold (e.g. Martin and Kennicutt 2001) and radial migration of stars (e.g. Martínez-Serrano et al. 2009; Roediger et al. 2012). The stellar disc of early-type spirals tends to be more massive than their gaseous disc, which implies a star-formation threshold around their break radius (Martin and Kennicutt 2001).

The disc-break in barred galaxies has also been associated with the bar radius and the Outer Lindlblad Resonance(OLR) (see Muñoz-Mateos et al. 2013; Laine et al. 2014), like in the case of FCC176. Flared discs in highly inclined galaxies like FCC115 (faintest galaxy) and FCC306 (bright dwarf) can produce a less-pronounced break (see e.g. Borlaff et al. 2016). The disruptions in the outskirts of their discs may have resulted as a consequence of the gravitational potential well of the cluster core.

FCC179 and FCC290 (Type II) are spiral galaxies without cold gas in their outer disc (see Sect. 2.5 and 2.7.1). The former is located within the X-ray halo (see Fig. 2.1), while the latter is located beyond the X-ray halo. The break radius of these galaxies are not only associated with the absence of molecular gas in their outer disc but also the absence of spiral arms.

Though Erwin, Gutiérrez, and Beckman (2012) found that there was an absence of Type II profiles in Virgo cluster S0s, suggesting that the Type II profiles can transition into Type I, in a cluster environment, or that Type I

were turning into Type II profiles (no models have predicted this yet), there might be other mechanisms that could also cause them to form a Type III break. As such, the processes (internal and external) causing disc-breaks are a part of the evolutionary phases of LTGs in the Fornax cluster.

What can the average ($g - i$) colour of the inner and outer discs of LTGs indicate?

We find that Type II galaxies have bluer outer discs, while Type III galaxies have redder outer discs. In addition, the molecular gas detection is only within the break radius of six LTGs. Both findings might suggest that there is a stellar population gradient across the disc (e.g. Bell and de Jong 2000). Since we do not find any segregation inside the virial radius of the cluster for Type II and Type III discs, this might indicate that different processes acted in different regions of the cluster.

There have been numerous studies concerning the outer-colour of LTGs with disc-breaks (see e.g. Bakos, Trujillo, and Pohlen 2008; Roediger et al. 2012; Laine, Laurikainen, and Salo 2016; Watkins et al. 2019, and references therein), but no conclusive results have been given to explain these findings. External mechanisms like ram-pressure stripping (removal of cold gas) and strangulation (removal of hot gas), or stellar migration (e.g Roškar et al. 2008) have been found to cause reddening in cluster LTGs (e.g. Steinhauser, Schindler, and Springel 2016; Pranger et al. 2017). The ram-pressure stripping or strangulation could have been responsible for the reddening in the outer Type III discs in FCC263 and FCC121, which are located (projected distance) in the transition region from high-to-low density region of the cluster, where the X-ray emission is decreasing (see Fig. 2.1). For the other two Type III galaxies (FCC267 and FCC312) far away from the cluster core, with a significant colour gradient between inner and outer disc, a different process could have been responsible for the redder colours in the outskirts. Both of them, show also evident signs of past merging (see Appendix 2.B.7 and Appendix 2.B.14).

Simulations by Hwang et al. (2018) have shown that LTGs entering a cluster could have encounters with ETGs, and during this phase, they can have strong star-formation activity yet losing their cold gas, which can also cause the presence of bluer outer discs. This could be the case of Type II galaxies inside the high density regions of the cluster, as FCC176 and FCC179 that show a colour difference larger than the error estimate (see Table. 2.6) and an ongoing star formation in the centre (see Appendix 2.B.4 and Appendix 2.B.5).

2.8 Concluding remarks and future perspectives

FDS data allow us to map the light distribution of galaxies down to the faintest magnitudes where the effects of the environment on the evolutionary stages of Fornax cluster galaxies can be studied in depth. In this work we have shown how such studies are especially useful in the analysis of disc-breaks, which in turn provides a ground in further analysis of the stellar

populations beyond the break radius. Despite the limited size of our LTG sample (13 objects), the morphological segregation of LTGs inside the virial radius of the Fornax cluster is clearly detected and is consistent with previous results that suggest that high-density ETG-dominated zones inhibit the formation of LTGs ($5 < T \leq 9$) in a cluster environment.

We have used the results derived from the break radius as a means to discern the different mechanisms (external and internal) causing the structural evolution of LTGs inside the virial radius of the Fornax cluster. Their structural evolution would eventually cause a morphological transition. Since the sample is small, we do not give a generic conclusion that disc-breaks are indeed good proxies, but rather for the Fornax cluster. Some of the important results from our disc-break analysis is that the average $(g - i)$ colour of the outer disc, that is, beyond the break radius of LTGs, depends on their disc-break type. For galaxies detected in CO(1–0), if star formation differences created their disc-breaks, then molecular gas within their primary break radius could define the break radius.

Further investigation on the stellar population content of the discs in LTGs from the Fornax 3D data (Sarzi et al. 2018; Iodice et al. 2019a) and infall time via phase-space analysis (e.g. Rhee et al. 2017) could address the origin of the different colour gradients in Type II and Type III in the Fornax cluster. In Chapter 3, we provide a detailed comparison of structure and evolution of LTGs in the cluster core and LTGs in the infalling south-west subgroup centred on Fornax A, which is a different environment mainly populated by LTGs (Iodice et al. 2017b).

Appendix

2.A The sample: LTGs inside the virial radius

In this section, we give a detailed description of the main properties of each galaxy analysed in this paper.

2.A.1 FCC113

FCC113, is an ScdIII pec, was classified as a star forming dwarf galaxy by Drinkwater, Gregg, and Colless (2001a), but is a late type lopsided spiral galaxy with effective radius 1.98 kpc. Unlike the other regular late type galaxies studied, as part of this paper, FCC113 is located near the low-density region of galaxies in the virial radius of the Fornax cluster, at a projected distance of 1.209 deg. This galaxy, following on similar substructures, explained in the Sect. 2.A.8. Drinkwater, Gregg, and Colless (2001a) point out to the ongoing star formation of this galaxy, which can be seen in the bright knots irregularly distributed in the northern regions of this galaxy. It appears to look like the galaxy is being pulled into the cluster centre, in the southern direction.

2.A.2 FCC115

FCC115, an Sdm (edge on) galaxy, is the faintest galaxy in our sample. Due to the edge-on characteristics of this galaxy, it is difficult to discern the presence of spiral arms. It is located at a projected distance D_{core} = 1.05 deg from the cluster centre, in the low-density regime. From Appendix 2.B.2, the SB image shows a dust lane in the centre, which is presumably the spiral arm (see Appendix 2.B.2). This galaxy has a Type II profile, with a break radius of 1.47 kpc. The outer disc is bluer with SB of 23.52 $mag/arcsec^2$ at the break radius.

2.A.3 FCC121

Also known as the great barred spiral galaxy NGC 1365 has been studied in the past mostly concerning the supermassive black hole present in its core. The bar of this galaxy has dust and star formation that extends to the end of the spiral arms. With an effective radius of 12.74 kpc, this galaxy is located at a projected distance D_{core} = 1.06 deg from the cluster centre. It has a Type III profile, with a break radius of 18.46 kpc, and redder outer disc.

2.A.4 FCC176

FCC176, also known as NGC 1369 is an SBa galaxy, consists of a bar and an outer ring formed by its spiral arms. It is located in the X-ray regions of NGC 1399 in the central cluster. The effective radius of this galaxy is 2.68 kpc. It is at a projected distance D_{core} = 0.82 deg from the cluster centre. The asymmetric halo (in the SE direction) and the outer ring which show intrinsic characteristics in the disc, suggest that this is an early type spiral galaxy (Elmegreen et al. 1992; Mastropietro et al. 2005), where the star formation in the outer regions appears to be stalled. This galaxy has a Type II profile with a B_r of 3.73 kpc. The outer disc is bluer with average $(g-i)$ colour of 0.76 ± 0.2 mag (refer Table. 2.6).The break radius is beyond the ring (OLR) of the galaxy at a SB of 22.20 $mag/arcsec^2$.

2.A.5 FCC179

FCC179, also known as NGC 1386 is an Sa, Seyfert 2 galaxy, located at a projected distance D_{core}= 0.55 deg from the central galaxy, in the X-ray regions of the Fornax cluster. It has an effective radius of 2.68 kpc. This galaxy has been a topic of interest concerning its outflows (e.g. Rodríguez-Ardila et al. 2017) and gas kinematics (e.g. Lena et al. 2015). Being in the hot, high-density regime of the Fornax cluster, the spiral arms of this galaxy are concentrated in its central regions of 1 arcmin diameter. These spiral arms contains a lot of dust, which can be seen in its $g-i$ colour map at a level of 1.1 mag (see Appendix 2.B.5. This galaxy has a Type II profile, with a break radius of 7.01 kpc, that is $\sim$ 2.5 times the effective radius in r-band.

2.A.6 FCC263

FCC263 is classified as a SBcd-III, barred spiral, located at D_{core}= 0.79 deg from the cluster centre. With an effective radius of 2.06 kpc, this galaxy is detected in HI and CO(1–0), showing signs of ongoing star formation in its spiral arms (see Zabel et al. 2019; Schröder, Drinkwater, and Richter 2001). This galaxy has a Type III profile, with a break radius of 2.32 kpc. Zabel et al. (2019) point out to the irregular distribution of molecular gas, suggesting the possibility of tidal encounters or past minor mergers. Though we include this in our morphological segregation of regular spiral galaxies at smaller projected distance to the cluster centre, it is not clear if this galaxy is indeed within the X-ray halo or farther away, yet appears to have its spiral arms stripped. The outer isophotes are not aligned with the inner isophotes, and the galaxy is more thickened along the direction pointing towards the cluster centre.

2.A.7 FCC267

FCC267, a Sm(IV) galaxy, is located at farthest projected distance (1.73 deg) from the cluster centre. This galaxy's spiral arms are concentrated in the

innermost regions with double nucleus. It has an effective radius of 1.92 kpc. This galaxy has a Type III profile with a break radius of 1.43 kpc.

2.A.8 FCC285

FCC 285, also known as NGC 1437A , is an Sd-III galaxy. In the SB image, the galaxy's extended spiral arms are marked. This galaxy is detected in HI (Schröder, Drinkwater, and Richter 2001) and studied in FIR (Fuller et al. 2014) and is located at D_{core} = 1.17 deg from the cluster centre, with an effective radius of 4.90 kpc. According to the De Vaucouleurs system of classification, Sd galaxies are usually diffuse, with a faint central bulge. These galaxies also have irregular star forming regions or star clusters spread out (see Appendix 2.B.8). NGC 1437A has a similar arrow-shaped optical appearance as NGC 1427A and seems to be travelling in a southeast direction (based on the location of its own star-forming region) that is parallel with the orientation of NGC 1427A. The tail shows low SB regions, and the top part is elongated with the south, moving in opposite directions. NGC 1437A has about one third the HI mass as NGC 1427A and the velocity difference between these dIrrs is 1150 km/s, which is three times higher than the velocity dispersion of the Fornax cluster (Lee-Waddell et al. 2018) with no indication of recent tidal interactions.

2.A.9 FCC290

FCC290, also known as NGC 1436 is an ScII galaxy at a projected distance D_{core}= 1.05 deg from the cluster centre, located within the X-ray regions of the central galaxy, with an effective radius of 4.64 kpc. The inner spiral arms have about a size of 2 arcmin consisting of dust lanes. As the spiral arms are concentrated in the central regions (within $1R_e$) of the galaxy, with a regular shape of disc in the outer regions, this galaxy appears to be moving to an S0 phase in its morphological evolution. This galaxy has a Type II profile with a break radius of 4.54 kpc. CO(1–0) detection (Zabel et al. 2019) shows presence of molecular gas in its spiral arms, within its break radius (see Appendix 2.B.9).

2.A.10 FCC302

FCC302 is a diffuse, nearly edge-on galaxy with fairly uniform surface brightness, and possibly an irregular galaxy (Matthews and Gallagher 1997), located at a projected distance D_{core} = 1.305 deg. It has an effective radius of 2.76 kpc and a companion galaxy close to symmetric centre of this galaxy (NED).

2.A.11 FCC306

FCC306, is a SBmIII, classified as a dwarf galaxy by Drinkwater, Gregg, and Colless (2001a). It is the smallest galaxy of the sample we present, with an effective radius of 0.94 kpc. Though past research says that there is no evidence of substructure because of its small velocity dispersion in the Fornax cluster Drinkwater, Gregg, and Colless (2001a), we speculate that there are spiral arms at SB level of 29 mag in north-west and south-east directions marked in the contours of the SB image (see Appendix 2.B.12). FCC306 lies in the beam of FCC308 and has been confirmed in a FLAIR observation with v = 915 ±15 km/s using emission lines (Schröder 1995).

2.A.12 FCC308

FCC308, also known as NGC 1437b, is an Sd galaxy, at a projected distance D_{core} = 0.3 deg to the bright dwarf galaxy FCC306, with an effective radius of 4.46 kpc. The structure of this galaxy is similar to that of FCC312. Sd galaxies are usually edge-on, with ill-defined spiral arms (Buta 2011). One can say that the uneven distribution of star forming regions can be accounted for the spiral arms loosely wound, as marked in the $g - i$ colour map of this galaxy (see Appendix 2.B.11). There is a lot of dust present in the central regions of this galaxy, which can be seen in the $g - i$ colour map as well as the $g - i$ colour profile, where the dust extinction can be recognised out in the regions between 2-20 arcsec of the central galaxy. Flares on the outskirts of the disc is clear because of the deep images of FDS (see Appendix 2.B.11).

2.A.13 FCC312

FCC312, is an Scd galaxy, with high stellar mass, detected in HI (Schröder, Drinkwater, and Richter 2001) and CO(1–0) (Zabel et al. 2019), and studied in FIR (250 μm, Fuller et al. 2014). It has an effective radius of 11.30 kpc and has been a topic of interest in the past, concerning its structure, molecular clouds and regions of star formation. The central regions show the traces of ongoing star formation, which can be seen in the $g - i$ colour profile. It is located at a projected distance D_{core} = 1.59 deg from the cluster centre. Being further away from the high-density regions of the central cluster, this galaxy shows the most extended disc (boxiness) which is visible in the azimuthally averaged SB images shown in Appendix 2.B.14. It has a Type III profile with a break radius of 6.91 kpc, around the same regions of star formation (see Appendix 2.B.14). The boxy shape of edge-on spiral galaxies is said to be related to the vertical distribution of light (Bureau and Freeman 1999). Although past research (e.g. Bureau and Freeman 1999) suggest that the presence of a boxy or peanut shaped bulge is due to the presence of a bar, this galaxy does not display a boxy bulge, but rather a boxy disc, with regions of high star formation surrounding the centre. The dust reddening of this galaxy makes the colour magnitude appear to be redder than bluer, and is clearly visible in the $g - i$ colour map of this galaxy (see Appendix 2.B.14). The extended tail of

the disc is at 25.6 mag/arcsec^2, which can be a sign of a recent minor merger event or due to instabilities caused in the disc.

2.B The sample: images and profiles

In this section, we show the g-band VST images of LTGs inside the virial radius of the Fornax cluster, surface brightness profile normalised to the effective radius, $g-i$ colour maps, $(g-i)$ deconvolved (black) and original profiles (grey). For ten of the galaxies with disc-breaks in our sample, we also mark the break radius on the g-band images in surface brightness (black dashed lines) and $(g-i)$ colour profiles (red dashed lines). For six galaxies that were detected in CO(1–0), we plot the CO contours (Zabel et al. 2019) in white.

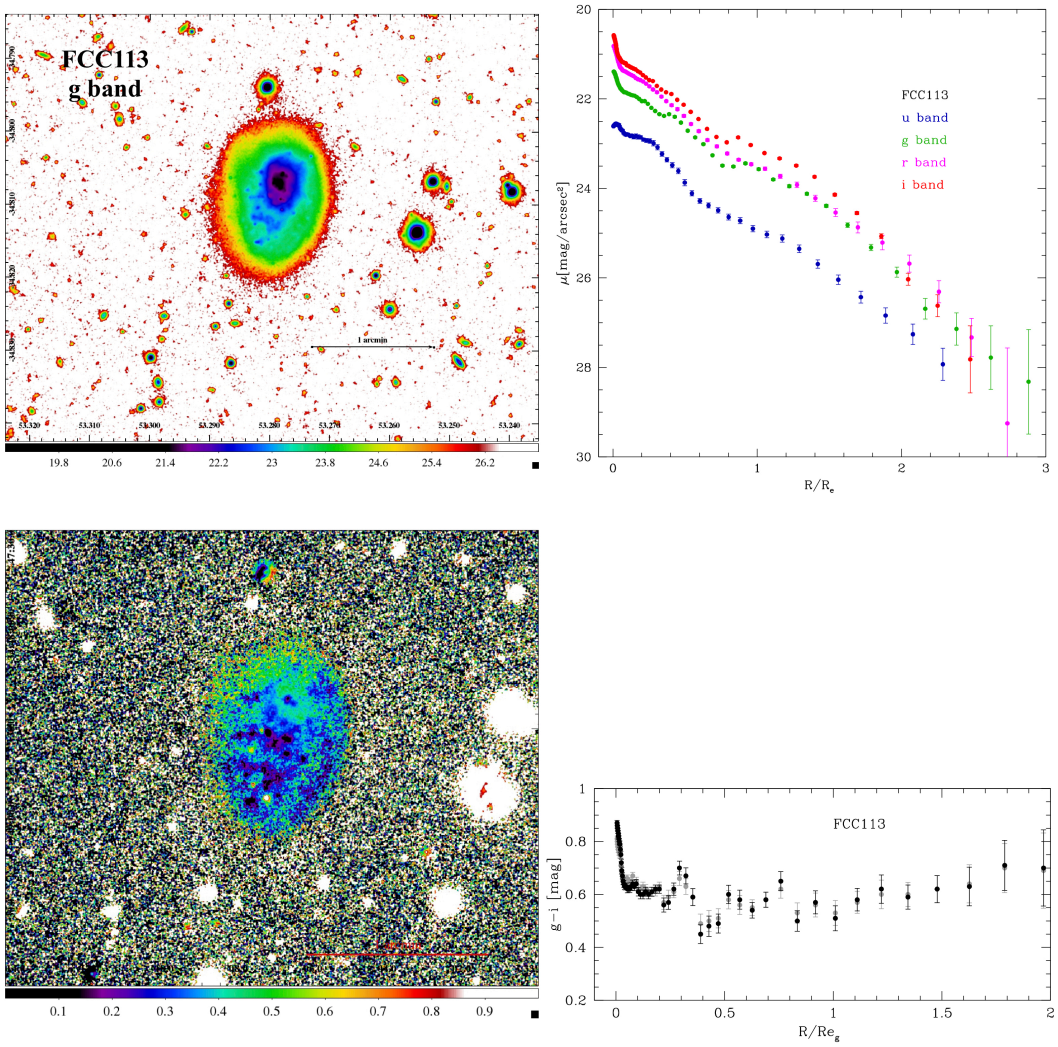


FIGURE 2.B.1: Surface photometry of FCC113

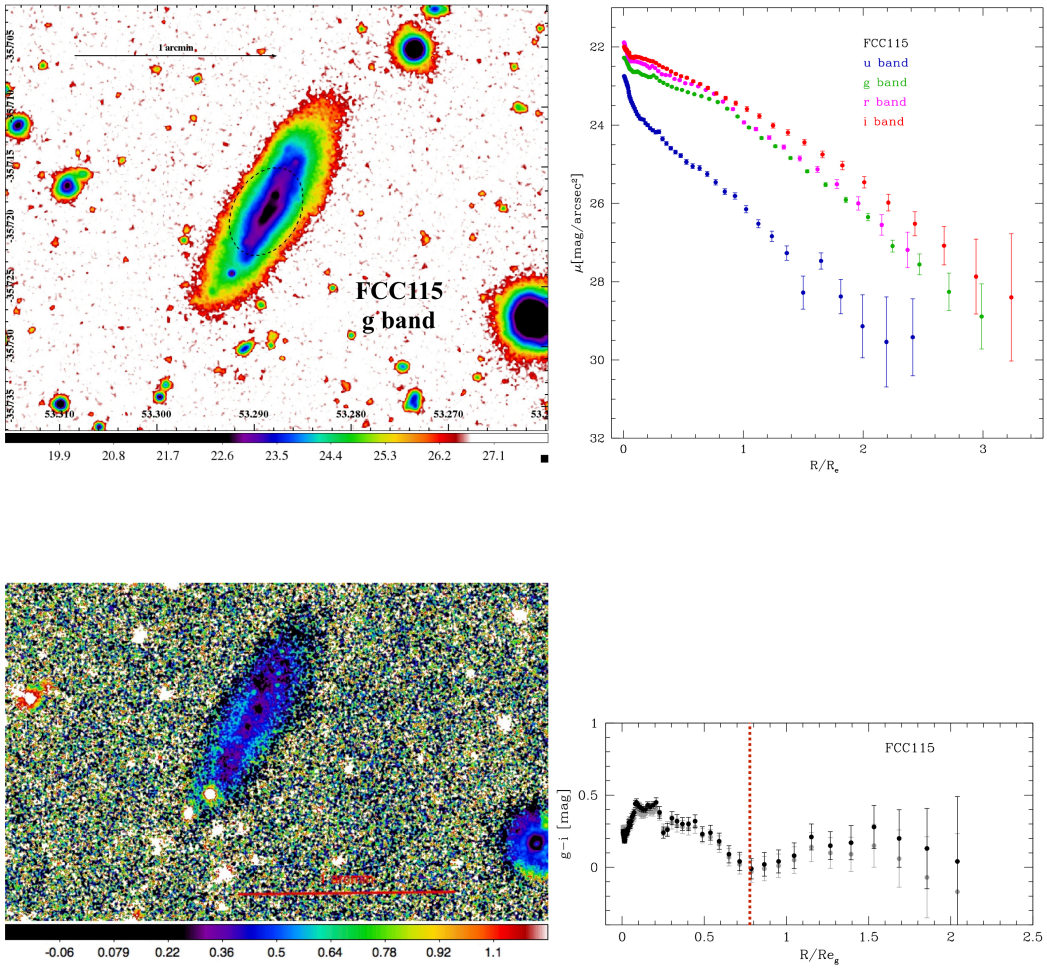


FIGURE 2.B.2: Surface photometry of FCC115. SB image: Black dashed lines represent the break radius (Type II). $(g - i)$ colour profile: Red dashed lines represent the break radius normalised to Re_g.

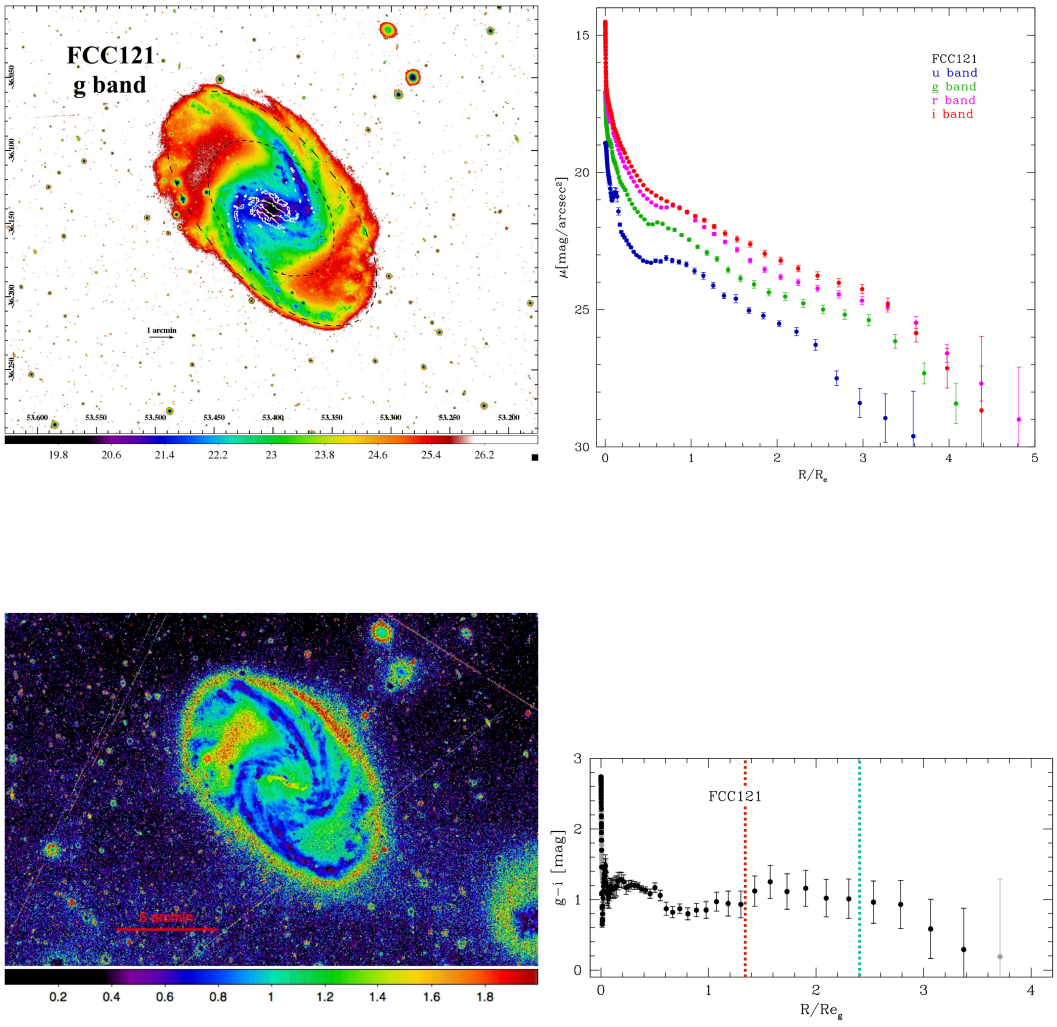


FIGURE 2.B.3: Surface photometry of FCC121. SB image: Black dashed lines represent the inner break radius (Type III) and outer break radius (Type II). CO(1–0) contours are in white. $(g - i)$ colour profile: Red dashed lines and cyan dashed lines represent the inner and outer break radii normalised to Re_g.

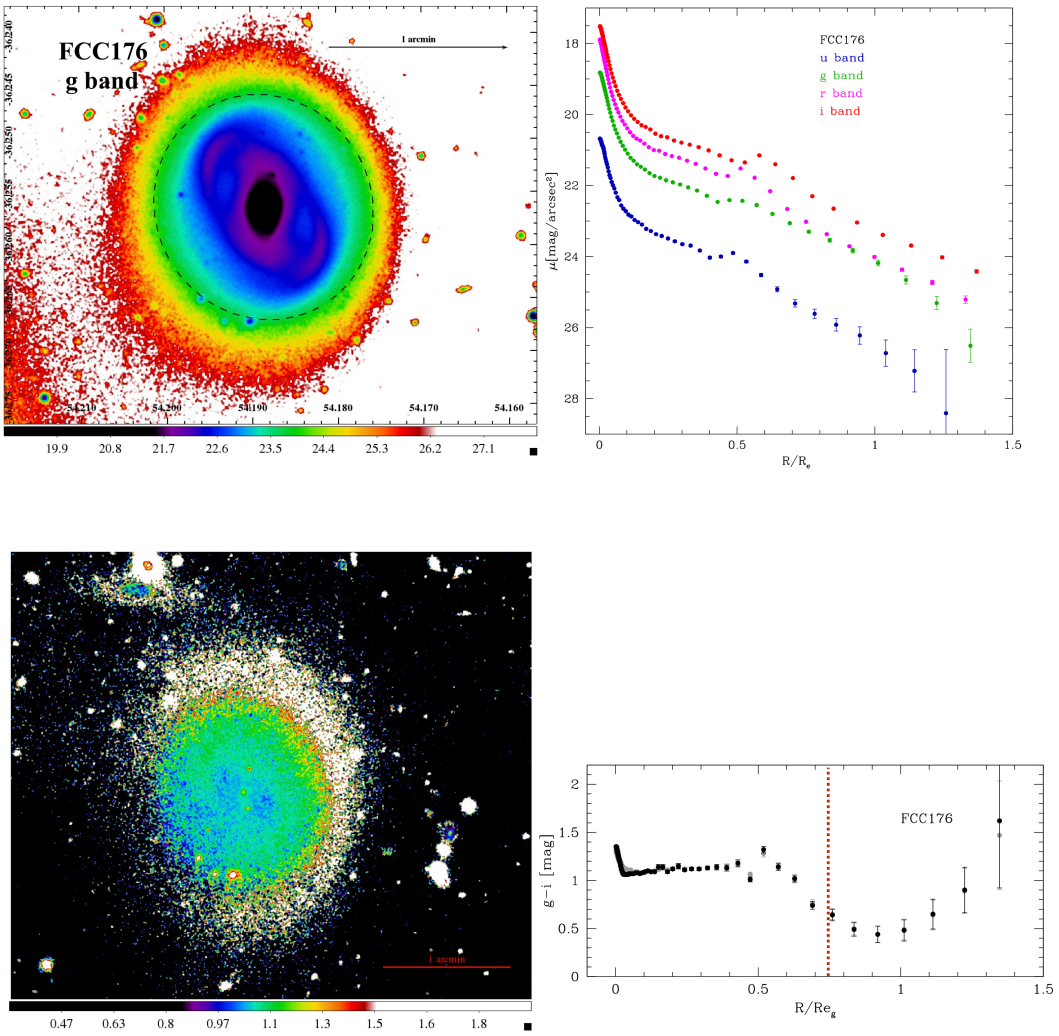


FIGURE 2.B.4: Surface photometry of FCC176. SB image: Black dashed lines represent the break radius (Type II). $(g - i)$ colour profile: Red dashed lines represent the break radius normalised to Re_g.

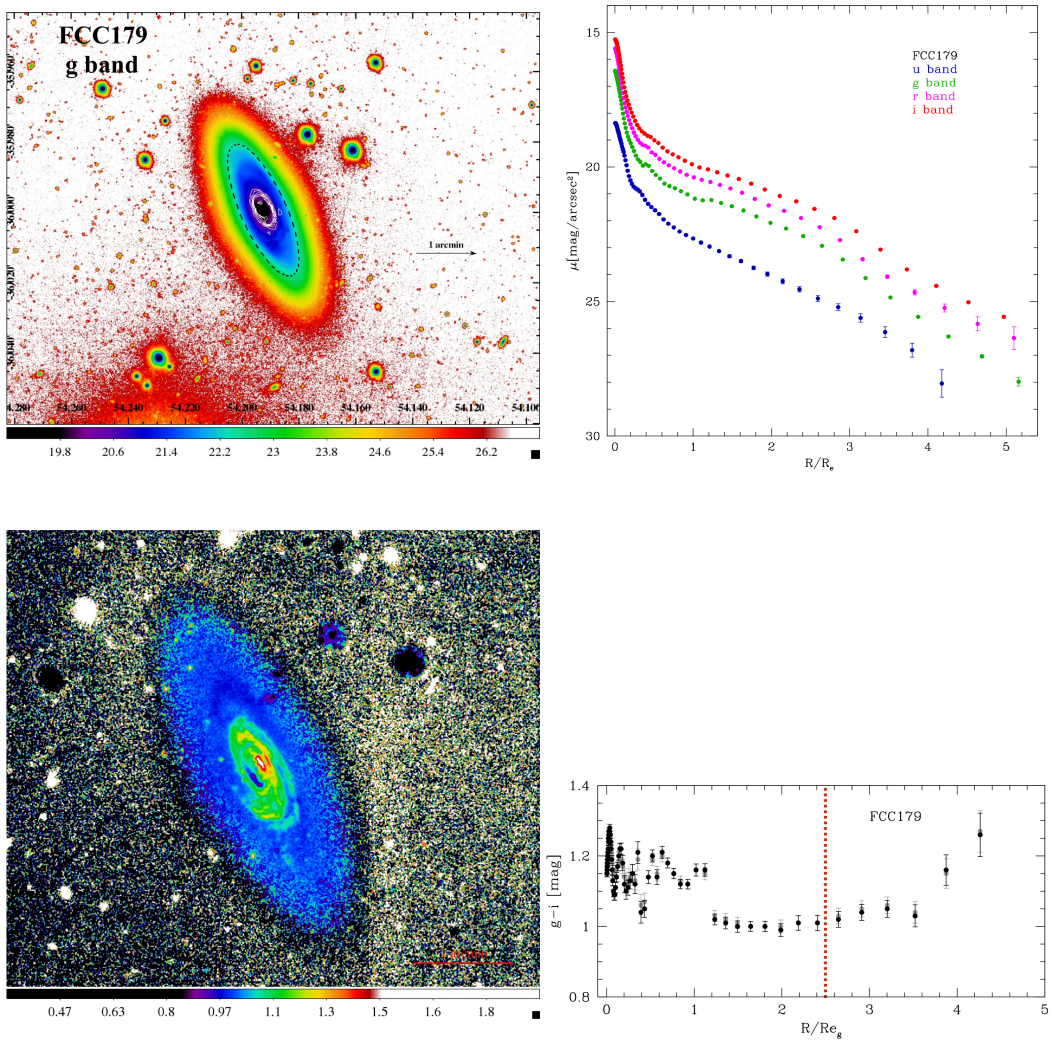


FIGURE 2.B.5: Surface photometry of FCC179. SB image: Black dashed lines represent the break radius (Type II). CO(1–0) contours are in white. $(g-i)$ colour profile: Red dashed lines represent the break radius normalised to Re_g.

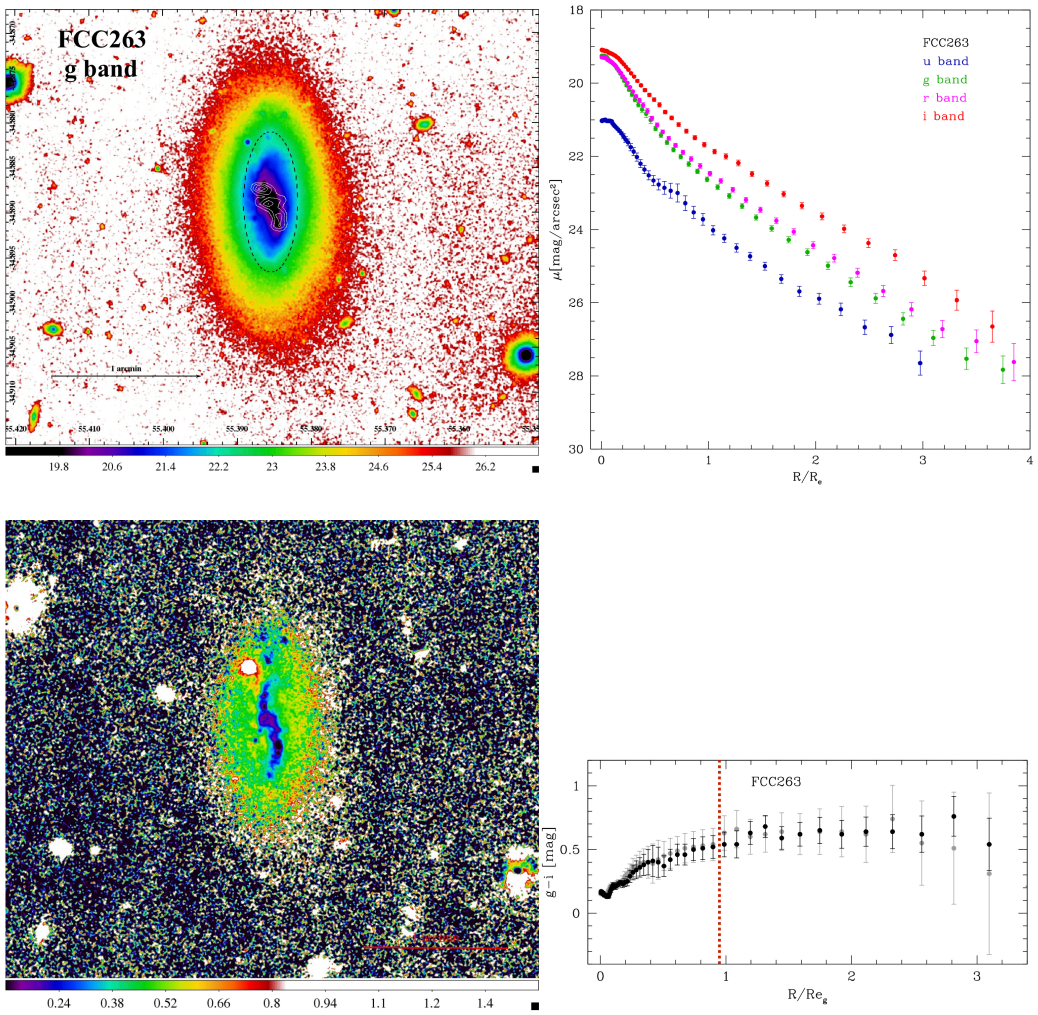


FIGURE 2.B.6: Surface photometry of FCC263. SB image: Black dashed lines represent the break radius (Type III). CO(1–0) contours are in white. $(g-i)$ colour profile: Red dashed lines represent the break radius normalised to Re_g.

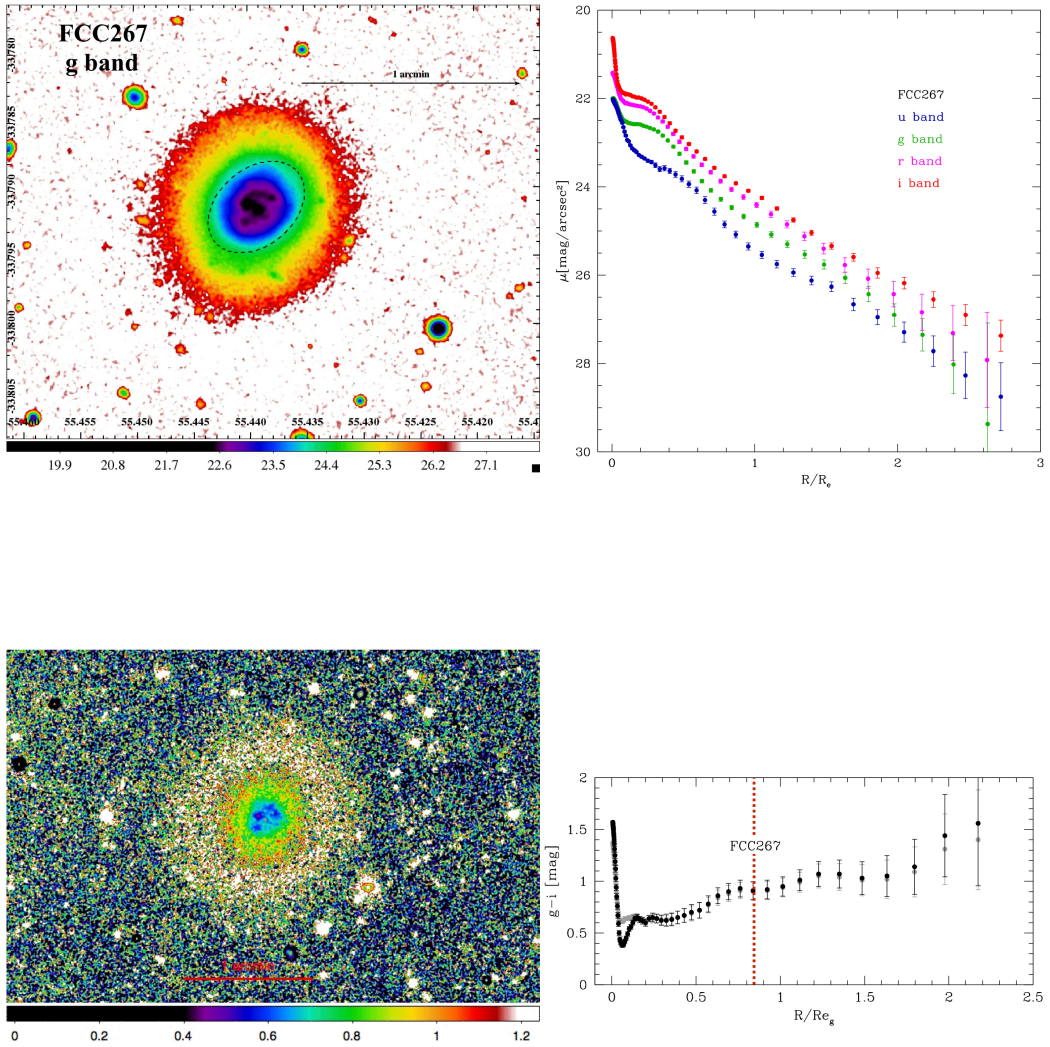


FIGURE 2.B.7: Surface photometry of FCC267. SB image: Black dashed lines represent the break radius (Type III). $(g-i)$ colour profile: Red dashed lines represent the break radius normalised to Re_g.

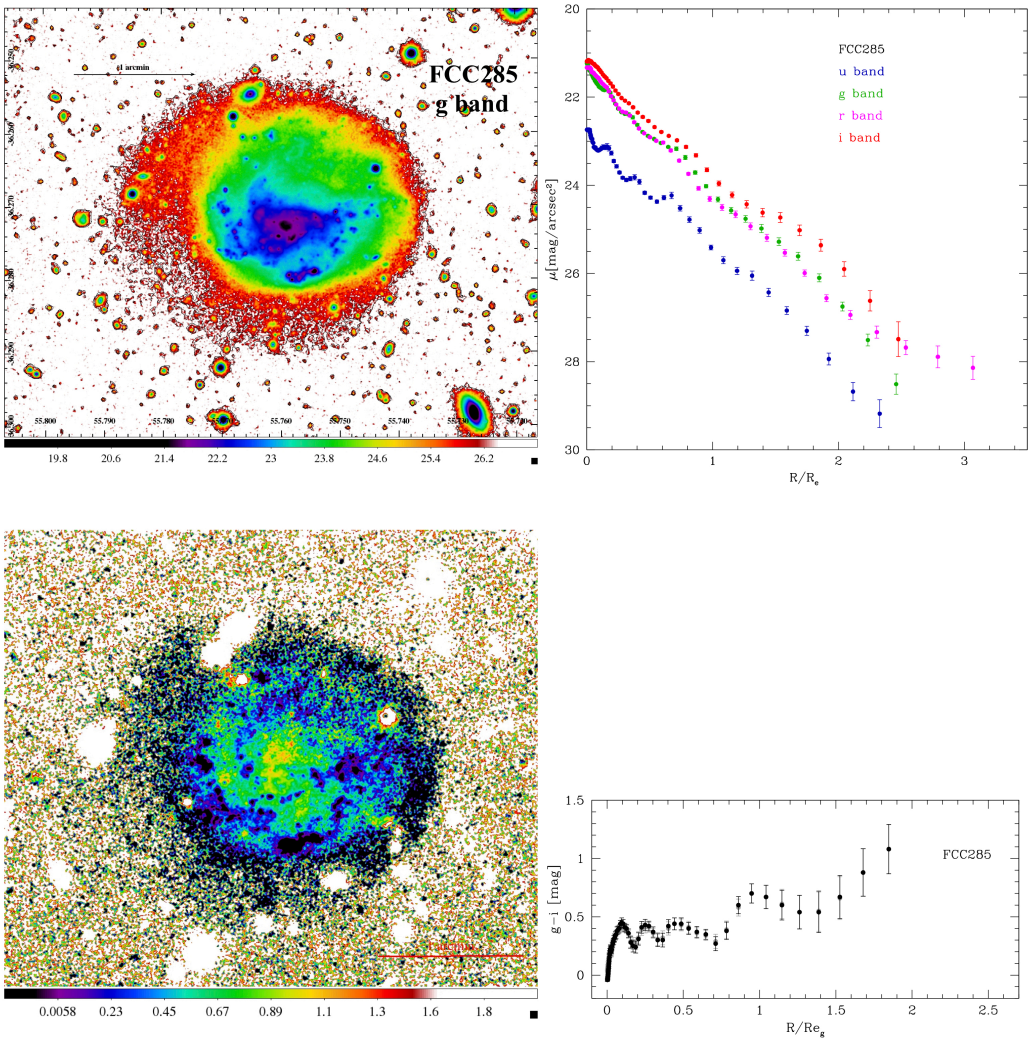


FIGURE 2.B.8: Surface photometry of FCC285.

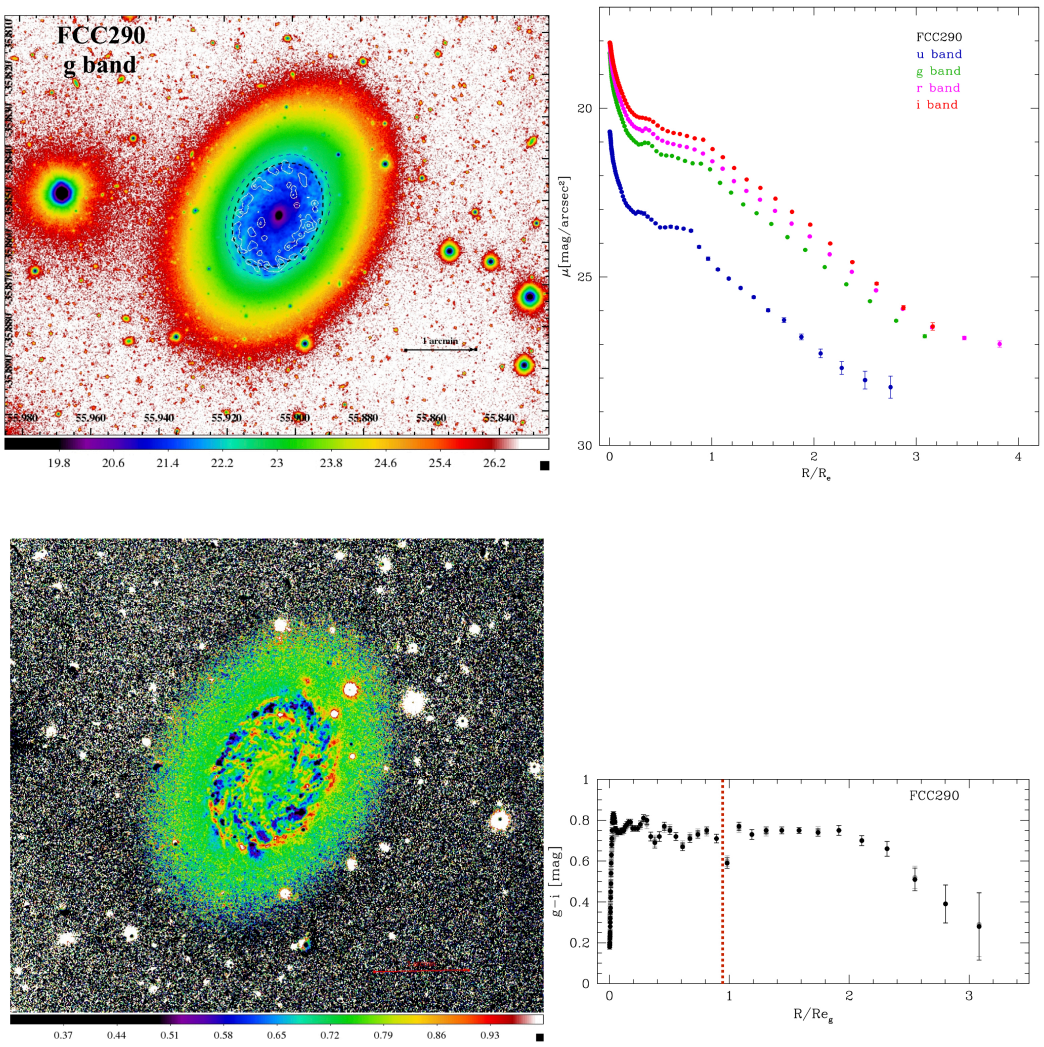


FIGURE 2.B.9: Surface photometry of FCC290. SB image: Black dashed lines represent the break radius (Type II). Blue dashed lines represent $B_r + 2\sigma$. CO(1–0) contours are in white. $(g - i)$ colour profile: Red dashed lines represent the break radius normalised to Re_g.

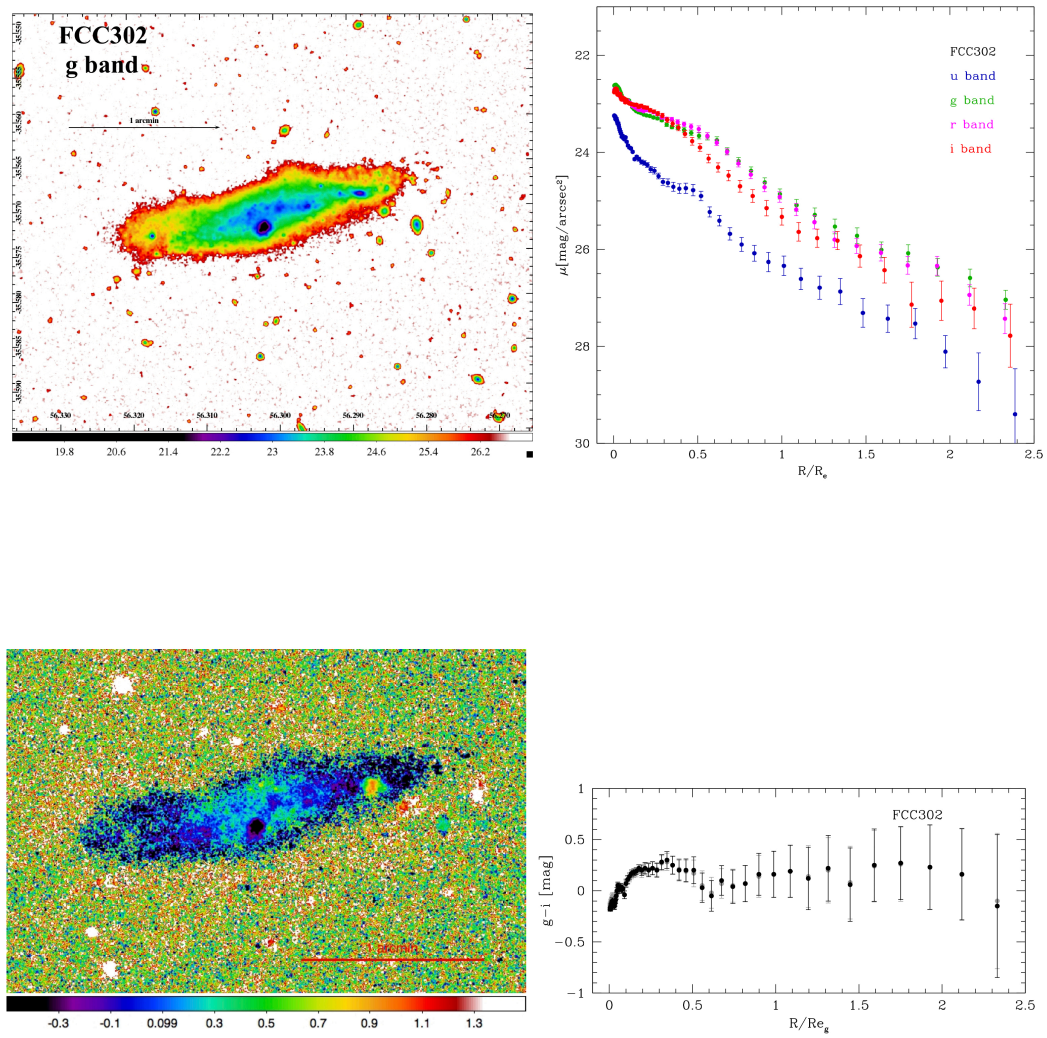


FIGURE 2.B.10: Surface photometry of FCC302.

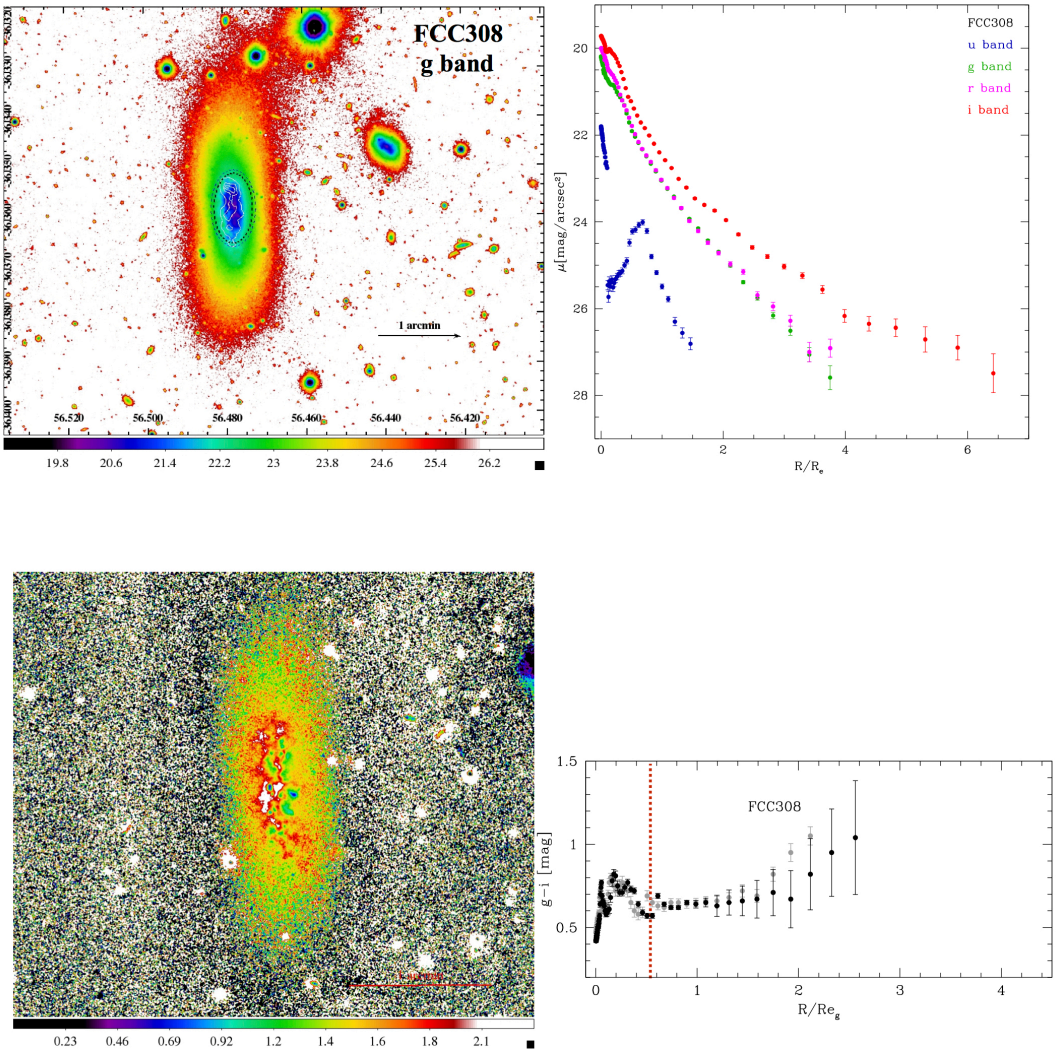


FIGURE 2.B.11: Surface photometry of FCC308. SB image: Black dashed lines represent the break radius (Type III) and blue dashed lines represent $B_r + 2\sigma$. CO(1–0) contours are in white. $(g - i)$ colour profile: Red dashed lines represent the break radius normalised to Re_g.

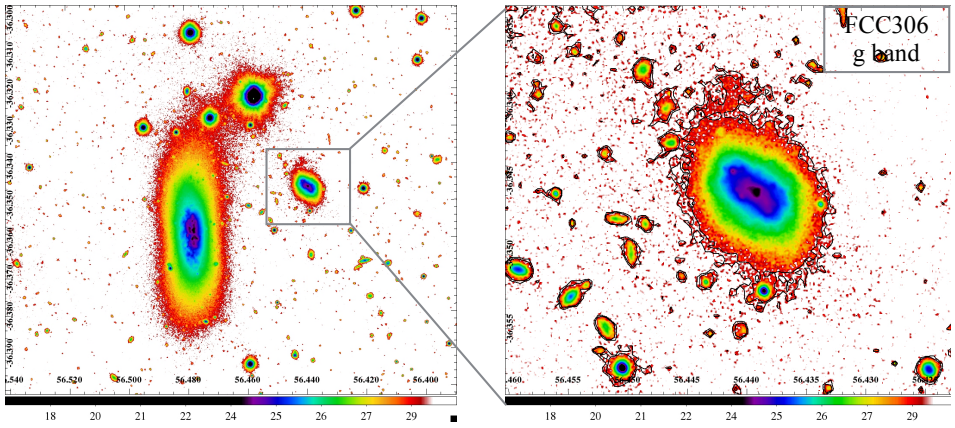
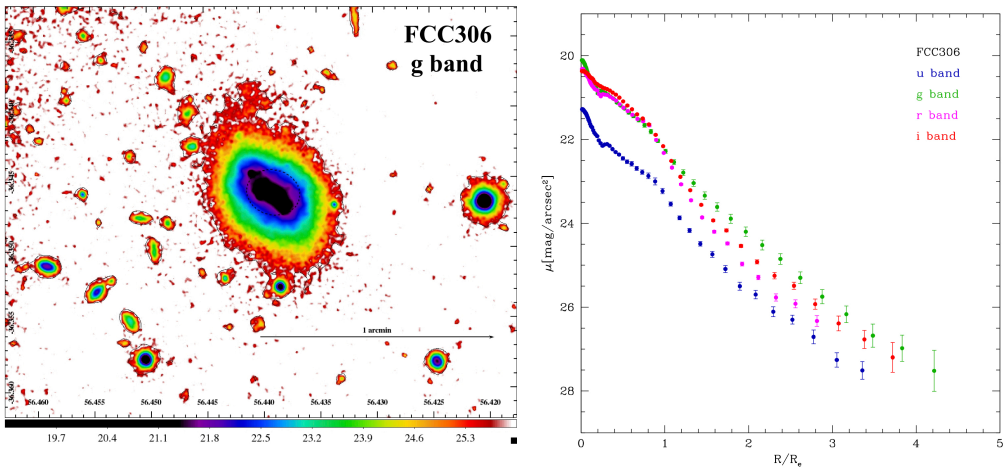


FIGURE 2.B.12: FCC306 in zoom



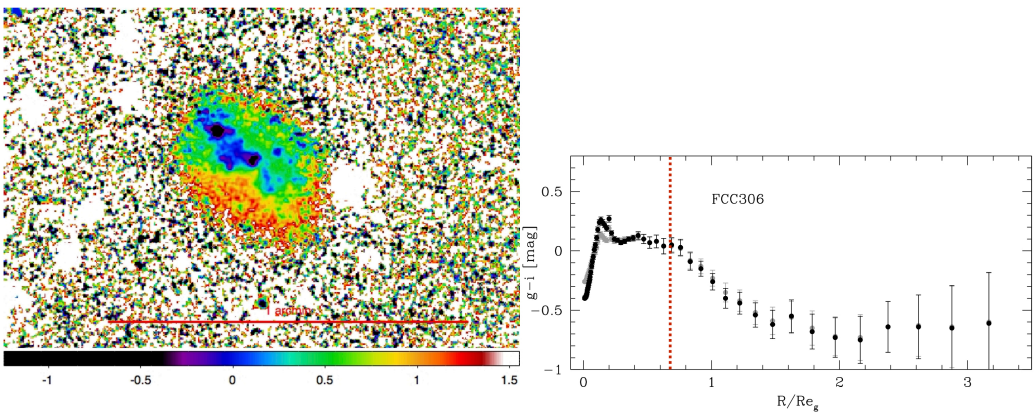


FIGURE 2.B.13: Surface photometry of FCC306. SB image: Black dashed lines represent the break radius (Type II). $(g-i)$ colour profile: Red dashed lines represent the break radius normalised to Re_g.

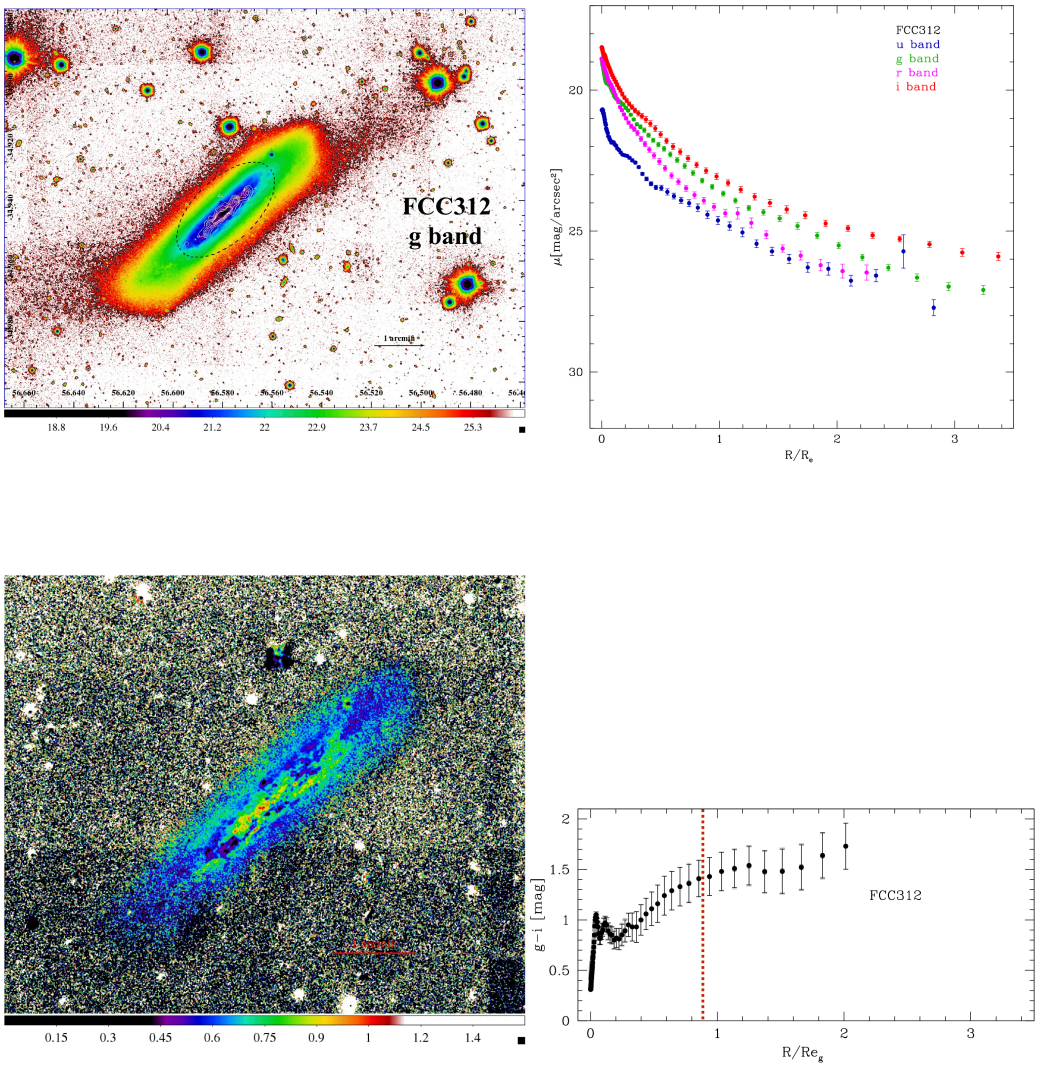


FIGURE 2.B.14: Surface photometry of FCC312. SB image: Black dashed lines represent the break radius (Type III). CO(1–0) contours are in white. $(g - i)$ colour profile: Red dashed lines represent the break radius normalised to Re_g.

2.C Methodologies

In this section, we show the results of the reliability test for the method of deconvolution we adopt, and the parameters of the best fit from the algorithm we developed for deriving break radii.

2.C.1 Reliability test

In order to test the reliability of the method of deconvolution we use, we adopt the method illustrated by Borlaff et al. (2017, hereafter B+17).

According to B+17, images are deconvolved using the following operation:

$$Residuals = Image\ raw - PSF * Model_{GALFIT} \tag{2.2}$$

$$Deconvolved\ image = Model_{GALFIT} + Residuals \tag{2.3}$$

Where $PSF * Model_{GALFIT}$ is the 2D model (with best-fitted parameters) convolved with the adopted PSF, obtained from `GALFIT3.0` (Peng et al. 2010a), and $Model_{GALFIT}$ is the 2D model obtained using the best fit parameters of the galaxy from $PSF * Model_{GALFIT}$, that is, the model of the galaxy without PSF convolution.

We apply this method to three of the galaxies in our sample: FCC179 and FCC290 (Type II with a second break) and FCC263 (Type III). For each of these galaxies, we use sersic+single exponential disc models to derive `GALFIT3.0` models with PSF convolution. We fix the parameters obtained from their $PSF * Model_{GALFIT}$ to extract another model, $Model_{GALFIT}$, that is, without PSF convolution. We then deconvolve the images using the above method. We extract the surface brightness profiles using ELLIPSE and (see Sect. 2.3) compare it with the method (LR algorithm) given by SP+17 (see Fig. 2.C.1). We derive the break radius from the aforementioned radial profiles. From Fig. 2.C.1, it is clear that our method of deconvolution (LR algorithm) is consistent with the above method, and that deconvolution does not affect the location of the primary break radius (within the σ_{nB_r}) as well as the break-type, as the break radius we estimate is within the regions unaffected by the PSF. In the case of FCC179 and FCC290, a possible secondary break radius occurs in the regions that are affected by the PSF, where the contribution of the scattered light is accounted for with deconvolution.

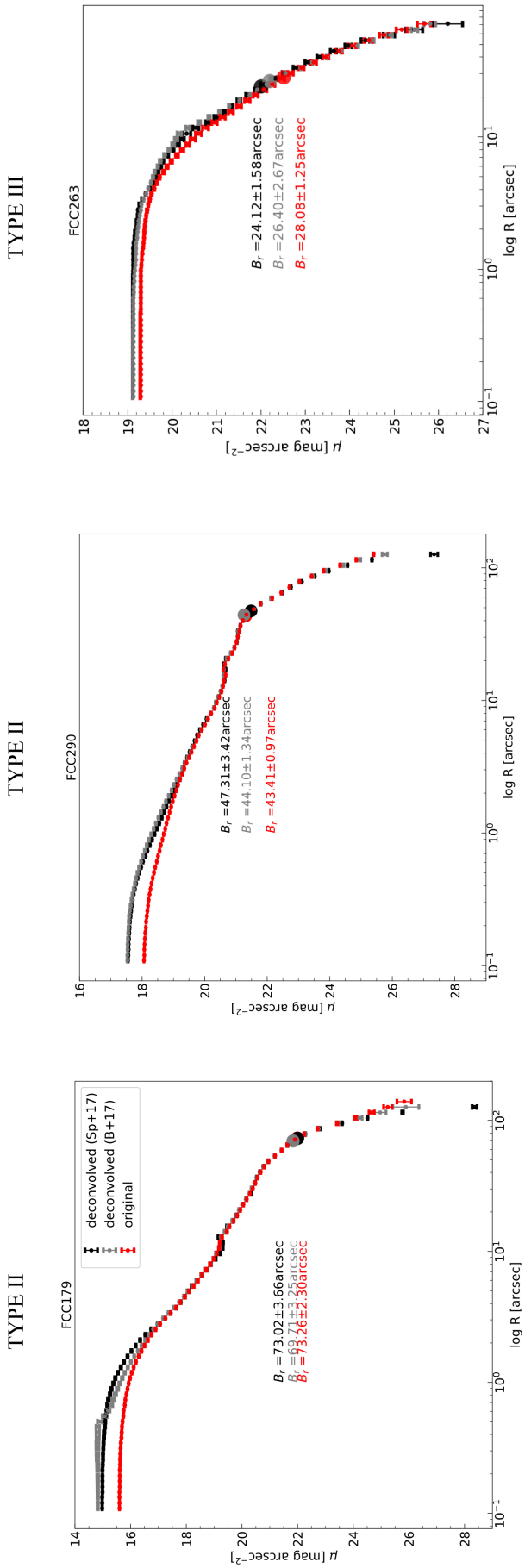


FIGURE 2.C.1: Deconvolved SB profiles using SP+17 method (black) and the method by Borlaff et al. (2017) (grey) overplotted on the original (red) profiles for Type II (FCC179 and FCC290) and Type III (FCC263).

2.C.2 Algorithm

Parameters of the best fit of LTGs with disc-breaks are given in Table. 2.C.1 with an example (FCC179) of the best fits produced by the algorithm shown in Fig. 2.C.2, 2.C.3, 2.C.4.

TABLE 2.C.1: **Parameters of the best fit of LTGs with disc-breaks, inside the virial radius.** *Col.1* - LTGs with disc-break; *Col.2* - slope of the fitted median model h_{in} and its corresponding *rms residuals*; *Col.3* - slope of the fitted median model h_{out} and its corresponding *rms residuals*

object	h_{in}		h_{out}	
	slope	*rms residuals*	slope	*rms residuals*
(1)	(2)		(3)	
FCC115	0.09 ± 0.03	0.02	0.11 ± 0.1	0.02
FCC121	0.02 ± 0.1	0.02	0.10 ± 0.2	0.07
FCC176	0.04 ± 0.1	0.09	0.06 ± 0.1	0.05
FCC179	0.04 ± 0.1	0.08	0.08 ± 0.7	0.23
FCC263	0.12 ± 0.1	0.08	0.07 ± 0.02	0.02
FCC267	0.17 ± 0.03	0.02	0.91 ± 0.03	0.02
FCC290	0.03 ± 0.1	0.07	0.05 ± 0.1	0.08
FCC306	0.20 ± 0.01	0.01	0.27 ± 0.1	0.08
FCC308	0.10 ± 0.1	0.05	0.05 ± 0.1	0.11
FCC312	0.05 ± 0.04	0.04	0.02 ± 0.1	0.06

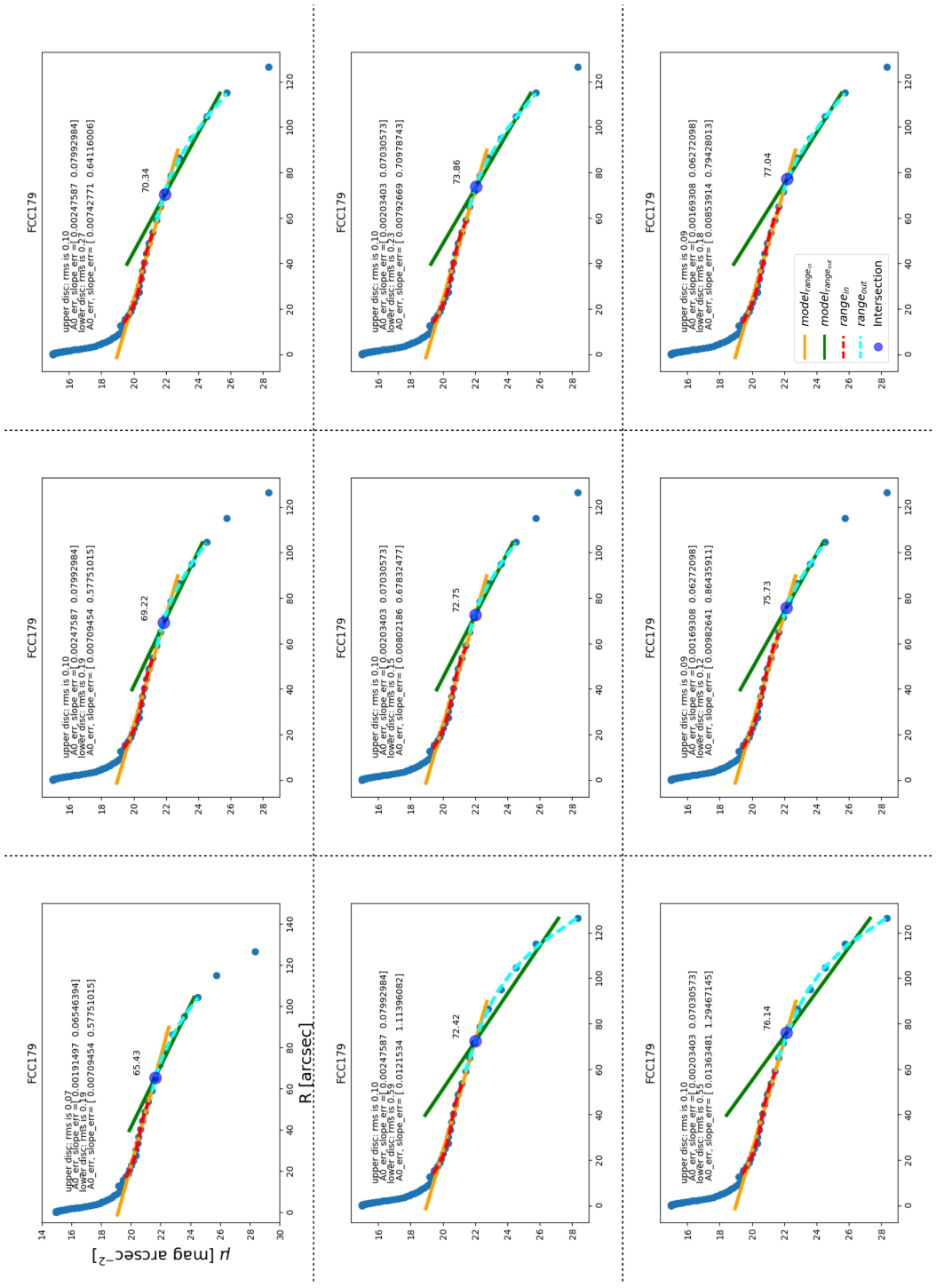


FIGURE 2.C.2: $(n+1)^3$ combinations of best fits on the inner and outer scale-lengths with minimal standard deviation, for FCC179 (here n =2). $range_{in}$ is represented with a red spline, and $range_{out}$ is represented with a cyan spline. $model_{range_{in}}$ is marked in orange, while $model_{range_{out}}$ is marked in green. The break radius is marked at the intersecting point. Rms residuals, errors of the intercept, and slope of the fitted models for the inner and outer discs are mentioned in each plot.

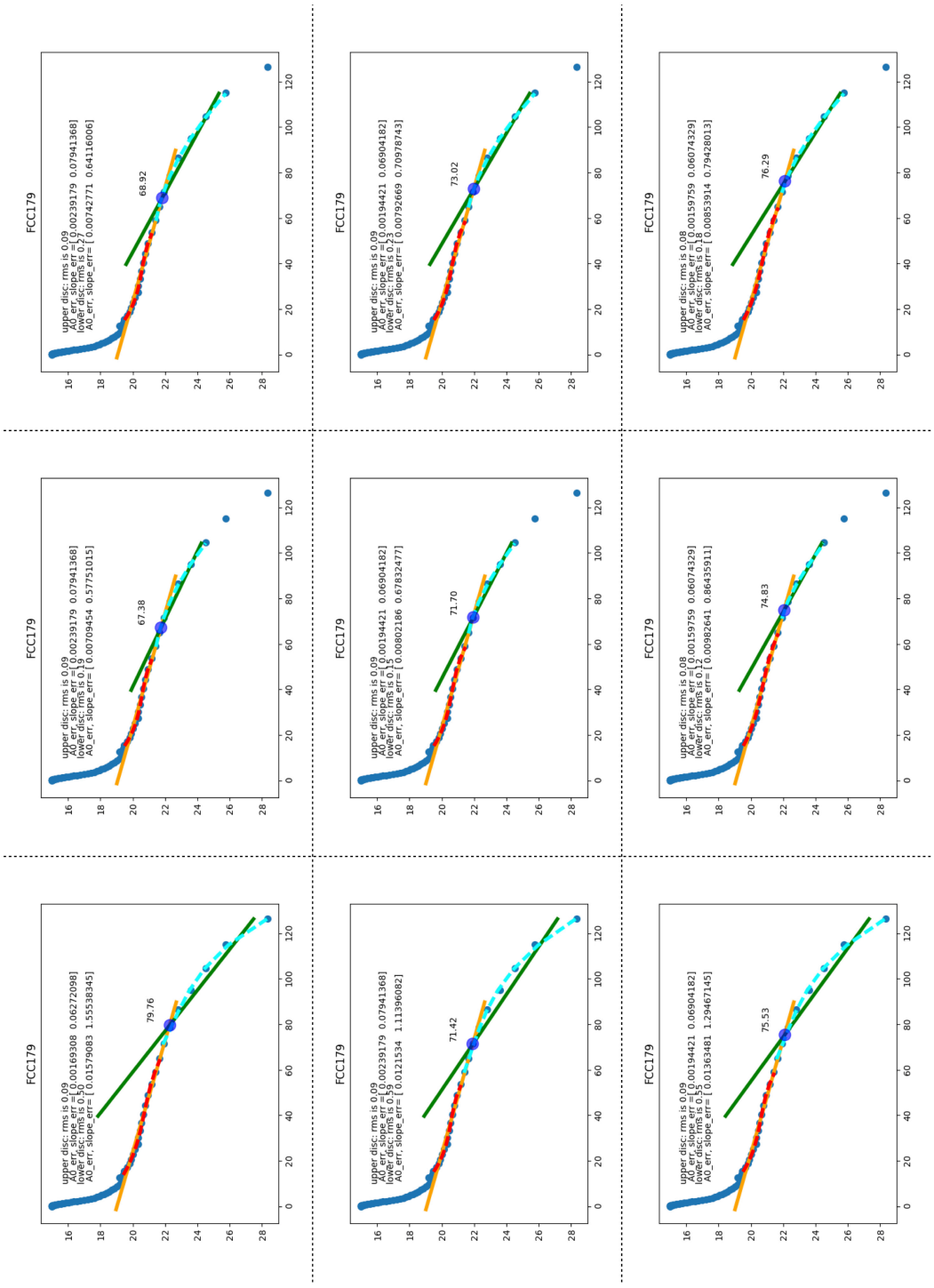


FIGURE 2.C.3: Appendix 2.C.2 continued.

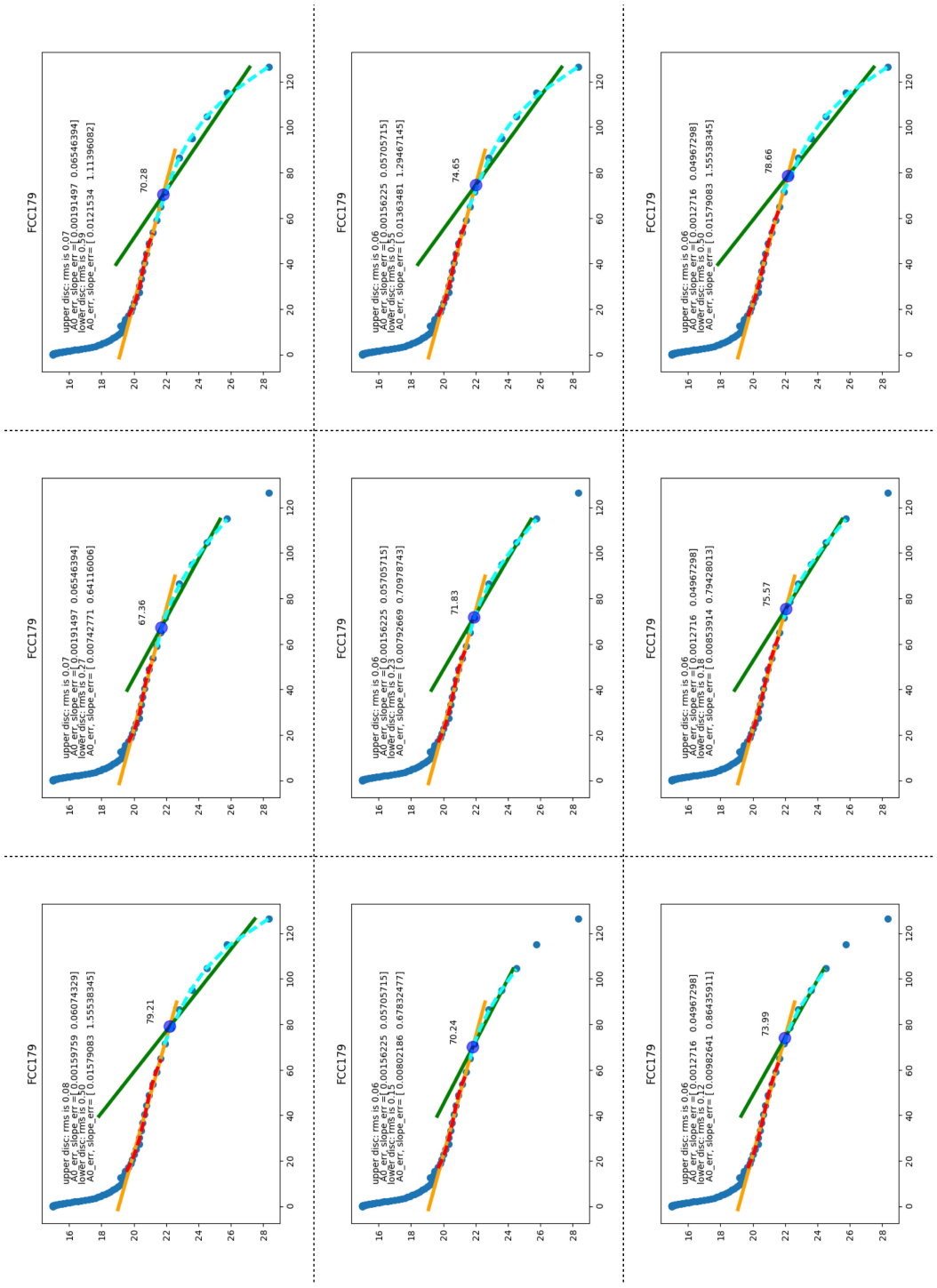


FIGURE 2.C.4: Appendix 2.C.2 continued.

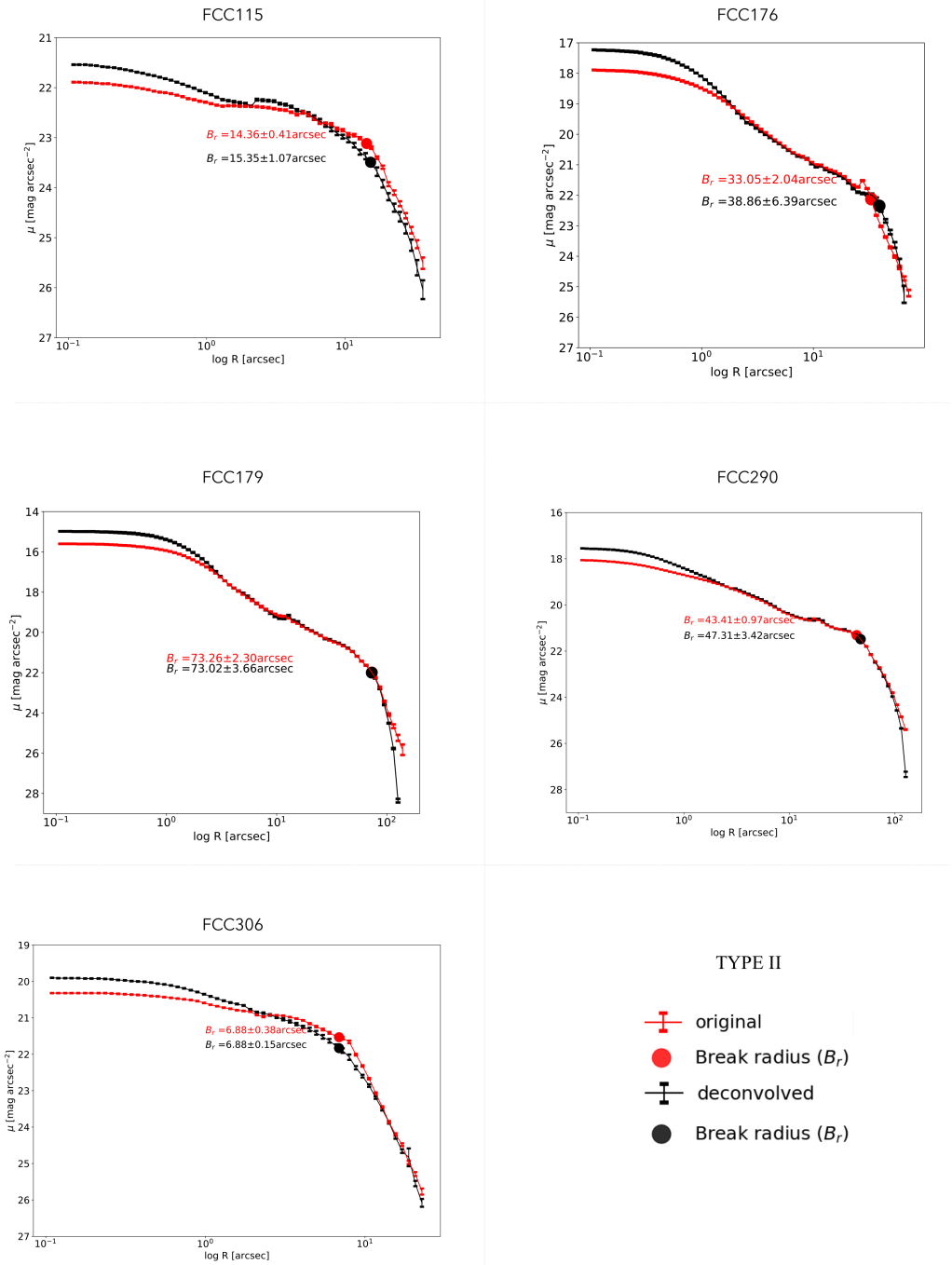


FIGURE 2.C.5: Type II deconvolved (black) and original (red) profiles in *r*-band with B_r marked in their corresponding colours of each profile.

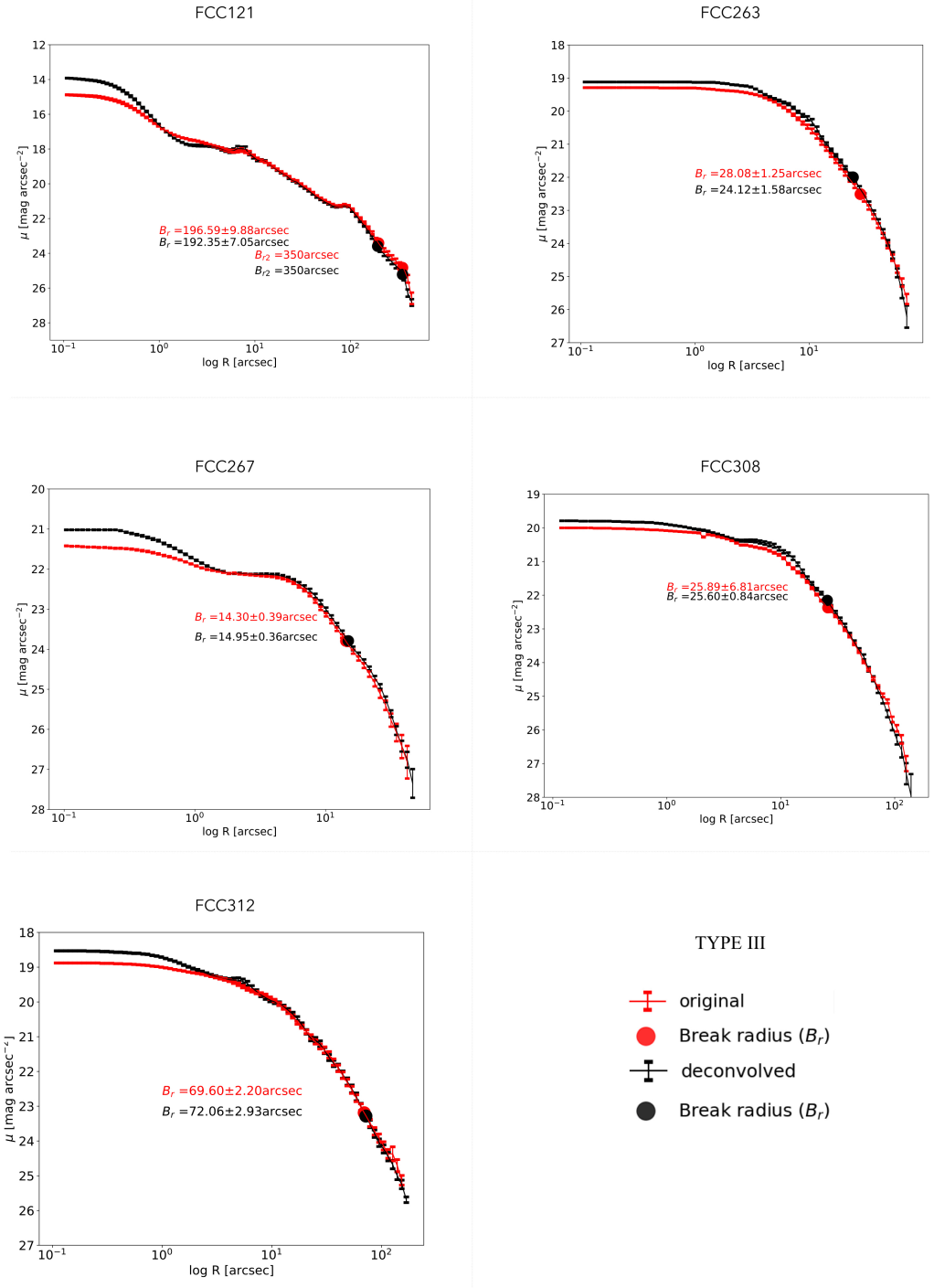


FIGURE 2.C.6: Type III (same as Fig. 2.C.5)

Chapter 3

On the assembly history of the bright galaxies in the Fornax A subgroup

This chapter is based on the paper:
Raj, M.A.; Iodice,E.; Napolitano,N.R.; Hilker, M.; Spavone,M.; Peletier,R.F.; Su,H.-S.; Falcon Barroso, J.; van de Ven, G.; Cantiello, M.; Kleiner. D; Venhola, A; Mieske, S.; Capaccioli, M.; Schipani, P.; *The Fornax Deep Survey with VST, X. On the assembly history of the bright galaxies and intra-group light in the Fornax A subgroup* , 2020, accepted to be published in Astronomy & Astrophysics.

Abstract

We present the study of the bright group members ($m_B < 16$ mag) in the south-west group of the Fornax cluster centred on the brightest group galaxy (BGG) Fornax A, observed as part of the Fornax Deep Survey (FDS). The main objective of this work is to investigate the assembly history of the Fornax A group and to compare its physical quantities as a function of the environment to that of the Fornax cluster core. For all galaxies, we extract the azimuthally averaged surface brightness profiles in three optical bands (g, r, i) by modelling the galaxy's isophotes. We derive their colour ($g - i$) profiles, total magnitude, effective radius in all respective bands, stellar mass, and the break radius in r-band. The majority of galaxies in the Fornax A group are late-type-galaxies (LTGs), spanning a range of stellar mass of $8 < log(M_* M_\odot) < 10.5$. Six out of nine LTGs show a Type-III (up-bending) break in their light profiles, which is either suggestive of strangulation halting star-formation in their outskirts or their HI-richness causing enhanced star-formation in their outer-discs. Overall, we do not find any correlations of their physical properties with group-centric distance. The Fornax A group appears to be in an early-stage of assembly with respect to the cluster core. The environment of the Fornax A group is not as dense as that of the cluster core, with all galaxies except the BGG showing similar morphology, comparable colours and stellar masses, and Type-III disc-breaks, without any clear trend of these properties with group-centric distances.

3.1 Introduction

Galaxies tend to gather in gravitationally bound systems during their evolution, which are seen as dense knots in the cosmic web filaments. In the local universe, it has been found that about half of the population of galaxies are found in groups and clusters (Karachentsev 2005). According to the hierarchical structure formation, these galaxy clusters are formed from merging of smaller structures like galaxy groups (e.g. Blumenthal et al. 1984; Sommer-Larsen 2006; Rudick et al. 2009). The terminology 'galaxy group' and 'galaxy cluster' depends on various factors e.g. the galaxy number density, the virial mass, X-ray luminosity, velocity dispersion. Groups of galaxies or poor clusters have masses in the range from 10^{13} to $10^{14} M_{\odot}$ (Bower and Balogh 2004; Mamon 2007), and rich clusters are more massive $> 10^{14} M_{\odot}$ (e.g. Bahcall 1996). In addition to this, the intracluster-medium (ICM) of rich clusters is hotter (X-ray temperature= 2–14 keV) than that of poor clusters and groups, and the radial velocity dispersion of galaxies in rich clusters is higher than that of groups (e.g. Bahcall 1988, 1996).

The definition of these gravitationally bound systems range from binary galaxies to superclusters, all of which are important in the studies of environmental mechanisms. Several surveys have shown variations in observed properties of galaxies in different environments i.e. from the field to the core of clusters in the local universe (e.g. Lewis et al. 2002; Kauffmann et al. 2004; Peng et al. 2010b; Grootes et al. 2017; Barsanti et al. 2018) and also at higher redshifts, up to $z \sim 1$ (e.g. Poggianti et al. 2008; Lubin et al. 2009; Cucciati et al. 2010; Cooper et al. 2012; Muzzin et al. 2012; Cucciati et al. 2017; Paulino-Afonso et al. 2018; Guglielmo et al. 2019). Such transitions in galaxy properties typically occur around cluster/group scales of $\sim$ 2–3 virial radii (Gómez et al. 2003). One such observed property is the decrease in star formation rate in galaxies of given morphological type in groups/clusters that is visible out to $2r_{200}$ (Lewis et al. 2002). The mechanisms causing such changes are proposed to depend on the local density of the environment and hence, they are different in groups and clusters.

The physical processes which are prominent in dense environments of clusters are ram-pressure stripping (Gunn and Gott 1972) and harassment (Moore et al. 1996). Ram-pressure stripping is not prevalent in poor clusters and galaxy groups as it depends on the velocity of the galaxy and the hot ICM. Mergers and strangulation are more common in groups of galaxies (e.g. Barnes 1985; Zabludoff and Mulchaey 1998). Major mergers can significantly alter the morphology of spiral galaxies by destroying their discs and therefore producing a major remnant that resembles an elliptical galaxy (Dekel et al. 2005). Sometimes, the disc can survive gas-rich mergers albeit resulting in the build-up of a galactic bulge (e.g. Stewart et al. 2009; Hopkins et al. 2010). On the other hand, disc-strangulation is a result of the tidal forces in the group/cluster that suppresses the infall of gas onto the discs of galaxies which in turn reduces star-formation (Larson, Tinsley, and Caldwell 1980b). The aforementioned processes that occur in groups of galaxies are most-effective when the velocity dispersion of the group is similar to that of

its galaxy members (Barnes 1985; Zabludoff and Mulchaey 1998).

Overall, high density environments provide a plethora of information for galaxy formation and evolution. There have been several studies on the effect of the environment on galaxy structures and properties in the local universe (e.g. Dressler 1980; Pastoriza et al. 1994; de Mello, Wiklind, and Maia 2002; Lewis et al. 2002; Gómez et al. 2003; Bower and Balogh 2004; Boselli et al. 2006; Mamon 2007; Huertas-Company et al. 2013; Tully et al. 2014; Deeley et al. 2017; Finn et al. 2018, and references therein) and at higher redshifts, up to $z \sim 1$ (e.g. Cooper et al. 2006; van der Wel et al. 2007; Tasca et al. 2009; Nantais et al. 2013; Kelkar et al. 2015; Allen et al. 2016; Krywult et al. 2017; Paulino-Afonso et al. 2019, and references therein).

As such, the Fornax cluster has been an environment of interest. It is the second most massive galaxy concentration within 20 Mpc, after the Virgo cluster, with a virial mass of $M_{\rm vir} = 7 \times 10^{13}$ $M_{\odot}$ (Drinkwater, Gregg, and Colless 2001a). The Fornax cluster has been extensively studied by several surveys in multiple wavelengths (e.g. Martin and GALEX Team 2005; Scharf, Zurek, and Bureau 2005; Jordán et al. 2007a; Davies et al. 2013; Muñoz et al. 2015; Su et al. 2017; Eigenthaler et al. 2018; Zabel et al. 2019; Serra et al. 2019).

The Fornax Deep Survey (FDS) with VST (described in Chapters 1 and 2) is one of the deepest and widest datasets mapping the Fornax cluster out to the virial radius ($\sim$ 0.7 Mpc). The analysis of the deep images from FDS suggests that the Fornax cluster is not completely relaxed inside the virial radius. The bulk of the gravitational interactions between galaxies takes place in the west-northwest core region, where most of the bright ETGs are located and where the intra-cluster baryons (i.e. diffuse light, GCs, and PNe) are found (Pota et al. 2018; Spiniello et al. 2018; Iodice et al. 2019a).

In this chapter, we focus on the SW Fornax A group using the FDS data in order to study the bright group members ($m_B < 16$ mag) and their physical properties as a function of the environment and thus, compare them with those observed for LTGs in the Fornax cluster. Maddox et al. (2019) presented a spectroscopic census of all the galaxies in the Fornax environment, covered by FDS which also includes background objects. Using this data, we are also able to study, and thus compare, the kinematics of the assembly history of the bright galaxies in the Fornax A subgroup to those of the core.

The outline of this chapter is as follows. In Sect. 3.2, we give a brief summary of FDS. In Sect. 3.3, we describe our methods of analysis along with the estimated parameters. In Sect. 3.4, we explain the results based on the surface photometry analysis. In Sect. 3.5, we address the assembly history of the bright galaxies in Fornax A. In Sect. 3.6, we compare the environments of the Fornax cluster core and Fornax subgroup. In Sect. 3.7, we summarise our results.

3.2 The Fornax Deep Survey: data

FDS data sample 26 deg^2 around the Fornax cluster, which also includes the in-falling Fornax A subgroup (Iodice et al. 2017b). Detailed explanations of the observing strategy and reduction are given by Iodice et al. (2016) and Iodice et al. (2017a) and Venhola et al. (2018). The FWHM (arcsec) and depth (mag/arsec^2) of the FDS fields in each filter (g, r, i), used in this work, are given in Tab. 3.2.1 (see also Venhola et al. 2018).

Catalogues and data products provided by FDS were presented by Venhola et al. (2018) on dwarf galaxies in the Fornax cluster, Iodice et al. (2019a) on photometry of ETGs, and Raj et al. (2019) (Chapter 2) on LTGs in the central 9 deg^2.

The g-band mosaic covering 3.6×2 deg ^{2} around NGC 1316 and the SW side of the Fornax cluster with named circles indicating the galaxies studied in this work, is shown in Fig. 3.2.1. In this image, we also mark all galaxies taken from the catalogue by Venhola et al. (2019) that are part of the Fornax A subgroup for the purpose of group-environmental analysis. The galaxies marked in Fig. 3.2.1 are grouped into giant LTGs ($m_B < 16$ mag), dwarf elliptical (dE), and dwarf late-type (dl) galaxies. The sample of spiral galaxies (m_B <16 mag) has been selected from Ferguson (1989) and are listed in Tab. 3.3.1.

TABLE 3.2.1: **Image quality of FDS fields used in this work.** *Col.1* -FDS fields ;*Col.2-Col.4* average seeing and rms of the FWHM, and surface brightness corresponding to 1σ S/N per arcsec^2 for g, r, i bands. The PSF FWHM and depth of each filter in all fields are adopted from Venhola et al. (2018).

Field	g band		r band		i band	
	$FWHM$ [arcsec]	depth [$\frac{mag}{arcsec^2}$]	$FWHM$ [arcsec]	depth [$\frac{mag}{arcsec^2}$]	$FWHM$ [arcsec]	depth [$\frac{mag}{arcsec^2}$]
(1)	(2)		(3)		(4)	
F22	1.04 ± 0.07	26.52	0.81± 0.05	25.90	0.85 ± 0.07	25.16
F25	1.11 ± 0.10	26.63	0.77± 0.06	25.84	0.85 ± 0.07	25.11
F26	0.93 ± 0.07	25.89	0.81± 0.05	25.96	0.91 ± 0.07	25.06
F27	1.07 ± 0.10	26.39	0.78± 0.06	25.63	0.89 ± 0.10	24.88
F28	1.08 ± 0.14	26.31	0.79± 0.06	25.57	0.92 ± 0.09	24.89

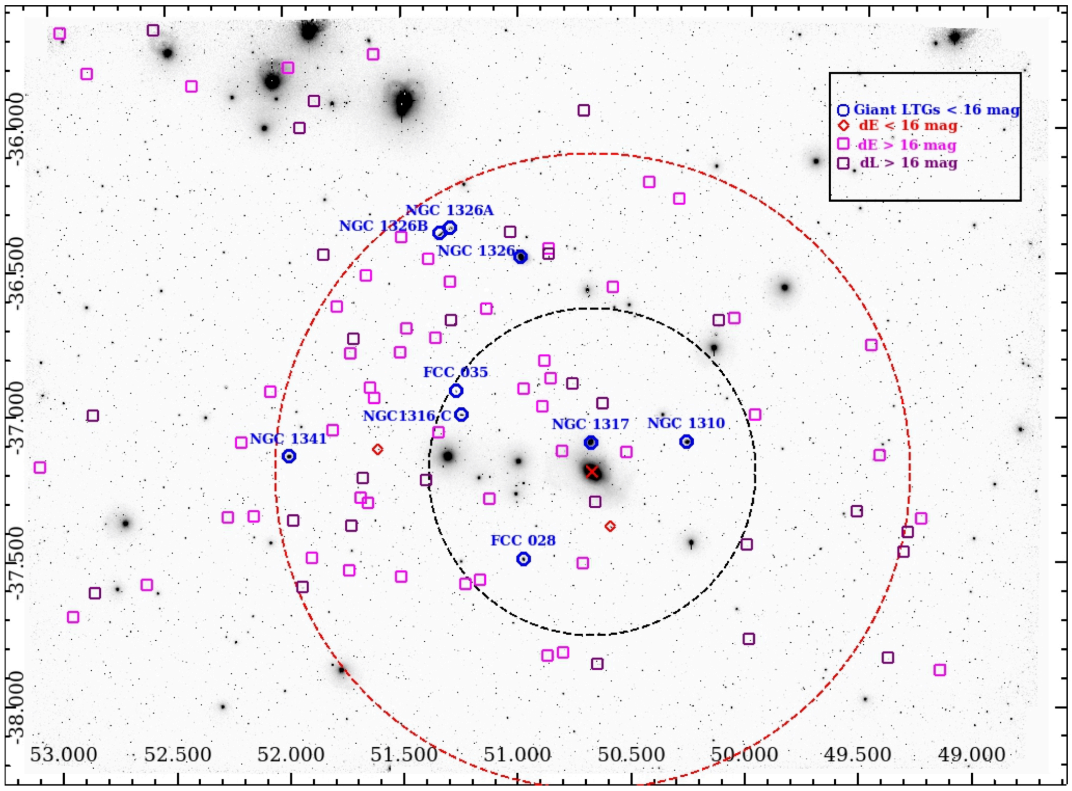


FIGURE 3.2.1: VST mosaic in g-band of the Fornax A subgroup covering 3 $\times$ 2 sq. deg. The red dashed circle is an approximate measure of the virial radius of the group, which is $\sim$1 deg^2 (Drinkwater, Gregg, and Colless 2001b). The black dashed circle (r= 0.58 deg) is the region where the intra-group light is estimated (discussed in Chapter 4). All galaxies part of the Fornax cluster and Fornax A subgroup, taken from Venhola et al. (2019) are indicated. The red cross indicates NGC 1316. Bright galaxies (m_B <16 mag) are represented with blue circles. Red diamond represents dE (m_B < 16 mag), pink squares represent dE (m_B > 16 mag), and purple squares represent LTGs (m_B > 16 mag).

3.3 Analysis

In this section, we briefly describe the procedures to derive galaxy parameters. We adopt the methods presented in Chapter 2 (see also Iodice et al. 2019a). Results for individual galaxies of the sample are given in Appendix 3.A.

TABLE 3.3.1: **LTGs brighter than $m_B < 16$ mag in the Fornax A subgroup.** *Col.1* - Fornax A subgroup members from Ferguson (1989); *Col.2 & Col.3* - Right Ascension and Declination; *Col.4* - Morphological type from Ferguson (1989); *Col.5* - Heliocentric radial velocity obtained from NED; *Col.6* - total magnitude in *B* band as given in NED *Col.7* - Location in the FDS Field; *Col.8* - Alternative catalogue names

FCC name	α	δ	Morph. type	radial velocity	m_B	FDS Field	Alternative names
	h:m:s	d:m:s		km/s	mag		
(1)	(2)	(3)	(4)	(5)	(6)	(7)	(8)
FCC013	03 21 03.4	-37 06 06	SBcII	1805	12.55	F28	NGC 1310, ESO 357- G 019
FCC022	03 22 44.3	-37 06 13	Sa pec	1941	11.91	F26	NGC 1317, ESO 357- G 023
FCC028	03 23 54.2	-37 30 33	SmIII	1405	13.88	F26	ESO 301-IG 011
FCC029	03 23 56.4	-36 27 53	SBa(r)	1360	12.20	F25	NGC1326, ESO 357- G 026
FCC033	03 24 58.4	-37 00 34	SdIII pec	1800	14.32	F26	NGC 1316C, ESO 357- G 027
FCC035	03 25 04.2	-36 55 39	SmIV	1800	15.3	F26	
FCC037	03 25 08.5	-36 21 50	SBcIII	1831	13.77	F25	NGC 1326A, ESO 357-IG 028
FCC039	03 25 20.3	-36 23 06	SdIII	999	13.59	F25	NGC 1326B, ESO 357- G 029
FCC062	03 27 58.4	-37 09 00	SbcII	1876	13.21	F22	NGC 1341, ESO 358- G 008

3.3.1 Isophote fitting

The azimuthally averaged surface brightness (SB) profiles of each source were extracted in three bands (g, r, i) using the IRAF task ELLIPSE[14] (Jedrzejewski 1987). As preliminary steps to the isophote fitting, we have masked all bright sources (e.g. galaxies, stars) that are close to the galaxies in the sample. In some cases, for galaxies that are close in projection to each other (NGC 1326A and NGC 1326B; NGC 1316 and NGC 1317), we adopted an iterative process by modelling the neighbouring source using the BMODEL task in IRAF. This model is created from the results of the isophotal analysis (ELLIPSE) and then subtracted from the original image. In the fitting routine, we adopted the k-sigma clipping algorithm for cleaning deviant sample points at each annulus[15].

Isophotes are fit in elliptical annuli, starting from the centre[16] of the galaxy to the edge of the FDS field ($\sim$ 0.5 deg). Since most of the galaxies have dust absorption and/or irregular shape close to their center, we keep the geometrical centre fixed, while the position angle and ellipticity are free parameters. According to Iodice et al. (2016), the intensity profiles are then

TABLE 3.3.2: **Limiting radius of intensity profiles.** *Col.1* - Fornax A group members from Ferguson (1989); *Col.2*- Limiting radius in r-band ; *Col.3*- Surface brightness at the limiting radius.

object	R_{lim}	μ
	arcsec	mag/arcsec^2
(1)	(2)	(3)
FCC013 (NGC 1310)	120.5	27.07$\pm$ 0.3
FCC022 (NGC 1317)	132.5	25.26$\pm$0.5
FCC028	99.57	27.24$\pm$0.2
FCC029 (NGC 1326)	213.4	25.82$\pm$0.5
FCC033 (NGC 1316C)	109.5	27.48$\pm$0.8
FCC035	82.29	27.68$\pm$0.5
FCC037 (NGC 1326A)	145.8	27.66$\pm$0.5
FCC039 (NGC 1326B)	160.4	27.22$\pm$0.4
FCC062 (NGC 1342)	145.8	28.16$\pm$0.6

used to derive (i) the limiting radius (R_{lim}) that corresponds to the outer-most

[14]IRAF is distributed by the National Optical Astronomy Observatories, which are operated by the Association of Universities for Research in Astronomy, Inc., under cooperative agreement with the National Science Foundation

[15]Overall, the manual masking, 3σ clipping and model-subtraction improve the isophotal fitting, ensuring the rejection of unmasked sources and defects.

[16]In the dust-free galaxies, the centre corresponds to the intensity peak. If the galaxy light is strongly affected by the dust absorption, we adopted the geometric centre of the isophotes.

annulus (see Tab. 3.3.2), where the light of the source blends into the average background level (it is the residual after subtracting the sky frame resulting in a value close to zero); (ii) derive the residual sky background of each source from their outer annuli in three respective bands. The limiting radius and the residual background levels are locally estimated for each galaxy in the sample. The background levels are computed at $R \geq R_{lim}$ as the average counts out to the edge of the image.

3.3.2 Products: total magnitude, effective radius, colours, stellar mass

For each galaxy of the sample we derive the 'total magnitude', 'effective radius' R_e, average '$g-i$' and '$g-r$' colours following the method presented by Iodice et al. (2019a) and Chapter 2 (Raj et al. 2019). All parameters are presented in Tab. 3.3.3.

1. Intensity profiles from the output of the isophote fit are used to derive azimuthally averaged SB profiles. The residual background level estimated at $R \geq R_{lim}$ of each band for all galaxies is subtracted. We also take into account the uncertainties on the photometric calibration and sky subtraction in the estimation of errors on magnitudes (see Capaccioli et al. 2015; Iodice et al. 2016; Iodice et al. 2019a).

2. $g-i$ colour profiles and colour maps are derived for all galaxies in the sample. They are shown in Appendix 3.B.

3. We derive total magnitudes and effective radii in g, r, i bands of all galaxies in our sample using the growth curve from the isophote fits.

4. We estimate the stellar mass M_* using the empirical relation from Taylor et al. (2011) which assumes a Chabrier IMF i.e. $log_{10}\,\frac{M_*}{M_\odot}$ = 1.15 + 0.70$(g-i)$- 0.4M_i. Here M_i is the absolute magnitude in i-band, $g-i$ is the average colour derived in the previous step. We then estimate the stellar mass-to-light ratio M_*/L_i with 1σ accuracy of 0.1 dex (see Taylor et al. 2011). The estimated parameters are shown in Tab. 3.3.4.

3.3.3 Products: break radius, scale-lengths, disc colours

Using the algorithm developed by Raj et al. (2019) (see Chapter 2), we derive the break radius B_r, inner and outer scale-lengths (h_{in} and h_{out}) [17] from the deconvolved SB profiles in r-band. The $(g-i)$ colours of the scale-lengths (h_{in} and h_{out}) are also derived from deconvolved SB profiles. The deconvolution method is briefly described in the following.

In the process of detecting disc-breaks, we make sure to account for the effect of the point spread function (PSF). This is to avoid false detection of disc-breaks as a result of the scattered light from a galaxy's bright core in the regions around them. We first measure the PSF out to the galaxy's disc and

[17] The disc scale-length refers to the region of the disc before and after the break radius.

TABLE 3.3.3: **Derived Parameters of LTGs in Fornax A subgroup.** *Col.1* - Fornax A subgroup members from Ferguson (1989); *Col.2 to Col.4* - Total magnitude in the g, r and i bands respectively, derived from the isophote fit. Values were corrected for the galactic extinction, using the absorption coefficient by Schlegel, Finkbeiner, and Davis (1998); *Col.5 to Col.7* - Effective radius in the g, r and i bands respectively, derived from the isophote fit.

object	m_g	m_r	m_i	Re_g	Re_r	Re_i
	mag	mag	mag	arcsec	arcsec	arcsec
(1)	(2)	(3)	(4)	(5)	(6)	(7)
FCC013 (NGC 1310)	12.48 ± 0.04	11.91 ± 0.02	11.58 ± 0.03	27.59 ± 0.2	29.44 ± 0.1	33.78 ± 0.7
FCC022 (NGC 1317)	11.15 ± 0.01	10.38 ± 0.01	10.16 ± 0.01	35.36 ± 0.03	31.1 ± 0.1	38.41 ± 0.1
FCC028	13.33 ± 0.02	12.76 ± 0.02	12.35 ± 0.03	22.12 ± 0.5	24.1 ± 0.5	34.05 ± 0.8
FCC029 (NGC 1326)	10.62 ± 0.02	10.0 ± 0.02	9.61 ± 0.02	47.9 ± 1.1	39.95 ± 0.9	39.41 ± 0.3
FCC033 (NGC 1316C)	13.81 ± 0.03	13.12 ± 0.03	12.84 ± 0.01	22.56 ± 0.5	24.11 ± 0.4	20.07 ± 0.2
FCC035	14.79 ± 0.03	14.62 ± 0.03	14.61 ± 0.02	17.15 ± 0.4	18.86 ± 0.4	13.1 ± 0.2
FCC037 (NGC 1326A)	13.55 ± 0.03	13.04 ± 0.1	12.60 ± 0.1	41.0 ± 0.8	48.2 ± 0.9	66.05 ± 2.5
FCC039 (NGC 1326B)	12.87 ± 0.1	12.55 ± 0.1	12.14 ± 0.1	53.03 ± 1.7	51.1 ± 1.7	67.07 ± 3.1
FCC062 (NGC 1341)	12.37 ± 0.02	11.89 ± 0.02	11.42 ± 0.02	20.64 ± 0.4	21.28 ± 0.4	37.0 ± 0.8

then the PSF is characterised from the VST images so that the broadening effect of the seeing on the galaxies is taken into account (Capaccioli et al. 2015). In Chapter 2, we showed how the effect of the PSF can affect the SB profiles of galaxies of various sizes (also see Capaccioli et al. 2015). We then deconvolve galaxies with the PSF, using the Lucy-Richardson algorithm (Lucy 1974; Richardson 1972).

We briefly explain the main steps of the algorithm used to derive the break radius.

1. The disc regions are determined from the 1D multi-component (bulge and disc) fits explained in Appendix. 3.C (the multi-component best fits are shown in Fig. 3.C.1 and the corresponding best fit parameters are listed in Tab. 3.C.1) . The starting point is the intersection between the bulge and disc components. The regions are provided to the algorithm to define inner disc limit $range_{in}$ and outer disc limit $range_{out}$, within R_{lim}.

2. The algorithm produces $(n+1)^2$ best linear fits by varying $range_{in}$ and $range_{out}$, and $(n+1)^3$ estimates of the break radius, where $n = 2$ in both cases.

3. The median of the $(n+1)^3$ intersecting points is chosen as the final break radius B_r, and the standard deviation of the $(n+1)^3$ estimates is given as sigma σ_{nB_r} on the estimation of the break radius.

4. Through iterations[18] of the previous steps, a minimal standard deviation of the $(n+1)^3$ break radii is obtained which in turn provides the best selection of the disc scale-lengths h_{in} and h_{out}.

5. The average $(g-i)$ colours of the inner and outer discs are derived for the regions h_{in} and h_{out}.

The break radius (in arcsec and kpc) of six galaxies along with σ_{nB_r}, surface brightness at the break μ_{B_r}, and average $(g-i)$ colour for the components h_{in} and h_{out} are listed in Tab. 3.3.5. Fitting results are shown in Fig. 3.3.1.

[18]The number of iterations varies for each galaxy with a minimum of five until a minimal standard deviation of the $(n+1)^3$ break radii is obtained.

TABLE 3.3.4: **Stellar mass estimates of LTGs in the i -band.** *Col.1* - Fornax A subgroup members from Ferguson (1989); *Col.2*- Projected distance from the galaxy centre in degree, i.e. from NGC 1316 (FCC021); *Col.3*- Absolute magnitude in r-band, derived using the distance modulus from NED and Tully et al. (2009); *Col.4* - Effective radius (kpc) in i-band;*Col.5 & 6*- Average $g-r$ and $g-i$ colours ; *Col.7 & Col. 8*- Stellar mass and mass-to-light (M/L) in i-band.

object	D_{core}	M_i	R_e	$g-r$	$g-i$	M_*	M/L
	deg	mag	kpc	mag	mag	$10^{10}M_\odot$	
(1)	(2)	(3)	(4)	(5)	(6)	(7)	(8)
FCC013 (NGC 1310)	0.254	-19.74	3.4	0.57 ± 0.1	0.9 ± 0.1	0.47	0.76
FCC022 (NGC 1317)	0.025	-20.98	3.9	0.77 ± 0.02	0.99 ± 0.02	1.71	0.88
FCC028	0.28	-19.07	3.4	0.57 ± 0.04	0.98 ± 0.05	0.29	0.87
FCC029 (NGC 1326)	0.68	-21.53	4.0	0.62 ± 0.04	1.01 ± 0.04	2.94	0.91
FCC033 (NGC 1316C)	0.37	-18.3	2.0	0.69 ± 0.1	0.97 ± 0.04	0.14	0.85
FCC035	0.44	-17.39	1.3	0.17 ± 0.1	0.18 ± 0.1	0.017	0.24
FCC037 (NGC 1326A)	0.868	-18.54	6.7	0.51 ± 0.1	0.95 ± 0.1	0.17	0.83
FCC039 (NGC 1326B)	0.865	-19.00	6.8	0.32 ± 0.1	0.73 ± 0.1	0.18	0.58
FCC062 (NGC 1341)	0.92	-19.72	3.7	0.54 ± 0.04	1.01 ± 0.04	0.55	0.91

TABLE 3.3.5: **Parameters of LTGs with a disc break.** *Col.1* - LTGs with a disc break; *Col.2* - Break Radius in units of arcsec and kpc (1 arcsec = 0.101 kpc); *Col.3* - Standard deviation of the break radii from $(n+1)^3$ combinations; *Col.4*- Surface brightness at the break radius; *Col.5* - inner scale-length in units of arcsec, and average $g-i$ colour for h_{in}; *Col.6*- outer scale-length in units of arcsec, and average $g-i$ colour for h_{out}; *Col.7*- Profile classification; *Col.8*- Hubble stage T taken from Drinkwater et al. (2001).

object	B_r		σ_{nB_r}	μ_{B_r}	h_{in}		h_{out}		Hubble	Break
	[arcsec]	[kpc]	[arcsec]	$[\frac{mag}{arcsec^2}]$	[arcsec]	$g-i$ [mag]	[arcsec]	$g-i$ [mag]	Type (T)	Type
(1)	(2)		(3)	(4)	(5)		(6)		(7)	(8)
FCC013(NGC 1310)	76.8	7.8	3.7	25.01	54.2	0.83±0.03	43.7	1.27 ± 0.1	III	5
FCC022(NGC 1317)	-		-	-	-	-	-		I	1
FCC028	38.8	3.9	1.6	23.60	24.0	0.83 ± 0.1	60.8	0.87 ± 0.1	III	9
FCC029(NGC 1326)	53.6	5.4	1.5	21.82	24.76	0.92 ± 0.1	159.8	0.68 ± 0.03	III	1
FCC033(NGC 1316C)	-		-	-	-	-	-		I	7
FCC035	27.6	2.8	0.3	23.94	25.64	-0.57 ± 0.02	34.2	-0.93 ± 0.1	III	9
FCC037(NGC 1326A)	-		-	-	-	-	-		I	5
FCC039(NGC 1326B)	95.5	9.6	8.2	25.01	94.9	0.52 ± 0.02	37.0	0.88 ± 0.2	III	7
FCC062(NGC 1341)	52.3	5.3	2.3	24.03	38.9	0.78± 0.02	68.2	0.86 ± 0.03	III	4

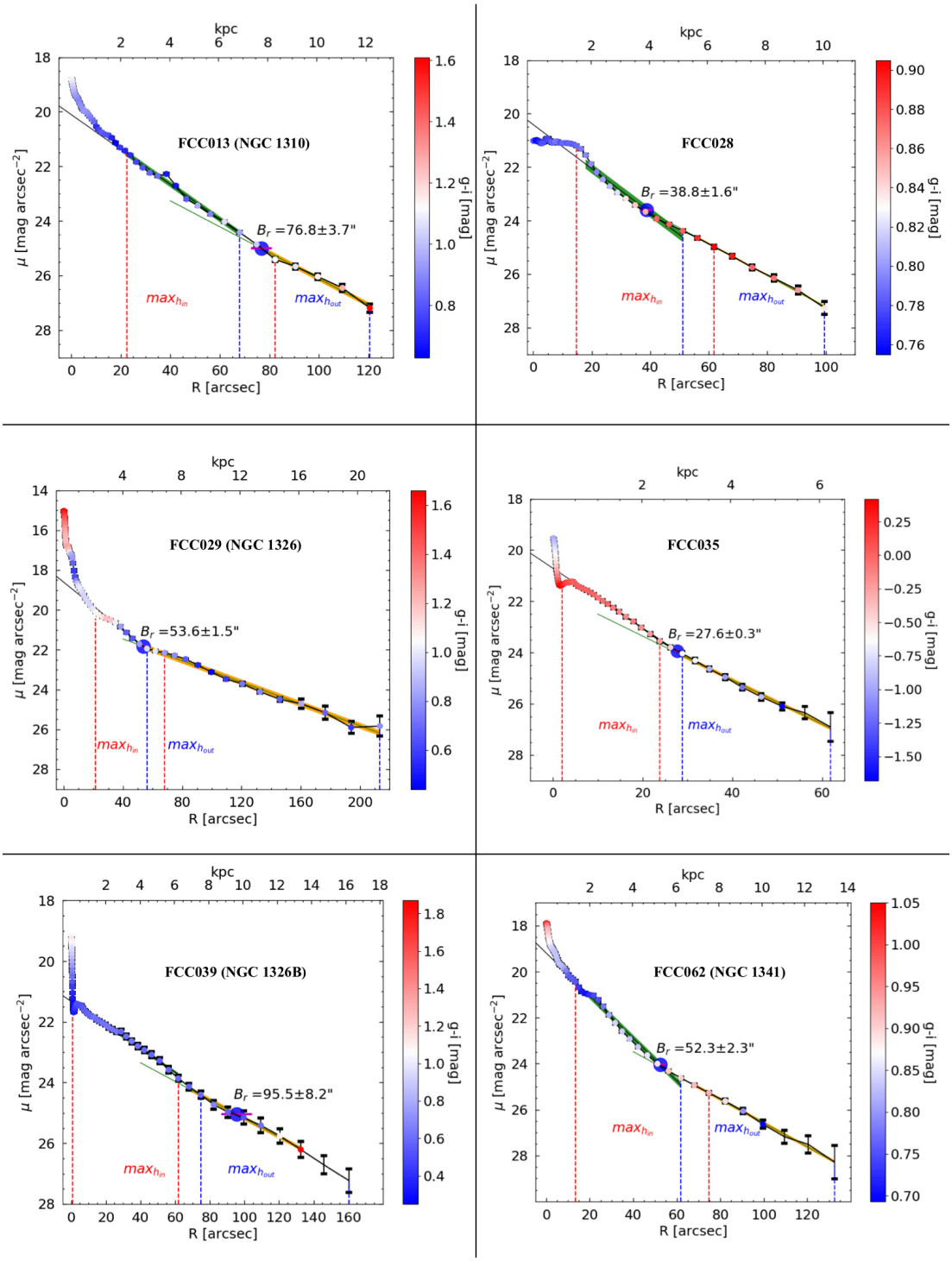


FIGURE 3.3.1: Surface brightness profiles of galaxies with Type III disc break, with $(g-i)$ colour as a third parameter. In each plot, the break radius (B_r) is marked at the intersecting point of the linear fits performed between h_{in} and h_{out}, with σ_{nB_r} as the median of $(n+1)^3$ combinations of best fits on the inner and outer scale-lengths. The vertical dashed lines ($max_{h_{in}}$ and $max_{h_{out}}$) indicate the regions for $max_{range_{in}} = range_{in} \pm n$ and $max_{range_{out}} = range_{out} \pm n$ where the algorithm produces $(n+1)^2$ linear least square fits. The shaded regions on h_{in} and h_{out} indicate the median of the rms of the residuals for $(n+1)^2$ linear least square fits.

3.4 Results

3.4.1 Morphology and colour analysis of galaxies in the Fornax A subgroup

The Fornax A subgroup is populated with bright ($m_B < 16$ mag) LTGs and only one giant peculiar ETG i.e. NGC 1316 as its central galaxy. Most of the bright galaxies ($> 75\%$) in the sample are located in the north-east (NE) side of the Fornax A group. Whitmore 1993 showed that in low-density environments, the galaxy population is dominated by LTGs. In Fig. 3.4.1, we plot the morphological stage parameter T as a function of projected distances from the group centre. This shows that the sample of LTGs is heterogeneous, similar to that of the Fornax cluster core (see Chapter 2). In this section, we analyse the morphology, structure, colours, and stellar mass, as a function of group-centric distance.

Galaxies with morphological type $1 \leq T \leq 4$ are NGC 1317, NGC 1326, NGC 1341. NGC 1317 ($T = 1$) is located nearest (in projected distance) to NGC 1316, while NGC 1341 ($T = 4$) is the farthest. NGC 1326 ($T = 1$) is the brightest galaxy in the LTG sample, located at 0.68 deg in projection from NGC 1316. Galaxies with morphological type $5 \leq T \leq 7$ are NGC 1310, NGC 1316C, NGC 1326A, and NGC 1326B. NGC 1310 ($T = 5$) is located in the NW side in projection to NGC 1316, while the other galaxies, NGC 1316C ($T = 7$), NGC 1326A ($T = 5$), and NGC 1326B ($T = 7$) are in the NE side. Very late-type galaxies ($T = 9$) are FCC028 and FCC035. They are located within $D_{core} = 0.5$ deg. FCC035 is the faintest galaxy in the sample ($m_B = 15.3$ mag). Overall, we do not find any morphological segregation of galaxies in the group.

All LTGs in the Fornax A group have stellar masses in the range $8 < log(M_*)[M_\odot] < 10.5$, uniformly distributed inside the group (see top panel of Fig. 3.4.2). As expected, from the colour-magnitude relation, the fainter galaxies ($M_i \leq -18$ mag) in the group have bluer colours, $g - i \leq 0.5$ mag (see lower panel of Fig. 3.4.2).

ETGs and LTGs follow a different size-mass relation (see Shen et al. 2003) and this is likely the reason for the difference in the size-mass relation driven by the massive galaxy NGC 1316 and a less-pronounced relation observed for the bright spiral galaxies in the Fornax A subgroup (top panel of Fig. 3.4.3). We do not find any correlation of effective radius as a function of the projected distance from NGC 1316 (lower panel of Fig. 3.4.3). The effective radii of all bright spiral galaxies in the Fornax A subgroup are $R_e \leq 70$ arcsec (~ 7.07 kpc).

As found for the other properties derived for the LTGs in Fornax A group (i.e. morphology and stellar mass), the colour distribution also appears to be quite uniform inside the group, without any evident colour segregation with the group-centric distance (see Fig. 3.4.4).

A slight, but not significant trend (Pearson's correlation coefficient and the correlation significance are -0.41 and 0.26) might be observed in $(g - r)$ colours as a function of projected distance, whereas, on average, most

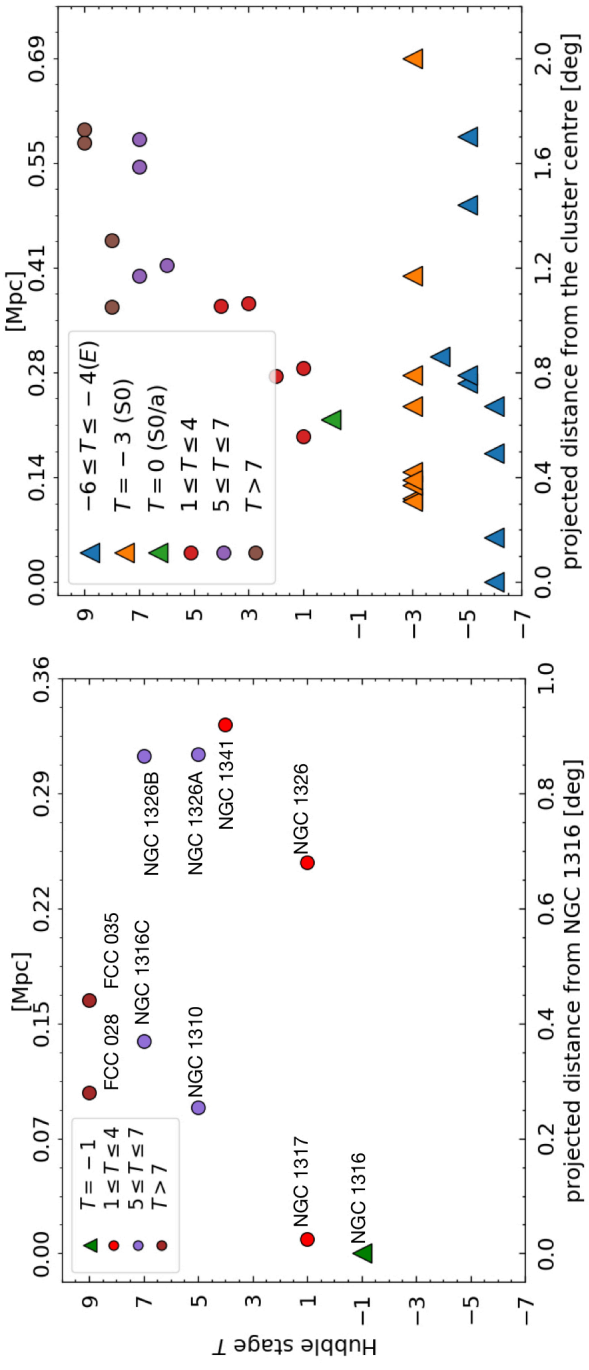


FIGURE 3.4.1: Hubble Type T as a function of group/cluster-centric distance for bright galaxies in the Fornax A subgroup (left panel) and Fornax cluster core (right panel).

($\sim$ 90%) of the LTGs in the Fornax A subgroup have colours in the range $0.7 \leq g - i \leq 1$ mag. The very blue outlier FCC035 ($g - i = 0.17 \pm 0.1$ mag) has a nuclear star cluster in its central region and this contributes to its blue ($g - i$) colour.

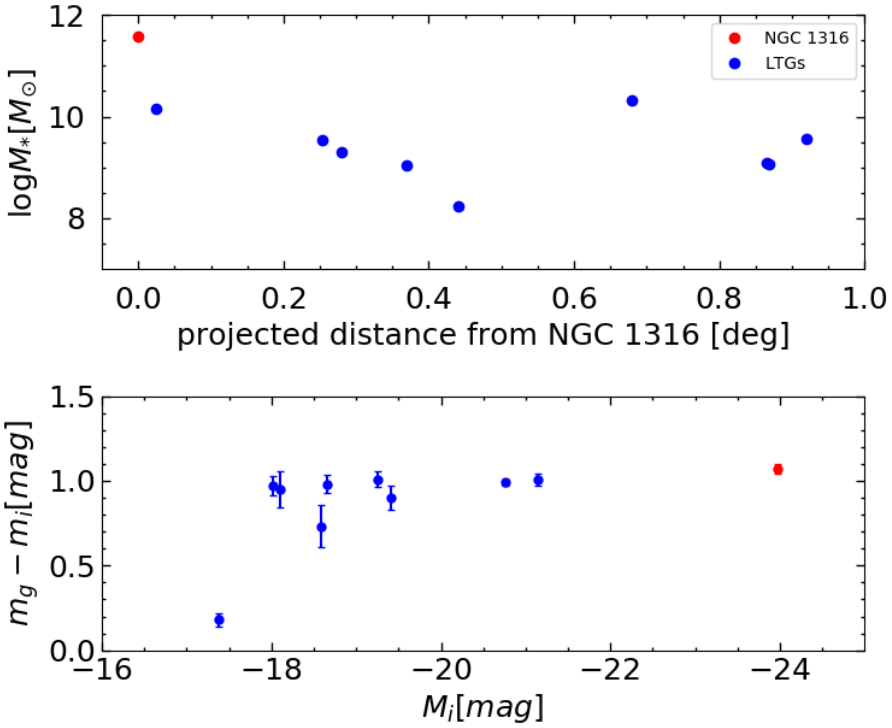


FIGURE 3.4.2: Stellar mass as function of projected distance from NGC 1316 (top panel) and colour-magnitude relation (lower panel) for bright spiral galaxies inside the virial radius of the Fornax A subgroup.

3.4.2 Analysis of the discs

Similar to our analysis in Chapter 2 (Raj et al. 2019) for the galaxies in the virial radius of the Fornax cluster, we study the discs of the galaxies in the group as well. Our results of the disc-breaks show that six galaxies have Type III profiles, indicating ongoing star formation (Raj et al. in prep) in their central regions.

The sample is too small to identify significant trends, but in order to compare with the results of the trends observed for the LTGs in the Fornax cluster core, we plot their parameters (e.g. stellar mass, total magnitude) to understand the environment of the Fornax A subgroup.

We do not find any disc-break trends in Fig. 3.4.5 with regard to the stellar mass (top left panel). The same can be said for (i) total magnitude as a function of break radius normalised to the effective radius in r (top right panel of Fig. 3.4.5) and (ii) absolute magnitude as a function of scale lengths (h_{in} and

h_{out}; lower panels in Fig. 3.4.5). Galaxies in the Fornax A subgroup have disc breaks located at different scale lengths, irrespective of their effective radius

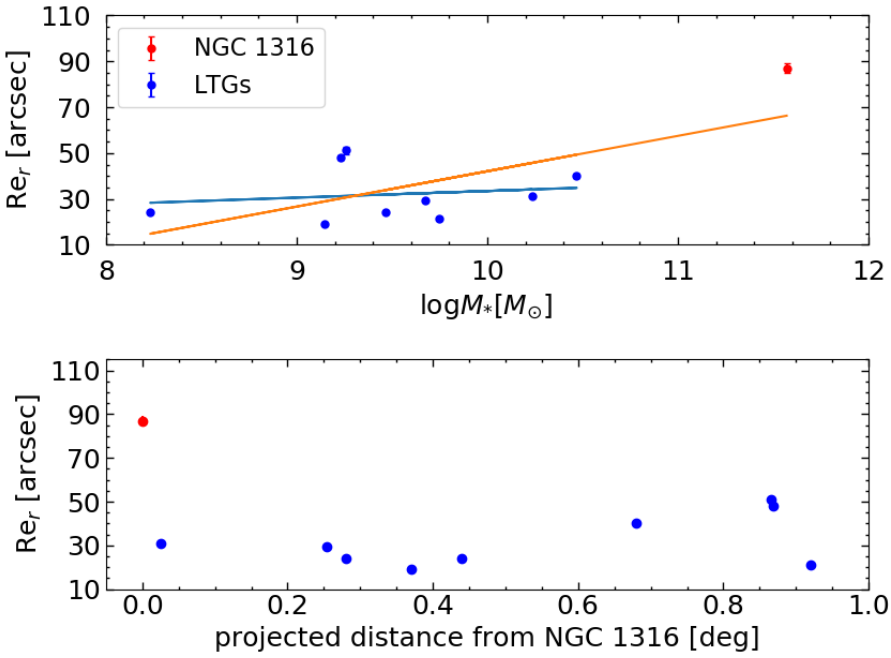


FIGURE 3.4.3: Size-mass relation (top panel) and effective radius as a function of projected distance from NGC 1316 (lower panel) for all the bright spiral galaxies in the Fornax A subgroup. A least square fit to the data is shown in orange (including NGC 1316) and blue (excluding NGC 1316).

and total magnitude, unlike the galaxies in the cluster core (Chapter 2) where there were observed trends (e.g. increasing inner scale length with absolute magnitude). For all six galaxies, the break radius is located beyond $1R_e$.

Except for NGC 1326 ($g - i_{h_{out}-h_{in}} = -0.24$ mag) and FCC035 ($g - i_{h_{out}-h_{in}} = -0.36$ mag), the other four galaxies show redder outer discs. FCC035 is a very late-type galaxy ($T = 9$) and is the faintest galaxy with minor disturbances in its outskirts, while NGC 1326 ($T = 1$) is the brightest in the LTG sample with the presence of a double bar (Erwin, Beckman, and Pohlen 2005). Nevertheless, we do not draw any conclusions from this observation since each galaxy's morphology, structure, and location in the group have to be taken into account to fully comprehend their individual evolutionary phases.

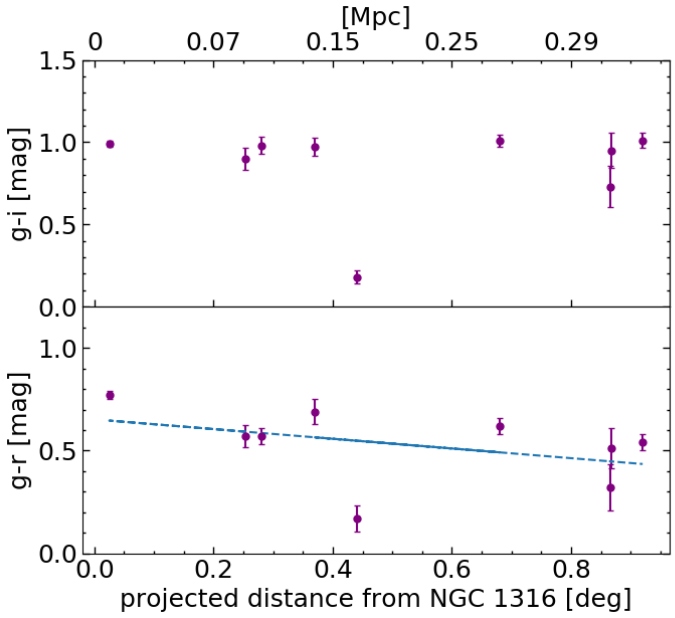


FIGURE 3.4.4: $g-i$ (top panel) and $g-r$ (lower panel) colours as a function of projected distance from NGC 1316 in degrees and Mpc. A least square fit to the $g-r$ data is shown.

3.5 Assembly history of the bright LTGs in Fornax A

Recently, studies concerning the location of galaxies in phase-space have gained importance (e.g. Mahajan, Mamon, and Raychaudhury 2011; Hernández-Fernández et al. 2014; Muzzin et al. 2014; Rhee et al. 2017). These studies show the connection between a galaxy's phase-space location and its effect on star-formation and stellar mass. This helps to further understand the effect of the environment on the evolution of galaxies, following on the morphology-density relation (Dressler 1980). As such, we adopt the method of analysis on phase-space given by Rhee et al. (2017). Through this analysis, we discuss the assembly history of the bright spiral galaxies in the Fornax A subgroup.

We used the published catalogue of spectroscopic redshifts by Maddox et al. (2019) to plot the phase-space diagram for 15 galaxies part of Fornax-A group. Using a sample of 40 galaxies within a radius of 0.7 Mpc, Maddox et al. (2019) found the central velocity of the Fornax A subgroup to be 1778 km/s with a velocity dispersion of 204 km/s. Using the relation between the dynamical mass of a cluster M_{dyn} and velocity dispersion σ_v, as given by Saro et al. (2013), Maddox et al. estimated the mass of the Fornax A subgroup to be 1.6 $\times 10^{13} M_{\odot}$. This estimation is also in agreement with Drinkwater, Gregg, and Colless (2001b), which is 2 $\times 10^{13} M_{\odot}$ (assuming that the Fornax A subgroup is virialised given that M/L ratio is the same as that of the Fornax cluster). In this work, we use 1.1 deg $\sim$ 0.38 Mpc as the virial radius of the Fornax A group.

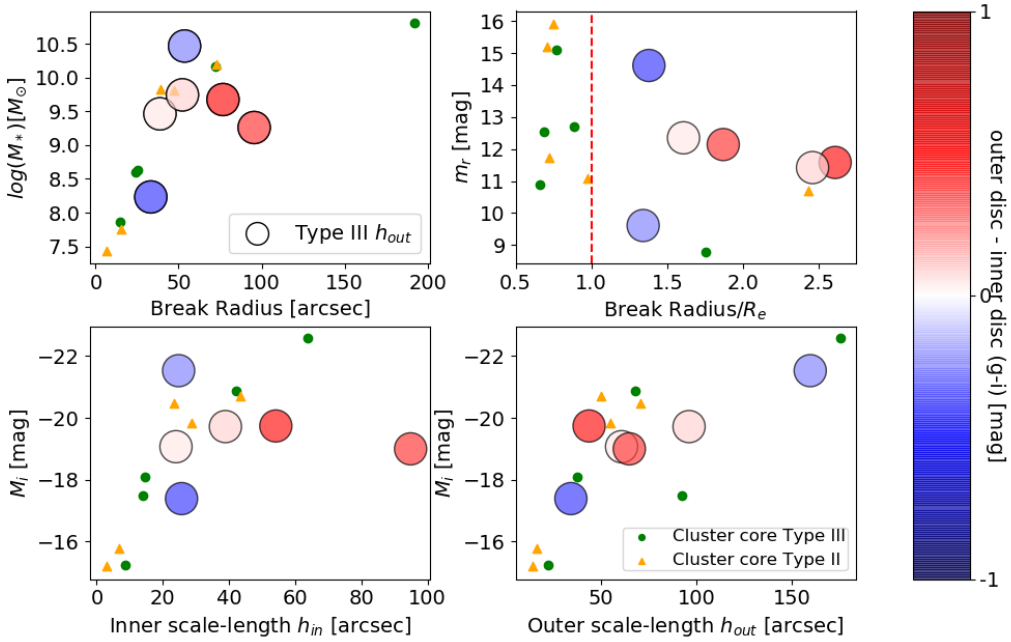


FIGURE 3.4.5: Analysis of galaxies with a break in their surface brightness profiles. Circles represent Type-III, with average $(g-i)$ colour of h_{out}-h_{in} as colour map. Orange triangles and green circles represent Type-II and Type-III galaxies in the Fornax cluster core (refer Chapter 2). Top panel (left): Stellar mass as a function of break radius; Top panel (right): Total magnitude as a function of break radius normalised to effective radius. The red dashed line indicates 80% of the Fornax cluster core galaxies; Bottom Panel: Absolute magnitude in i-band as a function of inner scale-length h_{in} (left) and outer scale-length h_{out} (right).

Rhee et al. (2017) used cosmological hydrodynamic N-body simulations of clusters and groups to study the effect of the environment on galaxies by understanding their phase-space location. Assuming a Navarro-Frenk-White (NFW) halo density profile (Navarro, Frenk, and White 1996), they derived the escape velocity[19] v_{esc}, with a concentration parameter c=6 (Gill et al. 2004).

In Fig. 3.5.1, we plot the velocities (normalised to the group velocity dispersion) as a function of the projected distance (normalised to the virial radius). Along with this, we also plot the trajectory curve v_{esc}. According to Rhee et al. (2017), the regions E, D, B are not strictly defined and they translate to ancient infallers ($t < 8$ Gyr), intermediate infallers ($t <$ 4–7 Gyr), and recent infallers ($t < 1$ Gyr). Rhee et al. explained the origin of these regions by comparing them to the trajectory such that galaxies falling for the first time will be close to the escape velocity curve, and as they pass through the pericentre, they start gaining velocity. Over time, after passing through the apocentre and many more pericentres, they eventually end up in

[19]The escape velocity $v_{esc} = \sqrt{\frac{2GM_{vir}}{R_{vir}}K(s)}$, where $K(s) = g_c\frac{ln(1+cs)}{s}$, $s = \frac{R_{3D}}{R_{proj}}$ and $g_c = [ln(1+c) - \frac{c}{1+c}]^{-1}$.

the region of ancient infallers. As ancient infallers, there are the central and massive galaxy NGC 1316 and the close (in projection) barred spiral galaxy NGC 1317 (see also Fig. 3.B.2). Most of the bright spiral galaxies in the For-

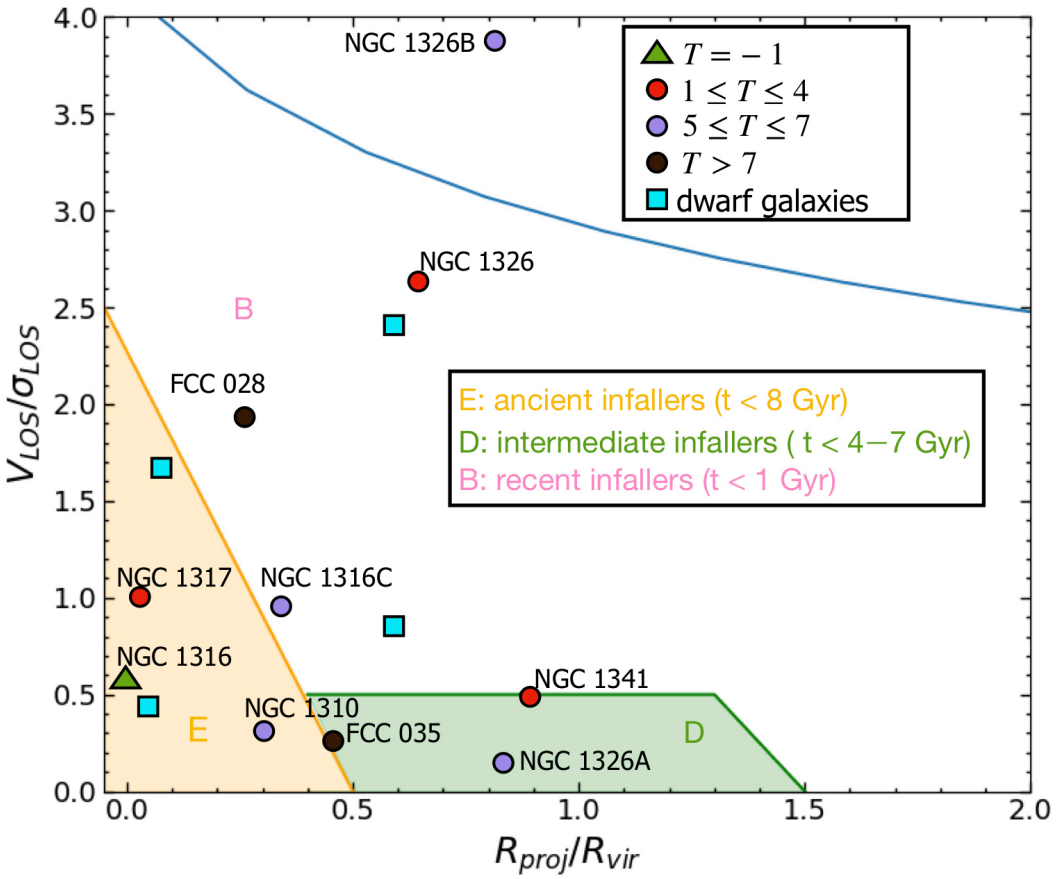


FIGURE 3.5.1: Projected phase-space diagram of galaxies in the Fornax A subgroup within a group-centric distance of 1.05 deg $\sim$ 0.38 Mpc. The blue trajectory corresponds to the escape velocity of the group. Regions E (orange), D (green), B (pink) represent ancient, intermediate, and recent infallers as defined by Rhee et al. (2017). The bright spiral galaxies are indicated with coloured circles based on their morphological type T (red, purple, brown), NGC 1316 is indicated with a green triangle ($T = -1$) and dwarf galaxies are indicated with blue squares.

nax A group (NGC 1310, NGC 1326A, FCC035, and NGC 1341) seem to be intermediate infallers. Except for FCC035, galaxies in this region have average colour $0.9 < g - i < 1$ mag. Although the Fornax A group is not as dense as the Fornax cluster, the group potential should somehow impact the outskirts of the discs. This is what we mainly observe for NGC 1316C, FCC028, NGC 1326 and NGC 1326B (see Fig. 3.B.3, Fig. 3.B.5, Fig. 3.B.7 and Fig. 3.B.8) that belong to the region of recent infallers. NGC 1326, the most massive LTG in the sample, also shows plenty of star-forming regions.

Six of the galaxies in the region of intermediate and recent infallers also show a Type-III disc-break. We explain the possible mechanisms for the formation of this break in Sect. 3.6.

Finally, according to the projected phase-space (PPS), the interacting system NGC 1326A and NGC 1326B may not be interacting, and that NGC 1326B is experiencing a fair amount of tidal interaction through its first infall, which would explain the star-forming regions in its outer-disc.

3.6 The tale of the Fornax environment

It is known that galaxies are redder and brighter in dense environments than in low-density environments (Faber 1973; Oemler 1974; Visvanathan and Sandage 1977; Butcher and Oemler 1984). The Fornax environment, comprising the cluster core and the Fornax A group, can tell the tale of 'pre-processing' of galaxies. In particular, how late-type galaxies evolve to the observed early-type galaxies in the cluster core. From literature, the proposed physical processes that galaxies undergo in groups and sub-clusters are strangulation and merging. In this section, we compare the properties of the group to that of the cluster core thus showing the different evolutionary stages for these environments.

3.6.1 Galaxy populations

The Fornax cluster core has 18 bright ($m_B < 15$ mag) ETGs (Iodice et al. 2019a) and 13 bright ($m_B < 16.6$ mag) LTGs (Chapter 2). The total number of dwarf galaxies in the cluster is 564 (Venhola et al. 2018; Venhola et al. 2019). However, the Fornax A group has nine bright ($m_B < 16$ mag) LTGs and one peculiar ETG i.e. the central galaxy NGC 1316. The total number of dwarf galaxies is ~ 60 within R_{vir} =1.0 deg (Venhola et al. 2019). Overall, the number of galaxies in the Fornax cluster core is nearly ten times more than that of the Fornax A group.

3.6.2 Morphological segregation

Nearly 70% of the ETGs ($T \leq -2$) are located within 0.8 deg of the cluster core (see Fig. 3.4.1). This region, where the bulk of the X-ray emission is also found, correspond to the high-density region of the cluster (Iodice et al. 2019a). Beyond this region, i.e. $D_{core} > 1$ deg, 60% of the LTGs are located (see Chapter 2). These results are consistent with the morphology-density relation (Dressler 1980). We do not observe the same for the galaxies in the Fornax A group (see Fig. 3.4.1). This suggests that the environment is not as dense as the Fornax cluster core, where the late-type star-forming galaxies are slowly transforming into passively evolved cluster members (e.g. Oemler 1974). The absence of ETGs in the Fornax A group and the morphological segregation confirm that the group is at a different stage of evolution.

3.6.3 Colour segregation

In the cluster core is observed a strong colour segregation as function of the cluster-centric radius, where the redder and massive ETGs populate the high-density region of the cluster (Iodice et al. 2019a). Most of the blue LTGs are found in the low-density region of the cluster. The Fornax A group, dominated by LTGs, does not show any colour segregation (see Fig. 3.4.4). The LTGs are about the same in $(g-i)$ colours as the LTGs in Fornax core (see left panel of Fig. 3.6.1). Fig. 3.6.1 (right panel) also shows that there are LTGs with lower stellar mass in the Fornax core ($7 < log(M_\star)[M_\odot] < 8$). Hence the overall stellar mass range of LTGs, both in the core and the group is $7 < log(M_\star)[M_\odot] < 11$.

3.6.4 Structure of LTGs

The LTGs in the cluster core exhibit very different substructures that are well-correlated with their locations in the cluster core (see Chapter 2). As for the LTGs in Fornax A group, their substructures are almost similar showing regular star-forming regions in their spiral arms. Although we find that Hubble stage T is heterogeneous in both samples, LTGs in the core show more irregularities in their structures (e.g. lopsidedness, tidal tails, boxy discs) in comparison to those in Fornax A group, where almost none show any such irregularities (except for NGC 1327B). This suggests that the environment of the cluster core has played a major role in the structure-transformation of LTGs, while galaxies in the Fornax A subgroup are undergoing minor changes or have not undergone any changes yet.

3.6.5 X-ray emission

The main contributions to the X-ray emission in Fornax A group are provided by the centre of the BGG, NGC 1316, and by two of the most luminous stellar loops in the outskirts (L1 in the south and L2 on the east of the galaxy, Mackie and Fabbiano 1998). In addition, there is an elongated region of X-ray emission to the NW of NGC 1316, corresponding to the region of the plume (Iodice et al. 2017b). The total luminosity of the X-ray emission is 3.1×10^{40} erg/s (Kim and Fabbiano 2003) is an order of magnitude fainter than the total X-ray luminosity in the Fornax core which is 5×10^{41} erg/s (Jones et al. 1997). Moreover, the X-ray emission in the core of the cluster, which peaks on the BCG NGC 1399, is much more extended, reaching $\sim 0.4 R_{vir} \sim 0.3$ Mpc. Most of the brightest and massive galaxies in the core are located inside the X-ray emission and all of them are ETGs (Iodice et al. 2019a). Therefore, most of the processes linked to the galaxy harassment that happened in this region of the cluster, and that shaped most of the observed galaxy properties, cannot be taken into account in the Fornax A group. This is further consistent with the homogeneous population of LTGs found in this group and with the overall picture that the Fornax A group is not as evolved as the cluster core.

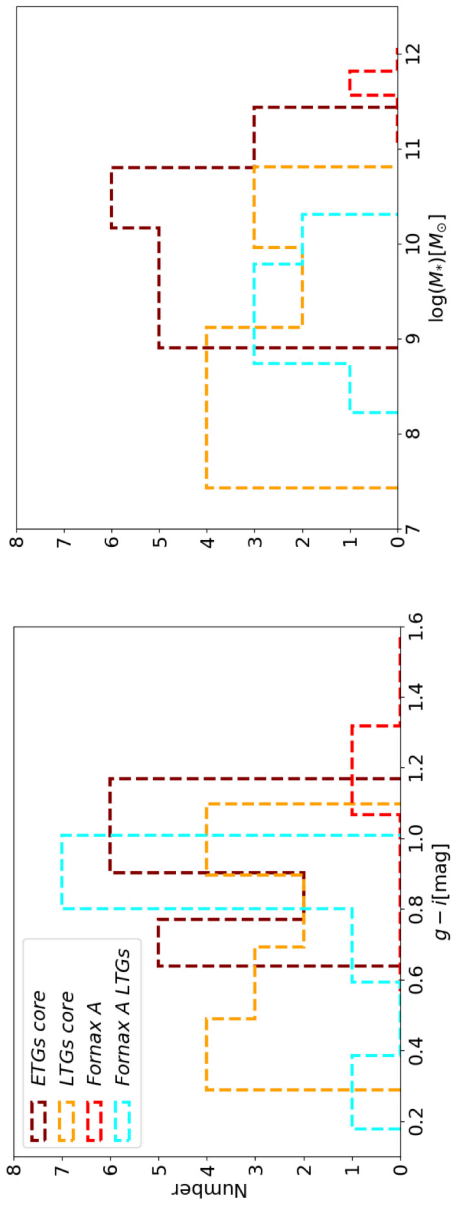


FIGURE 3.6.1: Histogram of the colour $(g - i)$ distribution (left) and of the stellar mass (right) for the bright galaxies in the Fornax core and Fornax A subgroup.

3.6.6 Disc-breaks of LTGs

We find that many of the galaxies in the Fornax core have undergone pre-processing, star-formation quenching in their outskirts during their time in the cluster (see Chapter 2; Zabel et al. 2019; Iodice et al. 2019b). This is also clearly seen through their disc-breaks i.e. the break radius of most (80%)of these galaxies is located within $1R_e$. Beyond this radius, there are no sub-structures (e.g. spiral arms) or star-forming regions. However, the observed Type III disc break dominates in the group, unlike in the cluster core. Moreover, the break radius of galaxies in the Fornax A subgroup is located beyond $1R_e$. This suggests that the environmental processes in the group have not severely altered the structures of the galaxies therein.

Mergers and strangulation are common phenomena in the group environment (Barnes 1985; Zabludoff and Mulchaey 1998; Hashimoto and Oemler 2000), but this assumption is not enough to understand the origin of Type-III disc-breaks alone. While they have been many explanations for their occurrence (e.g. Bakos, Trujillo, and Pohlen 2008; Younger et al. 2007; Laine, Laurikainen, and Salo 2016; Watkins et al. 2019), we state a few which depend on the HI content, such that if the gas is not replenished, star-formation is eventually halted. It is also important to consider internal mechanisms e.g. formation of bars, which can also form a Type-III disc-break (e.g. Erwin, Beckman, and Pohlen 2005; Pohlen and Trujillo 2006). The main possibilities are as following:

1. Wang et al. (2018) showed that Type-III disc-breaks were prevalent in HI-rich galaxies with low-spin. The *in-situ* star-formation from gas accretion builds the outer-disc of these Type-III galaxies.

2. Enhanced star-formation in the inner-discs of galaxies can cause steeper inner-discs than outer discs (Hunter and Elmegreen 2006). Gas in outer-discs are vulnerable to the tidal forces in a dense environment. In this case, the gas that falls inwards can cause star-bursts in the inner central regions (e.g. Barnes and Hernquist 1991; Barnes and Hernquist 1996; Hopkins et al. 2013, and references therein). If LTGs in the Fornax A subgroup are undergoing strangulation, their outer-discs will not have cold gas to fuel star-formation.

HI data is required to confirm if Type-III disc-breaks in LTGs part of the Fornax A subgroup, have formed as a consequence of HI-richness (case 1) or the contrary (case 2).

3.7 Summary and conclusions

With FDS data, we have been able to analyse the structure, morphology and other properties of nine bright ($m_B < 16$ mag) LTGs in the Fornax A group. In the study of disc-breaks of LTGs in different environments, we have been able to compare the break radius of LTGs in the cluster core to that of the subgroup. Since the Fornax cluster has been studied by several surveys, we

have made the best use of available public data, in this case, the spectroscopic redshift by Maddox et al. (2019) to look at the group members in phase-space. Thus, for the first time, we give a complete picture of the environment of the Fornax A subgroup, and compare it to that of the Fornax cluster core. We summarise our results of this work as follows:

1. In contrast to what is observed in the core of the Fornax cluster, in the Fornax A group there is no observed morphological, mass and colour segregation of galaxies. LTGs in the Fornax A group have stellar masses in the range $8 < log(M_*)[M_\odot] < 10.5$), while there are less massive LTGs in the Fornax cluster core ($7 < log(M_*)[M_\odot] < 11$).

2. We detect only Type-III (up-bending) disc-breaks in the SB profiles of galaxies in the Fornax A group. Of them, four galaxies have outer discs redder than their inner discs, and two galaxies have bluer outer discs. On the contrary, in the Fornax core we detected all types of disc-breaks, suggesting a variety of mechanisms and interactions with the environment (see Chapter 2). The formation of the breaks in the Fornax A group needs more investigations of their HI content, in order to investigate whether HI-rich galaxies can cause enhanced star-formation in the galaxy's outer-disc, or whether these galaxies are experiencing strangulation which halts star-formation in the outer-discs.

3. The break radii of six galaxies in the Fornax A subgroup are located beyond $1R_e$. This is contrary to the results of the galaxies in the Fornax cluster core where the break radii of galaxies (80% of the sample) are located within $1R_e$. This suggests that the environmental mechanisms in the Fornax A group are not as strong as those in the cluster core, where the latter has altered the structures of the galaxies' disc.

4. Through phase-space analysis, we find that most (80%) of the group members are intermediate and recent infallers, consistent with a younger assembly epoch with respect to the Fornax core, where the PPS is equally populated by ancient infallers (that dominate the high-density region of the cluster) and by intermediate and recent infallers that are symmetrically distributed around the cluster core in the low-density region (Iodice et al. 2019b).

According to the above results and the whole analysis performed in this work, the Fornax A group appears to be in an early-stage of assembly with respect to the cluster core. The environment of the Fornax A subgroup is not as dense as that of the cluster core, with all galaxies except the BGG showing similar morphology, comparable colours and stellar masses, and Type-III disc-breaks, without any clear trend of these properties with group-centric distances. .

As future perspectives, in order to analyse the star-formation and therefore, compare with the detected disc-breaks, we will study the Hα distribution of the brightest LTGs in the Fornax A group (Raj et al. in prep). A comparison of the overall structural parameters of galaxies in the cluster

core and the group is currently analysed by Su et al. (in prep). All of the mentioned work is part of FDS, thus providing a detailed analysis of the Fornax environment and galaxies therein.

Appendix

3.A Bright LTGs in the Fornax A subgroup

In this section, we briefly describe the galaxies analysed in this work.

3.A.1 FCC013

Also known as NGC 1310, is a barred-spiral galaxy (SBcII) with morphological type $T = 5$, located at a projected distance $D_{core} = 0.25$ deg from NGC 1316. The HI disc of this galaxy is more extended than its stellar disc, with $M_{HI} = 48.0 \pm 0.9 \times 10^7 M_\odot$ (Serra et al. 2019). The galaxy has an effective radius $R_{e,r} = 27.6$" and star-forming spiral arms. We detect a Type-III disc-break in its SB profile and hence the break radius is 7.8 kpc. The outer disc appears redder than the inner disc with average $(g-i)_{h_{out}-h_{in}} = 0.44$ mag. The origin of the Type-III break in this galaxy is likely due to its high HI content.

3.A.2 FCC022

Also known as NGC 1317, is a spiral galaxy (SA pec) with morphological type $T = 1$, located at closest projected distance from NGC 1316 i.e. $D_{core} = 0.025$ deg from NGC 1316. The HI disc of the galaxy is confined to its stellar disc and has HI mass $M_{HI} = 26.4 \pm 0.6 \times 10^7 M_\odot$ (Horellou et al. 2001; Serra et al. 2019), while in the central part of this galaxy i.e. at $R \sim 0.5'$, a star-forming ring is visible. It appears to be an early-type spiral, with almost no star-forming regions beyond $R \sim 0.5'$, which can be seen in its SB image (Appendix. 3.B.2). This can be justified with the results from phase-space analysis that FCC022 has passed through the pericentre and lost its neutral gas through interactions with the intra-group medium (also see Serra et al. 2019).

3.A.3 FCC028

FCC028 is a spiral galaxy (SmIII) with morphological type $T = 9$, located at projected distance $D_{core} = 0.28$ deg from NGC 1316. From literature, the galaxy has been associated to a ring galaxy (Few and Madore 1986; Corwin, de Vaucouleurs, and de Vaucouleurs 1985; Lauberts 1982). The ring can be seen as star forming regions in the SB image (Appendix. 3.B.3), which has likely originated from a collision (Maddox et al. 2019). The HI disc of the galaxy is more extended than its stellar disc and has HI mass

$M_{HI} = 13.7 \pm 0.6 \times 10^7 M_\odot$ (Serra et al. 2019). We detect a Type-III disc-break in its SB profile and its break radius is at 3.9 kpc. The outer disc of this galaxy is redder than its inner disc with an average $(g-i)_{h_{out}-h_{in}} = 0.04$ mag.

3.A.4 FCC029

Also known as NGC 1326, is a barred-spiral galaxy (SBa(r)) with morphological type $T = 1$ is located at a projected distance $D_{core} = 0.68$ deg from NGC 1316. Erwin (2004) describe it as a double barred galaxy. It is the most luminous, massive galaxy in our sample of LTGs with $M_i = -21.53$ and $M_* = 2.94 \times 10^{10} M_\odot$. We detect a Type-III disc-break with a break radius = 5.4 kpc. The outer disc is bluer than its inner disc with $(g-i)_{h_{out}-h_{in}} = -0.24$ mag. This can be associated to the presence of star-forming regions in its outskirts.

3.A.5 FCC033

Also known as NGC 1316C, is a spiral galaxy (SdIII pec) with morphological type $T = 7$, located at a projected distance $D_{core} = 0.37$ deg from NGC 1316. The spiral arms are within $R = 10$". The effective radius of this galaxy is $R_{e,g} = 22.6 \pm 0.5$" and has a faint corona (Corwin, de Vaucouleurs, and de Vaucouleurs 1985).

3.A.6 FCC035

FCC035 is a spiral galaxy (SmIV) with morphological type $T = 9$, and is located at a projected distance $D_{core} = 0.44$ deg from NGC 1316. It is the faintest galaxy in our sample $M_i = -17.39$ and $M_* = 0.017 \times 10^{10} M_\odot$. We detect a Type-III disc break in its SB profile with break radius = 2.8 kpc. The outer disc is bluer than its inner disc with $(g-i)_{h_{out}-h_{in}} = -0.36$ mag. The Hα (Raj et al. in prep) distribution in the galaxy is concentrated in a star-forming region located in its spiral arms, which explains the blue $(g-i)$ colours. This can also be associated to its very-late morphological type and irregularities in its spiral structure.

3.A.7 FCC037

Also known as NGC 1326A, is a barred-spiral galaxy (SBcIII) with morphological type $T = 5$, located at a projected distance $D_{core} = 0.87$ deg. This galaxy has been studied as an interacting system along with FCC039 (NGC 1327B). However, from our analysis in PPS (data taken from Maddox et al. 2019), we find the velocity difference between these galaxies is large and thus, they might not be interacting.

3.A.8 FCC039

Also known as NGC 1327B, is a spiral galaxy (SdIII) with morphological type $T = 7$, located at a projected distance $D_{core} = 0.86$ deg from NGC 1316. This galaxy has irregular spiral (dusty) arms, and disruptions in outer disc as a result of its recent interaction with the tidal field of the Fornax environment. We detect a Type-III disc-break in its surface brightness profile and a break radius = 9.6 kpc. As mentioned in Appendix. 3.A.7, this galaxy might not be interacting with FCC037 (NGC 1327A). However, it can be a fly-by thus showing faint tidal tails in its outskirts. The outer disc of this galaxy is redder than its inner disc with $(g-i)_{h_{out}-h_{in}} = 0.36$ mag.

3.A.9 FCC062

Also known as NGC 1341, is a barred-spiral galaxy (SbcII) with morphological type $T = 4$, located at furthest distance from NGC 1316 i.e., $D_{core} = 0.92$ deg. We detect a Type-III disc-break in its SB profile with disc break = 5.28 kpc. The outer disc of this galaxy is redder than its inner disc with spiral arms, Type-III disc break with $(g-i)_{h_{out}-h_{in}} = 0.08$ mag.

3.B The sample: images and profiles

In this section, we show the g-band VST images (in surface brightness level) of LTGs in the Fornax A subgroup, surface brightness profiles, $g-i$ colour maps and $(g-i)$ profiles. For six of the galaxies with disc-breaks, we mark the break radius on the g-band images in surface brightness level (black dotted lines), the $g-i$ colour maps (white dotted lines), and $(g-i)$ colour profiles (red dotted lines).

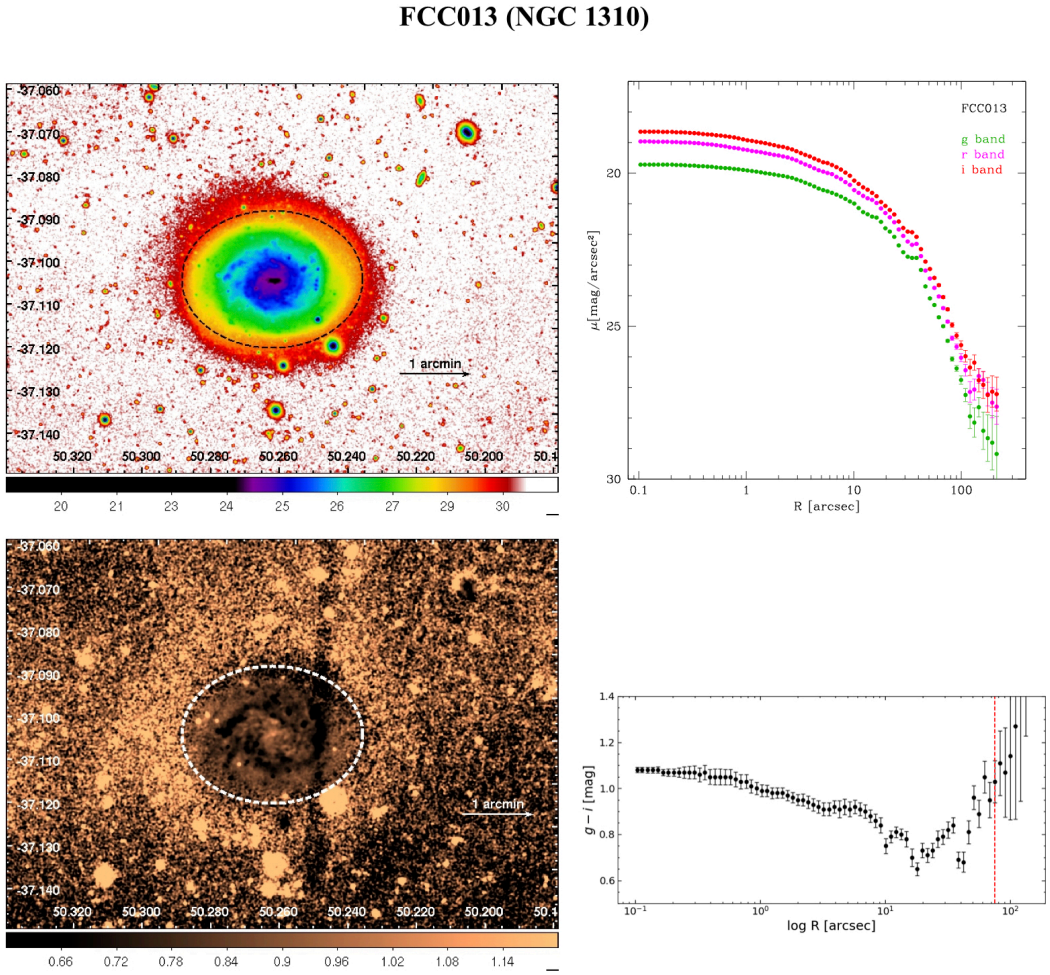


FIGURE 3.B.1: Surface Photometry of FCC013. Top left panel: g-band image in SB level with black dotted lines representing the break-radius. Top right panel: SB profiles in g, r, i bands. Bottom left panel: $g-i$ colour map with white dotted lines indicating the break-radius. Bottom right panel: $g-i$ colour profile with red dotted line indicating the break radius.

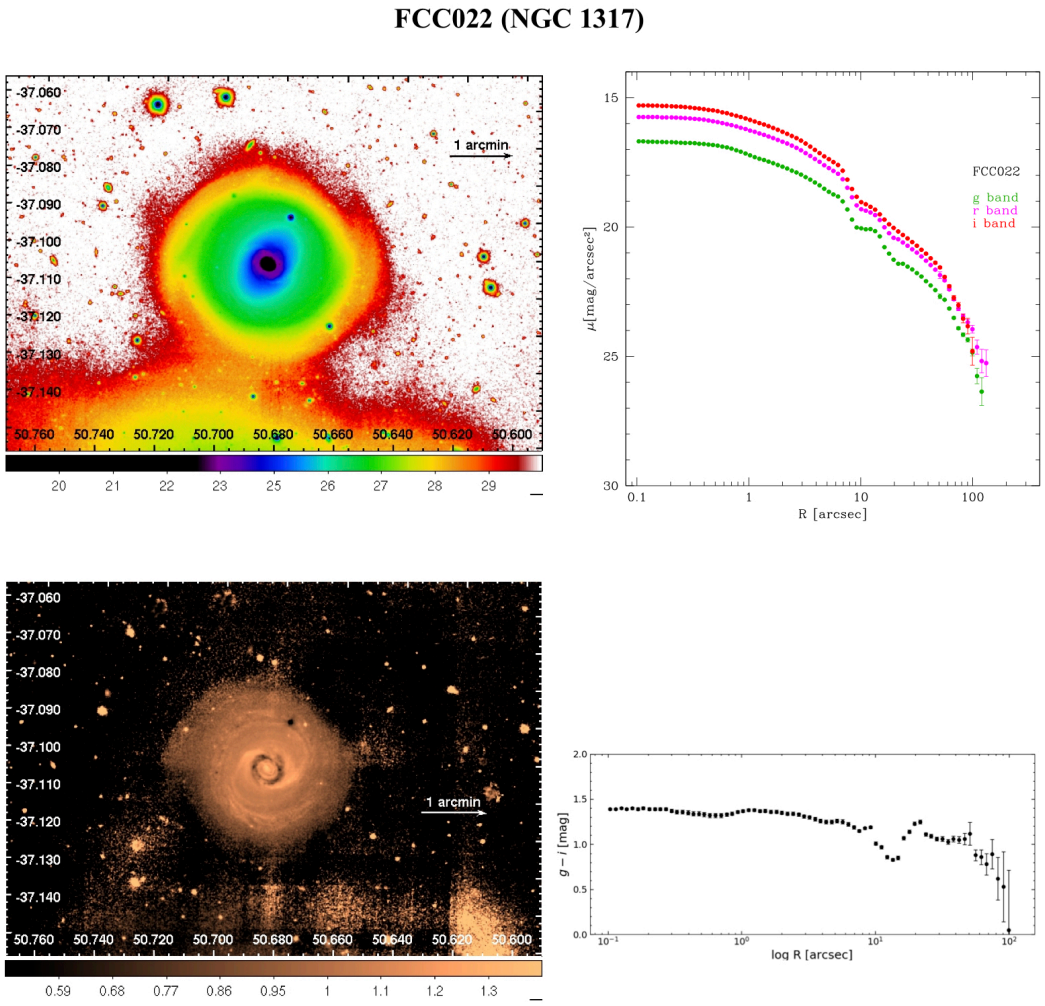


FIGURE 3.B.2: Surface Photometry of FCC022. Top left panel: g-band image in SB level. Top right panel: SB profiles in g, r, i bands. Bottom panels: $g - i$ colour map (left) and $g - i$ colour profile (right).

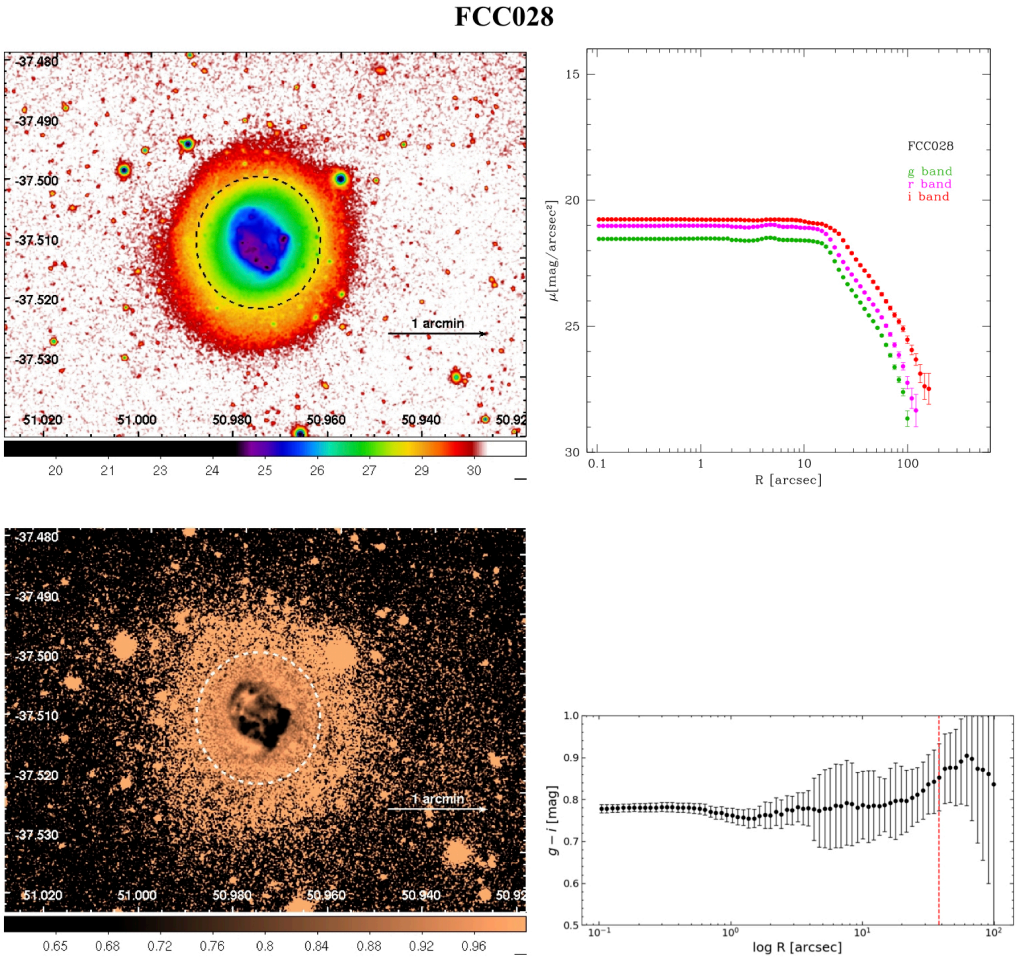


FIGURE 3.B.3: Surface Photometry of FCC028. Description same as Fig. 3.B.1.

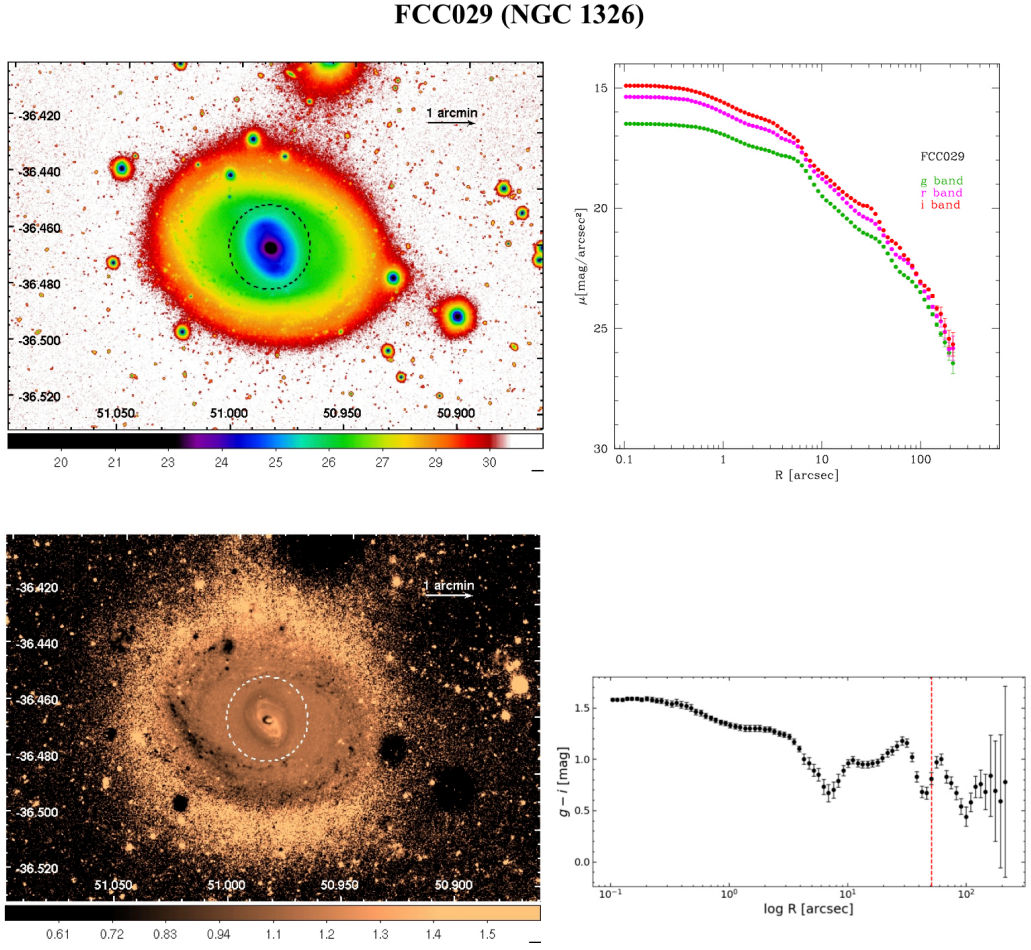


FIGURE 3.B.4: Surface Photometry of FCC029. Description same as Fig. 3.B.1.

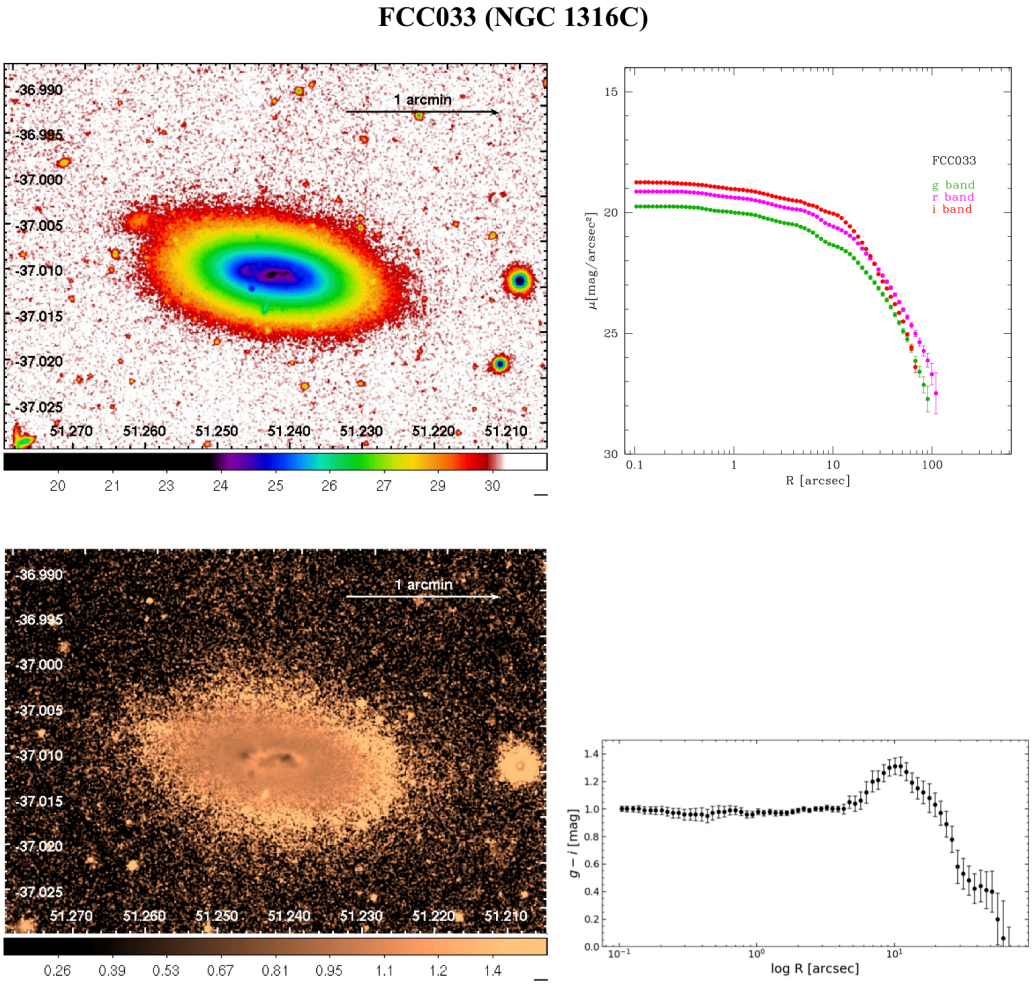


FIGURE 3.B.5: Surface Photometry of FCC033. Description same as Fig. 3.B.2.

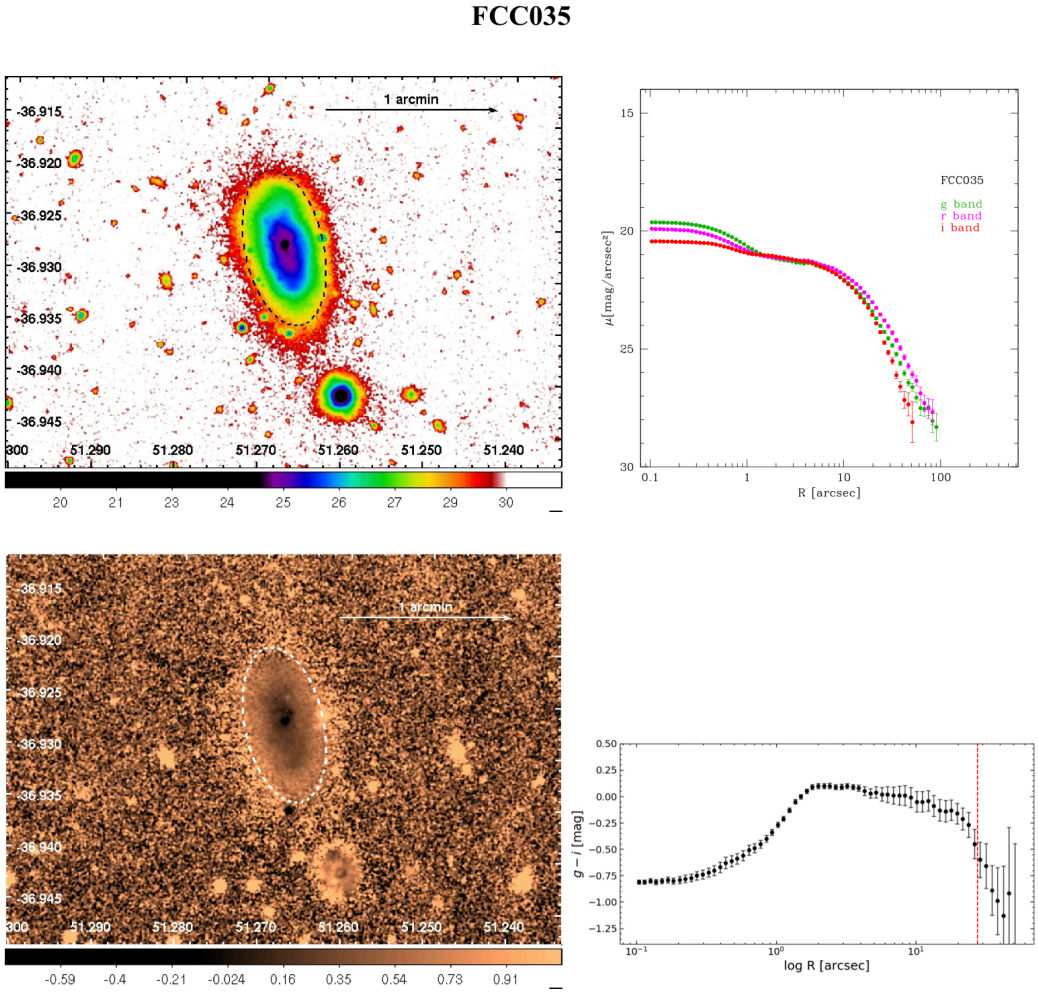


FIGURE 3.B.6: Surface Photometry of FCC035. Description same as Fig. 3.B.1.

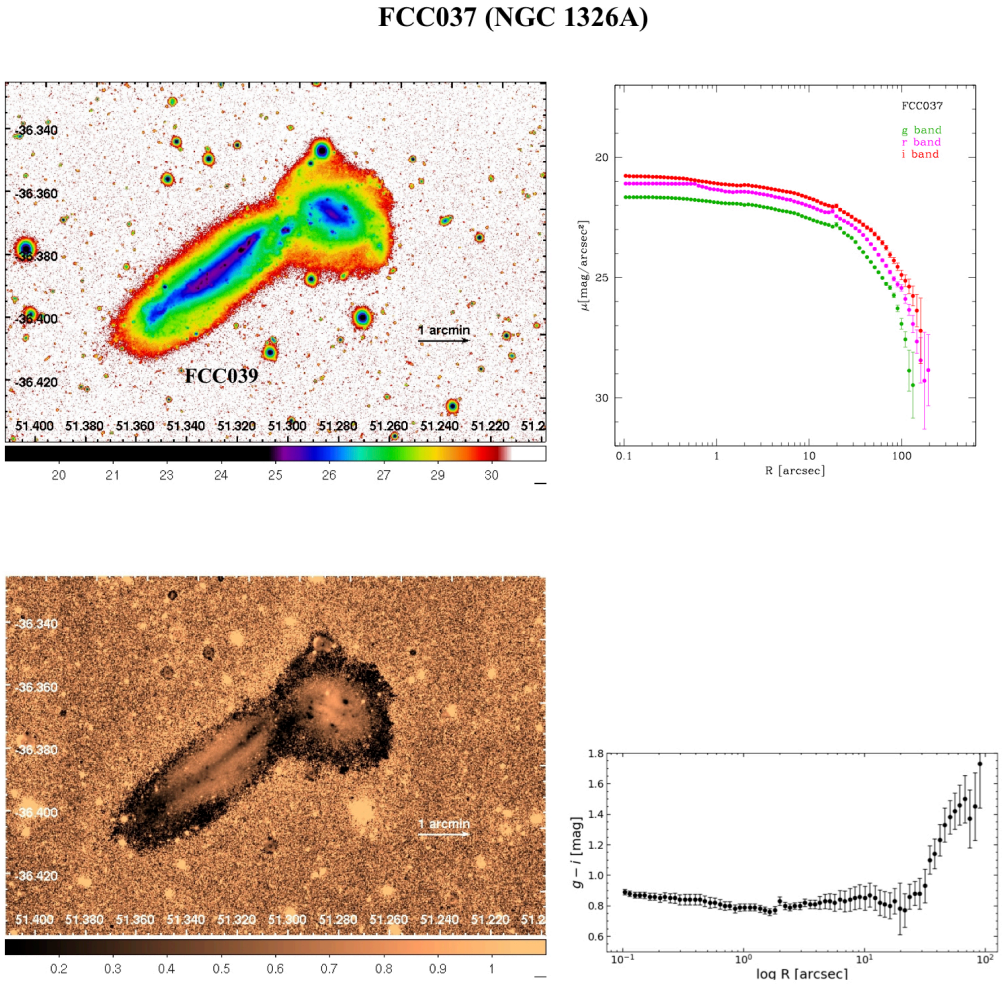


FIGURE 3.B.7: Surface Photometry of FCC037. Description same as Fig. 3.B.2.

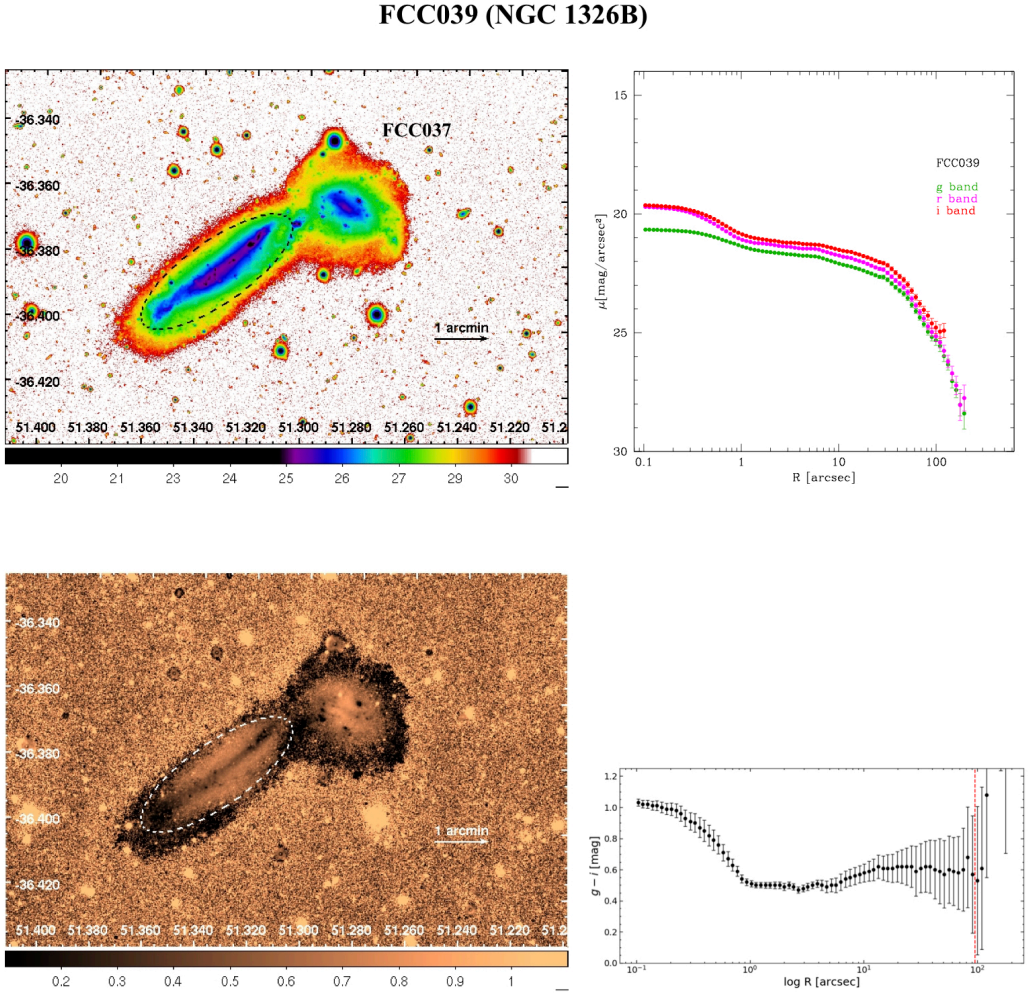


FIGURE 3.B.8: Surface Photometry of FCC039. Description same as Fig. 3.B.1.

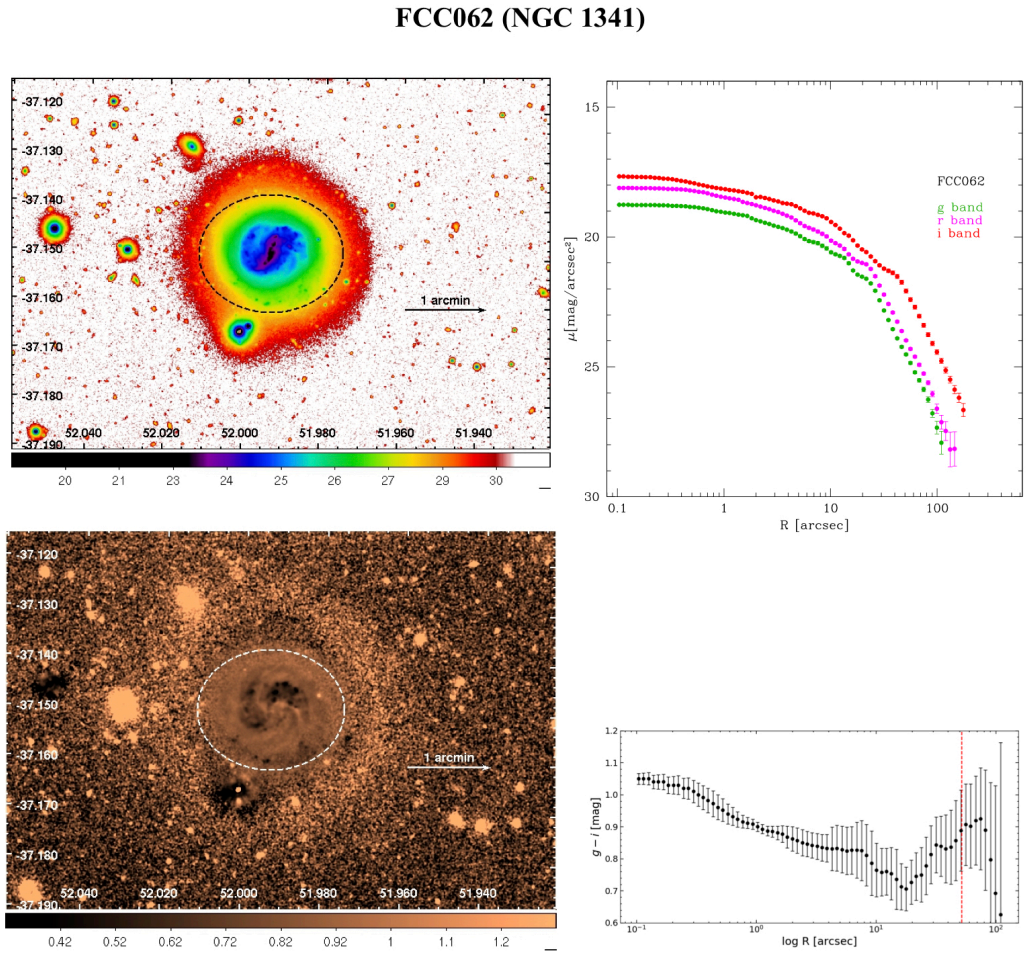


FIGURE 3.B.9: Surface Photometry of FCC062. Description same as Fig. 3.B.1.

3.C Methodologies: Multi-component fits of the light distribution

In this section, we briefly describe the 1D multi-component fitting method we adopt, published by Spavone et al. (2017b) and Spavone et al. (2020). This is done to determine the starting point of the disc regions for the break-radius algorithm (described in Sect. 3.3.3).

We perform a multi-component fit to the deconvolved surface brightness profiles of five galaxies (FCC013, FCC029, FCC035, FCC039, FCC062). The bulge component is fitted with a Sérsic law (Sérsic 1963; Caon, Capaccioli, and D'Onofrio 1993),

$$\mu(R) = \mu_e + k(n)\left[\left(\frac{R}{r_e}\right)^{1/n} - 1\right] \tag{3.1}$$

where $k(n) = 2.17n + 0.35$, R is the galactocentric radius, r_e, μ_e are the effective radius and surface brightness. The disc component is fitted with an exponential profile ($n = 1$),

$$\mu(R) = \mu_0 + 1.086 \times R/r_h \tag{3.2}$$

where μ_0 and r_h are the central surface brightness and exponential scale length. The parameters are not fixed for the Sérsic component. The fitting procedure adopted here performs least-square fits using a Levenberg-Marquadt algorithm in which the function to be minimised is the rms scatter (see Seigar, Graham, and Jerjen 2007), defined as $\Delta = \frac{\sum_{i=1}^{n} \delta_i^2}{m}$ where m is the number of data points and δ_i is i^{th} residual. The best fits are shown in Fig. 3.C.1 and their corresponding fitting parameters are listed in Tab. 3.C.1.

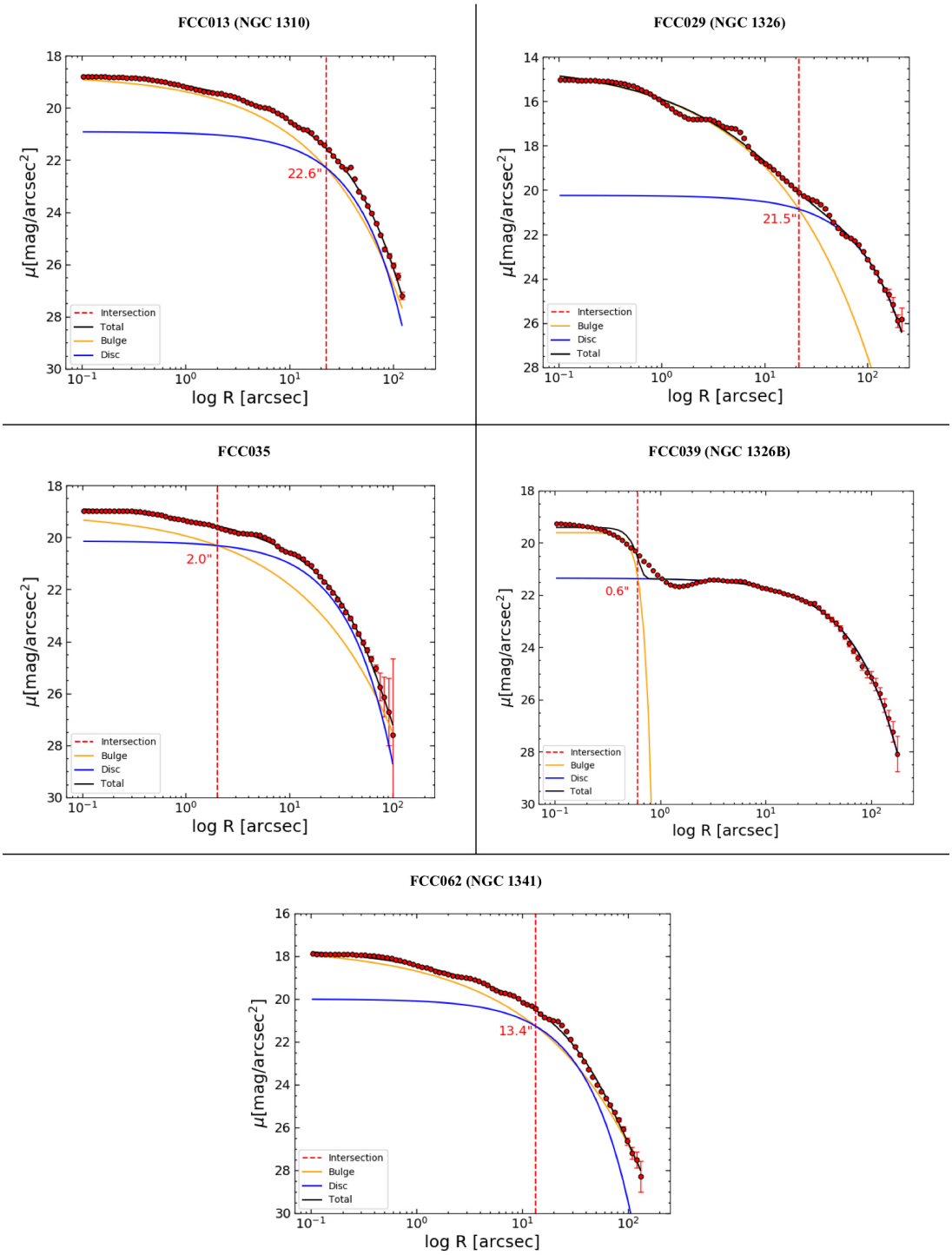


FIGURE 3.C.1: Multi-component fits of the surface brightness profiles (*r*-band) of galaxies with Type III disc break. In each plot, the multi-component fits i.e. bulge is indicated in orange, exponential disc is indicated in blue, and total(bulge+disc) is indicated in black. The intersecting point of the two components is indicated with a red dashed line.

TABLE 3.C.1: **Best-fitting parameters for five galaxies with detected disc-breaks in the Fornax A subgroup.** *Col.1* - Fornax A group members with detected disc-breaks; *Col.2*- effective surface brightness, effective radius, and Sérsic index for the bulge component of each fit; *Col.3*- central surface brightness and scale length for the exponential component; *Col.4*- radius at the intersection between the bulge and the disc component of the fits.

Object	Bulge			Disc		$r_{intersection}$
	μ_e	r_e	n	μ_0	r_h	
	[mag/arcsec^2]	[arcsec]		[mag/arcsec^2]	[arcsec]	[arcsec]
(1)		(2)		(3)		(4)
FCC013	22.34 ± 0.5	23.05 ± 1	1.83 ± 0.4	20.91 ± 0.2	17.65 ± 3.1	22.6
FCC029	18.70 ± 0.2	8.96 ± 1	2.2 ± 0.1	20.24 ± 0.6	37.57 ± 0.9	21.5
FCC035	23.16 ± 0.9	22.47 ± 0.2	0.7 ± 0.5	20.14 ± 0.7	12.63 ± 0.1	2.0
FCC039	20.93 ± 0.3	0.49 ± 0.1	0.65 ± 0.2	21.26 ± 0.1	27.1 ± 0.3	0.6
FCC062	22.0 ± 0.7	19.92 ± 0.3	2.21 ± 0.8	20.0 ± 0.1	11.56 ± 0.7	13.4

Chapter 4

The intra-cluster baryons in Fornax

This chapter is based on the paper:
Raj, M.A.; Iodice,E.; Napolitano,N.R.; Hilker, M.; Spavone,M.; Peletier,R.F.; Su,H.-S.; Falcon Barroso, J.; van de Ven, G.; Cantiello, M.; Kleiner. D; Venhola, A; Mieske, S.; Capaccioli, M.; Schipani, P.; *The Fornax Deep Survey with VST, X. On the assembly history of the bright galaxies and intra-group light in the Fornax A subgroup* , 2020, accepted to be published in Astronomy & Astrophysics.

Abstract

We present the study of the intra-group light (IGL) in the Fornax A subgroup, observed with the Fornax Deep Survey (FDS). The main objective of this work is to investigate the formation history of the IGL in the Fornax A group and to compare this to other loose as well as the intra-cluster light (ICL) of the Fornax cluster core, thus providing a complete picture of the intra-cluster baryons in the Fornax cluster. The long integration time and deep photometry allow us to estimate the IGL. The estimated luminosity of the IGL is $6 \pm 2 \times 10^{10} L_{\odot}$ in g-band which corresponds to about 16% of the total light in the group. The Fornax A group is in an early-stage of assembly with respect to the cluster core. The low amount of IGL is consistent with this result, since there were no significant gravitational interactions between galaxies that modified the galaxies' structure and contributed to the build-up of the IGL. The main contribution to the IGL is from the minor merging in the outskirts of the BGG NGC 1316 and, probably, the disrupted dwarf galaxies close to the group center.

4.1 Introduction

During the infall of galaxy groups to form a cluster, various dynamical processes separate stars from their host galaxies. The stripped material of galaxies will settle to constitute the intra-group light (IGL) or the intra-cluster light (ICL; Napolitano et al. 2003; Fujita 2004; Contini et al. 2014). Therefore, the ICL/IGL is a fossil record of past interactions and mergers as its growth and evolution over time provide a link to the assembly state of the cluster/group (Mihos 2015). The stripped material that is mainly composed of intergalactic stars in galaxy clusters was first proposed by Zwicky (1937). The ICL/IGL component is not easy to define as it comprises of the stellar halo of the brightest cluster/group galaxy (BCG/BGG, e.g. Zibetti et al. 2005). The stellar halo is a faint, diffuse component of stars formed by the gradual accretion of satellite galaxies (see Mihos et al. 2017). Surface brightness profile decomposition has been used to provide a distinction between the BCG/BGG and ICL/IGL (e.g. Zibetti et al. 2005). Apart from the diffuse starlight component, the ICL/IGL consists of intracluster globular clusters (e.g. Peng et al. 2011, and references therein), intracluster supergiant (e.g. Ohyama and Hota 2013, and references therein) and red-giant (e.g. Ferguson, Tanvir, and von Hippel 1998, and references therein) stars, intracluster novae (Neill, Shara, and Oegerle 2005) and supernovae (e.g. Barbary et al. 2012, and references therein), HII regions (Gerhard et al. 2002) and planetary nebulae (Gerhard et al. 2007). Tracing these components allow us to understand the stellar population and metallicity of the ICL/IGL (e.g Montes and Trujillo 2014).

Slow interactions between galaxies which lead to tidal stripping are more common in a group environment; this process produces tidal tails and streams. As groups merge to form clusters of galaxies, more material is stripped and along with this, the aforementioned tidal tails and streams is mixed with the ICL (Rudick, Mihos, and McBride 2006; Rudick et al. 2009). Recent works (e.g. Brough et al. 2006b; Brough et al. 2006a; Karachentsev 2005; Mamon 2007; Tully et al. 2014; Spavone et al. 2018; Fouad et al. 2019; Cattapan et al. 2019; Iodice et al. 2020, and references therein) give detailed analysis of the IGL and BGGs of the respective groups. Especially with the advent of deep photometry (e.g. Zibetti et al. 2005), exploring faint regions of galaxy outskirts and ICL/IGL have gained importance over the last years (e.g. Rudick et al. 2009; Mihos et al. 2017; Iodice et al. 2016; Spavone et al. 2017a; Iodice et al. 2017b; Iodice et al. 2017a; Spavone et al. 2018, and references therein).

Since the IGL is considered to be a contributor to the ICL (Mihos 2015), a comparison between them provides necessary clues on the assembly of the environment and galaxies therein. Moreover, in the context of the Fornax environment, it is crucial to have an estimate of the ICL in the Fornax cluster core as well as the Fornax A subgroup.

As such, we have estimated the IGL in the Fornax A subgroup and in the following sections, we give a brief overview of the faint outskirts of NGC 1316 and the ICL in the Fornax cluster. We then explain the method

of estimating the IGL and compare the results to other groups.

4.1.1 An overview of the outskirts of NGC 1316

In order to estimate the IGL, it is important to understand the structure of NGC 1316. As discussed in Chapter 3, the Fornax A subgroup is dominated by bright LTGs and only one peculiar ETG. This would suggest that the bulk of the IGL is where the stellar envelope of NGC 1316 starts to dominate. In this section, we give a literature review of the faint outskirts and formation history of NGC 1316 along with its detected globular clusters (GCs).

Faint features

The well known outskirts characterised by loops and substructures (sharp boundaries and plumes) were first identified by Schweizer (1980) and Richtler et al. (2014). In addition to the known loops (L1, L2, L3, L4), Iodice et al. (2017b) detected three other fainter loops at a SB level of $\mu_g \sim 29$–30 mag/arcsec^2, which they names L6, L7, L8, and the faintest ($\mu_g > 30$ mag/arcsec^2) loop L9 in the NW region. L5 is the the most extended loop in the SW of NGC 1316 with an appearance of a filament. In the SE part of this loop, there are bright knots, and in the west part, there is more diffuse structure and contaminated by the faint halo of the stars (Iodice et al. 2017b). In this loop, Schweizer (1980) detected HII regions.

Apart from loops, Iodice et al. (2017b) also detected a connecting bridge between L1 and L4, shells protruding from the plume, and bright ripples R1 and R2. To summarise, these shells, plume and bright ripples are features inside the transition radius $R_{tr} = 5.5'$. The loops L1 to L9 contribute to the light from the outer stellar envelope. The bright loops are shown in Fig. 4.1.1.

Formation history

The faint outskirts of a galaxy provide a direct link to the formation history. As such, Serra et al. (2019) provided an estimate of the HI mass within and around NGC 1316 and through their analysis supported the hypothesis on its formation history i.e. through the merger between a dominant gas-poor ETG and a smaller gas-rich spiral galaxy. The oldest merger is traced by the most extended loops L5 and L9 (Schweizer 1980; Iodice et al. 2017b). The fainter loops L2 and L1 are likely the result of subsequent mergers. Through HI detection in L5 and L9, Serra et al. (2019) suggest that the oldest merger was gas-rich and fainter detection in other loops suggest that the subsequent mergers were gas-poor.

4.2 The ICL in the Fornax cluster

As mentioned in Sect. 4.1, the stellar envelope of the galaxies in the cluster contribute to the ICL. By fitting the light distribution of the bright ETGs inside the virial radius of the Fornax cluster, Spavone et al. (2020) estimated

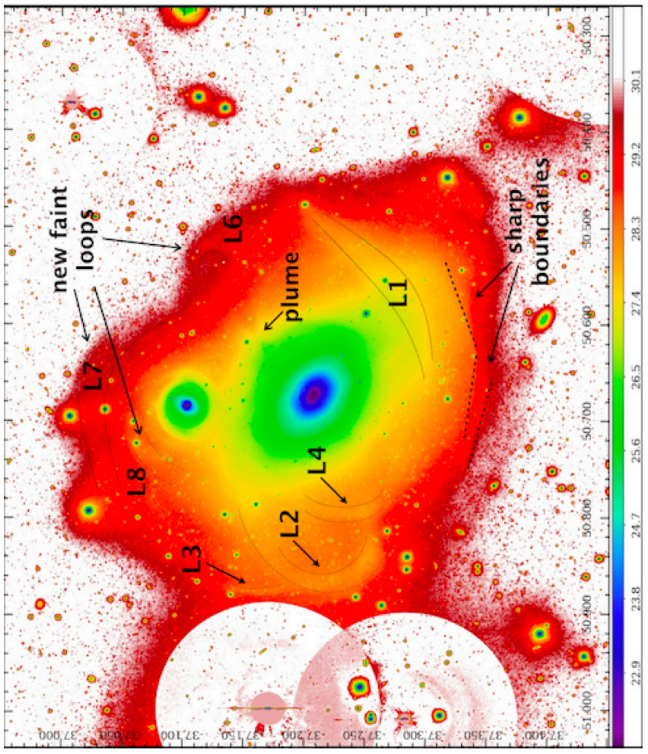


FIGURE 4.1.1: Images of NGC 1316 in SB level with the detected loops are shown in the left panel except for SW and NW loops; the latter are shown in the right panel. The adapted image is Fig. 2 and Fig. 3 in Iodice et al. (2017b).

the luminosity of the ICL in r-band to be $2.6 \pm 0.1 \times 10^{11} L_{\odot}$, which translates to a fraction of 34% of the total luminosity of the cluster core. Apart from the stellar envelope ($R > R_{tr2}$) of all galaxies, the total amount of ICL in the Fornax cluster also includes the stellar bridge connecting NGC 1399 and NGC 1387 (Iodice et al. 2016), and the patch of diffuse light detected by Iodice et al. (2017b). Below, we summarise the main results on the ICL in the Fornax cluster core.

4.2.1 The stellar bridge connecting NGC 1399 and NGC 1387

The material expelled by a galaxy that is interacting with a massive companion perturbing it produces tidal tails with similar age and metallicity to that of its parent galaxy. Alternatively, if a low-mass galaxy disrupts the halo of a massive galaxy, the tidal streams is made up of material different form that of the parent galaxy (Duc et al. 2015). As such, Iodice et al. (2016) detected such stellar streams between NGC 1399 and NGC 1387 which are at SB levels of 29 mag/arcsec^2. They suggested that these streams, which they called 'stellar bridge' were formed due to the ongoing interactions between NGC 1399 and NGC 1387. In the same region, blue GCs were detected (Bassino et al. 2006; D'Abrusco et al. 2016). The origin of these blue GCs is due to the tidal stripping of the stellar envelope of NGC 1399 and NGC 1387.

4.2.2 The diffuse light in the central regions of Fornax cluster core

By subtracting the 2D model of the light distribution of the bright ETGs in the central region i.e. from 40' to over an area of 430 arcmin^2, Iodice et al. (2017a) detect several patches of diffuse light in the north and north-west regions of NGC 1399. The bulk of the ICL is concentrated between three bright ETGs (NGC 1387, NGC 1379, NGC 1381). These patches appear to be connecting bridges between the bright ETGs (see Fig. 4.2.1) and are contributing to the growth of the ICL through tidal interactions. The gravitational interactions between the aforementioned galaxies happened in the west-northwest (W-NW) sub-clump of the cluster. The intra-cluster baryons found here are the result of these interactions that modified the structures of the massive galaxies therein (Iodice et al. 2019a). Venhola et al. (2017) showed that there was a significant drop in the number density of LSB dwarf galaxies below cluster-centric distance $r = 0.6$ deg (180 kpc; see Fig. 4.2.2) suggesting that a fraction of the ICL population here also comes from the disrupted low-mass dwarf galaxies (Venhola et al. 2017; Iodice et al. 2019a).

4.2.3 The intracluster GCs and PNe

In Fig. 4.2.1, Iodice et al. (2017a) also show the intracluster GCs detected by D'Abrusco et al. (2016) and Cantiello et al. (2018). The overdensity of the GC system was found to connect NGC 1399 to its neighbouring galaxies and that their asymmetric nature suggests that the galaxies in the Fornax cluster core

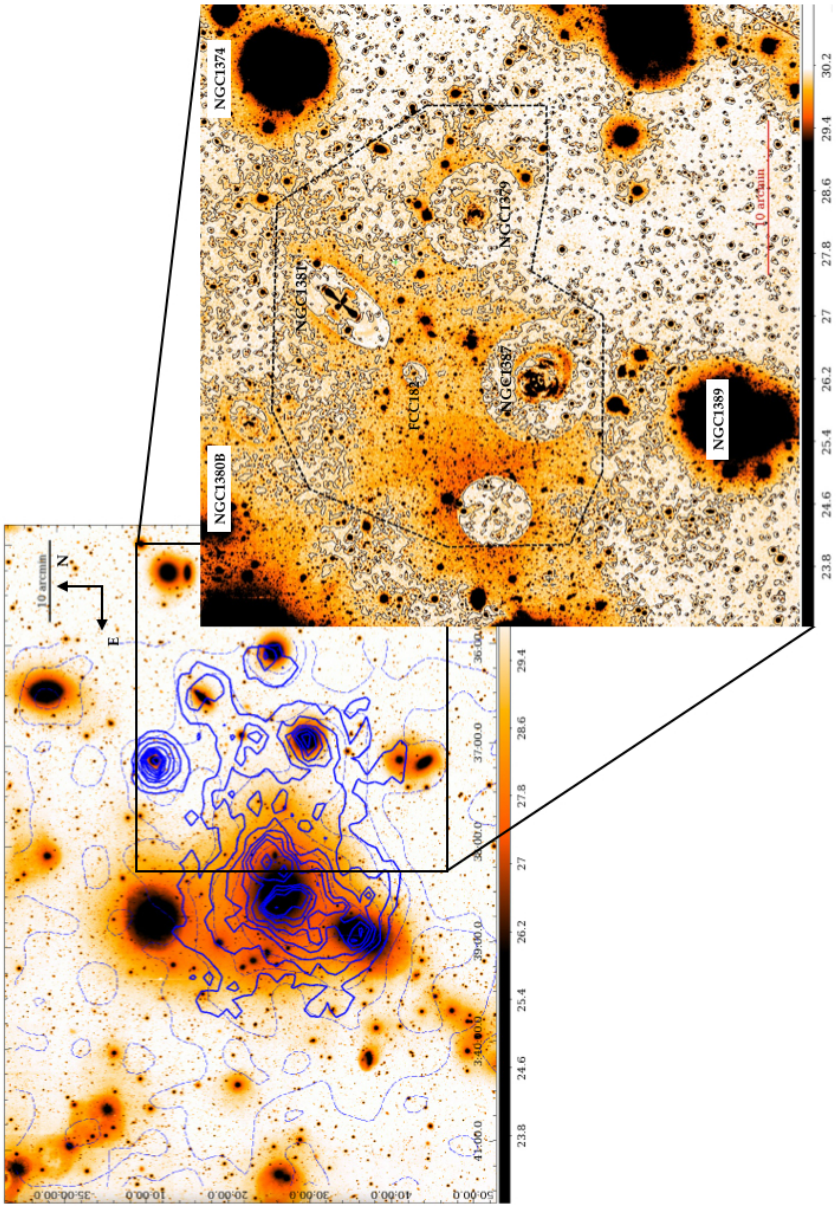


FIGURE 4.2.1: The central regions around NGC 1399 where Iodice et al. (2017a) detect diffuse patches of ICL. The GCs detected by D'Abrusco et al. (2016) and Cantiello et al. (2018) are marked in blue. The adapted figure is Fig. 1 in Iodice et al. (2017a).

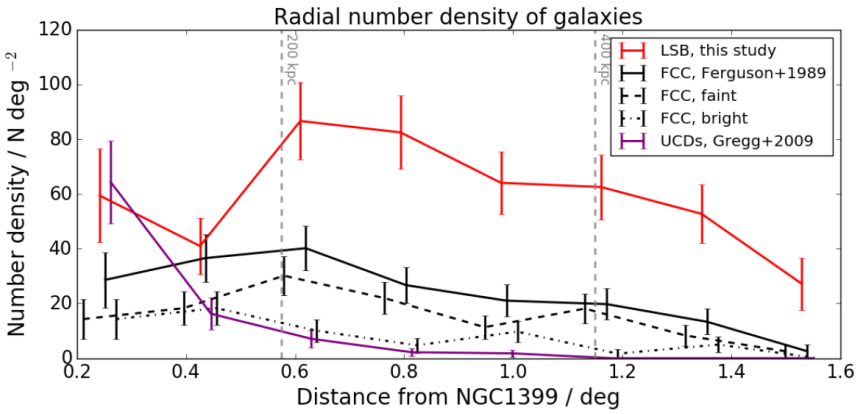


FIGURE 4.2.2: Radial density of the galaxy population as a function of the cluster-centric distance. The red line indicates the radial density of LSB galaxies in the Fornax cluster. Other samples are also indicated. The adapted image is Fig. 13 in Venhola et al. (2017).

have undergone several interactions and this is suggestive of the red GCs. On the other hand, the spatial distribution of blue GCs is due to them being stripped from the haloes of massive galaxies (D'Abrusco et al. 2016). The ICL is the counterpart of this overdensity of blue GCs (Iodice et al. 2017a). In the same regions of the 'connecting bridge' between NGC 1399 and NGC 1387, (Spiniello et al. 2018) found a high-velocity PNe. Moreover, Spiniello et al. showed that the PNe are not bound to NGC 1399 beyond R $\sim$ 400".

4.2.4 The ICL of Fornax cluster compared to other local clusters

The estimated ICL fraction of the Virgo cluster ranges between 7% and 15% (Mihos et al. 2017), and of the Coma cluster ranges between 25% and 50% (Jiménez-Teja et al. 2019, and references therein). For nearby clusters, Ciardullo et al. (2004) found that the ICL fraction spans a range of 15%–35%. The high ICL fraction in the Fornax cluster is consistent with predictions that it is in an evolved state where most of its bright members ($m_B < 15$ mag) are ETGs and has an ETG/LTG ratio of 1.6. The ICL fraction in the Fornax cluster is comparable to that of the Coma cluster which has an ETG/LTG ratio of 6 (Colless 2000). The Virgo cluster has a low ETG/LTG ratio (0.6) and is indicative of its evolutionary phase and hence has a low fraction of ICL.

4.3 Estimation of the IGL

The IGL is estimated from the mosaic in g and r bands as their surface brightness limit is fainter than that of the i-band (see Tab. 3.2.1). The brightest stars and galaxies surrounding NGC 1316 are modelled using the IRAF tasks ELLIPSE and BMODEL as explained in Sect. 3.3.1, and then subtracted from the image. The resultant residual image is used to derive the radial profiles and

thus 2D model of NGC 1316, which is also subtracted from the image. The final residual image is used to estimate the IGL[20] using the IRAF task PHOT, which computes integrated flux inside a specified aperture. The uncertainties on the estimate of the IGL take into account 1) the error on the background estimate ($\simeq$ 10% in g, $\simeq$ 50% in r); 2) the poissonian error on the flux ($\simeq$ 26% in g and r) and 3) the error on the photometric calibration ($\simeq$ 0.1% in g and r).

According to Iodice et al. (2016), the stellar envelope of NGC 1316 starts to dominate at $R > R_{tr} = 5.5'$, where R_{tr} is the transition radius[21]. Taking this into account, we mask this region of NGC 1316. The IGL is estimated in a region $\sim$33.5 arcmin^2 surrounding NGC 1316, which covers nearly 60% of the group including the bright galaxies. In Fig. 4.3.1, we show the final g-band image used in the estimation of the IGL of the Fornax A subgroup. In this image, we also mark the loops that are part of the stellar envelope (also see Iodice et al. 2017b).
Through our deep photometry of this group, we also find a new patch of diffuse light in the SW part of NGC 1316, which also contributes to the IGL (see Fig. 4.3.1).

The total magnitude[22] of the IGL in the Fornax A group, within an area of $\sim$33.5 arcmin^2 around NGC 1316, is $m_g = 10.1 \pm 0.3$ mag and $m_r = 9.2 \pm 0.3$ mag in g and r bands, respectively. Therefore, the total luminosity is $6 \pm 2 \times 10^{10} L_\odot$ in g-band and $7 \pm 2 \times 10^{10} L_\odot$ in r-band. As pointed out earlier, the IGL estimate includes the stellar envelope of NGC 1316. The fraction of the IGL luminosity to the (i) luminosity of the BGG NGC 1316 is $L_{IGL,g}/L_{BGG,g} \sim 19\%$; (ii) total luminosity of all group members (including dwarf galaxies) inside the virial radius is $L_{IGL,g}/L_{group,g} \sim 16 \pm 4\%$. The total luminosity of NGC 1316 ($L_{BGG,g} = 3.11 \times 10^{11} L_\odot$) is given by Iodice et al. (2017b). The total luminosity for dwarf galaxies ($9 \times 10^8 L_\odot$ in g-band) is provided by Venhola et al. (2019). The total luminosity for all bright LTGs in the sample studied in this work are derived from magnitudes listed in Tab. 3.3.3.

The contribution to the IGL (in g-band) of the luminous loops in the stellar envelope of NGC 1316 (loops L1, L2, L9, SW loop L5) is 22%. According to Iodice et al. (2017b), the total luminosity from these loops is $1.3 \times 10^{10} L_\odot$ in g-band. We stress that the IGL estimation is a lower limit as it is not possible to estimate the diffuse component which is in the line-of-sight of masked objects.

[20] This method of estimating the IGL is not affected by the point-spread function (PSF; e.g. Montes and Trujillo 2014) i.e. effect of the contamination from a galaxy's bright core, (see Chapters 2 and 3) which scatters the light in the regions around them.

[21] The transition radius R_{tr} is defined as the distance from the centre of the galaxy to the region where an inflection (evident in their SB profiles) in the stellar halo occurs (Cooper et al. 2010; Cooper et al. 2013).

[22] Values were corrected for Galactic extinction using the absorption coefficient by Schlegel, Finkbeiner, and Davis (1998).

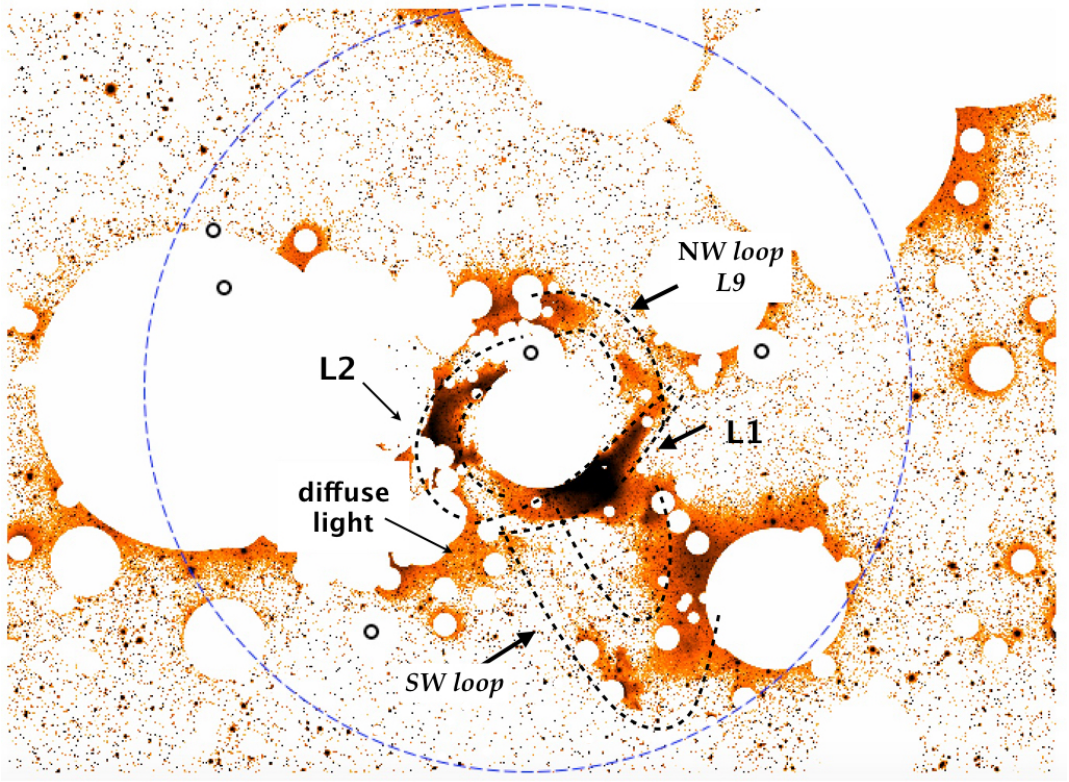


FIGURE 4.3.1: Residual image in g-band used for the estimation of the IGL. The image size is $\sim$ 87.7 $\times$ 63.4′. The blue dotted circle is the circular aperture with radius = 33.5′; the IGL is estimated in this region. All bright galaxies are marked with black circles. The known luminous structures— loops L1, L2, L5 (SW loop), L9 (NW loop) are indicated (also see Iodice et al. 2017b). A patch of diffuse light is also indicated.

4.4 On the build-up of the IGL in the Fornax A subgroup

In this section, we summarise relevant results from this work and those from previous works on the Fornax A group that will help to understand the formation history of its IGL and then discuss in detail how predictions from models fit in well with our results from observations. The IGL in the Fornax A group is estimated within a region $\sim$35 arcmin^2 ($\sim$0.5 deg), which covers most of the group extension (see Sect. 4.3). Inside this radius, Venhola et al. (2019) found a significant drop in the number of dwarf galaxies ($\sim$ 50%; see also Fig. 4.4.1). This might be an indication that the IGL in the Fornax A group was assembled by past merger of NGC 1316 (see Iodice et al. 2017b; Serra et al. 2019) and disruption of satellite galaxies on infall, which also contributed to the build-up of the extended stellar envelope around NGC 1316. This hypothesis is further supported by comparing the IGL fraction in the Fornax A subgroup with theoretical predictions from Contini et al. (2014) (see Fig. 4.4.2). According to Contini et al. (2014), galaxies that get destroyed while falling into the cluster/group make the accreted component of the

ICL/IGL. Since IGL in the Fornax A subgroup fits well in both regions from tidal disruption and merger channels, this suggests that, at the present epoch, both mechanisms contributed to the build-up of this component.

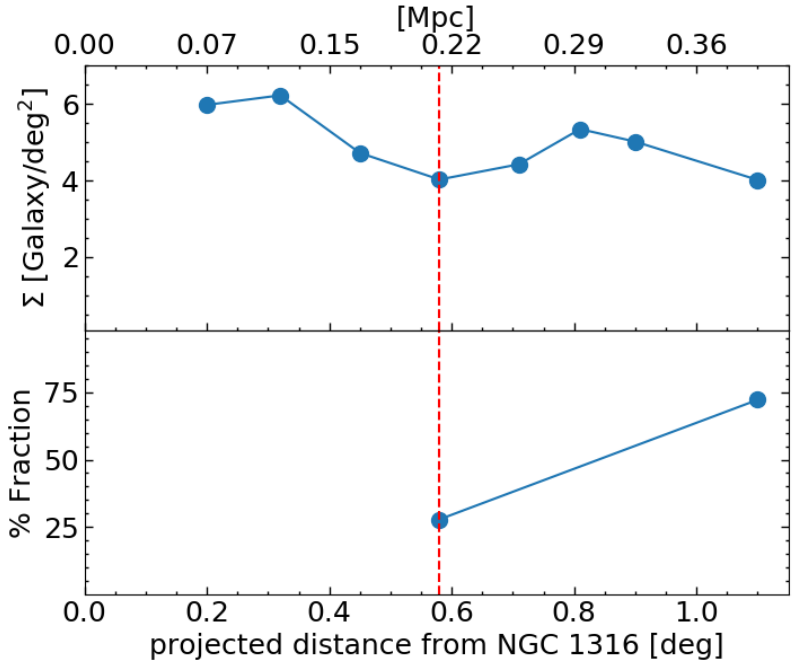


FIGURE 4.4.1: Top panel: Radial density of the galaxy population as a function of the group-centric distance. Lower panel: Percentage fraction of galaxies within an annulus = 0.6 deg and outside this annulus. The red dashed line indicates the radius within which the IGL is estimated.

In Fig. 4.4.2 we also compare the IGL derived for the Fornax A group with values obtained for other groups of galaxies, from observations of comparable depth and with the same image analysis. In particular, we plot the fraction of IGL to the total luminosity of the bright member galaxies as a function of the BGG stellar mass (in the range 10^{11} – 10^{12} $M_{\odot}$) for four groups: Fornax A (NGC 1316), NGC 5018 (Spavone et al. 2018), NGC 1533 (Cattapan et al. 2019), and IC 1459 (Iodice et al. 2020). Compared with theoretical predictions, the IGL fraction in each group reflects their assembly history. The main contribution to the IGL in the NGC 5018 group comes from the extended tidal tail that is tracing an ongoing merger (Spavone et al. 2018). In the Fornax A group, as well as in the NGC 1533 triplet (Cattapan et al. 2019), that have a comparable IGL fraction, mergers would have partly contributed to the IGL, and signs of past mergers are confined in the BGG's envelope (in the form of loops and shells). As pointed out by Iodice et al. (2020), given the low IGL fraction ($\sim$ 2%) and the structure and properties of galaxy members, the IC 1459 group is still in an early mass assembly phase.

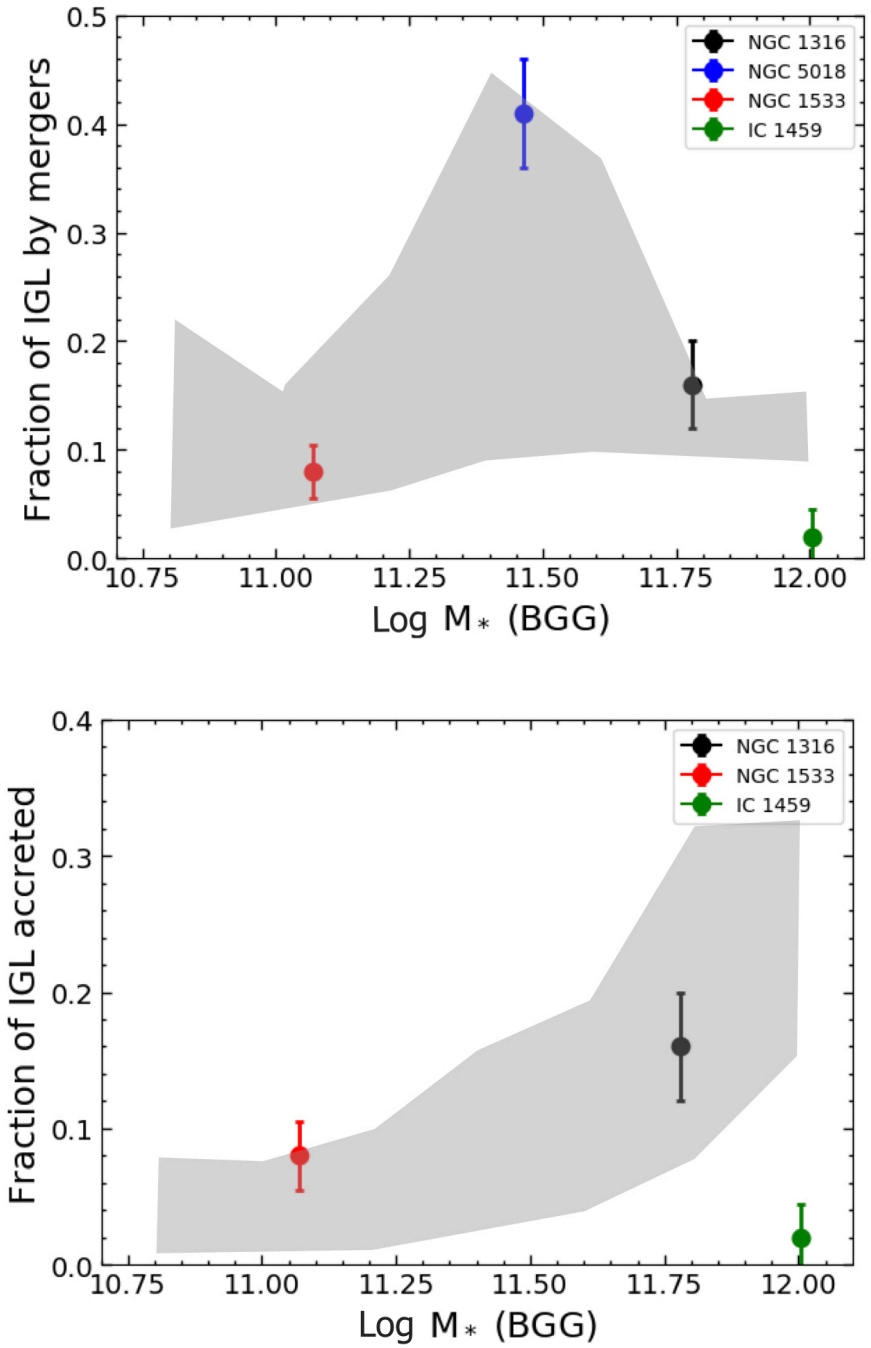


FIGURE 4.4.2: Fraction of IGL by mergers (top panel) and fraction of IGL accreted (bottom panel), as a function of the BGG stellar mass for four groups: NGC 1316, NGC 5018 (Spavone et al. 2018), NGC 1533 (Cattapan et al. 2019), IC 1459 (Iodice et al. 2020). The shaded areas represent the 20th and 80th percentile of the *model disruption* described by Contini et al. (2014).

The connection between the IGL fraction and evolution is also consistent with the different ratios of ETG-to-LTG galaxies. In the Fornax A group, ETG/LTG=0.11, since it has only one peculiar ETG (NGC 1316) and nine bright LTGs. NGC 5018 and NGC 1533 groups have ETG/LTG=1.6, while IC 1549 ETGs/LTGs=0.3. Although the Fornax A subgroup has the lowest ratio among the groups discussed above, a major fraction of the IGL with respect to the IC 1459 group, which has comparable ETG-to-LTG ratio, comes from the past merger of NGC 1316 and disrupted dwarf galaxies. In the IC 1459, no signs of interactions are found with a galaxy of comparable mass (Iodice et al. 2020).

4.4.1 The HI content versus diffuse light

As mentioned in Sect. 4.1, the presence of HI clumps in the loops of NGC 1316 points to its past merger (Serra et al. 2019). For all bright LTGs in the Fornax A subgroup, there are HI-detections (Schröder, Drinkwater, and Richter 2001; Serra et al. 2019). Moreover, for some of these galaxies, their HI disc is beyond their stellar disc (Serra et al. 2019). This is expected as the group is in its early stage of assembly.

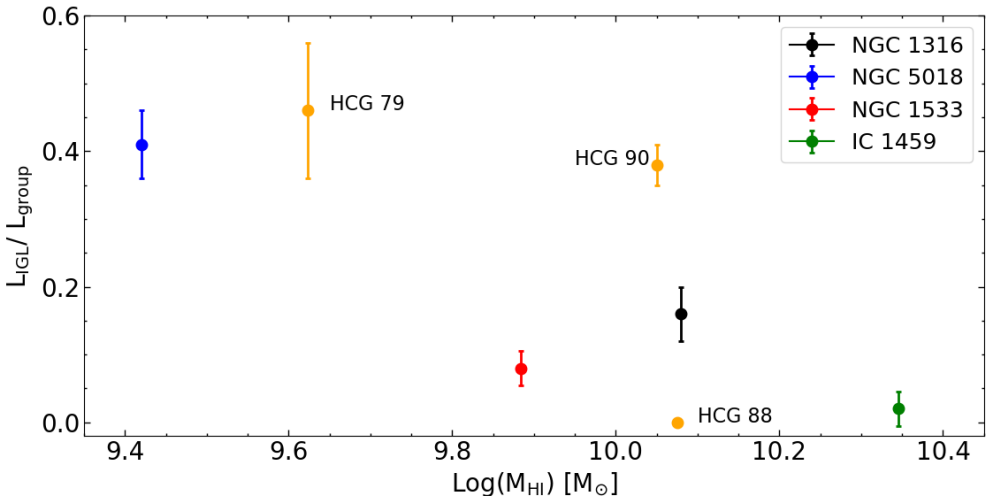


FIGURE 4.4.3: Fraction of IGL as a function of the total HI mass for four loose groups (NGC 5018, NGC 1533, IC 1459, NGC 1316) and Hickson Compact Groups (HCG). Data for HC 79, HCG 88, HCG 90 are taken from Ribeiro et al. (1998), Da Rocha and Mendes de Oliveira (2005), Da Rocha, Ziegler, and Mendes de Oliveira (2008), and Borthakur, Yun, and Verdes-Montenegro (2010)

Iodice et al. (2020) find that the total HI mass of three loose groups (NGC 1533, NGC 5018, IC 1459) inversely correlates with the fraction of the IGL. The total HI mass of the Fornax A subgroup is $M_{HI} = 1.2 \times 10^{10} M_\odot$ (private communication with Dane Kleiner and Paolo Serra). As done in Iodice et al. (2020), we include NGC 1316 in Fig. 4.4.3 and the observed trend applies here as well. This, as previously suggested, shows that groups with low fractions of IGL have higher HI masses.

4.4.2 IGL as the progenitor of the ICL

There are three well-defined groups in the cluster: *core, north-south clump* and the *infalling galaxies* (Iodice et al. 2019a; Spavone et al. 2020); and references therein). Each of these groups exhibit different properties in their light distribution, structure, stellar populations (Iodice et al. 2019a). In particular, galaxies in the north-south clump are more metal-rich and massive than other galaxies in the cluster (Iodice et al. 2019b). On the other hand, the infalling galaxies show signs of interaction with evidence from their tidal tails and disturbed molecular gas (Zabel et al. 2019 and Chapter 2).

As mentioned earlier, the bulk of the ICL comes from the W-NW subclump of galaxies. According to Iodice et al. (2019a), this clump may have resulted from the early accretion of a group of galaxies during the assembly of the cluster.

The fraction of IGL in the Fornax A subgroup is 16%, while that of the Fornax cluster core is 34%. Clearly, both of these environments are at different stages of evolution. Simulations by Rudick et al. (2009, and references therein) show that during the process of infall, the IGL mixes with the ICL. Due to the low-velocity dispersion of galaxies in groups, 'pre-processing' of groups before falling onto the cluster is what contributes to the detected intra-cluster baryons.

4.5 Summary and conclusions

In this chapter, we have given an overview of the faint outskirts of the BCG NGC 1399, BGG NGC 1316, and the ICL in the Fornax cluster core. We then described the method used in the estimation of the IGL and addressed its formation history. The main results and conclusions are as follows:

- The luminosity of IGL in the Fornax A group is estimated to be $6 \pm 2 \times 10^{10} L_{\odot}$ in g. Compared to the total luminosity of the group, the fraction of IGL is $\sim$ 16%. Our estimates are in good agreement with model predictions from Contini et al. (2014). Thus, we address the formation history of the IGL in the Fornax A group which is mainly through the past merger of NGC 1316 and the disruption of dwarf galaxies in the same region. This is further supported by the significant drop in the number of dwarf galaxies ($\sim$ 50%) towards the group centre found by Venhola et al. (2019).

- We confirm that HI content of NGC 1316 is inversely correlated with the fraction of the IGL, as found by Iodice et al. (2020) in three loose groups, suggesting that Fornax A group is in an early stage of assembly.

- The fraction of ICL in the Fornax cluster is 34% (Spavone et al. 2020), which is higher than that of the Fornax A subgroup. This clearly shows that both environments are at different stages of evolution.

By analysing the intra-cluster baryons in the Fornax cluster, we have shown how hierarchical merging of groups in the cluster forms the ICL.

Chapter 5

Discussion and future perspectives

In this chapter, I summarise the key results of the work presented in this thesis and discuss how they help us understand 'pre-processing' of galaxies part of groups before cluster-infall. By doing so, I trace the evolutionary path of LTGs in the Fornax cluster and therefore predict their fate in the cluster environment. Finally, I draw conclusions and give the future perspectives of the work undertaken in this thesis.

5.1 Discussion

The work undertaken in this thesis is part of a deep imaging survey FDS, which covers a diverse range of topics concerning the assembly history and evolution of the Fornax cluster. By exploring the faint regions of the galaxy outskirts, estimating and studying the build-up of the ICL/IGL, investigating the properties of the galaxies themselves, FDS aims to provide a new and comprehensive view of the Fornax cluster and of galaxies therein.

As such, my contribution to this survey and to the overall understanding of the Fornax cluster is the study of the bright LTGs ($m_B < 16$ mag) residing in the core of the cluster and compare relevant properties to those in the subgroup. By doing so, we are able to comprehend the processes taking place in the cluster environment that contribute to the structure transformation and evolution of galaxies in the cluster.

In this thesis, I have presented the surface photometry analysis of 22 LTGs in the Fornax cluster i.e. 13 in the core and nine in the subgroup, observed with FDS. In Chapter 2, I gave a detailed explanation of the methods to derive structural parameters, average colours, and stellar mass. In order to detect and derive the break-radius, I explained the algorithm I developed and therefore provided an accurate estimate of the break radius. I discussed the morphology, structure, average colours, break-radii, break type of all 13 LTGs. In the context of the morphology-density relation, I also compared some parameters to those of the ETGs and thus showed how dense environments play a major in the evolution of their constituent galaxies. In Chapter 3, using the same method of analysis from Chapter 2, I compared the results of nine LTGs in the subgroup to those in the cluster core. By doing so, I showed how different the impact of both these environments are on the LTGs. I combined results from surface photometry to their time of infall, as seen in the PPS diagram therefore providing the assembly history of the LTGs in the subgroup. In order to justify how different the cluster core is, in comparison to the group, I estimated the IGL of the latter. Thus, in Chapter 4, I provided a thorough explanation of the method used to estimate the IGL and through theoretical models, I discussed the formation history of the IGL and compared this to other loose groups. Since the IGL is the precursor of the ICL, I also gave an overview of the formation history of the ICL in the cluster core thus providing a complete analysis of the total ICL in the Fornax cluster.

The main results of the work presented in this thesis are:

Bright LTGs in the Fornax cluster core: In the Fornax cluster core, galaxies with Type-II disc-breaks have blue average $(g - i)$ colours in their outer discs while galaxies with Type-III disc-breaks have red average colours $(g - i)$ in their outer discs. The inner and outer discs increase with stellar mass and decrease with molecular gas-fractions. Beyond the break radius, there is no cold gas detected. We showed how the dense environment of the cluster core causes segregation in morphology and stellar mass such that LTGs with morphological type $5 < T \leq 9$ are located beyond the high density regions

of the cluster core, which are populated by the most massive ETGs.

Bright LTGs in the Fornax A subgroup: In the Fornax A subgroup, LTGs span a range of stellar mass $8 < logM_*M_\odot < 11$. Six out of nine LTGs exhibit a Type-III disc-break, which is either suggestive of strangulation halting the star-formation in their outer discs or a consequence of HI-richness. The evolutionary phase of the Fornax A group is different from that of the cluster core, and is evident in the absence of morphology and colour segregation with group centric distance. This is further supported by the effect of the environment on the structure of LTGs such that the break radius was detected beyond $1R_e$ in the case of the group LTGs, and is contrary to those in the cluster core ($<1R_e$).

The intra-cluster baryons in Fornax: The luminosity of the IGL is $6 \pm 2 \times 10^{10} L_\odot$ in g-band and corresponds to a fraction of 16% of the total light in the group. The fraction of ICL to the total light in the cluster core is 34%. The bulk of the ICL as given in previous works is in the region of the W-NW clump which is believed to be a group of galaxies suggesting how the IGL contributes to the ICL.

All of the mentioned work plays a bigger role in understanding the difference in the evolutionary path of galaxies falling into a dense environment that were part of a group or from the field. In the Fornax cluster, we see groups of galaxies as well as galaxies from the field. This is crucial in the investigation of the mass assembly of the cluster as well as the fate of its constituent LTGs. In the next section, I discuss how all of the above results have helped us to further understand pre-processing of galaxies in groups before falling into a cluster.

5.1.1 On the account of pre-processing of galaxies in the Fornax cluster core

In this thesis, I have analysed LTGs in the core of the cluster and compared them to those in the infalling group. The basis for this is to see how environments influence the morphological transformation of galaxies upon infall. In the local Universe, the abundance of quiescent ETGs over LTGs has been interpreted as the result of the various processes that occur in rich clusters by quenching star-formation. The same can be suggested for the evolution of galaxies in the Fornax cluster. However, the question would be if these were pre-processed before cluster-infall. Based on the ΛCDM, clusters are formed through hierarchical merging of smaller structures like groups. As previously mentioned, there are three significant groups in the Fornax cluster. In order to trace their evolutionary history, we have to analyse their faint features, time since infall, and other observational properties. This way, we also predict the evolutionary path of LTGs in the infalling sub-group and thus map the fate of the Fornax cluster itself.

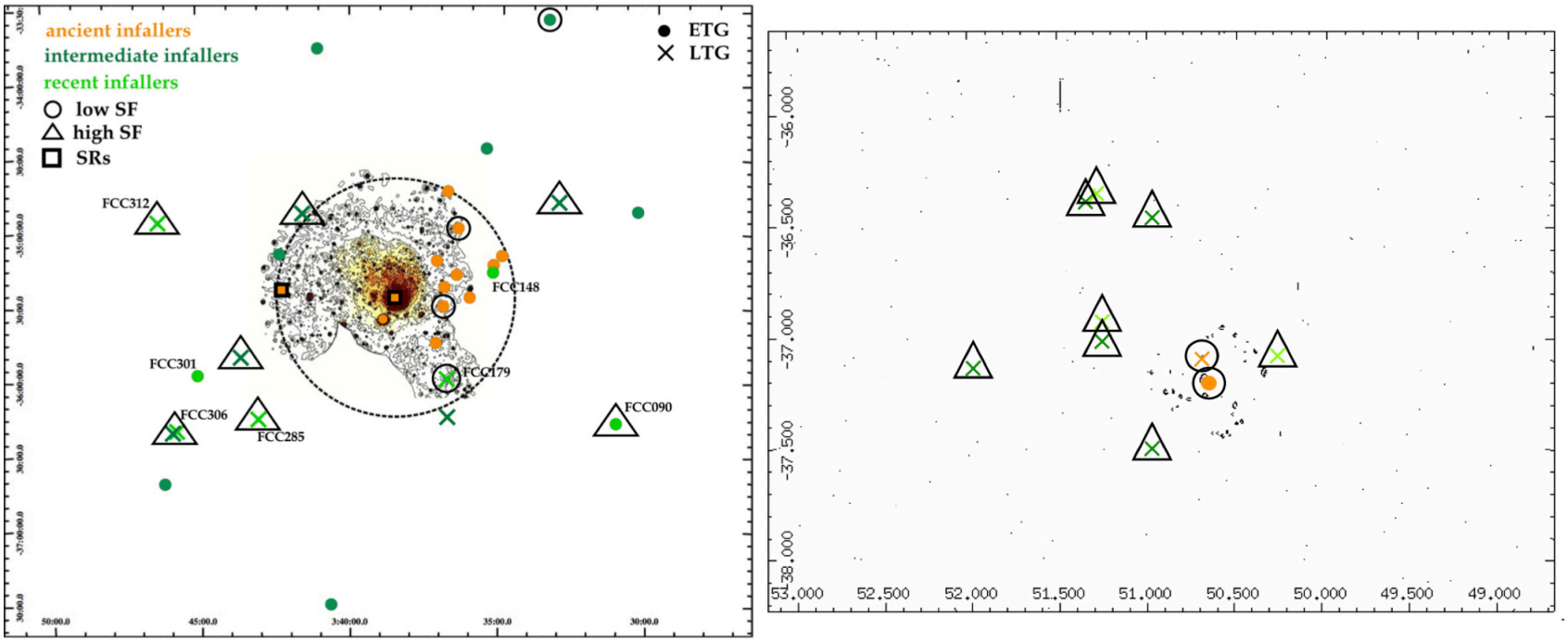


FIGURE 5.1.1: ETGs and LTGs in the Fornax cluster core (left panel) and Fornax A subgroup (right panel) are indicated with circles and crosses. Orange, green, and light-green symbols represent ancient, intermediate, and recent infallers according to the PPS diagram. Open triangles and circles indicate high and low star-formation (SF). Left panel: The X-ray emission is in the energy range 0.4–1.3 keV as measured by XMM-Newton (Frank et al. 2013). The adapted image is Fig. 7 in Iodice et al. (2019b). Right panel: The X-ray emission is in the energy range 0.5–0.6 keV (Kim and Fabbiano 2003). We assumed the star-formation activity based on the Hα emission (Raj et al. prep) in the bright galaxies.

Clues from phase-space diagrams

With Fornax 3D MUSE data, Iodice et al. (2019b) traced the assembly history of bright galaxies in the Fornax cluster core. Their findings provide further evidence to the processes and mechanisms proposed by other works (Zabel et al. 2019; Iodice et al. 2019a; Raj et al. 2019) on the evolution of galaxies in the Fornax cluster. As described in Chapter 3, the PPS diagram gives an approximate time since infall and by combining results from stellar kinematics, star-formation, and stellar populations of the bright galaxies, Iodice et al. (2019b) concluded that the main cluster consists of three groups: the *core*, the *north-south clump*, and the *infalling galaxies*. Bright galaxies part of the Fornax 3D sample (Iodice et al. 2019b) are shown in Fig. 5.1.1 (right panel). In this section, I summarise results from past works which provide clues on 'pre-processing' of galaxies before cluster-infall.

W-NW clump: According to Iodice et al. (2019b), the *north-south clump* is the result of the accretion of a group of galaxies during the cluster-collapse. Galaxies in the clump are found to be redder and more metal-rich than other galaxies in the cluster, while their outskirts have lower metallicity than their bright central regions. As discussed in Chapter 4, the bulk of the ICL is also found in the clump. Galaxies in this region have spent over 8 Gyr in the cluster core. In addition to this, Spavone et al. (submitted) found that ETGs in the clump have the highest accreted mass fraction and flat colour profiles in their outskirts. As these galaxies were part of a group before infall, they have undergone a fair amount of 'pre-processing', which has significantly modified their structures and contributed to the growth of their stellar halos (Iodice et al. 2019b, Spavone et al. submitted). Findings from the aforementioned works are also consistent with those from Pinna et al. (2019b) and Pinna et al. (2019a), where they show that three of the S0 galaxies in the clump have thick discs.

LTGs: Most of the LTGs in the Fornax cluster core are recent (FCC179, FCC263, FCC285, FCC306, FCC312) and intermediate (FCC290, FCC308, FCC113) infallers. From Chapter 2, it is evident that the tidal forces of the cluster environment have caused minor disturbances in thee outskirts of recent infallers. In particular, the tidal tails of FCC312 and FCC285 are signs of interaction with the cluster potential or past minor merging events.

Except for FCC179, the recent infallers are star-forming (see Fig. 5.1.1: left panel). Due to the velocity difference between FCC179 and that of the cluster, Makarov and Karachentsev (2011) classified the galaxy to be that of a group. This would explain its low star-formation rate (SFR) in comparison to other LTGs of comparable stellar mass. Moreover, HII regions (Weaver, Wilson, and Baldwin 1991) and molecular gas (Zabel et al. 2019) are only detected in its spiral arms. So far, there has been no HI detection (Schröder, Drinkwater, and Richter 2001). All of these results support that this galaxy has undergone 'pre-processing'.

Evidence from break-radius

One of the main results of the work in this thesis is that the break radii of galaxies in the Fornax cluster core are within $1R_e$ while those of galaxies in the subgroup are beyond $1R_e$. In the Fornax cluster core, FCC179 and FCC290 are of comparable stellar mass but the former has low SFR. In addition to this, the break radius of FCC179 is at $\sim 2.5R_e$ making it an outlier, while that of FCC290 is at $\sim 1R_e$. As concluded in Chapter 2, there are no sub-structures (e.g. spiral arms) beyond the break radius of the cluster LTGs suggesting that the dense environment has significantly altered their outskirts, slowly transforming them into S0 galaxies. This further supports that FCC179 has undergone 'pre-processing' Although being a recent infaller, it appears to be transitioning into an S0. The other LTGs in the cluster core are undergoing structure transformation in the cluster environment. In the case of the Fornax cluster core, the break radius is more of a component-transition radius, beyond which there is no molecular gas or star-forming regions. For galaxies in the Fornax A subgroup, their Type-III breaks is either suggestive of strangulation or HI-richness.

Recently, IllustrisTNG simulations by Joshi et al. (2020) found that there was no significant difference in the degree of morphological change of pre-processed galaxies in comparison to those from the field, but insisted that pre-processing of galaxies should be considered in understanding the effect of the environment on *galaxy evolution* as a cluster consists of galaxies with different morphologies and accretion times.

5.1.2 The fate of LTGs in the Fornax cluster

As done for the bright galaxies in the Fornax cluster core in Iodice et al. (2019b) (also see Fig. 5.1.1: left panel), I reproduced a similar image (see Fig. 5.1.1: right panel) to compare the effect of the environment on the evolution of LTGs. From Fig. 5.1.1 (right panel), it is evident that the processes in dense environments can remove gas from the galaxies thereby halting star-formation and changing their morphology. In the Fornax A subgroup, most of the bright LTGs are intermediate and recent infallers, meaning that they have only passed through the pericenter once. These galaxies also exhibit star-forming regions in their spiral arms, as seen through their Hα-distribution (Raj et al. in prep; also see Chapter 3). Recent and intermediate infallers in the Fornax cluster core also have higher SFR than ancient infallers. Recently, IllustrisTNG simulations by Joshi et al. (2020) show that cluster disc galaxies that spend the longest time in the cluster experience the largest change in morphology by $z = 0$. This is true in the case of FCC176, which is an ancient infaller and is devoid of gas with no evidence of star-formation activity (see Iodice et al. 2019b). All of this suggest that the dense environment of the Fornax cluster core is significantly transforming the structure of LTGs therein.

5.2 Conclusions and future perspectives

The main results of the work presented in this thesis provide a better understanding of the structure and evolution of LTGs in the Fornax cluster. In particular, deep imaging data have helped us to trace the formation history of these galaxies and the ICL by exploring their light distribution down to faint SB levels (> 28 mag/arcsec^2). In order to investigate the effect of the environment on the evolution of its constituent galaxies, combining results from multiple wavelengths is essential. In this context, the break radius has proven to be a useful parameter in providing further support to the predictions of galaxies being 'pre-processed'. All in all, the Fornax cluster is one of the most preferred regions in the local Universe to test out theories concerning the evolution of galaxies, from the biggest to the faintest. In this thesis, I have compared the LTGs in two different environments to predict their fate to show how their hosting cluster affects their evolutionary path.

Within the Fornax cluster, we have seen how different the impact is on the structure transformation of galaxies therein. In the era of deep imaging data, the questions we can ask are (i) *How do the outskirts and structure of LTGs in other groups and clusters in the local Universe vary from the Fornax cluster?* (ii) *Can we detect disc-breaks and truncations beyond $z \sim 1$? What will it suggest of their local environment? Will we expect a trend on large-scales?*

With greater image depth and resolution of the Vera C. Rubin Observatory Legacy Survey of Space and Time (LSST; Ivezić et al. 2019), we will be able to explore a large area ($\sim 20{,}000^2$ deg) of the sky. The Extremely Large Telescope (ELT) will provide a ground for investigating the formation history of the ICL in different environments at higher redshifts. Euclid will provide photometric redshifts for a large (overlap of $\sim 11{,}000^2$ deg) area using the measurements from LSST. With the advent of the future telescopes, we will be able to discover many more aspects of *galaxy evolution*.

Apart from the work presented in Chapters 2, 3, and 4, as part of my PhD, I have also contributed to the following works, published in first-quartile refereed journals:

- Spavone, M.; Iodice, E.; van de Ven, G.; Falcon-Barroso, J.; **Raj, M. A.**; Hilker, M.; Peletier, R. F.; Capaccioli, M.; Mieske, S.; Venhola, A.; Napolitano, N. R.; Cantiello, M.; Paolillo, M.; Schipani. P.; *The Fornax Deep Survey with VST. VIII. Connecting the accretion history with the cluster density*, in press, A&A, 2020 (arXiv:2005.00025)

- Scognamiglio, D.; Tortora, C.; Spavone, M.; Spiniello, C.; Napolitano, N.R.; D'Ago, G.; La Barbera, F.; Getman, F.; Roy, N.; **Raj, M. A.**; Radovich, M.; Brescia, M.; Cavuoti, S.; Koopmans, L. V. E.; Kuijken, K. H.; Longo, G.; and Petrillo, C. E.; *Building the largest spectroscopic sample of ultra-compact massive galaxies with the Kilo Degree Survey*, ApJ, 2020, 893, 4. DOI: 10.3847/1538-4357/ab7db3

- Tortora, C.; Napolitano, N. R.; Spavone, M.; La Barbera, F.; D'Ago, G.; Spiniello, C.; Kuijken, K. H.; Roy, N.; **Raj, M. A.**; Cavuoti, S.; Brescia, M.; Longo, G.; Pota, V.; Petrillo, C. E.; Radovich, M.; Getman, F.; Koopmans, L. V. E.; Trujillo, I.; Verdoes Kleijn, G.; Capaccioli, M. Grado, A.; Covone, G.; Scognamiglio, D.; Blake, C.; Glazebrook, K.; Joudaki, S.; Lidman, C.; Wolf, C.,*The first sample of spectroscopically confirmed ultra-compact massive galaxies in the Kilo Degree Survey*, 2018, MNRAS, 481, 4728. DOI: 10.1093/mnras/sty2564

- Roy, N.; Napolitano, N. R.; La Barbera, F.; Tortora, C.; Getman, F.; Radovich, M.; Capaccioli, M.; Brescia, M.; Cavuoti, S.; Longo, G.; **Raj, M. A.**; Puddu, E.; Covone, G.; Amaro, V.; Vellucci, C.; Grado, A.; Kuijken, K.; Verdoes Kleijn, G.; Valentijn, E., *Evolution of galaxy size-stellar mass relation from the Kilo-Degree Survey*, 2018, MNRAS, 480, 1057. DOI: 10.1093/mnras/sty1917

Acknowledgements

I wish to express my deepest gratitude to my thesis advisors, Dr Enrichetta Iodice and Prof Nicola R. Napolitano, for their encouragement, guidance, and continuous support throughout my PhD study and related research work. Their immense knowledge, undivided attention, and patience have contributed a great deal to my current level of expertise in the work presented in this thesis. Enrica and Nicola's motivation helped me realise my potential and made this project a success; it has indeed been a fruitful experience.

The PhD project has received funding from the European Union Horizon 2020 research and innovation programme under the Marie Skłodowska-Curie grant agreement n. 721463 to the SUNDIAL-ITN. The work undertaken in this thesis is based on visitor mode observations collected at the European Organisation for Astronomical Research in the Southern Hemisphere under the following VST GTO programs: 094.B-0512(B), 094.B-0496(A), 096.B-0501(B), 096.B-0582(A). This research has made use of the (i) NASA/IPAC Extragalactic Database (NED), which is operated by the Jet Propulsion Laboratory, California Institute of Technology, under contract with the National Aeronautics and Space Administration; (ii) Python packages Astropy (`http://www.astropy.org`), a community-developed core Python package for Astronomy (Astropy Collaboration et al. 2013; Astropy Collaboration et al. 2018), Scipy (Jones, Oliphant, Peterson, et al. 2001–), Numpy (Oliphant 2006–), Matplotlib (Hunter 2007); (iii) Software SAODS9 (Joye and Mandel 2003), `GALFIT3.0` (Peng et al. 2010b), IRAF (Tody 1986, 1993).

I should never forget to thank Prof Reynier F. Peletier, who has played an essential role in this PhD project. Reynier is the coordinator of the SUNDIAL-ITN within which, I have had the opportunity to learn and gain knowledge in various fields of astronomy as well as machine learning. I have also had the chance to work with Reynier, whose insights and guidance have helped with the favourable progress of the PhD project.

My extended gratitude to the international collaborators of the Fornax Deep Survey whose comments and suggestions contributed majorly to the publication of our scientific articles. I also thank our collaborators within the Kilo-Degree Survey (especially Crescenzo Tortora, Chiara Spiniello, Nivya Roy, Fedor Getman, Francesco La Barbera). Special thanks to (i) members of the AstroWISE team (especially to Jelte de Jong and Gijs Verdoes Kleijn for the tutorials and know-hows of AstroWISE); (ii) collaborators within the Fornax 3D team whose contribution has helped with the scientific analysis in the project.

Of course, one gets the opportunity to interact with scientists, colleagues, and many more during their PhD journey; the list is long. Nevertheless, there are those with prominent roles, without whom, a significant part of one's life would not be the same. As such, I wish to show my gratitude to Prof Johan Knapen for the continuous support, motivation and counsel that helped me complete this project. I am also sincerely grateful to Guido Celentano for the numerous times he has helped me in the past three years.

I am thankful for the support of my colleagues (especially Marilena, Giulia, Fabio) at the INAF Astronomical Observatory of Capodimonte, Naples, and at the University of Naples "Federico II". To the other 13 ESRs (Caroline, Thanh, Nushkia, Shivangee, Aleke, Alex, Alan, Teymoor, Marco, Michele, Mohammad, Bahar, Abolfazl) of the SUNDIAL-ITN: it has been a wonderful and memorable experience— learning, working, collaborating, and travelling together with them; some friendships go a long way and I wish them the very best. Special thanks to collaborators (especially to Ignacio Trujillo for his comments and insights on some of the aspects in the scientific project) and members (especially to Marlies van de Weijgaert and Wiebe Zijlstra) within the SUNDIAL-ITN.

I am grateful to have had the chance to travel widely to attend meetings and give talks during my PhD work, through which I got to communicate with experts and see a new side of the world. In particular, my special thanks go to the staff, collaborators, and fellow PhD students (especially to Sara, Jon, Adrian and many others for the great times we have had together; my best wishes to them) at the University of Groningen and ESO Garching.

We would also like to show our gratitude to Prof. Tim de Zeeuw and Prof. Johan Knapen for their comments, suggestions, and fair evaluation of this thesis.

I must not forget my family and friends who are not scientifically involved with the PhD project yet whose tremendous support and encouragement have helped me reach this commendable stage in life. In particular, my younger brother, Alwyn, and best friend, Roshni; it takes a small conversation with them to brighten my day. My heartfelt thanks to Silvana, without whom, living in Naples would not have been an enjoyable experience. I am indebted to my parents. My mother, who is my constant support and whose unconditional love has made me the person I am today. My father, who educated me and believed in my potential, but could not make it to the end of this PhD journey; he will always be my inspiration to move forward and pursue my passion.

To those whom I have forgotten to mention, I am still grateful for their assistance and support. I must again extend my gratitude to Enrica, for not only her professional guidance but also for her valuable time and kindness; she is a remarkable human being. Lastly, I am thankful for that *unseen force* in this Universe which has blessed me abundantly.

Bibliography

[1] M. G. Abadi, B. Moore, and R. G. Bower. "Ram pressure stripping of spiral galaxies in clusters". In: *MNRAS* 308 (Oct. 1999), 947–954. doi:10.1046/j.1365-8711.1999.02715.x. eprint: astro-ph/9903436.

[2] Mario G. Abadi et al. "Simulations of Galaxy Formation in a Λ Cold Dark Matter Universe. II. The Fine Structure of Simulated Galactic Disks". In: *ApJ* 597.1 (Nov. 2003), 21–34. doi:10.1086/378316. arXiv: astro-ph/0212282 [astro-ph].

[3] Rebecca J. Allen et al. "Differences in the Structural Properties and Star-formation Rates of Field and Cluster Galaxies at z$_\sim$1". In: *ApJ* 826.1, 60 (July 2016), 60. doi:10.3847/0004-637X/826/1/60. arXiv: 1605.05314 [astro-ph.GA].

[4] M. Arnaboldi et al. "A tale of two tails and an off-centered envelope: diffuse light around the cD galaxy NGC 3311 in the Hydra I cluster". In: *A&A* 545, A37 (Sept. 2012), A37. doi:10.1051/0004-6361/201116752. arXiv: 1205.5289 [astro-ph.CO].

[5] Magda Arnaboldi et al. "Intracluster Planetary Nebulae in Virgo: Photometric Selection, Spectroscopic Validation, and Cluster Depth". In: *AJ* 123.2 (Feb. 2002), 760–771. doi:10.1086/338313. arXiv: astro-ph/0110522 [astro-ph].

[6] Halton Arp. "Atlas of Peculiar Galaxies". In: *ApJS* 14 (1966), 1. doi:10.1086/190147.

[7] Astropy Collaboration et al. "Astropy: A community Python package for astronomy". In: *A&A* 558, A33 (Oct. 2013), A33. doi:10.1051/0004-6361/201322068. arXiv: 1307.6212 [astro-ph.IM].

[8] Astropy Collaboration et al. "The Astropy Project: Building an Open-science Project and Status of the v2.0 Core Package". In: *AJ* 156.3, 123 (Sept. 2018), 123. doi:10.3847/1538-3881/aabc4f. arXiv: 1801.02634 [astro-ph.IM].

[9] Neta A. Bahcall. "Clusters and dark matter". In: *Dark Matter*. Ed. by Stephen S. Holt and Charles L. Bennett. Vol. 336. American Institute of Physics Conference Series. July 1995, 201–207. doi:10.1063/1.48326.

[10] Neta A. Bahcall. "Clusters and superclusters of galaxies". In: *arXiv e-prints*, astro-ph/9611148 (Nov. 1996), astro–ph/9611148. arXiv: astro-ph/9611148 [astro-ph].

[11] Neta A. Bahcall. "Large-scale structure in the universe indicated by galaxy clusters." In: *Annual Review of Astron and Astrophys* 26 (Jan. 1988), 631–686. doi:10.1146/annurev.aa.26.090188.003215.

[12] J. Bakos, I. Trujillo, and M. Pohlen. "Color Profiles of Spiral Galaxies: Clues on Outer-Disk Formation Scenarios". In: *ApJL* 683 (Aug. 2008), L103. doi:10.1086/591671. arXiv: 0807.2776.

[13] Fabio D. Barazza, Shardha Jogee, and Irina Marinova. "Bars in Disk-dominated and Bulge-dominated Galaxies at z ∼0: New Insights from ∼3600 SDSS Galaxies". In: *ApJ* 675.2 (Mar. 2008), 1194–1212. doi:10.1086/526510. arXiv: 0710.4674 [astro-ph].

[14] K. Barbary et al. "The Hubble Space Telescope Cluster Supernova Survey. II. The Type Ia Supernova Rate in High-redshift Galaxy Clusters". In: *ApJ* 745.1, 32 (Jan. 2012), 32. doi:10.1088/0004-637X/745/1/32. arXiv: 1010.5786 [astro-ph.CO].

[15] J. Barnes. "The dynamical state of groups of galaxies." In: *MNRAS* 215 (1985), 517–536. doi:10.1093/mnras/215.3.517.

[16] Joshua E. Barnes. "Transformations of Galaxies. I. Mergers of Equal-Mass Stellar Disks". In: *ApJ* 393 (July 1992), 484. doi:10.1086/171522.

[17] Joshua E. Barnes and Lars Hernquist. "Transformations of Galaxies. II. Gasdynamics in Merging Disk Galaxies". In: *ApJ* 471 (Nov. 1996), 115. doi:10.1086/177957.

[18] Joshua E. Barnes and Lars E. Hernquist. "Fueling Starburst Galaxies with Gas-rich Mergers". In: *ApJL* 370 (Apr. 1991), L65. doi:10.1086/185978.

[19] S. Barsanti et al. "Galaxy and Mass Assembly (GAMA): Impact of the Group Environment on Galaxy Star Formation". In: *ApJ* 857.1, 71 (Apr. 2018), 71. doi:10.3847/1538-4357/aab61a. arXiv: 1803.05076 [astro-ph.GA].

[20] L. P. Bassino et al. "Large-scale study of the NGC 1399 globular cluster system in Fornax". In: *A&A* 451.3 (June 2006), 789–796. doi:10.1051/0004-6361:20054563. arXiv: astro-ph/0603349 [astro-ph].

[21] Kenji Bekki, Warrick J. Couch, and Yasuhiro Shioya. "Passive Spiral Formation from Halo Gas Starvation: Gradual Transformation into S0s". In: *ApJ* 577.2 (Oct. 2002), 651–657. doi:10.1086/342221. arXiv: astro-ph/0206207 [astro-ph].

[22] E. F. Bell and R. S. de Jong. "The stellar populations of spiral galaxies". In: *MNRAS* 312 (Mar. 2000), 497–520. doi:10.1046/j.1365-8711.2000.03138.x. eprint: astro-ph/9909402.

[23] Ralf Bender et al. "Structure and Formation of cD Galaxies: NGC 6166 in ABELL 2199". In: *ApJ* 807.1, 56 (July 2015), 56. doi:10.1088/0004-637X/807/1/56. arXiv: 1411.2598 [astro-ph.GA].

[24] George J. Bendo and Joshua E. Barnes. "The line-of-sight velocity distributions of simulated merger remnants". In: *MNRAS* 316.2 (Aug. 2000), 315–325. doi:10.1046/j.1365-8711.2000.03475.x. arXiv: astro-ph/0003248 [astro-ph].

[25] G. M. Bernstein et al. "The Luminosity Function of the Coma Cluster Core for -25<M/R<-9.4". In: *AJ* 110 (Oct. 1995), 1507. doi:10.1086/117624. arXiv: astro-ph/9503102 [astro-ph].

[26] B. Binggeli, G. A. Tammann, and A. Sandage. "Studies of the Virgo cluster. VI - Morphological and kinematical structure of the Virgo cluster". In: *AJ* 94 (Aug. 1987), 251–277. doi:10.1086/114467.

[27] J. Binney and S. Tremaine. *Galactic dynamics*. 1987.

[28] John P. Blakeslee et al. "The ACS Fornax Cluster Survey. V. Measurement and Recalibration of Surface Brightness Fluctuations and a Precise Value of the Fornax-Virgo Relative Distance". In: *ApJ* 694.1 (Mar. 2009), 556–572. doi:10.1088/0004-637X/694/1/556. arXiv: 0901.1138 [astro-ph.CO].

[29] M. R. Blanton and J. Moustakas. "Physical Properties and Environments of Nearby Galaxies". In: *Annual Review of Astron and Astrophys* 47 (Sept. 2009), 159–210. doi:10.1146/annurev-astro-082708-101734. arXiv: 0908.3017.

[30] G. R. Blumenthal et al. "Formation of galaxies and large-scale structure with cold dark matter." In: *Nature* 311 (1984), 517–525. doi:10.1038/311517a0.

[31] A. Borlaff et al. "Evolution of the anti-truncated stellar profiles of S0 galaxies since z = 0.6 in the SHARDS survey. I. Sample and methods". In: *A&A* 604, A119 (Aug. 2017), A119. doi:10.1051/0004-6361/201630282. arXiv: 1705.05850.

[32] A. Borlaff et al. "Formation of S0 galaxies through mergers. Antitruncated stellar discs resulting from major mergers ". In: *A&A* 570, A103 (Oct. 2014), A103. doi:10.1051/0004-6361/201424299. arXiv: 1407.5097.

[33] A. Borlaff et al. "Type-II surface brightness profiles in edge-on galaxies produced by flares". In: *A&A* 591, L7 (June 2016), L7. doi:10.1051/0004-6361/201628868. arXiv: 1606.00448.

[34] Sanchayeeta Borthakur, Min Su Yun, and Lourdes Verdes-Montenegro. "Detection of Diffuse Neutral Intragroup Medium in Hickson Compact Groups". In: *ApJ* 710.1 (Feb. 2010), 385–407. doi:10.1088/0004-637X/710/1/385. arXiv: 0912.0297 [astro-ph.CO].

[35] A. Boselli and G. Gavazzi. "Environmental Effects on Late-Type Galaxies in Nearby Clusters". In: *Public. of the Astron. Soc. Pac.* 118 (Apr. 2006), 517–559. doi:10.1086/500691. eprint: astro-ph/0601108.

[36] A. Boselli et al. "The Fate of Spiral Galaxies in Clusters: The Star Formation History of the Anemic Virgo Cluster Galaxy NGC 4569". In: *ApJ* 651 (Nov. 2006), 811–821. doi:10.1086/507766. eprint: astro-ph/0609020.

[37] F. Bournaud, C. J. Jog, and F. Combes. "Galaxy mergers with various mass ratios: Properties of remnants". In: *A&A* 437.1 (July 2005), 69–85. doi:10.1051/0004-6361:20042036. arXiv: astro-ph/0503189 [astro-ph].

[38] Richard G. Bower and Michael L. Balogh. "The Difference Between Clusters and Groups: A Journey from Cluster Cores to Their Outskirts and Beyond". In: *Clusters of Galaxies: Probes of Cosmological Structure and Galaxy Evolution*. Ed. by J. S. Mulchaey, A. Dressler, and A. Oemler. 2004, 325. arXiv: astro-ph/0306342 [astro-ph].

[39] Sarah Brough et al. "Eridanus - a supergroup in the local Universe?" In: *MNRAS* 369.3 (2006), 1351–1374. doi:10.1111/j.1365-2966.2006.10387.x. arXiv: astro-ph/0603778 [astro-ph].

[40] Sarah Brough et al. "Southern GEMS groups - I. Dynamical properties". In: *MNRAS* 370.3 (2006), 1223–1246. doi:10.1111/j.1365-2966.2006.10542.x. arXiv: astro-ph/0605279 [astro-ph].

[41] M. Bureau and K. C. Freeman. "The Nature of Boxy/Peanut-Shaped Bulges in Spiral Galaxies". In: *AJ* 118 (July 1999), 126–138. doi:10.1086/300922. eprint: astro-ph/9904015.

[42] R. Buta and F. Combes. "Galactic Rings". In: *Fund. Cosmic Phys.* 17 (Jan. 1996), 95–281.

[43] R. Buta and D. A. Crocker. "Metric Characteristics of Nuclear Rings and Related Features in Spiral Galaxies". In: *AJ* 105 (Apr. 1993), 1344. doi:10.1086/116514.

[44] R. J. Buta. "Galaxy Morphology". In: *arXiv e-prints* (Feb. 2011). arXiv: 1102.0550 [astro-ph.CO].

[45] Ronald J. Buta et al. "A Classical Morphological Analysis of Galaxies in the Spitzer Survey of Stellar Structure in Galaxies (S4G)". In: *ApJS* 217.2, 32 (Apr. 2015), 32. doi:10.1088/0067-0049/217/2/32. arXiv: 1501.00454 [astro-ph.GA].

[46] H. Butcher and Jr. Oemler A. "The evolution of galaxies in clusters. V. A study of populations since Z 0.5." In: *ApJ* 285 (1984), 426–438. doi:10.1086/162519.

[47] Nelson Caldwell. "Dwarf Elliptical Galaxies in the Fornax Cluster. I. A Catalogue and Luminosity Function". In: *AJ* 94 (Nov. 1987), 1116. doi:10.1086/114549.

[48] M. Cantiello et al. "VEGAS-SSS. II. Comparing the globular cluster systems in NGC 3115 and NGC 1399 using VEGAS and FDS survey data. The quest for a common genetic heritage of globular cluster systems". In: *A&A* 611, A93 (Apr. 2018), A93. doi:10.1051/0004-6361/201730649.

[49] N. Caon, M. Capaccioli, and M. D'Onofrio. "On the shape of the light profiles of early-type galaxies." In: *MNRAS* 265 (Dec. 1993), 1013–1021. doi:10.1093/mnras/265.4.1013. arXiv: astro-ph/9309013 [astro-ph].

[50] M. Capaccioli et al. "VEGAS: A VST Early-type GAlaxy Survey. I. Presentation, wide-field surface photometry, and substructures in NGC 4472". In: *A&A* 581, A10 (Sept. 2015), A10. doi:10.1051/0004-6361/201526252. arXiv: 1507.01336.

[51] Arianna Cattapan et al. "VEGAS: A VST Early-type GAlaxy Survey. IV. NGC 1533, IC 2038, and IC 2039: An Interacting Triplet in the Dorado Group". In: *ApJ* 874.2, 130 (2019), 130. doi:10.3847/1538-4357/ab0b44. arXiv: 1903.04466 [astro-ph.GA].

[52] D. Christlein, D. Zaritsky, and J. Bland-Hawthorn. "A spectroscopic study of the Hα surface brightness profiles in the outer discs of galaxies". In: *MNRAS* 405 (July 2010), 2549–2560. doi:10.1111/j.1365-2966.2010.16631.x. arXiv: 1003.4872.

[53] R. Ciardullo et al. "The Systematics of Intracluster Starlight". In: *Recycling Intergalactic and Interstellar Matter*. Ed. by Pierre-Alain Duc, Jonathan Braine, and Elias Brinks. Vol. 217. IAU Symposium. June 2004, 88.

[54] V. Coenda, H. Muriel, and H. J. Martínez. "Comparing galaxy populations in compact and loose groups of galaxies". In: *A&A* 543, A119 (July 2012), A119. doi:10.1051/0004-6361/201118318. arXiv: 1205.3428 [astro-ph.CO].

[55] Valeria Coenda, Hernán Muriel, and Héctor J. Martínez. "Comparing galaxy populations in compact and loose groups of galaxies. III. Effects of environment on star formation". In: *A&A* 573, A96 (Jan. 2015), A96. doi:10.1051/0004-6361/201424870. arXiv: 1410.7780 [astro-ph.GA].

[56] Alison L. Coil. "The Large-Scale Structure of the Universe". In: *Planets, Stars and Stellar Systems* (2013), 387–421. doi:10.1007/978-94-007-5609-0_8. http://dx.doi.org/10.1007/978-94-007-5609-0_8.

[57] M. Colless. "Coma Cluster". In: *Encyclopedia of Astronomy and Astrophysics*. Ed. by P. Murdin. 2000, 2600. doi:10.1888/0333750888/2600.

[58] F. Combes and R. H. Sanders. "Formation and properties of persisting stellar bars." In: *A&A* 96 (Mar. 1981), 164–173.

[59] E. Contini, S. K. Yi, and X. Kang. "Theoretical Predictions of Colors and Metallicity of the Intracluster Light". In: *ApJ* 871.1, 24 (2019), 24. doi:10.3847/1538-4357/aaf41f. arXiv: 1811.03253 [astro-ph.GA].

[60] E. Contini et al. "On the formation and physical properties of the intracluster light in hierarchical galaxy formation models". In: *MNRAS* 437.4 (2014), 3787–3802. doi:10.1093/mnras/stt2174. arXiv: 1311.2076 [astro-ph.CO].

[61] A. P. Cooper et al. "Galactic stellar haloes in the CDM model". In: *MNRAS* 406.2 (2010), 744–766. doi:10.1111/j.1365-2966.2010.16740.x. arXiv: 0910.3211 [astro-ph.GA].

[62] Andrew P. Cooper et al. "Galactic accretion and the outer structure of galaxies in the CDM model". In: *MNRAS* 434.4 (2013), 3348–3367. doi:10.1093/mnras/stt1245. arXiv: 1303.6283 [astro-ph.CO].

[63] Michael C. Cooper et al. "The Arizona CDFS Environment Survey (ACES): A Magellan/IMACS Spectroscopic Survey of the Chandra Deep Field-South". In: *MNRAS* 425.3 (Sept. 2012), 2116–2127. doi:10.1111/j.1365-2966.2012.21524.x. arXiv: 1112.0312 [astro-ph.CO].

[64] Michael C. Cooper et al. "The DEEP2 Galaxy Redshift Survey: the relationship between galaxy properties and environment at z ∼1". In: *MNRAS* 370.1 (July 2006), 198–212. doi:10.1111/j.1365-2966.2006.10485.x. arXiv: astro-ph/0603177 [astro-ph].

[65] H. G. Corwin, A. de Vaucouleurs, and G. de Vaucouleurs. "Southern Galaxy Catalogue." In: *Univ. Texas Monogr. Astron., Vol. 4, p. 1 (1985)*. Vol. 4. 1985, 1.

[66] S. Courteau. "Deep r-Band Photometry for Northern Spiral Galaxies". In: *ApJS* 103 (Apr. 1996), 363. doi:10.1086/192281.

[67] O. Cucciati et al. "The VIMOS Public Extragalactic Redshift Survey (VIPERS). The decline of cosmic star formation: quenching, mass, and environment connections". In: *A&A* 602, A15 (June 2017), A15. doi:10.1051/0004-6361/201630113. arXiv: 1611.07049 [astro-ph.GA].

[68] O. Cucciati et al. "The VIMOS-VLT deep survey: the group catalogue". In: *A&A* 520, A42 (Sept. 2010), A42. doi:10.1051/0004-6361/200911831. arXiv: 0911.3740 [astro-ph.CO].

[69] C. Da Rocha and C. Mendes de Oliveira. "Intragroup diffuse light in compact groups of galaxies: HCG 79, 88 and 95". In: *MNRAS* 364.3 (Dec. 2005), 1069–1081. doi:10.1111/j.1365-2966.2005.09641.x. arXiv: astro-ph/0509908 [astro-ph].

[70] C. Da Rocha, B. L. Ziegler, and C. Mendes de Oliveira. "Intragroup diffuse light in compact groups of galaxies - II. HCG 15, 35 and 51". In: *MNRAS* 388 (Aug. 2008), 1433–1443. doi:10.1111/j.1365-2966.2008.13500.x. arXiv: 0805.4015.

[71] R. D'Abrusco et al. "The Extended Spatial Distribution of Globular Clusters in the Core of the Fornax Cluster". In: *ApJL* 819, L31 (Mar. 2016), L31. doi:10.3847/2041-8205/819/2/L31. arXiv: 1602.06076.

[72] L. Danese et al. "Projection effects and virial masses of groups of galaxies". In: *ApJ* 244 (Mar. 1981), 777–779. doi:10.1086/158754.

[73] J. I. Davies et al. "Low surface brightness galaxies in the Fornax cluster : automated galaxy surface photometry. III." In: *MNRAS* 232 (May 1988), 239–258. doi:10.1093/mnras/232.2.239.

[74] J. I. Davies et al. "The Herschel Fornax Cluster Survey - I. The bright galaxy sample". In: *MNRAS* 428 (Jan. 2013), 834–844. doi:10.1093/mnras/sts082. arXiv: 1210.4448.

[75] T. A. Davis et al. "The ATLAS^{3D} Project - XIV. The extent and kinematics of the molecular gas in early-type galaxies". In: *MNRAS* 429 (Feb. 2013), 534–555. doi:10.1093/mnras/sts353. arXiv: 1211.1011.

[76] R. S. de Jong. "B, V, R, I, H and K images of 86 face-on spiral galaxies". In: *Journal of Astronomical Data* 2 (1996). eprint: astro-ph/9611003.

[77] D. F. de Mello, T. Wiklind, and M. A. G. Maia. "Environmental effects in galaxies. Molecular gas, star formation, and activity". In: *A&A* 381 (2002), 771–782. doi:10.1051/0004-6361:20011566. arXiv: astro-ph/0110702 [astro-ph].

[78] A. de Vaucouleurs and G. de Vaucouleurs. "New redshifts of bright galaxies." In: *AJ* 72 (Aug. 1967), 730–737. doi:10.1086/110301.

[79] G. de Vaucouleurs. "Photographic dimensions of the brighter galaxies". In: *AJ* 64 (Nov. 1959), 397. doi:10.1086/107959.

[80] G. de Vaucouleurs. "Revised Classification of 1500 Bright Galaxies." In: *ApJS* 8 (Apr. 1963), 31. doi:10.1086/190084.

[81] G. de Vaucouleurs. "Structure, Dynamics and Statistical Properties of Galaxies (invited Paper)". In: *The Formation and Dynamics of Galaxies*. Ed. by John R. Shakeshaft. Vol. 58. IAU Symposium. Jan. 1974, 1.

[82] G. de Vaucouleurs and A. de Vaucouleurs. "Photometry of Intergalactic Matter in the Coma Cluster". In: *Astrophys. Lett.* 5 (Jan. 1970), 219.

[83] Victor P. Debattista et al. "The Secular Evolution of Disk Structural Parameters". In: *ApJ* 645.1 (July 2006), 209–227. doi:10.1086/504147. arXiv: astro-ph/0509310 [astro-ph].

[84] Simon Deeley et al. "Galaxy and Mass Assembly (GAMA): formation and growth of elliptical galaxies in the group environment". In: *MNRAS* 467.4 (June 2017), 3934–3943. doi:10.1093/mnras/stx441. arXiv: 1702.07641 [astro-ph.GA].

[85] A. Dekel et al. "Lost and found dark matter in elliptical galaxies". In: *Nature* 437.7059 (2005), 707–710. doi:10.1038/nature03970. arXiv: astro-ph/0501622 [astro-ph].

[86] R. Delgado-Serrano et al. "How was the Hubble sequence 6 Gyr ago?" In: *Astronomy and Astrophysics* 509 (2010), A78. ISSN: 1432-0746. doi:10.1051/0004-6361/200912704. http://dx.doi.org/10.1051/0004-6361/200912704.

[87] Clare Dobbs and Junichi Baba. "Dawes Review 4: Spiral Structures in Disc Galaxies". In: *Publications of the Astronomical Society of Australia* 31, e035 (Sept. 2014), e035. doi:10.1017/pasa.2014.31. arXiv: 1407.5062 [astro-ph.GA].

[88] M. D'Onofrio, P. Marziani, and L. Buson. "The transformation of Spirals into S0 galaxies in the cluster environment". In: *Frontiers in Astronomy and Space Sciences* 2, 4 (Aug. 2015), 4. doi:10.3389/fspas.2015.00004. arXiv: 1508.04572.

[89] A. Dressler. "Galaxy morphology in rich clusters - Implications for the formation and evolution of galaxies". In: *ApJ* 236 (Mar. 1980), 351–365. doi:10.1086/157753.

[90] M. J. Drinkwater, M. D. Gregg, and M. Colless. "Substructure and Dynamics of the Fornax Cluster". In: *ApJL* 548 (Feb. 2001), L139–L142. doi:10.1086/319113. eprint: astro-ph/0012415.

[91] M. J. Drinkwater et al. "The evolution and star formation of dwarf galaxies in the Fornax Cluster". In: *MNRAS* 326.3 (Sept. 2001), 1076–1094. doi:10.1046/j.1365-8711.2001.04646.x. arXiv: astro-ph/0106376 [astro-ph].

[92] Michael J. Drinkwater, Michael D. Gregg, and Matthew Colless. "Substructure and Dynamics of the Fornax Cluster". In: *ApJL* 548.2 (2001), L139–L142. doi:10.1086/319113. arXiv: astro-ph/0012415 [astro-ph].

[93] Pierre-Alain Duc et al. "The ATLAS^{3D} project - XXIX. The new look of early-type galaxies and surrounding fields disclosed by extremely deep optical images". In: *MNRAS* 446.1 (Jan. 2015), 120–143. doi:10.1093/mnras/stu2019. arXiv: 1410.0981 [astro-ph.GA].

[94] O. J. Eggen, D. Lynden-Bell, and A. R. Sandage. "Evidence from the motions of old stars that the Galaxy collapsed." In: *ApJ* 136 (1962), 748. doi:10.1086/147433.

[95] Paul Eigenthaler et al. "The Next Generation Fornax Survey (NGFS). II. The Central Dwarf Galaxy Population". In: *ApJ* 855.2, 142 (2018), 142. doi:10.3847/1538-4357/aaab60. arXiv: 1801.02633 [astro-ph.GA].

[96] B. G. Elmegreen. "Grand design, multiple arm, and flocculent spiral galaxies". In: *Annals of the New York Academy of Sciences* 596 (June 1990), 40–52. doi:10.1111/j.1749-6632.1990.tb27410.x.

[97] D. M. Elmegreen et al. "Properties and simulations of interacting spiral galaxies with transient "ocular" shapes." In: *A&A* 244 (Apr. 1991), 52.

[98] D. M. Elmegreen et al. "The influence of environment on outer rings and pseudo-rings in galaxies". In: *A&A* 257 (Apr. 1992), 17–23.

[99] Debra Meloy Elmegreen and Bruce G. Elmegreen. "Arm Classifications for Spiral Galaxies". In: *ApJ* 314 (Mar. 1987), 3. doi:10.1086/165034.

[100] Debra Meloy Elmegreen et al. "Grand Design and Flocculent Spirals in the Spitzer Survey of Stellar Structure in Galaxies (S^{4}G)". In: *ApJ* 737.1, 32 (Aug. 2011), 32. doi:10.1088/0004-637X/737/1/32. arXiv: 1106.4840 [astro-ph.GA].

[101] P. Erwin, J. E. Beckman, and M. Pohlen. "Antitruncation of Disks in Early-Type Barred Galaxies". In: *ApJL* 626 (June 2005), L81–L84. doi:10.1086/431739. eprint: astro-ph/0505216.

[102] P. Erwin, L. Gutiérrez, and J. E. Beckman. "A Strong Dichotomy in S0 Disk Profiles between the Virgo Cluster and the Field". In: *ApJL* 744, L11 (Jan. 2012), L11. doi:10.1088/2041-8205/744/1/L11. arXiv: 1111.5027 [astro-ph.CO].

[103] P. Erwin, M. Pohlen, and J. E. Beckman. "The Outer Disks of Early-Type Galaxies. I. Surface-Brightness Profiles of Barred Galaxies". In: *AJ* 135 (Jan. 2008), 20–54. doi:10.1088/0004-6256/135/1/20. arXiv: 0709.3505.

[104] Peter Erwin. "Double-barred galaxies. I. A catalog of barred galaxies with stellar secondary bars and inner disks". In: *A&A* 415 (2004), 941–957. doi:10.1051/0004-6361:20034408. arXiv: astro-ph/0310806 [astro-ph].

[105] S. M. Faber. "Variations in Spectral-Energy Distributions and Absorption-Line Strengths among Elliptical Galaxies". In: *ApJ* 179 (1973), 731–754. doi:10.1086/151912.

[106] S. M. Fall and G. Efstathiou. "Formation and rotation of disc galaxies with haloes". In: *MNRAS* 193 (Oct. 1980), 189–206. doi:10.1093/mnras/193.2.189.

[107] John J. Feldmeier et al. "Intracluster Planetary Nebulae in the Virgo Cluster. III. Luminosity of the Intracluster Light and Tests of the Spatial Distribution". In: *ApJ* 615.1 (Nov. 2004), 196–208. doi:10.1086/424372. arXiv: astro-ph/0407274 [astro-ph].

[108] H. C. Ferguson. "Population studies in groups and clusters of galaxies. II - A catalog of galaxies in the central 3.5 deg of the Fornax Cluster". In: *AJ* 98 (Aug. 1989), 367–418. doi:10.1086/115152.

[109] H. C. Ferguson and A. Sandage. "Population studies in groups and clusters of galaxies. I - The luminosity function of galaxies in the Fornax Cluster". In: *AJ* 96 (Nov. 1988), 1520–1533. doi:10.1086/114903.

[110] Henry C. Ferguson, Nial R. Tanvir, and Ted von Hippel. "Detection of intergalactic red-giant-branch stars in the Virgo cluster". In: *Nature* 391.6666 (Jan. 1998), 461–463. doi:10.1038/35087. arXiv: astro-ph/9801228 [astro-ph].

[111] J. A. Fernley and S. P. Bhavsar. "The virial masses of clusters of galaxies and the effects of contamination." In: *MNRAS* 210 (Oct. 1984), 883–890. doi:10.1093/mnras/210.4.883.

[112] Laura Ferrarese et al. "The Next Generation Virgo Cluster Survey (NGVS). I. Introduction to the Survey". In: *ApJS* 200.1, 4 (May 2012), 4. doi:10.1088/0067-0049/200/1/4.

[113] Jane M. A. Few and Barry F. Madore. "Ring galaxies- II. Classification and statistics". In: *MNRAS* 222 (1986), 673–682. doi:10.1093/mnras/222.4.673.

[114] Rose A. Finn et al. "The Local Cluster Survey. I. Evidence of Outside-in Quenching in Dense Environments". In: *ApJ* 862.2, 149 (Aug. 2018), 149. doi:10.3847/1538-4357/aac32a. arXiv: 1807.03388 [astro-ph.GA].

[115] Holland C. Ford et al. "Advanced camera for the Hubble Space Telescope". In: *Proc. SPIE*. Ed. by Pierre Y. Bely and James B. Breckinridge. Vol. 3356. Society of Photo-Optical Instrumentation Engineers (SPIE) Conference Series. 1998, 234–248. doi:10.1117/12.324464.

[116] Ahmed M. Fouad et al. "Colour similarity study among small galaxy groups members". In: *NRIAG Journal of Astronomy and Geophysics* 8.1 (2019), 15–21. doi:10.1080/20909977.2019.1615793. arXiv: 1812.10803 [astro-ph.GA].

[117] K. A. Frank et al. "Characterization of Intracluster Medium Temperature Distributions of 62 Galaxy Clusters with XMM-Newton". In: *ApJ* 764.1, 46 (Feb. 2013), 46. doi:10.1088/0004-637X/764/1/46. arXiv: 1212.2239 [astro-ph.CO].

[118] K. C. Freeman. "On the Disks of Spiral and S0 Galaxies". In: *ApJ* 160 (June 1970), 811. doi:10.1086/150474.

[119] Yutaka Fujita. "Pre-Processing of Galaxies before Entering a Cluster". In: *Publications of the Astronomical Society of Japan* 56 (Feb. 2004), 29–43. doi:10.1093/pasj/56.1.29. arXiv: astro-ph/0311193 [astro-ph].

[120] Yutaka Fujita and Masahiro Nagashima. "Effects of Ram Pressure from the Intracluster Medium on the Star Formation Rate of Disk Galaxies in Clusters of Galaxies". In: *ApJ* 516.2 (May 1999), 619–625. doi:10.1086/307139. arXiv: astro-ph/9812378 [astro-ph].

[121] C. Fuller et al. "The Herschel Fornax Cluster Survey II: FIR properties of optically selected Fornax cluster galaxies". In: *MNRAS* 440 (May 2014), 1571–1589. doi:10.1093/mnras/stu369. arXiv: 1403.0589.

[122] D. A. Gadotti and S. Dos Anjos. "Stellar Populations, Bars and Secular Evolution in Late-Type Galaxies". In: *Galaxy Disks and Disk Galaxies*. Ed. by José G. Funes and Enrico Maria Corsini. Vol. 230. Astronomical Society of the Pacific Conference Series. Jan. 2001, 237–238. arXiv: astro-ph/0008395 [astro-ph].

[123] H. Gao et al. "The Carnegie-Irvine Galaxy Survey. VII. Constraints on the Origin of S0 Galaxies from Their Photometric Structure". In: *ApJ* 862, 100 (Aug. 2018), 100. doi:10.3847/1538-4357/aacdac. arXiv: 1806.06350.

[124] O. Gerhard et al. "The kinematics of intracluster planetary nebulae and the on-going subcluster merger in the Coma cluster core". In: *A&A* 468.3 (June 2007), 815–822. doi:10.1051/0004-6361:20066484. arXiv: astro-ph/0703770 [astro-ph].

[125] Ortwin Gerhard et al. "Isolated Star Formation: A Compact H II Region in the Virgo Cluster". In: *ApJL* 580.2 (Dec. 2002), L121–L124. doi:10.1086/345657. arXiv: astro-ph/0211341 [astro-ph].

[126] Stuart P. D. Gill et al. "The evolution of substructure - II. Linking dynamics to environment". In: *MNRAS* 351.2 (2004), 410–422. doi:10.1111/j.1365-2966.2004.07913.x. arXiv: astro-ph/0404255 [astro-ph].

[127] R. Giovanelli and M. P. Haynes. "The HI extent and deficiency of spiral galaxies in the Virgo cluster." In: *AJ* 88 (July 1983), 881–908. doi:10.1086/113376.

[128] Percy L. Gómez et al. "Galaxy Star Formation as a Function of Environment in the Early Data Release of the Sloan Digital Sky Survey". In: *ApJ* 584.1 (2003), 210–227. doi:10.1086/345593. arXiv: astro-ph/0210193 [astro-ph].

[129] A. Grado et al. "VST processing facility: first astronomical applications". In: *Memorie della Societa Astronomica Italiana Supplementi* 19 (2012), 362. arXiv: 1102.1588 [astro-ph.IM].

[130] C. J. Grillmair. "Substructure in Tidal Streams: Tributaries in the Anticenter Stream". In: *ApJL* 651.1 (Nov. 2006), L29–L32. doi:10.1086/509255. arXiv: astro-ph/0609449 [astro-ph].

[131] C. J. Grillmair et al. "The velocity dispersion of globular clusters in NGC 1399". In: *ApJL* 422 (Feb. 1994), L9–L12. doi:10.1086/187199.

[132] M. W. Grootes et al. "Galaxy And Mass Assembly (GAMA): Gas Fueling of Spiral Galaxies in the Local Universe. I. The Effect of the Group Environment on Star Formation in Spiral Galaxies". In: *AJ* 153.3, 111 (Mar. 2017), 111. doi:10.3847/1538-3881/153/3/111. arXiv: 1612.07322 [astro-ph.GA].

[133] V. Guglielmo et al. "The XXL Survey. XXXVII. The role of the environment in shaping the stellar population properties of galaxies at $0.1 \leq z \leq 0.5$". In: *A&A* 625, A112 (May 2019), A112. doi:10.1051/0004-6361/201834970. arXiv: 1903.12293 [astro-ph.GA].

[134] J. E. Gunn and J. R. Gott III. "On the Infall of Matter Into Clusters of Galaxies and Some Effects on Their Evolution". In: *ApJ* 176 (Aug. 1972), 1. doi:10.1086/151605.

[135] Maan H Hani et al. "Interacting galaxies in the IllustrisTNG simulations – II: star formation in the post-merger stage". In: *Monthly Notices of the Royal Astronomical Society* 493.3 (2020), 3716–3731. ISSN: 1365-2966. doi:10.1093/mnras/staa459. http://dx.doi.org/10.1093/mnras/staa459.

[136] Yasuhiro Hashimoto and Jr. Oemler Augustus. "The Effect of Environment on Galaxy Interactions". In: *ApJ* 530.2 (2000), 652–659. doi:10.1086/308383.

[137] Martha P. Haynes, Ricardo Giovanelli, and Guido L. Chincarini. "The Influence of Envirionment on the H I Content of Galaxies". In: *Annual Review of Astron and Astrophys* 22 (Jan. 1984), 445–470. doi:10.1146/annurev.aa.22.090184.002305.

[138] Jonathan D. Hernández-Fernández et al. "Star formation activity and gas stripping in the Cluster Projected Phase-Space (CPPS)". In: *MNRAS* 438.3 (2014), 2186–2200. doi:10.1093/mnras/stt2354. arXiv: 1312.1346 [astro-ph.GA].

[139] P. W. Hodge. "Surface photometry of bright members of the Fornax cluster of galaxies." In: *ApJS* 37 (Aug. 1978), 429–441. doi:10.1086/190536.

[140] P. W. Hodge, D. M. Pyper, and C. J. Webb. "Dwarf galaxies in the Fornax cluster." In: *AJ* 70 (Oct. 1965), 559. doi:10.1086/109781.

[141] David W. Hogg. *Distance measures in cosmology*. 1999. arXiv: astro-ph/9905116 [astro-ph].

[142] Philip F. Hopkins et al. "Mergers and Bulge Formation in ΛCDM: Which Mergers Matter?" In: *ApJ* 715.1 (May 2010), 202–229. doi:10.1088/0004-637X/715/1/202. arXiv: 0906.5357 [astro-ph.CO].

[143] Philip F. Hopkins et al. "Star formation in galaxy mergers with realistic models of stellar feedback and the interstellar medium". In: *MNRAS* 430.3 (Apr. 2013), 1901–1927. doi:10.1093/mnras/stt017. arXiv: 1206.0011 [astro-ph.CO].

[144] C. Horellou et al. "Atomic and molecular gas in the merger galaxy NGC 1316 (Fornax A) and its environment". In: *A&A* 376 (Sept. 2001), 837–852. doi:10.1051/0004-6361:20011039. arXiv: astro-ph/0107390 [astro-ph].

[145] E. P. Hubble. "Extragalactic nebulae." In: *ApJ* 64 (1926), 321–369. doi:10.1086/143018.

[146] John P. Huchra et al. "The 2MASS Redshift Survey—Description and Data Release". In: *ApJS* 199.2, 26 (Apr. 2012), 26. doi:10.1088/0067-0049/199/2/26. arXiv: 1108.0669 [astro-ph.CO].

[147] M. Huertas-Company et al. "No Evidence for a Dependence of the Mass-Size Relation of Early-type Galaxies on Environment in the Local Universe". In: *ApJ* 779.1, 29 (Dec. 2013), 29. doi:10.1088/0004-637X/779/1/29. arXiv: 1212.4143 [astro-ph.CO].

[148] Deidre A. Hunter and Bruce G. Elmegreen. "Broadband Imaging of a Large Sample of Irregular Galaxies". In: *ApJS* 162.1 (Jan. 2006), 49–79. doi:10.1086/498096. arXiv: astro-ph/0509189 [astro-ph].

[149] J. D. Hunter. "Matplotlib: A 2D graphics environment". In: *Computing in Science & Engineering* 9.3 (2007), 90–95. doi:10.1109/MCSE.2007.55.

[150] H. S. Hwang et al. "Environmental dependence of local luminous infrared galaxies". In: *A&A* 522, A33 (Nov. 2010), A33. doi:10.1051/0004-6361/201014807. arXiv: 1006.2166.

[151] J.-S. Hwang et al. "Evolution of Late-type Galaxies in a Cluster Environment: Effects of High-speed Multiple Encounters with Early-type Galaxies". In: *ApJ* 856, 160 (Apr. 2018), 160. doi:10.3847/1538-4357/aab3ce. arXiv: 1803.09915.

[152] E. Iodice et al. "Intracluster Patches of Baryons in the Core of the Fornax Cluster". In: *ApJ* 851, 75 (Dec. 2017), 75. doi:10.3847/1538-4357/aa9b30. arXiv: 1711.04681.

[153] E. Iodice et al. "The Fornax Deep Survey with the VST. V. Exploring the faintest regions of the bright early-type galaxies inside the virial radius". In: *A&A* 623, A1 (Mar. 2019), A1. doi:10.1051/0004-6361/201833741. arXiv: 1812.01050 [astro-ph.GA].

[154] E. Iodice et al. "The Fornax Deep Survey with VST. I. The Extended and Diffuse Stellar Halo of NGC 1399 out to 192 kpc". In: *ApJ* 820, 42 (Mar. 2016), 42. doi:10.3847/0004-637X/820/1/42. arXiv: 1602.02149.

[155] E. Iodice et al. "The Fornax Deep Survey with VST. II. Fornax A: A Two-phase Assembly Caught in the Act". In: *ApJ* 839, 21 (Apr. 2017), 21. doi:10.3847/1538-4357/aa6846. arXiv: 1703.07989.

[156] E. Iodice et al. "The Fornax3D project: Tracing the assembly history of the cluster from the kinematic and line-strength maps". In: *A&A* 627, A136 (2019), A136. doi:10.1051/0004-6361/201935721. arXiv: 1906.08187 [astro-ph.GA].

[157] Enrichetta Iodice et al. "VEGAS: a VST Early-type GAlaxy Survey. V. IC 1459 group: Mass assembly history in low-density environments". In: *A&A* 635, A3 (Mar. 2020), A3. doi:10.1051/0004-6361/201936435. arXiv: 1912.07452 [astro-ph.GA].

[158] Željko Ivezić et al. "LSST: From Science Drivers to Reference Design and Anticipated Data Products". In: *ApJ* 873.2, 111 (Mar. 2019), 111. doi:10.3847/1538-4357/ab042c. arXiv: 0805.2366 [astro-ph].

[159] R. I. Jedrzejewski. "CCD surface photometry of elliptical galaxies. I - Observations, reduction and results". In: *MNRAS* 226 (June 1987), 747–768. doi:10.1093/mnras/226.4.747.

[160] Y. Jiménez-Teja et al. "J-PLUS: Analysis of the intracluster light in the Coma cluster". In: *A&A* 622, A183 (Feb. 2019), A183. doi:10.1051/0004-6361/201833547. arXiv: 1810.01424 [astro-ph.GA].

[161] C. Jones et al. "X-Ray Emission from the Fornax Cluster". In: *ApJ* 482.1 (June 1997), 143–155. doi:10.1086/304104.

[162] Eric Jones, Travis Oliphant, Pearu Peterson, et al. *SciPy: Open source scientific tools for Python*. 2001–. http://www.scipy.org/.

[163] J. E. Jones and B. J. T. Jones. "The Fornax cluster of galaxies." In: *MNRAS* 191 (June 1980), 685–700. doi:10.1093/mnras/191.4.685.

[164] A. Jordán et al. "The ACS Fornax Cluster Survey. I. Introduction to the Survey and Data Reduction Procedures". In: *ApJS* 169 (Apr. 2007), 213–224. doi:10.1086/512778. eprint: astro-ph/0702320.

[165] Andrés Jordán et al. "The ACS Fornax Cluster Survey. I. Introduction to the Survey and Data Reduction Procedures". In: *ApJS* 169.2 (Apr. 2007), 213–224. doi:10.1086/512778. arXiv: astro-ph/0702320 [astro-ph].

[166] Gandhali D. Joshi et al. "The fate of disk galaxies in IllustrisTNG clusters". In: *arXiv e-prints*, arXiv:2004.01191 (Apr. 2020), arXiv:2004.01191. arXiv: 2004.01191 [astro-ph.GA].

[167] W. A. Joye and E. Mandel. "New Features of SAOImage DS9". In: *Astronomical Data Analysis Software and Systems XII*. Ed. by H. E. Payne, R. I. Jedrzejewski, and R. N. Hook. Vol. 295. Astronomical Society of the Pacific Conference Series. Jan. 2003, 489.

[168] I. D. Karachentsev. "The Local Group and Other Neighboring Galaxy Groups". In: *The Astronomical Journal* 129.1 (2005), 178–188. ISSN: 1538-3881. doi:10.1086/426368. http://dx.doi.org/10.1086/426368.

[169] Guinevere Kauffmann et al. "The environmental dependence of the relations between stellar mass, structure, star formation and nuclear activity in galaxies". In: *MNRAS* 353.3 (Sept. 2004), 713–731. doi:10.1111/j.1365-2966.2004.08117.x. arXiv: astro-ph/0402030 [astro-ph].

[170] Daisuke Kawata and John S. Mulchaey. "Strangulation in Galaxy Groups". In: *The Astrophysical Journal* 672.2 (2007), L103–L106. ISSN: 1538-4357. doi:10.1086/526544. http://dx.doi.org/10.1086/526544.

[171] Kshitija Kelkar et al. "Galaxy sizes as a function of environment at intermediate redshift from the ESO Distant Cluster Survey". In: *MNRAS* 450.2 (June 2015), 1246–1255. doi:10.1093/mnras/stv670. arXiv: 1503.08225 [astro-ph.GA].

[172] Jeffrey D. P. Kenney and Rebecca A. Koopmann. "Ongoing Gas Stripping in the Virgo Cluster Spiral Galaxy NGC 4522". In: *AJ* 117.1 (Jan. 1999), 181–189. doi:10.1086/300683. arXiv: astro-ph/9812363 [astro-ph].

[173] Dong-Woo Kim and G. Fabbiano. "Chandra X-Ray Observations of NGC 1316 (Fornax A)". In: *ApJ* 586.2 (2003), 826–849. doi:10.1086/367930. arXiv: astro-ph/0206369 [astro-ph].

[174] J. H. Knapen et al. "The Central Region in M100: Observations and Modeling". In: *ApJ* 454 (Dec. 1995), 623. doi:10.1086/176516. arXiv: astro-ph/9506098 [astro-ph].

[175] Johan H. Knapen, Isaac Shlosman, and Reynier F. Peletier. "A Subarcsecond Resolution Near-Infrared Study of Seyfert and "Normal" Galaxies. II. Morphology". In: *ApJ* 529.1 (Jan. 2000), 93–100. doi:10.1086/308266. arXiv: astro-ph/9907379 [astro-ph].

[176] Karen Knierman et al. "Tidal Tails of Minor Mergers: Star Formation Efficiency in the Western Tail of NGC 2782". In: *ApJ* 749, L1 (Apr. 2012), L1. doi:10.1088/2041-8205/749/1/L1. arXiv: 1205.1553 [astro-ph.CO].

[177] John Kormendy and Ralf Bender. "A Revised Parallel-sequence Morphological Classification of Galaxies: Structure and Formation of S0 and Spheroidal Galaxies". In: *ApJS* 198.1, 2 (Jan. 2012), 2. doi:10.1088/0067-0049/198/1/2. arXiv: 1110.4384 [astro-ph.CO].

[178] M. Kregel and P. C. van der Kruit. "Radial truncations in stellar discs in galaxies". In: *MNRAS* 355 (Nov. 2004), 143–146. doi:10.1111/j.1365-2966.2004.08307.x. eprint: astro-ph/0408125.

[179] J. Krywult et al. "The VIMOS Public Extragalactic Redshift Survey (VIPERS). The coevolution of galaxy morphology and colour to z 1". In: *A&A* 598, A120 (Feb. 2017), A120. doi:10.1051/0004-6361/201628953. arXiv: 1605.05502 [astro-ph.GA].

[180] K. Kuijken. "OmegaCAM: ESO's Newest Imager". In: *The Messenger* 146 (Dec. 2011), 8–11.

[181] J. Laine, E. Laurikainen, and H. Salo. "Influence of galaxy stellar mass and observed wavelength on disc breaks in S^{4}G, NIRS0S, and SDSS data". In: *A&A* 596, A25 (Nov. 2016), A25. doi:10.1051/0004-6361/201628397. arXiv: 1610.00610.

[182] J. Laine et al. "Morphology and environment of galaxies with disc breaks in the S^{4}G and NIRS0S". In: *MNRAS* 441 (July 2014), 1992–2012. doi:10.1093/mnras/stu628. arXiv: 1404.0559.

[183] R. B. Larson. "Models for the formation of disc galaxies". In: *MNRAS* 176 (July 1976), 31–52. doi:10.1093/mnras/176.1.31.

[184] R. B. Larson, B. M. Tinsley, and C. N. Caldwell. "The evolution of disk galaxies and the origin of S0 galaxies". In: *ApJ* 237 (May 1980), 692–707. doi:10.1086/157917.

[185] R. B. Larson, B. M. Tinsley, and C. N. Caldwell. "The evolution of disk galaxies and the origin of S0 galaxies". In: *ApJ* 237 (1980), 692–707. doi:10.1086/157917.

[186] A. Lauberts. *ESO/Uppsala survey of the ESO(B) atlas*. 1982.

[187] E. Laurikainen and H. Salo. "BVRI imaging of M51-type interacting galaxy pairs - III. Analysis of the photometric parameters". In: *MNRAS* 324.3 (June 2001), 685–698. doi:10.1046/j.1365-8711.2001.04347.x.

[188] R. J. Lavery and J. P. Henry. "Evidence for galaxy-galaxy interactions as an active agent of the 'Butcher-Oemler' effect at a redshift of 0.2". In: *ApJ* 330 (July 1988), 596–600. doi:10.1086/166496.

[189] K. Lee-Waddell et al. "Tidal origin of NGC 1427A in the Fornax cluster". In: *MNRAS* 474 (Feb. 2018), 1108–1115. doi:10.1093/mnras/stx2808. arXiv: 1710.09947.

[190] D. Lena et al. "The Complex Gas Kinematics in the Nucleus of the Seyfert 2 Galaxy NGC 1386: Rotation, Outflows, and Inflows". In: *ApJ* 806, 84 (June 2015), 84. doi:10.1088/0004-637X/806/1/84. arXiv: 1504.05089.

[191] Ian Lewis et al. "The 2dF Galaxy Redshift Survey: the environmental dependence of galaxy star formation rates near clusters". In: *MNRAS* 334.3 (2002), 673–683. doi:10.1046/j.1365-8711.2002.05558.x. arXiv: astro-ph/0203336 [astro-ph].

[192] C. C. Lin and F. H. Shu. "On the Spiral Structure of Disk Galaxies." In: *ApJ* 140 (Aug. 1964), 646. doi:10.1086/147955.

[193] C. C. Lin and Frank H. Shu. "On the Spiral Structure of Disk Galaxies." In: *ApJ* 140 (Aug. 1964), 646. doi:10.1086/147955.

[194] C. C. Lin and Frank H. Shu. "On the Spiral Structure of Disk Galaxies, II. Outline of a Theory of Density Waves". In: *Proceedings of the National Academy of Science* 55.2 (Feb. 1966), 229–234. doi:10.1073/pnas.55.2.229.

[195] Bertil Lindblad. "On the nature of the spiral nebulae". In: *MNRAS* 87 (Mar. 1927), 420. doi:10.1093/mnras/87.5.420.

[196] Bertil Lindblad. "On the possibility of a quasi-stationary spiral structure in galaxies". In: *Stockholms Observatoriums Annaler* 5 (Jan. 1963), 5.

[197] Chris Lintott et al. "Galaxy Zoo 1: data release of morphological classifications for nearly 900 000 galaxies". In: *MNRAS* 410.1 (Jan. 2011), 166–178. doi:10.1111/j.1365-2966.2010.17432.x. arXiv: 1007.3265 [astro-ph.GA].

[198] L. M. Lubin et al. "The Observations of Redshift Evolution in Large-Scale Environments (ORELSE) Survey. I. The Survey Design and First Results on CL 0023+0423 at z = 0.84 and RX J1821.6+6827 at z = 0.82". In: *AJ* 137.6 (June 2009), 4867–4883. doi:10.1088/0004-6256/137/6/4867. arXiv: 0809.2092 [astro-ph].

[199] L. B. Lucy. "An iterative technique for the rectification of observed distributions". In: *AJ* 79 (June 1974), 745. doi:10.1086/111605.

[200] D. Lynden-Bell and A. J. Kalnajs. "On the generating mechanism of spiral structure". In: *MNRAS* 157 (Jan. 1972), 1. doi:10.1093/mnras/157.1.1.

[201] G. Mackie and G. Fabbiano. "Evolution of Gas and Stars in the Merger Galaxy NGC 1316 (Fornax A)". In: *AJ* 115.2 (Feb. 1998), 514–524. doi:10.1086/300203.

[202] Natasha Maddox et al. "A spectroscopic census of the Fornax cluster and beyond: preparing for next generation surveys". In: *MNRAS* 490.2 (2019), 1666–1677. doi:10.1093/mnras/stz2530. arXiv: 1909.04379 [astro-ph.GA].

[203] Smriti Mahajan, Gary A. Mamon, and Somak Raychaudhury. "Erratum: The velocity modulation of galaxy properties in and near clusters: quantifying the decrease in star formation in backsplash galaxies". In: *MNRAS* 418.4 (2011), 2816–2816. doi:10.1111/j.1365-2966.2011.20068.x.

[204] Dmitry Makarov and Igor Karachentsev. "Galaxy groups and clouds in the local (z$\sim$ 0.01) Universe". In: *MNRAS* 412.4 (Apr. 2011), 2498–2520. doi:10.1111/j.1365-2966.2010.18071.x. arXiv: 1011.6277 [astro-ph.CO].

[205] G. A. Mamon. "The Evolution of Galaxy Groups and of Galaxies Therein". In: *Groups of Galaxies in the Nearby Universe*. Ed. by Ivo Saviane, Valentin D. Ivanov, and Jordanka Borissova. 2007, 203. doi:10.1007/978-3-540-71173-5_35. arXiv: astro-ph/0607482 [astro-ph].

[206] C. Martin and GALEX Team. "The Galaxy Evolution Explorer - Early Data". In: *Maps of the Cosmos*. Ed. by M. Colless, L. Staveley-Smith, and R. A. Stathakis. Vol. 216. IAU Symposium. Jan. 2005, 221.

[207] C. L. Martin and R. C. Kennicutt Jr. "Star Formation Thresholds in Galactic Disks". In: *ApJ* 555 (July 2001), 301–321. doi:10.1086/321452. eprint: astro-ph/0103181.

[208] I. Martín-Navarro et al. "A unified picture of breaks and truncations in spiral galaxies from SDSS and S^{4}G imaging". In: *MNRAS* 427 (Dec. 2012), 1102–1134. doi:10.1111/j.1365-2966.2012.21929.x. arXiv: 1208.2893 [astro-ph.CO].

[209] David Martinez-Delgado et al. "Discovery of a Giant Stellar Tidal Stream Around the Disk Galaxy NGC 4013". In: *arXiv e-prints*, arXiv:0801.4657 (Jan. 2008), arXiv:0801.4657. arXiv: 0801.4657 [astro-ph].

[210] David Martínez-Delgado et al. "The Ghost of a Dwarf Galaxy: Fossils of the Hierarchical Formation of the Nearby Spiral Galaxy NGC 5907". In: *ApJ* 689.1 (Dec. 2008), 184–193. doi:10.1086/592555. arXiv: 0805.1137 [astro-ph].

[211] F. J. Martínez-Serrano et al. "Disk Galaxies with Broken Luminosity Profiles from Cosmological Simulations". In: *ApJL* 705 (Nov. 2009), L133–L137. doi:10.1088/0004-637X/705/2/L133. arXiv: 0906.1118 [astro-ph.GA].

[212] C. Mastropietro et al. "Morphological evolution of discs in clusters". In: *MNRAS* 364 (Dec. 2005), 607–619. doi:10.1111/j.1365-2966.2005.09579.x. eprint: astro-ph/0411648.

[213] L. D. Matthews and J. S. Gallagher III. "B and V CCD Photometry of Southern, Extreme Late-Type Spiral Galaxies". In: *AJ* 114 (Nov. 1997), 1899. doi:10.1086/118613. eprint: astro-ph/9709145.

[214] Chris Mihos. "Intragroup and Intracluster Light". In: *IAU General Assembly*. Vol. 29. 2015, 2247903.

[215] J. Christopher Mihos. "Interactions and Mergers of Cluster Galaxies". In: *Clusters of Galaxies: Probes of Cosmological Structure and Galaxy Evolution*. Ed. by J. S. Mulchaey, A. Dressler, and A. Oemler. Jan. 2004, 277.

[216] J. Christopher Mihos et al. "The Burrell Schmidt Deep Virgo Survey: Tidal Debris, Galaxy Halos, and Diffuse Intracluster Light in the Virgo Cluster". In: *ApJ* 834.1, 16 (2017), 16. doi:10.3847/1538-4357/834/1/16. arXiv: 1611.04435 [astro-ph.GA].

[217] Trevor A. Miles et al. "The Group Evolution Multiwavelength Study (GEMS): bimodal luminosity functions in galaxy groups". In: *MNRAS* 355.3 (Dec. 2004), 785–793. doi:10.1111/j.1365-2966.2004.08356.x. arXiv: astro-ph/0408554 [astro-ph].

[218] Toshinobu Miwa and Masafumi Noguchi. "Dynamical Properties of Tidally Induced Galactic Bars". In: *ApJ* 499.1 (May 1998), 149–166. doi:10.1086/305611.

[219] Mireia Montes and Ignacio Trujillo. "Intracluster Light at the Frontier: A2744". In: *ApJ* 794.2, 137 (Oct. 2014), 137. doi:10.1088/0004-637X/794/2/137. arXiv: 1405.2070 [astro-ph.CO].

[220] B. Moore, G. Lake, and N. Katz. "Morphological Transformation from Galaxy Harassment". In: *ApJ* 495 (Mar. 1998), 139–151. doi:10.1086/305264. eprint: astro-ph/9701211.

[221] B. Moore et al. "Galaxy harassment and the evolution of clusters of galaxies". In: *Nature* 379 (Feb. 1996), 613–616. doi:10.1038/379613a0. eprint: astro-ph/9510034.

[222] R. P. Muñoz et al. "Unveiling a Rich System of Faint Dwarf Galaxies in the Next Generation Fornax Survey". In: *ApJL* 813, L15 (Nov. 2015), L15. doi:10.1088/2041-8205/813/1/L15. arXiv: 1510.02475.

[223] J. C. Muñoz-Mateos et al. "The Impact of Bars on Disk Breaks as Probed by S^4G Imaging". In: *ApJ* 771, 59 (July 2013), 59. doi:10.1088/0004-637X/771/1/59. arXiv: 1304.6083.

[224] Adam Muzzin et al. "The Gemini Cluster Astrophysics Spectroscopic Survey (GCLASS): The Role of Environment and Self-regulation in Galaxy Evolution at z $\sim$1". In: *ApJ* 746.2, 188 (Feb. 2012), 188. doi:10.1088/0004-637X/746/2/188. arXiv: 1112.3655 [astro-ph.CO].

[225] Adam Muzzin et al. "The Phase Space and Stellar Populations of Cluster Galaxies at z $\sim$1: Simultaneous Constraints on the Location and Timescale of Satellite Quenching". In: *ApJ* 796.1, 65 (2014), 65. doi:10.1088/0004-637X/796/1/65. arXiv: 1402.7077 [astro-ph.GA].

[226] J. B. Nantais et al. "Morphology with light profile fitting of confirmed cluster galaxies at z = 0.84". In: *A&A* 555, A5 (July 2013), A5. doi:10.1051/0004-6361/201321268. arXiv: 1305.0826 [astro-ph.CO].

[227] N. R. Napolitano et al. "The Planetary Nebula Spectrograph elliptical galaxy survey: the dark matter in NGC 4494". In: *MNRAS* 393 (Feb. 2009), 329–353. doi:10.1111/j.1365-2966.2008.14053.x. arXiv: 0810.1291.

[228] Nicola R. Napolitano et al. "Intracluster Stellar Population Properties from N-Body Cosmological Simulations. I. Constraints at z = 0". In: *ApJ* 594.1 (2003), 172–185. doi:10.1086/376860. arXiv: astro-ph/0305216 [astro-ph].

[229] O. G. Nasonova, J. A. de Freitas Pacheco, and I. D. Karachentsev. "Hubble flow around Fornax cluster of galaxies". In: *Astronomy & Astrophysics* 532 (2011), A104. ISSN: 1432-0746. doi:10.1051/0004-6361/201016004. http://dx.doi.org/10.1051/0004-6361/201016004.

[230] Julio F. Navarro, Carlos S. Frenk, and Simon D. M. White. "The Structure of Cold Dark Matter Halos". In: *ApJ* 462 (1996), 563. doi:10.1086/177173. arXiv: astro-ph/9508025 [astro-ph].

[231] James D. Neill, Michael M. Shara, and William R. Oegerle. "Tramp Novae between Galaxies in the Fornax Cluster: Tracers of Intracluster Light". In: *ApJ* 618.2 (Jan. 2005), 692–704. doi:10.1086/426049. arXiv: astro-ph/0409265 [astro-ph].

[232] Jr. Oemler Augustus. "The Systematic Properties of Clusters of Galaxies. Photometry of 15 Clusters". In: *ApJ* 194 (1974), 1–20. doi:10.1086/153216.

[233] P. A. Oesch et al. "A Remarkably Luminous Galaxy at z=11.1 Measured with Hubble Space Telescope Grism Spectroscopy". In: *ApJ* 819.2, 129 (2016), 129. doi:10.3847/0004-637X/819/2/129. arXiv: 1603.00461 [astro-ph.GA].

[234] Youichi Ohyama and Ananda Hota. "Discovery of a Possibly Single Blue Supergiant Star in the Intra-cluster Region of Virgo Cluster of Galaxies". In: *ApJL* 767.2, L29 (Apr. 2013), L29. doi:10.1088/2041-8205/767/2/L29. arXiv: 1304.2560 [astro-ph.CO].

[235] Travis Oliphant. *NumPy: A guide to NumPy*. USA: Trelgol Publishing. [Online; accessed <today>]. 2006–. http://www.numpy.org/.

[236] J. P. Ostriker. "Elliptical Galaxies are not Made by Merging Spiral Galaxies". In: *Comments on Astrophysics* 8 (Jan. 1980), 177.

[237] M. Paolillo et al. "Deep ROSAT HRI Observations of the NGC 1399/NGC 1404 Region: Morphology and Structure of the X-Ray Halo". In: *ApJ* 565 (Feb. 2002), 883–907. doi:10.1086/337919. eprint: astro-ph/0109342.

[238] M. G. Pastoriza et al. "Galaxy Properties in Different Environments. II. Star Formation in Bulges of Late-Type Spirals". In: *ApJ* 432 (1994), 128. doi:10.1086/174554.

[239] Ana Paulino-Afonso et al. "VIS^{3}COS. I. Survey overview and the role of environment and stellar mass on star formation". In: *A&A* 620, A186 (Dec. 2018), A186. doi:10.1051/0004-6361/201832688. arXiv: 1805.07371 [astro-ph.GA].

[240] Ana Paulino-Afonso et al. "VIS^{3}COS. II. Nature and nurture in galaxy structure and morphology". In: *A&A* 630, A57 (Oct. 2019), A57. doi:10.1051/0004-6361/201935137. arXiv: 1907.10062 [astro-ph.GA].

[241] C. Y. Peng et al. "Detailed Decomposition of Galaxy Images. II. Beyond Axisymmetric Models". In: *AJ* 139 (June 2010), 2097–2129. doi:10.1088/0004-6256/139/6/2097. arXiv: 0912.0731.

[242] Eric W. Peng et al. "The HST/ACS Coma Cluster Survey. IV. Intergalactic Globular Clusters and the Massive Globular Cluster System at the Core of the Coma Galaxy Cluster". In: *ApJ* 730.1, 23 (Mar. 2011), 23. doi:10.1088/0004-637X/730/1/23. arXiv: 1101.1000 [astro-ph.GA].

[243] Ying-jie Peng et al. "Mass and Environment as Drivers of Galaxy Evolution in SDSS and zCOSMOS and the Origin of the Schechter Function". In: *ApJ* 721.1 (Sept. 2010), 193–221. doi:10.1088/0004-637X/721/1/193. arXiv: 1003.4747 [astro-ph.CO].

[244] J. Perea, A. del Olmo, and M. Moles. "Mass estimation for systems of galaxies." In: *A&A* 237 (Oct. 1990), 319.

[245] S. P. C. Peters et al. "Stellar disc truncations and extended haloes in face-on spiral galaxies". In: *MNRAS* 470 (Sept. 2017), 427–444. doi:10.1093/mnras/stx1205. arXiv: 1705.03555.

[246] Annalisa Pillepich et al. "Simulating galaxy formation with the IllustrisTNG model". In: *MNRAS* 473.3 (Jan. 2018), 4077–4106. doi:10.1093/mnras/stx2656. arXiv: 1703.02970 [astro-ph.GA].

[247] F. Pinna et al. "The Fornax 3D project: Thick disks in a cluster environment". In: *A&A* 625, A95 (May 2019), A95. doi:10.1051/0004-6361/201935154. arXiv: 1904.01260 [astro-ph.GA].

[248] F. Pinna et al. "The Fornax 3D project: Unveiling the thick disk origin in FCC 170; possible signs of accretion". In: *A&A* 623, A19 (Mar. 2019), A19. doi:10.1051/0004-6361/201833193. arXiv: 1901.04310 [astro-ph.GA].

[249] Bianca M. Poggianti et al. "GASP. I. Gas Stripping Phenomena in Galaxies with MUSE". In: *ApJ* 844.1, 48 (July 2017), 48. doi:10.3847/1538-4357/aa78ed. arXiv: 1704.05086 [astro-ph.GA].

[250] Bianca M. Poggianti et al. "The Relation between Star Formation, Morphology, and Local Density in High-Redshift Clusters and Groups". In: *ApJ* 684.2 (Sept. 2008), 888–904. doi:10.1086/589936. arXiv: 0805.1145 [astro-ph].

[251] M. Pohlen and I. Trujillo. "The structure of galactic disks. Studying late-type spiral galaxies using SDSS". In: *A&A* 454 (Aug. 2006), 759–772. doi:10.1051/0004-6361:20064883. eprint: astro-ph/0603682.

[252] V. Pota et al. "The Fornax Cluster VLT Spectroscopic Survey - I. VIMOS spectroscopy of compact stellar systems in the Fornax core region". In: *MNRAS* 481 (Dec. 2018), 1744–1756. doi:10.1093/mnras/sty2149. arXiv: 1803.03275.

[253] F. Pranger et al. "The effect of environment on the structure of disc galaxies". In: *MNRAS* 467 (May 2017), 2127–2144. doi:10.1093/mnras/stx199. arXiv: 1605.08845.

[254] M. E. Putman et al. "FCC 35 and Its H i Companion: Multiwavelength Observations and Interpretation". In: *AJ* 115.6 (June 1998), 2345–2355. doi:10.1086/300367.

[255] P. J. Quinn, Lars Hernquist, and D. P. Fullagar. "Heating of Galactic Disks by Mergers". In: *ApJ* 403 (Jan. 1993), 74. doi:10.1086/172184.

[256] M. A. Raj et al. "The Fornax Deep Survey with the VST. VII. Evolution and structure of late type galaxies inside the virial radius of the Fornax cluster". In: *A&A* 628, A4 (2019), A4. doi:10.1051/0004-6361/201935433. arXiv: 1906.08704 [astro-ph.GA].

[257] Jesper Rasmussen, Trevor J. Ponman, and John S. Mulchaey. "Gas stripping in galaxy groups - the case of the starburst spiral NGC 2276". In: *MNRAS* 370.1 (July 2006), 453–467. doi:10.1111/j.1365-2966.2006.10492.x. arXiv: astro-ph/0604549 [astro-ph].

[258] Gibson Reaves. "Distribution of Dwarf Galaxies in the Virgo and Fornax Clusters." In: *AJ* 69 (Jan. 1964), 556. doi:10.1086/109461.

[259] J. Rhee et al. "Phase-space Analysis in the Group and Cluster Environment: Time Since Infall and Tidal Mass Loss". In: *ApJ* 843, 128 (July 2017), 128. doi:10.3847/1538-4357/aa6d6c. arXiv: 1704.04243.

[260] André L. B. Ribeiro et al. "Structural and Dynamical Analysis of the Hickson Compact Groups". In: *ApJ* 497.1 (Apr. 1998), 72–88. doi:10.1086/305442.

[261] W. H. Richardson. "Bayesian-Based Iterative Method of Image Restoration". In: *Journal of the Optical Society of America (1917-1983)* 62 (Jan. 1972), 55.

[262] T. Richtler et al. "The globular cluster system of NGC 1316. III. Kinematic complexity". In: *A&A* 569, A41 (Sept. 2014), A41. doi:10.1051/0004-6361/201423525. arXiv: 1406.2868 [astro-ph.GA].

[263] A. Rodríguez-Ardila et al. "Powerful outflows in the central parsecs of the low-luminosity active galactic nucleus NGC 1386". In: *MNRAS* 470 (Sept. 2017), 2845–2860. doi:10.1093/mnras/stx1401. arXiv: 1706.01370.

[264] J. C. Roediger et al. "Stellar Populations and Radial Migrations in Virgo Disk Galaxies". In: *ApJ* 758, 41 (Oct. 2012), 41. doi:10.1088/0004-637X/758/1/41. arXiv: 1201.6361.

[265] R. Roškar et al. "Riding the Spiral Waves: Implications of Stellar Migration for the Properties of Galactic Disks". In: *ApJL* 684 (Sept. 2008), L79. doi:10.1086/592231. arXiv: 0808.0206.

[266] Craig S. Rudick, J. Christopher Mihos, and Cameron McBride. "The Formation and Evolution of Intracluster Light". In: *ApJ* 648.2 (Sept. 2006), 936–946. doi:10.1086/506176. arXiv: astro-ph/0605603 [astro-ph].

[267] Craig S. Rudick et al. "Tidal Streams of Intracluster Light". In: *ApJ* 699.2 (July 2009), 1518–1529. doi:10.1088/0004-637X/699/2/1518. arXiv: 0906.1185 [astro-ph.GA].

[268] V. S. Safronov. "On the gravitational instability in flattened systems with axial symmetry and non-uniform rotation". In: *Annales d'Astrophysique* 23 (Feb. 1960), 979.

[269] Kanak Saha and Bruce Elmegreen. "Why Are Some Galaxies Not Barred?" In: *ApJ* 858.1, 24 (May 2018), 24. doi:10.3847/1538-4357/aabacd. arXiv: 1803.10445 [astro-ph.GA].

[270] H. Salo et al. "The Spitzer Survey of Stellar Structure in Galaxies (S^4G): Multi-component Decomposition Strategies and Data Release". In: *ApJS* 219, 4 (July 2015), 4. doi:10.1088/0067-0049/219/1/4. arXiv: 1503.06550.

[271] P. Sánchez-Blázquez et al. "The origin of the light distribution in spiral galaxies". In: *MNRAS* 398 (Sept. 2009), 591–606. doi:10.1111/j.1365-2966.2009.15133.x. arXiv: 0905.4579.

[272] Allan Sandage. "The Classification of Galaxies: Early History and Ongoing Developments". In: *Annual Review of Astron and Astrophys* 43.1 (2005), 581–624. doi:10.1146/annurev.astro.43.112904.104839.

[273] Allan Sandage. *The Hubble Atlas of Galaxies*. 1961.

[274] Craig L. Sarazin. "X-ray emission from clusters of galaxies". In: *Rev. Mod. Phys.* 58 (1 1986), 1–115. doi:10.1103/RevModPhys.58.1. https://link.aps.org/doi/10.1103/RevModPhys.58.1.

[275] Alex Saro et al. "Toward Unbiased Galaxy Cluster Masses from Line-of-sight Velocity Dispersions". In: *ApJ* 772.1, 47 (July 2013), 47. doi:10.1088/0004-637X/772/1/47. arXiv: 1203.5708 [astro-ph.CO].

[276] M. Sarzi et al. "The Fornax3D project: overall goals, galaxy sample, MUSE data analysis and initial results". In: *A&A, in press* (2018).

[277] C. A. Scharf, D. R. Zurek, and M. Bureau. "The Chandra Fornax Survey. I. The Cluster Environment". In: *ApJ* 633 (Nov. 2005), 154–164. doi:10.1086/444531. eprint: astro-ph/0406216.

[278] J. Schaye. "Star Formation Thresholds and Galaxy Edges: Why and Where". In: *ApJ* 609 (July 2004), 667–682. doi:10.1086/421232. eprint: astro-ph/0205125.

[279] Joop Schaye et al. "The EAGLE project: simulating the evolution and assembly of galaxies and their environments". In: *MNRAS* 446.1 (Jan. 2015), 521–554. doi:10.1093/mnras/stu2058. arXiv: 1407.7040 [astro-ph.GA].

[280] P. Schipani et al. "Removing static aberrations from the active optics system of a wide-field telescope". In: *Journal of the Optical Society of America A* 29 (July 2012), 1359. doi:10.1364/JOSAA.29.001359.

[281] D. J. Schlegel, D. P. Finkbeiner, and M. Davis. "Maps of Dust Infrared Emission for Use in Estimation of Reddening and Cosmic Microwave Background Radiation Foregrounds". In: *ApJ* 500 (June 1998), 525–553. doi:10.1086/305772. eprint: astro-ph/9710327.

[282] A. Schröder. PhD thesis. , Universität Basel., (1995), 1995.

[283] A. Schröder, M. J. Drinkwater, and O.-G. Richter. "The neutral hydrogen content of <ASTROBJ>Fornax cluster</ASTROBJ> galaxies". In: *A&A* 376 (Sept. 2001), 98–111. doi:10.1051/0004-6361:20010997. eprint: astro-ph/0107373.

[284] M. P. Schwarz. "How bar strength and pattern speed affect galactic spiral structure." In: *MNRAS* 209 (July 1984), 93–109. doi:10.1093/mnras/209.1.93.

[285] M. P. Schwarz. "The response of gas in a galactic disk to bar forcing". In: *ApJ* 247 (July 1981), 77–88. doi:10.1086/159011.

[286] F. Schweizer. "An optical study of the giant radio galaxy NGC 1316 (Fornax A)." In: *ApJ* 237 (1980), 303–318. doi:10.1086/157870.

[287] Marc S. Seigar, Alister W. Graham, and Helmut Jerjen. "Intracluster light and the extended stellar envelopes of cD galaxies: an analytical description". In: *MNRAS* 378.4 (July 2007), 1575–1588. doi:10.1111/j.1365-2966.2007.11899.x. arXiv: astro-ph/0612229 [astro-ph].

[288] J. A. Sellwood and A. Wilkinson. "Dynamics of barred galaxies". In: *Reports on Progress in Physics* 56.2 (Feb. 1993), 173–256. doi:10.1088/0034-4885/56/2/001. arXiv: astro-ph/0608665 [astro-ph].

[289] P. Serra et al. "Neutral hydrogen gas within and around NGC 1316". In: *A&A* 628, A122 (2019), A122. doi:10.1051/0004-6361/201936114. arXiv: 1907.08265 [astro-ph.GA].

[290] P. Serra et al. "The MeerKAT Fornax Survey". In: *MeerKAT Science: On the Pathway to the SKA*. Jan. 2016, 8. arXiv: 1709.01289 [astro-ph.GA].

[291] J. L. Sérsic. "Influence of the atmospheric and instrumental dispersion on the brightness distribution in a galaxy". In: *Boletin de la Asociacion Argentina de Astronomia La Plata Argentina* 6 (Feb. 1963), 41–43.

[292] Shiyin Shen et al. "The size distribution of galaxies in the Sloan Digital Sky Survey". In: *MNRAS* 343.3 (Aug. 2003), 978–994. doi:10.1046/j.1365-8711.2003.06740.x. arXiv: astro-ph/0301527 [astro-ph].

[293] Jesper Sommer-Larsen. "Properties of intra-group stars and galaxies in galaxy groups: 'normal' versus 'fossil' groups". In: *MNRAS* 369.2 (2006), 958–968. doi:10.1111/j.1365-2966.2006.10352.x. arXiv: astro-ph/0509849 [astro-ph].

[294] M. Spavone et al. "The Fornax Deep Survey with VST. VIII. Connecting the accretion history with the cluster density". In: *arXiv e-prints*, arXiv:2005.00025 (Apr. 2020), arXiv:2005.00025. arXiv: 2005.00025 [astro-ph.GA].

[295] M. Spavone et al. "VEGAS: A VST Early-type GAlaxy Survey. II. Photometric study of giant ellipticals and their stellar halos". In: *A&A* 603, A38 (July 2017), A38. doi:10.1051/0004-6361/201629111. arXiv: 1703.10835.

[296] Marilena Spavone et al. "VEGAS: A VST Early-type GAlaxy Survey. II. Photometric study of giant ellipticals and their stellar halos". In: *A&A* 603, A38 (July 2017), A38. doi:10.1051/0004-6361/201629111. arXiv: 1703.10835 [astro-ph.GA].

[297] Marilena Spavone et al. "VEGAS: A VST Early-type Galaxy Survey. III. Mapping the Galaxy Structure, Interactions, and Intragroup Light in the NGC 5018 Group". In: *ApJ* 864.2, 149 (2018), 149. doi:10.3847/1538-4357/aad6e9. arXiv: 1807.11204 [astro-ph.GA].

[298] C. Spiniello et al. "The Fornax Cluster VLT Spectroscopic Survey II - Planetary Nebulae kinematics within 200 kpc of the cluster core". In: *MNRAS* 477 (June 2018), 1880–1892. doi:10.1093/mnras/sty663. arXiv: 1803.03276.

[299] D. Steinhauser, S. Schindler, and V. Springel. "Simulations of ram-pressure stripping in galaxy-cluster interactions". In: *A&A* 591, A51 (June 2016), A51. doi:10.1051/0004-6361/201527705. arXiv: 1604.05193.

[300] Kyle R. Stewart et al. "Gas-rich Mergers in LCDM: Disk Survivability and the Baryonic Assembly of Galaxies". In: *ApJ* 702.1 (Sept. 2009), 307–317. doi:10.1088/0004-637X/702/1/307. arXiv: 0901.4336 [astro-ph.CO].

[301] Y. Su et al. "Gas Sloshing Regulates and Records the Evolution of the Fornax Cluster". In: *ApJ* 851, 69 (Dec. 2017), 69. doi:10.3847/1538-4357/aa989e. arXiv: 1711.01523 [astro-ph.HE].

[302] L. A. M. Tasca et al. "The zCOSMOS redshift survey: the role of environment and stellar mass in shaping the rise of the morphology-density relation from z ~1". In: *A&A* 503.2 (Aug. 2009), 379–398. doi:10.1051/0004-6361/200912213. arXiv: 0906.4556 [astro-ph.CO].

[303] E. N. Taylor et al. "Galaxy And Mass Assembly (GAMA): stellar mass estimates". In: *MNRAS* 418 (Dec. 2011), 1587–1620. doi:10.1111/j.1365-2966.2011.19536.x. arXiv: 1108.0635 [astro-ph.CO].

[304] Doug Tody. "IRAF in the Nineties". In: *Astronomical Data Analysis Software and Systems II*. Ed. by R. J. Hanisch, R. J. V. Brissenden, and J. Barnes. Vol. 52. Astronomical Society of the Pacific Conference Series. Jan. 1993, 173.

[305] Doug Tody. "The IRAF Data Reduction and Analysis System". In: *Proc. SPIE*. Ed. by David L. Crawford. Vol. 627. Society of Photo-Optical Instrumentation Engineers (SPIE) Conference Series. Jan. 1986, 733. doi:10.1117/12.968154.

[306] Alar Toomre. "Mergers and Some Consequences". In: *Evolution of Galaxies and Stellar Populations*. Ed. by Beatrice M. Tinsley and D. Campbell Larson Richard B. Gehret. Jan. 1977, 401.

[307] I. Trujillo and J. Fliri. "The hidden Universe". In: *Highlights of Spanish Astrophysics VIII*. May 2015, 348–353.

[308] I. Trujillo et al. "A Correlation between Light Concentration and Cluster Local Density for Elliptical Galaxies". In: *ApJL* 573 (July 2002), L9–L12. doi:10.1086/341883. eprint: astro-ph/0205291.

[309] R. B. Tully et al. "The Extragalactic Distance Database". In: *AJ* 138 (Aug. 2009), 323–331. doi:10.1088/0004-6256/138/2/323.

[310] R. Brent Tully et al. "The Laniakea supercluster of galaxies". In: *Nature* 513.7516 (2014), 71–73. doi:10.1038/nature13674. arXiv: 1409.0880 [astro-ph.CO].

[311] J. A. Tyson, F. Valdes, and R. A. Wenk. "Detection of Systematic Gravitational Lens Galaxy Image Alignments: Mapping Dark Matter in Galaxy Clusters". In: *ApJL* 349 (Jan. 1990), L1. doi:10.1086/185636.

[312] E. A. Valentijn et al. "Astro-WISE: Chaining to the Universe". In: *Astronomical Data Analysis Software and Systems XVI*. Ed. by R. A. Shaw, F. Hill, and D. J. Bell. Vol. 376. Astronomical Society of the Pacific Conference Series. Oct. 2007, 491. eprint: astro-ph/0702189.

[313] S. van den Bergh. "A new classification system for galaxies." In: *ApJ* 206 (June 1976), 883–887. doi:10.1086/154452.

[314] P. C. van der Kruit. "Optical surface photometry of eight spiral galaxies studied in Westerbork". In: *A&AS* 38 (Oct. 1979), 15–38.

[315] P. C. van der Kruit and K. C. Freeman. "Galaxy Disks". In: *Annual Review of Astron and Astrophys* 49.1 (Sept. 2011), 301–371. doi:10.1146/annurev-astro-083109-153241. arXiv: 1101.1771 [astro-ph.GA].

[316] P. C. van der Kruit and L. Searle. "Surface photometry of edge-on spiral galaxies. I - A model for the three-dimensional distribution of light in galactic disks." In: *A&A* 95 (Feb. 1981), 105–115.

[317] P. C. van der Kruit and L. Searle. "Surface Photometry of Edge-On Spiral Galaxies. II - the Distribution of Light and Colour in the Disk and Spheroid of NGC891". In: *A&A* 95 (Feb. 1981), 116.

[318] A. van der Wel et al. "The Evolution of the Field and Cluster Morphology-Density Relation for Mass-Selected Samples of Galaxies". In: *ApJ* 670.1 (Nov. 2007), 206–220. doi:10.1086/521783. arXiv: 0707.2787 [astro-ph].

[319] A. Venhola et al. "The Fornax Deep Survey with the VST. IV. A size and magnitude limited catalog of dwarf galaxies in the area of the Fornax cluster". In: *A&A* 620, A165 (Dec. 2018), A165. doi:10.1051/0004-6361/201833933. arXiv: 1810.00550.

[320] A. Venhola et al. "The Fornax Deep Survey with VST. III. Low surface brightness dwarfs and ultra diffuse galaxies in the center of the Fornax cluster". In: *A&A* 608, A142 (Dec. 2017), A142. doi:10.1051/0004-6361/201730696. arXiv: 1710.04616.

[321] Aku Venhola et al. "The Fornax Deep Survey (FDS) with VST. VI. Optical properties of the dwarf galaxies in the Fornax cluster". In: *A&A* 625, A143 (2019), A143. doi:10.1051/0004-6361/201935231. arXiv: 1904.08660 [astro-ph.GA].

[322] R. Vijayaraghavan and P. M. Ricker. "Pre-processing and post-processing in group-cluster mergers". In: *MNRAS* 435 (Nov. 2013), 2713–2735. doi:10.1093/mnras/stt1485. arXiv: 1308.1311 [astro-ph.CO].

[323] N. Visvanathan and A. Sandage. "The color - absolute magnitude relation for E and S0 galaxies. I. Calibration and tests for universality using Virgo and eight other nearby clusters." In: *ApJ* 216 (1977), 214–226. doi:10.1086/155464.

[324] G. Mark Voit. "Tracing cosmic evolution with clusters of galaxies". In: *Reviews of Modern Physics* 77.1 (Apr. 2005), 207–258. doi:10.1103/RevModPhys.77.207. arXiv: astro-ph/0410173 [astro-ph].

[325] B. Vollmer. "NGC 4654: Gravitational interaction or ram pressure stripping?" In: *A&A* 398 (Feb. 2003), 525–539. doi:10.1051/0004-6361:20021729. eprint: astro-ph/0211321.

[326] Jing Wang et al. "The prevalence of type III disc breaks in H I-rich and low-spin galaxies". In: *MNRAS* 479.4 (Oct. 2018), 4292–4306. doi:10.1093/mnras/sty1687. arXiv: 1806.09353 [astro-ph.GA].

[327] A. E. Watkins et al. "On the varied origins of up-bending breaks in galaxy disks". In: *arXiv e-prints* (Mar. 2019). arXiv: 1903.09384.

[328] Meryl Waugh et al. "The large-scale distribution of neutral hydrogen in the Fornax region". In: *MNRAS* 337.2 (Dec. 2002), 641–656. doi:10.1046/j.1365-8711.2002.05942.x. arXiv: astro-ph/0210170 [astro-ph].

[329] K. A. Weaver, A. S. Wilson, and J. A. Baldwin. "Kinematics and Ionization of Extended Gas in Active Galaxies. VI. The Seyfert 2 Galaxy NGC 1386". In: *ApJ* 366 (Jan. 1991), 50. doi:10.1086/169539.

[330] G. A. Welch, G. Chincarini, and H. J. Rood. "Study of three southern groups of galaxies." In: *AJ* 80 (1975), 77–82. doi:10.1086/111715.

[331] S. D. M. White and M. J. Rees. "Core condensation in heavy halos: a two-stage theory for galaxy formation and clustering." In: *MNRAS* 183 (1978), 341–358. doi:10.1093/mnras/183.3.341.

[332] Simon D. M. White and Carlos S. Frenk. "Galaxy Formation through Hierarchical Clustering". In: *ApJ* 379 (1991), 52. doi:10.1086/170483.

[333] B. C. Whitmore. "What determines the morphological fractions in clusters of galaxies?" In: *Evolution of Galaxies and their Environment*. Ed. by J. M. Shull and H. A. Thronson. Jan. 1993.

[334] J. D. Younger et al. "Antitruncated Stellar Disks via Minor Mergers". In: *ApJ* 670 (Nov. 2007), 269–278. doi:10.1086/521976. arXiv: 0707.4481.

[335] N. Zabel et al. "The ALMA Fornax Cluster Survey I: stirring and stripping of the molecular gas in cluster galaxies". In: *MNRAS* 483 (Feb. 2019), 2251–2268. doi:10.1093/mnras/sty3234. arXiv: 1811.11759.

[336] Ann I. Zabludoff and John S. Mulchaey. "The Properties of Poor Groups of Galaxies. I. Spectroscopic Survey and Results". In: *ApJ* 496.1 (1998), 39–72. doi:10.1086/305355. arXiv: astro-ph/9708132 [astro-ph].

[337] Stefano Zibetti et al. "Intergalactic stars in z∼0.25 galaxy clusters: systematic properties from stacking of Sloan Digital Sky Survey imaging data". In: *MNRAS* 358.3 (2005), 949–967. doi:10.1111/j.1365-2966.2005.08817.x. arXiv: astro-ph/0501194 [astro-ph].

[338] F. Zwicky. "On the Masses of Nebulae and of Clusters of Nebulae". In: *ApJ* 86 (1937), 217. doi:10.1086/143864.

Take pride in how far you have come, have faith in how far you can go.
— Anonymous